SEISMIC SOIL-STRUCTURE INTERACTION BEHAVIOR OF PILE-SUPPORTED WHARF SYSTEMS ON LIQUEFIABLE SOILS UNDER 3-D EXCITATION

by

Caner Gülenç

B.S., Civil Engineering, Dokuz Eylül University, 2010

M.S., Earthquake Engineering, Boğaziçi University, 2014

Submitted to the Kandilli Observatory and Earthquake Research Institute
in partial fulfillment of the requirements for the degree of
Doctor of Philosophy

Graduate Program in Earthquake Engineering

Boğaziçi University

2024

SEISMIC SOIL-STRUCTURE INTERACTION BEHAVIOR OF PILE-SUPPORTED WHARF SYSTEMS ON LIQUEFIABLE SOILS UNDER 3-D EXCITATION

APPROVED BY:

Prof. Eser Çaktı (Thesis Supervisor)	.....
Prof. M. Nuray Aydınoğlu (Thesis Co-supervisor)	.....
Prof. Ufuk Hancılar	.....
Prof. Özer Çinicioğlu	.....
Assoc. Prof. Barlas Özden Çağlayan (Istanbul Technical University)	.....
Assist. Prof. Eren Vuran (Yeditepe University)	.....

DATE OF APPROVAL: 25.07.2024

To my precious wife, Nihan

ACKNOWLEDGEMENTS

First of all, I would like to thank Prof. M. Nuray Aydınoğlu. His existence has profoundly affected my life. It is a great honour and source of immense happiness to be his student. I will strive to disseminate the knowledge and, more importantly, the values learned from him to others throughout my remaining life. I believe that by doing so, we can ensure his legacy lives on. His constant support, encouragement and invaluable contributions are gratefully acknowledged. I would like to thank Prof. Eser Çaktı for her contributions during the preparation period of this thesis, particularly during the project application periods to BAP and TUBITAK. I would like to express my gratitude to Osman Müyesser, who is my former boss, engineering teacher and lifelong mentor, for his endless support during my professional career and Ph.D. studies. He is truly one of the heroes directing my life in a positive way and certainly one of the best people I have ever known. I would like to thank the jury members, Assist. Prof. Eren Vuran, Prof. Ufuk Hancılar, Prof. Özer Çinicioğlu and Assoc. Prof. Ö. Barlas Çağlayan for their valuable contributions. I would like to thank Prof. Yasin Fahjan and Utku Celep, Ph.D. for their guidance at the initial stage of this Ph.D. thesis. I would like to thank my colleagues, Bilgen Özbay, Fatma S. Malcıoğlu, Ahmet Korkmaz, Tuğçe Tetik, Kökcan Dönmez, N. Merve Çağlar, Mahir Çetin, Fahrettin Kuran, Elif Yıldırım, Hakan A. Alçık, Hasibe Gül and Rıza Pektaş for their support and companionship. I would like to thank Yalçın Şadi for his friendship and encouragement during my Ph.D. studies. This thesis has been financially supported by Boğaziçi University BAP Doctorate Project Code: 19443. Their support is greatly acknowledged. I would like to thank the Itasca family for their support regarding the free use of FLAC3D within context of IEP program. I would like to express my deepest gratitude to my precious wife, Nihan, for her extraordinary patience, support and love during my lifelong studentship, specifically over the last two and a half years. Special thanks to my little son, Tan, whose existence makes my life meaningful and beautiful. Also, I would like to express my gratitude to my mother, father, sister and brother for their endless support throughout my life.

ABSTRACT

SEISMIC SOIL-STRUCTURE INTERACTION BEHAVIOR OF PILE-SUPPORTED WHARF SYSTEMS ON LIQUEFIABLE SOILS UNDER 3-D EXCITATION

The procedures currently used in the analysis and design of pile-supported wharf structures are inadequate to consider the important features of the systems under seismic excitation. Highly sophisticated analysis models employed in literature neglect the seismic excitation in longitudinal direction, while design approaches roughly incorporate this aspect but fail in accurate modeling of soil-structure interaction (SSI) effects. Despite widespread use of very long multi-segmented wharves in marine construction practice, seismic analysis of these systems is generally overlooked. It is likely that such long structures exhibit varying soil stratification along the embankment in the longitudinal direction. In this regard, three-dimensional soil-structure interaction models are developed for multi-segmented wharf systems situated on liquefiable soil conditions, addressing a realistic engineering challenge. The analyses of these systems are performed under three dimensional seismic excitation and the outputs are meticulously processed to clearly demonstrate the outcomes. Finally, the findings are presented in proper order. The results indicate that SSI modeling and soil liquefaction play a crucial role in the seismic behavior of wharves. The impact of longitudinal excitation in liquefiable soil conditions significantly affects both soil and structural responses. The torsional response of structural systems is negligibly small. Analysis of multi-segmented wharf systems may only be required when varying liquefiable soil layers exist along the embankment. This study is expected to be a pioneering effort in the field of marine geostructural engineering, potentially providing a base for the performance-based analysis and design of pile-supported wharf systems in the near future.

ÖZET

SIVILAŞABİLEN ZEMİNLER ÜZERİNDEKİ KAZIKLI RIHTIMLARIN ÜÇ BOYUTLU DEPREM ETKİSİ ALTINDA YAPI-ZEMİN ETKİLEŞİMİ DAVRANIŞLARI

Kazıklı rıhtımların analiz ve tasarımında halihazırda kullanılan yaklaşımlar, bu yapıların deprem etkisi altındaki önemli özelliklerini dikkate almakta yetersiz kalmaktadır. Literatürdeki son derece sofistike analiz modelleri bile boyuna doğrultudaki deprem etkisini ihmal ederken, pratikte kullanılan tasarım yaklaşımları genellikle bu etkileri kabaca da olsa dikkate alsa da, yapı-zemin etkileşiminin tutarlı şekilde modellenmesi bakımından yetersiz kalmaktadır. Öte yandan deniz inşaatı pratiğinde çok segmentli rıhtımlar yaygın olarak kullanılmasına rağmen, bu sistemlerin deprem analizi genellikle gözardı edilmektedir. Oysa böylesine uzun yapıların boyuna doğrultuda değişken zemin tabakalanmasına sahip olması kuvvetle muhtemeldir. Bu bağlamda, gerçekçi bir mühendislik problemi için sıvılaşabilir zemin tabakalarının üzerinde inşa edilen çok segmentli rıhtımların üç boyutlu yapı-zemin etkileşimi modelleri geliştirilmiştir. Bu sistemlerin analizleri iki ve üç boyutlu deprem etkileri altında gerçekleştirilmiş, elde edilen çıktılar işlenerek sonuçlar açık bir şekilde sunulmuştur. Sonuçlar, yapı-zemin etkileşimi modellemesinin ve zemin sıvılaşmasının rıhtımların deprem davranışındaki kritik rolünü göstermektedir. Sıvılaşabilir zemin koşullarında; boyuna doğrultudaki yer hareketinin etkisi, zemin ve yapısal tepkilerini önemli ölçüde etkilemektedir. Yapısal sistemlerin burulma davranışının ise ihmal edilebilir derecede olduğu gözlemlenmiştir. Çok segmentli rıhtım sistemlerinin analizinin, rıhtım boyuna doğrultusunda değişken, sıvılaşabilir zemin tabaklanmasının bulunduğu durumlarda gerekebileceği gözlemlenmiştir. Bu çalışmanın, deniz yapıları geo-yapısal mühendisliği alanında öncü bir çaba olması beklenmekte ve yakın gelecekte kazıklı rıhtım sistemlerinin performansa dayalı analiz ve tasarımı için bir temel sağlama potansiyeline sahip olabileceği düşünülmektedir.

TABLE OF CONTENTS

LIST OF FIGURES

LIST OF TABLES

LIST OF SYMBOLS

C_p	P-wave velocity of medium
C_s	S-wave velocity of medium
v_n	Input particle velocity in normal direction
v_s	Input particle velocity in shear direction
t_n	Traction vector of absorbing boundary in normal direction
t_s	Traction vector of absorbing boundary in shear direction
K	Bulk modulus of soil medium
G	Shear modulus of soil medium
F_x	Force at the node of near-field grid near boundary in X direction
F_y	Force at the node of near-field grid near boundary in Y direction
F_z	Force at the node of near-field grid near boundary in Z direction
F_x^{ff}	Force at the node of free-field grid in X direction
F_y^{ff}	Force at the node of free-field grid in Y direction
F_z^{ff}	Force at the node of free-field grid in Z direction
v_{xm}	Particle velocity at the node of near-field grid near boundary in X direction
v_{ym}	Particle velocity at the node of near-field grid near boundary in Y direction
v_{zm}	Particle velocity at the node of near-field grid near boundary in Z direction
v_x^{ff}	Particle velocity at the node of free-field grid in X direction
v_y^{ff}	Particle velocity at the node of free-field grid in Y direction
v_z^{ff}	Particle velocity at the node of free-field grid in Z direction
V_{s-min}	Minimum shear wave velocity
f_{max}	Highest frequency of ground motion

f_{min}	Central frequency used in Rayleigh Damping
f_{min}	Central frequency used in Rayleigh Damping
V	Tetrahedral subzone volume
A^f_{max}	Face area associated with the tetrahedral subzone
r	Radius
m_A	Hydrodynamic water mass
c_s	Adhesion factor for vertical interface element
c_n	Adhesion at pile-soil interface for lateral interface element
M_w	Moment magnitude
v_{s30}	Average shear wave velocity of the soil stratification of top 30 meters
AI	Arias intensity
V_s	Shear wave velocity
D_r	Relative density
c'	Effective cohesion
c_u	Undrained shear strength
$C40$	Concrete class with 40Mpa characteristic yield strength capacity in compression
E_c	Modulus of elasticity of concrete
f_{co}	Yield strength of unconfined concrete
E_s	Modulus of elasticity of steel
f_{sy}	Yield strength of reinforcing steel
f_{su}	Ultimate strength of reinforcing steel
E_{ss}	Modulus of elasticity of structural steel
f_{ssy}	Yield strength of structural steel
f_{ssu}	Ultimate strength of structural steel
$S355$	Structural steel class with 355Mpa characteristic yield strength capacity
f_{ce}	Expected yield strength of concrete in compression
$f_{ye,r}$	Expected yield strength of reinforcing steel
$f_{ye,s}$	Expected yield strength of structural steel

M_p	Plastic moment capacity
M_y	Yield moment
N_{1-60}	Corrected blow count
ρ	Density
σ_n	Applied stress in normal direction
σ_s	Applied stress in shear direction
ξ_{min}	Minimum damping ratio used in Rayleigh Damping
Δt_d	Time-step size used in analysis
Δt_{crit}	Critical time-step size
Δt_β	Critical time-step size associated with stiffness proportional damping
ω_{max}	Highest angular frequency
α	Fraction of critical damping at this frequency
β	Ratio of minimum damping ratio to central angular frequency
ω_{min}	Central angular frequency used in Rayleigh Damping
φ_s	Friction angle at pile-soil interface for vertical interface element
ϕ	Internal friction
φ_n	Friction angle at pile-soil interface for lateral interface element
ρ_{sat}	Central angular frequency used in Rayleigh Damping
ϕ'	Effective internal friction angle
γ_c	Concrete density
ν_c	Concrete poisson ratio
ϵ_{co}	Yield strain of unconfined concrete
ϵ_{cs}	Crushing strain of unconfined concrete
ϵ_{ss}	Spalling strain of unconfined concrete
ϵ_{sy}	Yield strain of reinforcing steel
ϵ_{sh}	Hardening strain of reinforcing steel
ϵ_{su}	Ultimate strain of reinforcing steel
ρ_{ss}	Density of structural steel

ν_{ss}	Structural steel poisson ratio
θ	Rotation

LIST OF ACRONYMS/ABBREVIATIONS

1-D	One Dimensional
2-D	Two Dimensional
3-D	Three Dimensional
ASCE	American Society of Civil Engineers
CD	Chart Datum
CLE	Contingency Level Earthquake
DE	Design Level Earthquake
DEM	Discrete Element Modeling
DL	Seabed (Dredging) Level
DMF	Dynamic Magnification Factor
DS	Dense Sand
DTL	Deck Top Level
FISH	FLAC-ISH FLAC3D Scripting Language
FGL	Final Grade Level
KZE	Kazık Zemin Etkileşimi
LCS	Longitudinally Changing Soil Stratification
MDS	Medium Dense Sand
MOTEM	Marine Oil Terminal Engineering and Maintenance Standards
MSL	Mean Sea Level
OLE	Operating Level Earthquake
PC	Precast Concrete
PEER	Pacific Earthquake Engineering Research Center
POLA	Port of Los Angeles
POLB	Port of Long Beach
POLB-WDC	Port of Long Beach Wharf Design Criteria
RC	Reinforced concrete
RSM	Relative Soil Movement
SE	Structural Eccentricity

SPT	Standard penetration test
SRSS	Square Root of Sum of Squares
SSI	Soil-structure interaction
StC	Stiff Clay
STRP	Wharf Strip Analysis
TS	Turkish Standard Instutite
TSCDMS	Turkish Seismic Code for the Design of Marine Structures
TSDCB	Turkish Seismic Design Code for the Buildings
US	United States
VDS	Very Dense Sand
VSS	Varying Soil Stratification
VStC	Very Stiff Clay

1. INTRODUCTION

The developments in non-linear seismic modeling/analysis procedures and performance-based assessment/design of structures within the last thirty years have changed our perspective considerably. This relatively new approach has been adopted and implemented successfully for various types of structures, particularly for buildings. Towards the end of 1990s, the application of non-linear modeling/analysis procedures has been extended to marine structures as well. However, the use of those methods for marine structures, particularly for pile-supported wharves, has not been satisfactory in many cases due to the reasons mentioned in the following paragraphs.

Unlike most of the building structures, the seismic behavior of pile-supported wharves is generally governed by the geotechnical system having soft and loose layers in marine environment. Lack of proper soil representation in analysis models coupled with an artificial and rather insufficient incorporation of the "kinematic soil-structure interaction" effects may be considered as the major weaknesses of the current design approach used for the wharf structures. On the other hand, current analysis models are almost entirely limited to two-dimensional response of system in the transverse direction to the shoreline. Seismic excitation and the behavior of the wharf soil-structure system in the longitudinal direction are completely disregarded or at best estimated through rather crudely approximate ways.

The starting point of this thesis is to demonstrate that a more realistic approach for the seismic assessment and design of a wharf structure would be to incorporate the full soil medium into "complete soil-structure interaction" model in three dimensions. In fact, today's hardware and software capabilities allows us to perform such a more sophisticated modeling and analysis of 3D wharf systems within the framework of the modern "performance-based seismic assessment/design" methodology.

Thus, the primary aim of this research is to demonstrate the possibility of seismic evaluation and design of wharf structures through large three-dimensional soil-structure interaction models. Eventually, it is aimed to develop a full understanding of the seismic behavior of realistically long, pile-supported, multi-segmented 3D wharf systems considering liquefiable soil conditions and changing soil stratigraphy under three-dimensional seismic excitation.

1.1. Scope

In Chapter-2, a general definition for the wharf systems including structural and geotechnical components is presented emphasizing the importance of these infrastructural systems, complexities and challenges encountered during the analysis and design.

A detailed literature review, which is classified into the topics related to SSI modeling, multi-segmented wharves, longitudinal excitation, rockfill modeling, case histories from past earthquakes and code procedures used in practice, is presented in Chapter-3.

In Chapter-4, essentials of dynamic analysis in SSI modeling, including structural and geotechnical components, the load conditions and some other details regarding modeling are presented. The ground motions used in the study with filtering and deconvolution analysis details are given in Chapter-5.

In Chapter-6 and Chapter-7, properties of wharf system models, materials used in analysis cases and some details regarding processing of output data are presented.

In Chapter-8, findings obtained through the analysis cases are presented and evaluated. Concluding remarks and potential future research are presented in Chapter-9 and Chapter-10.

1.2. General Approach

The general approach adopted in the preparation of this thesis can be itemized as follows:

- Review literature in detail and in a wider extent.
- Create a realistic engineering framework that can possibly reflect all features intended to be demonstrated,
- Model and analyze the problem in many ways, trying to simulate realistic cases as much as possible,
- Process and visualize the data to clearly reflect the conclusive results to readers,
- Conclude the findings in a proper order without exaggerating or understating.

2. WHARF SYSTEM

2.1. General Definition

Wharf systems can be formed in many ways. The wharves considered in this study are pile-supported wharf systems and will be referred to as only "wharf systems" hereinafter.

Wharves can be defined as geo-structural systems, which extends along natural shoreline and/or man-made fill, located at the interface of sea and land. In this respect, they can be considered as link structures between sea and the terminals constructed on land, which provide services such as mooring, berthing of vessels and operations carried out in the field of passenger/cargo transportation, tourism and energy supply etc. A typical general arrangement plan including wharves and other marine infrastructures is shown in Figure 2.1 [1].

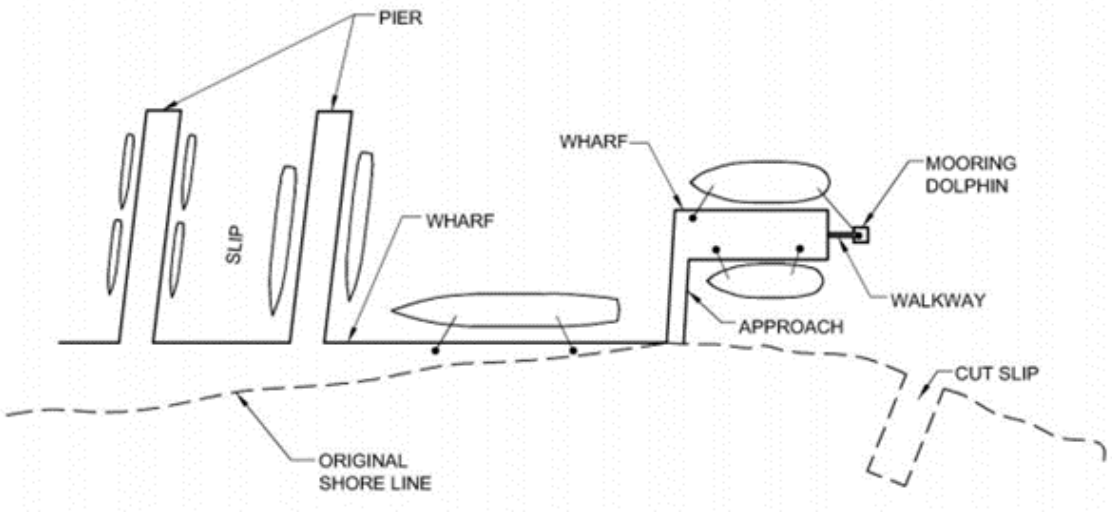

Figure 2.1. General Arrangement Plan for a Port (UFC Design: Piers and Wharves [1]).

2.2. Importance

Wharf systems are the main elements of marine terminals, which serve for international trade, global supply chain and other international maritime operations worldwide. Approximately 70% of international trade is realized through maritime transportation [2]. An interruption in port operations can cause billion dollars of cost as well as shortages in food, pharmacy, goods etc. The impact of such an interruption can be substantial on the economies of countries and social life of people.

Past earthquakes have shown such direct impacts on the countries' economies and people's life. Two man-made island accommodating container terminals in Kobe Port in Japan suffered from devastating Kobe Earthquake in 1995 [3]. The direct loss due to damage in Port of Kobe was estimated as 10 billion dollars by Ministry of Transportation. The port operations were disrupted during the reconstruction period, which lasted around two years [3].

Other important earthquake that has a considerable impact on ports and people's life is Haiti Earthquake, 2010 [4]. Port de Port-au-Prince, which was the largest port of Haiti at that time, was severely damaged. Emergency response and humanitarian aid could not be provided, because the port was unusable in the weeks after the earthquake [4].

Therefore, the seismic resilience of wharf structures is very important even though it is not directly related to life safety. Reliable seismic assessment/design of existing and newly designed wharves has been gaining importance with increasing demand of international trade volume in today's world.

2.3. Components

A wharf system is basically consisting of a geotechnical system and a structural system. The geotechnical system may include naturally existing soil strata with armour

layers, filter layer and backfill formed by rock placement based on the requirements of the facility. It may be directly formed on a cut-slope embankment by rock armouring through natural coastline or it may be formed on seabed by backfilling to create a reclamation area. Then, armour layers are formed by rock placement to protect the reclaimed area from wave actions. The construction methodology used to create reclamation areas can be varied from country to country depending on machinery, equipment, logistic conditions and materials used. For instance, quarry run can be used as backfill material if it is feasible to transport the material from mine and/or dredged soil material can be used as backfill material if suitable machinery and equipment are available.

The structural system of a wharf system consists of piles, pile heads, beams, slabs and shear keys. Piling can be again varied depending on the construction practice adopted in the country as well as the availability of machinery and equipment. Driven and bored piles can be used with steel and reinforced concrete material options. The deck of a wharf structural system can be steel or reinforced concrete. Steel deck systems have not been generally preferred recently because of their initial cost and maintenance costs due to the corrosive marine environments. Reinforced concrete deck system is generally a preferable option for wharves. After piling, RC pile heads or pile head beams are constructed depending on the adopted slab system. The connection between steel pile and RC deck system is provided by RC plugs elements, which is linked to the steel pile with shear connectors welded inside the piles and linked to the deck system via dowel bars. Cast in-situ and/or precast beam or slab options can be used to construct deck system. A typical wharf system of a container terminal is shown in Figure 2.2 [5].

The deck-on-pile wharf systems can be constructed as very long systems up to 1-2 km in longitudinal direction. To tolerate the expansions in longitudinal direction due to temperature change they are built as separated modules. To prevent the transverse movement between modules they are linked each other via shear keys constructed at the ends of modules.

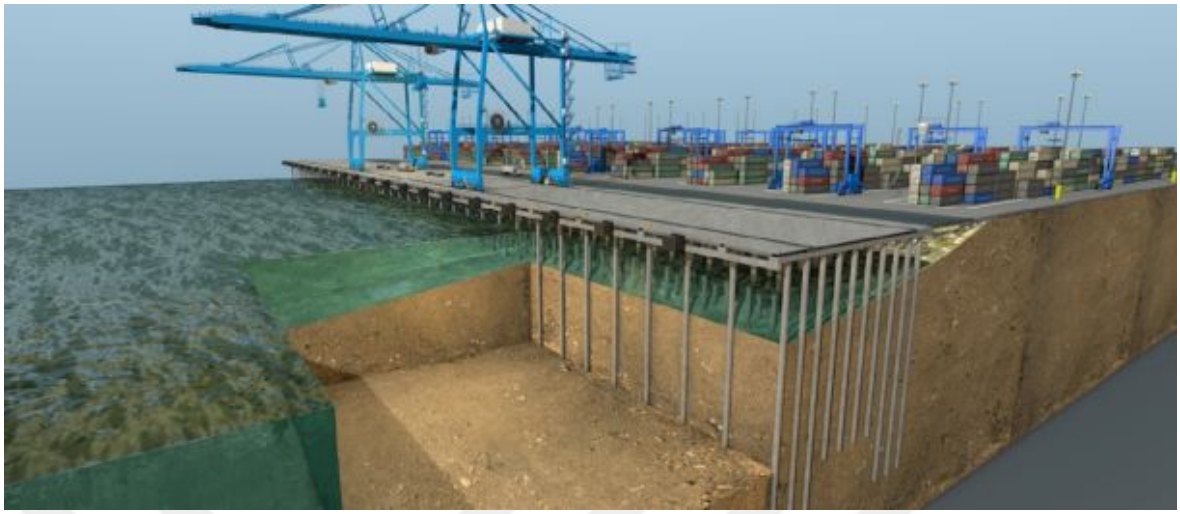

Figure 2.2. Typical Wharf System of a Container Terminal (Ramirez-Henao and Smith-Pardo [5]).

2.4. Complexity and Challenges

The seismic behavior of wharf system is mainly controlled by the seismic behavior of geotechnical system particularly if it contains loose and soft soils, which is a very common situation in marine environment. Therefore, the correct modeling of soil behavior is essential to represent the realistic behavior of the system. However, realistic modeling of geotechnical system is not an easy task. Components of geotechnical system may have considerable uncertainties in terms of dynamic properties and stratification along a long wharf system.

The studies treating the torsional response of wharf structural system state that the torsional behavior makes important contribution to the overall response of pile-supported wharves. However, these studies considered the structural systems only under inertial interaction. Torsional behavior of structural system interacting with three-dimensional soil medium may be more critical. When structural system consists of multiple modules linked each other via shear key, the situation may become even more complex.

The modeling and analysis of multi-segmented structural system together with the geotechnical system by direct analysis is a challenging task. But it is an inevitable necessity to consider the effects of soil-structure interaction, and accordingly to understand the realistic seismic behavior of the wharf system.

Not just the modeling and analysis of such large systems present challanges but also the post-processing of large output data is a complex problem.

3. LITERATURE REVIEW

Important developments regarding the seismic analysis and design of piled wharves in the modern era have started to occur after the major earthquakes, which happened in the first half of 1990s, and have continued at full steam up to today.

For the sake of clarity, the topics in literature review are classified, namely, dynamic soil-structure interaction (SSI) modeling and analysis techniques; longitudinal response and linked wharves; observations, case histories from past earthquakes and tests; rockfill-pile interaction, tests and modeling.

3.1. Dynamic SSI Modeling and Analysis Techniques

This section encompasses the literature survey regarding the methods of dynamic soil-structure interaction modeling and analysis employed for pile-supported wharves. The analysis methods used to consider the dynamic interaction of soil and structural systems can be divided into two groups [6]. The first one, which is employed within the context of this thesis, is called "direct interaction analysis". The second one is called "substructure analysis".

Direct interaction analysis is based on analyzing soil and structural systems simultaneously through a common analysis model, considering their direct interaction under dynamic or seismic excitation. This analysis can be performed in time or frequency domain. Since frequency domain solutions can only be applicable for linear systems, it is not preferable to implement in many situations in today's practice particularly in the case of highly nonlinear behaviour is expected. Today's hardware and software capacities allow us to implement nonlinear direct interaction analysis.

Substructure analysis method is based on the idea of analyzing soil and structural subsystems separately in two steps. In the first step, soil subsystem is analyzed under

seismic excitation and the foundation input motion, which is to be used in the second step, is calculated. Then, the soil springs, which is again to be used in the second step, are calculated by condensing the dynamic stiffness matrix of soil subsystem. In the second step, the structural subsystem is modeled incorporating the soil springs instead of real soil system. Then, the foundation input motion is imposed to the structural subsystem via soil springs and the response of structure incorporating dynamic soil-structure interaction is calculated. However, substructure analysis method is based on superposition approach and frequency domain analysis, thus, it is only applicable to linear systems. For this reason, conventional substructure method is generally not applied in today's practice. Instead, there are many applications, in which the various approximate substructure methods are applied in the time domain incorporating nonlinear behavior of subsystems.

On the other hand, there are some other studies including inertial and kinematic loading applications in the literature. These applications may be considered as a sort of approximate substructure analysis, which is treated separately in this study.

3.1.1. Direct Interaction Analysis

In this chapter, the studies incorporating the application of direct interaction analysis method are compiled and presented.

Series of analysis were conducted including simplified SPT-based liquefaction analysis, Newmark sliding block analysis and 2D fully coupled effective stress analysis in DYSAC2 by Muraleetharan et. al. [7]. The displacement results of dikes were compared with the ones obtained from case histories [8].

Yang [9] performed series of 2D effective stress analysis in FLAC [10] to investigate the optimum dimensions of the zone for soil improvement to reduce the detrimental effect of liquefaction on wharf response.

Roth et. al. [11] simulated the case histories from Loma Prieta earthquake (1989) by performing 2D effective stress analysis in FLAC.

McCullough [12] performed a set of 2D plane strain analysis in FLAC to validate the centrifuge test results and the response quantities of piled wharves observed in past earthquakes.

A comparative study for a pile-supported wharf was investigated via centrifuge model and simple 3D finite element model considering only one axis in longitudinal direction. The thickness of the piles were modeled via additional link elements by Takahashi [13]. This study is the first 3D finite element analysis model for pile-supported wharf systems.

Dickenson and McCullough [14] emphasized the importance of 3D modeling of pile-soil interaction to reduce uncertainties in geo-mechanical problems.

Lu [15] investigated the transverse response of a pile-supported wharf strip including number of piles by using 3D brick finite elements for soil modeling by parallel computing. Both linear and nonlinear time domain analyses were performed. It was a very sophisticated study at that time.

Chiaramonte [16] performed a set of 2D plane strain analyses of pile-supported wharf systems employing different pile-deck connection types by fiber modeling. The detailed explanations regarding finite element modeling and analysis carried out in OPENSEES framework were presented in this study.

Heidary-Torkamani et. al. [17] and Amirabadi et. al. [18] performed 2D plane strain analysis in OPENSEES incorporating fiber modeling of piles for the derivation of fragility curves of pile-supported wharf systems.

Ragued [19] study included 2D plain strain analyses of a wharf segment incorporating fiber modeling of piles in OPENSEES framework.

Su et. al. [20] investigated seismic behavior of a piled wharf system by 3D finite element modeling in OPENSEES framework. Even though only transverse behavior of 6.1m-wide wharf segment was investigated, pile-soil-pile interaction was considered by detailed model incorporating the effect of pile thickness. Large lateral deformation of soil and its effect on the wharf piles in downward direction was clearly depicted. The other important result of the study was significant axial forces occurred at the piles as a result of coupled vertical and lateral behavior of soil. It was able to be considered because of finite element modeling of soil around the piles. Such effects, probably, might not have been captured by uncoupled interaction springs to be used for representation of soil-structure interaction in structural analysis.

Su et. al. [21], Su et. al. [22] and Su et. al. [23] investigated fragility of piled wharves, the effects of soil permeability on fragility, retrofitting of wharves by different strategies, respectively, using the same 2D plane strain finite element model in OPENSEES framework.

Su et. al. [24] included the same 3D finite element model given in Su et al [20]. Performance-based assessment of given piled wharf was made as per the provisions of ASCE 61-14 considering only transverse behavior of the system.

Souri et. al. [25] performed 2D plane strain analysis in FLAC to investigate the effect of duration on the seismic response of pile-supported wharves.

Ozcebe et. al. [26] performed 2D plane strain analysis for a pile-supported wharf system incorporating crane system in OPENSEES framework and derived fragility curves for this system.

Souri et. al. [27] evaluated the efficiency of a soil constitutive model (PDMY03) and several analysis strategies to model 3D pile-soil interaction by 2D models. They performed 2D plane strain analysis and validate the results with the centrifuge data, which had been obtained within the context of McCullough [12].

Khosravifar and Souri [28] carried out a study incorporating direct analysis to compare the centrifuge test results with 3D simulation performed in FLAC3D. Note that this study only included one directional excitation. It was also stated that the estimation of reliable seismic response of wharves was important for performance-based design.

Wang et. al. [29] investigated the seismic response of pile-supported wharves under different types of near-field earthquakes, namely, forward directivity pulse-like, fling-step pulse-like and non-pulse-like records. 3D finite element simulation was performed for 18m wide wharf strip including 22 piles under only transverse excitation in OPENSEES framework.

Zhang et. al. [30] investigated the dynamic wharf-crane interaction by performing 3D finite element simulation considering only transverse excitation in OPENSEES framework. The analysis results were verified by physical model tests.

Common feature of these studies that both were performed by direct interaction analysis, disregarded longitudinal response of pile-supported wharf systems even though some of them was formed by three-dimensional brick elements instead of 2D plane strain model.

3.1.2. Substructure Analysis

In this chapter, the studies incorporating the application of approximate substructure analysis methods are compiled and presented herein.

Varun and Assimaki [31] had declared the development of macro-element model, which was later published by Varun [32], was able to simulate pile-soil interaction considering the effect of liquefaction, to be used as a Winkler-type spring in structural analysis.

Werner et. al. [33] explained the development of fragility models for container cargo wharves within the context of NEESR Grand Challenge Project. A procedure, which was to be used in probabilistic vulnerability assessment of pile-supported wharves, was proposed for the relatively rapid estimation of engineering demand parameters with respect to direct analysis. This two-step approximate substructure analysis procedure was consisting of free-field embankment analysis and structural analysis incorporating nonlinear macro-elements developed by Varun [32].

Shafieezadeh [34] PhD dissertation made important contributions to the literature of pile-supported wharf analysis. Most importantly, the Bouc-Wen type macro-element model [32], which make possible to incorporate the effect of liquefaction into structural analysis appropriately, was employed to define the soil-pile interaction. The procedure used in the analyses is based on the idea that the free-field soil displacements calculated at the first step were imposed to the macro-elements representing liquefiable soil layers and other p-y springs defined in structural analysis at the second step. These macro-elements monitored the pore-pressure data, which was obtained again from the free-field analysis, at the same time to adjust the stiffness and strength properties of springs in each time step. Note that these 2D free-field analyses had been performed by Vytiniotis [35].

Thomopoulos and Lai [36] used similar substructure analysis procedure, performing 2D free-field displacement responses at first step and imposing the displacements, calculated from the first step, to the end of p-y springs in structural analysis at the second step. As an alternative for the free field analysis performed in the first step, the embankment with embedded pile portions was performed as well. It was shown that employing the displacements of embankment with embedded pile model gave smaller

displacements at sloping ground than the ones computed from free-field analysis. Then, it was suggested the use of embedded pile model instead of free-field model for sloping ground conditions.

Panagiotidou [36] and Vytiniotis et. al. [37] evaluated the efficiency of a rapid soil improvement strategy with PV drains for pile-supported wharves using macro-element model [32] and 2D wharf model used by Shafieezadeh [34].

As a result, use of macro-element model developed by Varun [32] gains important advantage to structural analysis so that the effects of liquefaction on soil-pile interaction during the seismic excitation can be incorporated, thereby, increasing the efficiency of substructure analysis methods.

3.1.3. Inertial Loading and Kinematic Loading Analysis

In the first years of millennium, the idea of combination of kinematic and inertial response quantities was questionable, even generally neglected by some researchers on the grounds that the responses occurred due to the inertial and kinematic effects were happened at the different time intervals and they affected to the different locations of piles. As time goes by, the idea of combination has been getting popular in marine civil engineering community and causing a need of collaboration between structural and geotechnical engineers. This section covers the literature survey regarding the applications of inertial and kinematic loading analysis in marine civil engineering industry.

Weismair et. al. [38] addresses many important issues regarding pile-supported wharf design. The design considerations of Pier 400 were explained both in structural and geotechnical perspectives. Most probably, it is the study that performance-based design approach was adopted at the first time for a pile-supported wharf structure in the literature. Up-slope and down-slope p-y spring stiffnesses were considered in 2D pushover and 2D nonlinear time domain analyses. Only inertial analysis was per-

formed without considering kinematic effects in structural analyses. Then, 2D finite element analysis for geotechnical considerations was performed. However, the response quantities obtained from the analyses were not combined on the grounds that the peak responses of inertial and kinematic analyses would occur at different time phases.

McCullough et. al. [39] explained three common approaches used in pile design practice, namely, inertial loading, kinematic loading and direct analysis including both inertial and kinematic effects even though the names weren't referred literally. The importance of the kinematic effects was shown that the bending moments at the embedded parts of piles could be more than the ones obtained at the pile-deck connections. Also, the increase in the moments of piles at the soft-stiff soil layer interfaces was stated. In this regard, the inadequacy of point of fixity method used in structural analysis were emphasized.

Singh et. al. [40] came up with the requirement of combination for inertial and kinematic responses at least by a certain rate. They showed the interference of kinematic and inertial responses at the same time interval unlike the general opinion in engineering society. Also, it was stated that limit equilibrium and Newmark sliding block analyses were not reliable when weak soil conditions existed.

Roth et. al. [41] emphasized that performing only inertial interaction analysis for wharf systems was not correct way to design the systems by comparing the results of inertial analyses performed in SAP2000 [42], Perform 2D and the results of direct analyses performed in FLAC. Roth et. al. [11] emphasized the importance of soil deformations and the kinematic interaction of pile and surrounding soil for the design of pile-supported wharves as well.

Dickenson and McCullough [14] stated that the combination of inertial and kinematic interaction with a certain weighting scheme was not an easy task.

Vahdani et. al. [43] assessed the structural capacity of a pile-supported wharf by performing series of analysis including pushover analysis by SAP2000, Newmark analysis and direct analysis by FLAC. The displacements obtained from FLAC analysis imposed to each row of pile to calculate pile kinematic response. The kinematic responses were not combined with the ones calculated from inertial analysis because of the reason that a coupled action were not expected for the wharf under inertial and kinematic loading conditions.

Blandon [44] proposed a simplified method for single pile analysis regarding liquefaction induced kinematic loading on piles.

Arulmoli et. al. [45] stated that inertial and kinematic effects could be coupled or uncoupled during seismic excitation. The possibility of coupling might investigate during design stages.

Jain et. al. [46] covered an application for a newly designed wharf in line with MOTEM requirements. Inertial analyses in SAP2000 and direct analyses were performed by structural and geotechnical engineers to optimize the design.

Dickenson et. al. [47] emphasized that the determination and the use of weighting factors for kinematic and inertial interaction was a complex issue.

Percher and Iwashita [48] explained the methods of kinematic loading proposed by American codes. Also, the combination procedures for inertial and kinematic loadings, with weighting factors, were discussed.

Souri et. al. [49] compared the measured response of a pile-supported wharf obtained from the centrifuge tests by McCullough [12] with the results of LPILE single pile analyses to obtain the trends of inertial and kinematic demands of piles. It was recommended that, based on the comparative results, 100% inertial effect + 100% kinematic effect should be combined to obtain the response of piles located within

the part from pile-deck connection to 10D distance below ground. Also, only 100% kinematic effect was enough for the evaluation of the parts of piles below this level.

Galbraith et. al. [50] explained the details of procedures used in marine civil engineering industry at US for the practical application of inertial and kinematic loading and their combination. Common procedure used in practice to consider kinematic effects under liquefied soil and/or lateral spreading conditions was stated as post-kinematic analysis method. In this method, the kinematic effects obtained by geotechnical analysis was applied to the piles as either static force or displacement considering liquefied soil springs. Then, the inertial effects obtained from spectrum-based calculations was applied to the wharf at the second step. Kinematic displacement demand was incorporated in the calculation of target displacement for inertial loading. The weighting factors provided by geotechnical engineers for inertial and kinematic loading conditions were considered by taking the certain proportion of spectrum and/or kinematic displacement demand at the beginning of the analysis. The design was completed by checking the resultant strains of piles with given limiting strain values in the codes. This paper is important since there is no detailed guidance regarding the applications in practice about kinematic and inertial loading in practice even though it is mentioned in the codes.

Yao et. al. [51] explained a retrofit application implemented at the west coast of US incorporating kinematic effects due to liquefaction induced lateral deformations. Post-kinematic analysis method [50] used in design practice was employed.

Souri et al. [25] performed 2D plane strain analyses considering only inertial effects, only kinematic effects and considering both effects by direct analysis. It was stated that the deck displacement response was governed mainly by kinematic effects. The effects of inertia on deck displacements are minimal. It was also stated that the deck accelerations decreased when liquefaction was not considered.

Souri et. al. [52] made detailed analysis of the centrifuge tests, which had been carried out within the context of McCullough [12], to find out the relationships of peak moments, displacements and accelerations at the pile head, the embedded parts of piles and wharf deck.

Souri et. al. [53] developed a simplified static analysis procedure for the calculation of seismic response of pile-supported wharves based on the centrifuge tests, which had been carried out within the context of McCullough [12]. Also, the combination factors derived from these test results were presented for practical applications. It was proposed that only 100% peak inertial effects should be considered for the moments of pile head, only 100% peak kinematic effects should be considered for the moments of pile portions at the depths more than 10D (pile diameter) below grade and 30% to 100% peak inertial effects + 100% kinematic effects should be considered for the pile portions at the depths less than 10D below grade. A detailed collection regarding the combinations factors in the literature were presented in this study as well.

Literature survey regarding inertial and kinematic interaction show that people in marine civil engineering industry working as structural and geotechnical engineers have been getting close collaboration recently. Particularly, structural engineering community have recognized the importance of dynamic soil-structure interaction phenomenon and they have incorporated the kinematic effects, more or less, into their design stages in recent years. Also, the necessity of combination or the simultaneous evaluation of inertial and kinematic effects has been acknowledged recently even though there is still no consensus on the level of weighting factors in the literature.

The author opinion about this issue is that the attempts to find out the combination factors for the proper incorporation of kinematic and inertial effects can be good for our understanding of wharf seismic behavior, preliminary design purposes and the validation of finite element or finite difference simulations by test data. However, it cannot be the future aim for designing of wharf structures. This highly large (generally) and complex dynamic soil-structure interaction problem can incorporate many

uncertainties regarding soil conditions/stratification, the types of embankments, the dimensions of embankments, the dimensions/distribution of piles, ground motion etc. and cannot be generalized easily. Therefore, the models incorporating three dimensional soil behavior under three dimensional excitation will be the key solution for the reliable performance-based design of pile-supported wharf structures in near future.

3.2. Longitudinal Response and Linked Wharves

The seismic response of pile supported wharf systems having single module or multiple modules linked via shear keys each other have been scarcely investigated under longitudinal excitation. Most of the studies in which the longitudinal excitation is considered have disregarded the kinematic effects. Besides, only a few studies treating the seismic response of multi-segmented, pile-supported wharves exist in the literature. In this chapter, the studies dealing with the longitudinal response of pile-supported wharf systems and linked wharf systems are compiled and presented.

Weismair et. al. [38] stated that the longitudinal response of a wharf segment can be taken into account simply by increasing the calculated transverse response by 15% for the piles. Also, shear key forces were calculated but no details were given regarding calculation.

A procedure to estimate the longitudinal response of pile-supported wharves and shear key forces were proposed by Benzoni and Priestley [54]. This method idealized the piles of one wharf segment by super pile approach that four super piles placed at certain locations of the deck. Each super pile, which represented the piles and p-y springs placed at a quarter portion of each segment, was defined by a couple of spring representing the behavior in X and Y direction in deck plan. Analysis cost could be considerably reduced by idealizing 3D system as 2D model in plan as well as the eccentricity of a wharf segment due to asymmetrical geometry in longitudinal direction was taken into consideration by this approach. Note that this procedure took into account only inertial effects by time domain analysis.

One, two and three segmented (with or without corner segment) wharf systems were linked to each other via the shear keys, which was represented by two compression-only springs (in longitudinal direction) at both ends and one transverse spring at the middle of each segment [54]. Then, the multiple segmented wharves were analyzed and the response quantities in longitudinal direction were calculated. Also, so-called dynamic magnification factors (DMFs) were derived in order to obtain 3D response of the segmented wharf systems by just multiplying the transverse response quantities, which had been obtained by simple 2D transverse analysis. By this way, the design of piles located in any segment could be completed, without performing more complex 3D analysis, by just using DMFs for the multiple segmented wharves. The DMF value for intermediate segments were proposed 1.10 conservatively. Also, a simple formulation was proposed for the calculation of shear key force based on dimension, eccentricity, shear force at maximum displacement and a special coefficient derived from the numerical analyses [54].

Donahue et. al. [55] performed a three-dimensional structural analysis incorporating p-y springs in time domain for an existing wharf system to compare the results with measured response data recorded during Loma Prieta earthquake. Note that this study considered only inertial effects.

Blandon [44] covered many aspects regarding pile-supported wharf design. A set of parametric analysis for linked wharf system was implemented by using the method proposed by Benzoni and Priestley [54] by incorporating an extended parameter context. The effects of soil stiffness, hazard levels, number of wharf modules on wharf seismic response and shear key forces were investigated. One novel idea incorporated in addition to Benzoni and Priestley [51] was use of delta (three spring) and penta (five spring) shaped p-y spring options instead of commonly used two-spring option in orthogonal directions. Note that this study considered only inertial effects as well.

Varun and Assimaki [31] expressed the importance of 3D modeling and coupled transverse and longitudinal response of pile-supported wharves highlighting the com-

plexity of soil-pile interaction.

Thach and Yang [56] developed a formulation for displacement magnification factors (DMF) (in similar manner to Benzoni and Priestley [54]) performing inertial analyses for a set of wharf geometry having different soil conditions.

Jaradat et. al. [57] study covered a design application implemented for a project in Port of Long Beach (POLB), US. Super pile approach [54] and 2D non-linear time domain analysis was performed to calculate DMF values and shear key forces for the wharf segments as proposed in POLB Wharf Design Criteria (POLB-WDC) [58]. The length of berth, consisting of six wharf segments, was approximately 1300m. The important point of this paper was that different soil stratification for the wharf system were considered by taking varying characteristics of soil stiffness along the system in structural analysis and design process. Even though POLB-WDC procedure takes into account only inertial effects by super pile approach, it is a good attempt to observe realistic behavior of the wharf structure considering changing soil stratification. Other interesting point considered in this paper is that one of the ground motions, which was sourced by the fault located at the closest distance, was applied considering the real angle of exact fault location with respect to the wharf segments.

Doran et. al. [59] and Erdogan et. al. [60] dealt with the seismic performance assessment of existing piled wharf systems by three-dimensional structural models considering only inertial effects as per the Turkish Seismic Code for Marine, Railway and Airport Structures [61].

Karakas [62] investigated the effect of linked behavior of double-segmented wharves on three-dimensional seismic response considering only inertial interaction of soil and piles.

Another DMF formulation was derived to consider 3D response of a wharf segment from 2D transverse response by Gao et. al. [63] for single wharf module solutions.

The aforementioned studies up to this paragraph have considered only inertial effects on the seismic response of wharves by either pushover analysis or time domain analysis. Only two studies treated the seismic response of pile-supported wharves considering both kinematic and inertial effects by Shafieezadeh [34] and Shafieezadeh et. al. [64]. In the first paper, any considerable difference between two-dimensional and three-dimensional response of pile-supported wharves was not reported [34]. It was clearly depicted that the longitudinal response of wharves negligibly small when it was compared with the transverse response. However, it should not be forgotten that these analyses were performed for a very loose soil stratification, which had loose sand layer with 18m thickness approximately, was highly susceptible to large transverse deformation due to liquefaction. Furthermore, the ground motion imposed in longitudinal direction was generated artificially by using a very crude matching technique developed by Burden [65] since only free-field transverse response existed [35].

In the same study, one attempt to calculate three-dimensional linked system response including kinematic effects was made by using a simplified model [34]. However, it could not be completed due to the fact that this simplified model did not give reliable results [34]. Time domain analysis was abandoned and structural response was calculated by pushover analysis for the calculation of fragility curve generation.

Shafieezadeh et. al. [64] stated that the effect of longitudinal excitation on the seismic response of pile-supported wharves was very significant when impulsive near field earthquakes were considered whereas the longitudinal excitation almost had no effect on total response when far field earthquake records were employed. However, this conclusion was drawn by the results of two records only, one for far field, one for the near field. For this reason, generalization may not be correct. Moreover, there was no explanation regarding scaling of these ground motions. It was clearly understood from the response spectra of two records that the level of pseudo acceleration for near field record was notably greater than the ones of far field record in almost any frequency. Any other far field record having the similar intensity levels with the near field record employed in that study might cause significant longitudinal response. Conversely, any

other near field record having lower intensity level in the frequency range of interest might cause lower effect on the longitudinal response.

More importantly, again, the ground motion in longitudinal direction used in structural analysis were generated artificially by using a matching technique very crudely [65] due to the lack of free-field analysis in longitudinal direction [35]. Before this technique was applied, the downslope permanent deformation of embankment happened was eliminated [64]. The effect of these approximations on the characteristics of longitudinal ground response was not elucidated. Because of the fact that the seismic behavior of pile-supported wharf system mainly depends on embankment's behavior, neglecting actual longitudinal behavior of embankment may cause misguided response of wharf system. Undoubtedly, use of ground motion data obtained from free field analysis in longitudinal direction would have been much better to understand realistic response of wharves as well as to eliminate the suspicions in this regard.

In conclusion, Shafieezadeh [34] and Shafieezadeh et. al. [64] studies are important because these are the only studies in the literature not disregarding the existence of longitudinal direction and incorporating dynamic soil-structure interaction by an approximate substructure method. However, the approximations used in the method to calculate the longitudinal excitation being applied to the structural system didn't have neither a theoretical nor a logical basis.

Besides these papers, there are some papers expressing observations and clues regarding the importance of longitudinal response from past earthquakes, presented as follows.

Donahue et. al. [55] presented seismic motion data recorded during Loma Prieta earthquake at free field and at the wharf deck. According to this data, the longitudinal displacement response of wharf deck was larger than the transverse displacement response under low to moderate level (recorded PGAs were 0.22g and 0.28g for both orthogonal directions) ground motions. Secondly, observed torsional response, which

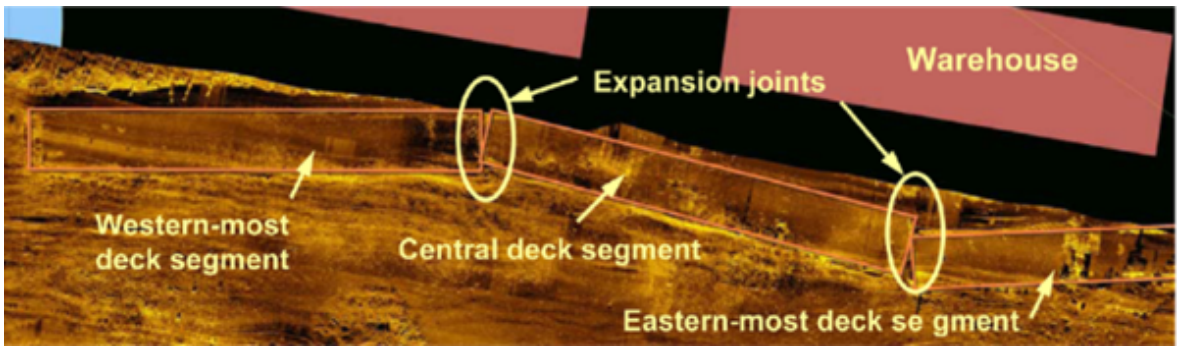

Figure 3.1. Sonar image of Port-au-Prince after Haiti Earthquake, 2010 (Werner et. al. [4])

even stated as in low level, was depicted clearly in time domain. Torsional response was attributed to slight in-coherent seismic action along the long wharf (493m). It was also stated that liquefaction occurred at one side of the long wharf. All in all, these findings give an idea about how 3D modeling can be important for the correct evaluation of wharf seismic response.

Yin et. al. [66] indicated the importance of longitudinal response of piled wharves emphasizing the damages observed at piled wharves during San Fernando Earthquake, 1971.

Werner et. al. [4] presented a sonar image, showing collapsed view of a three-segmented wharf system at Port-au-Prince, taken after Haiti, 2010 earthquake. Liquefaction-induced excessive soil deformation was stated as a reason of collapse. It is interesting to note that the final collapsed position at the image implies the presence of torsion. Although it is not easy to grasp the collapse phenomenon by just looking at one final image, it gives an idea regarding the significance of three-dimensional seismic behavior of wharves. The sonar image is given in Figure 2.1.

Smith-Pardo and Ospina [67] shared the observations regarding permanent damage, which indicated torsional behavior of the wharf segments possibly, happened at the wharf segments at San Vicente Terminal after Chile Earthquake 2010.

Common feature of the studies above is that both are performed by structural analysis incorporated interaction (p-y) springs. Most of these studies incorporating longitudinal direction response of a single or a linked wharf system have considered only inertial effects, disregarded soil deformations due to wave propagation and kinematic interaction. Only Shafieezadeh [34] and Shafieezadeh et. al. [64] studies calculated longitudinal response of the wharf system including kinematic effects by an approximate substructure analysis method. However, free-field embankment response in longitudinal direction was not calculated from site response analysis but it generated indirectly. Therefore, it is difficult to say that free-field embankment response, accordingly, wharf response, in longitudinal direction was attributed to the given soil/embankment conditions in these studies. Based on these approximations and insufficient data used in the analyses, the author is having the opinion that this field has not been enlightened clearly and still open to investigation.

3.3. Observations, Case Histories from Past Earthquakes and Tests

In this section, the observations from past earthquakes and the centrifuge tests carried out to validate case histories for pile-supported wharf systems are presented.

Hung and Werner [68] stated that the major damage source for marine structures was caused by liquefaction-induced soil deformations. They also stated that there was not much evidence in the literature that the marine structures had been seriously affected by the vibration-induced deformations.

Muraleetharan et. al. [8] stated that Berth 121-126 and Pier-300 at POLA had moderate damage during Northridge Earthquake, 1995. The embankments of mentioned berths had been formed by hydraulically placed dredging fill material, which was consisting of loose sands and soft clays. After the earthquake, cracks and settlement along the berth was observed and it was believed that the source of the wharf deformations was the liquefaction of the hydraulically placed dredged material. Similar observations regarding the reason of damage for Berth 121-126 at POLA were reported

by Buslov et. al. [69] as well.

After several major earthquakes occurred, Loma Prieta (1989), Northridge (1994) and Kobe (1995), it was observed that the wharf damages based on liquefaction-induced soil deformations were getting pivotal issue for wharf seismic design [9]. Particularly, because the backyards of wharves were formed by hydraulically placed dredging fill, which was highly susceptible to liquefaction, soil improvement strategies behind dikes were getting important. Dong-Shan Yang [9] calculated the optimum dimensions of required soil improvement parts behind the dikes to provide better seismic performance.

It is reported that extensive damage was observed in piled marine structures after Kocaeli earthquake particularly for the ones with batter piles. Boulanger et. al. [70] stated that liquefaction was the main source of extensive soil deformations.

McCullough emphasized [12] that pile-supported wharf analysis and design methods had never been examined due to lack of well-documented case histories and tests implemented. In this context, several centrifuge tests were conducted to contribute to this field. Detailed evaluation from past earthquake reconnaissance and case histories reports was presented. The common point of these reports was that damages occurred at pile-supported wharves had been sourced by permanent soil deformation during and/or after seismic excitation. The comparative results regarding centrifuge tests and case histories were evaluated and presented.

The results of centrifuge tests highlighted that the kinematic effects was more critical than inertial effects for the wharf systems having unstable rockfill/soil stratification [12]. Larger bending moments, as compared with pile-deck connections, were obtained for the parts of piles located at the interfaces of rockfill/soil layers and at the locations where the permanent soil deformation was occurred due to liquefaction. Therefore, the observations from past earthquakes regarding the seismic behavior of pile-supported wharves was validated by the centrifuge test results. The importance of kinematic effects for pile-supported wharf design was emphasized clearly [12].

The observations from past earthquakes and centrifuge tests have shown that extensive soil deformations due to liquefaction in marine environment are mainly responsible for damage.

3.4. Rockfill-Pile Interaction, Tests and Modeling

Rockfill modeling in pile-supported wharf analysis is very important due to its unique characteristic and the amount that can be used in construction. Rockfill is granular material but its mechanical behavior and interaction with piles is different from sand and gravel. It has a specific nature mainly because of individual material size. The size of individual rock element can reach up to the size of pile or even larger than that. Besides, the amount of rockfill used in construction plays determining role in the seismic behavior of pile-supported wharves. This section covers literature survey regarding rockfill behavior, rockfill-pile interaction and its modeling.

Diaz et. al. [71] is the first paper presenting the results of full-scale tests conducted at sloping rockfill during the project which was carried out for a new container terminal at POLA (Port of Los Angeles). McCullough and Dickenson [72] stated that Diaz et. al. [71] derived the correction factors from the tests to show the effect of rockfill in sloping ground. A substantial strength increase at shallower depth was found out. The reason of this increase was attributed to the particle size effect and/or interlocking of rockfill. This full-scale test clearly showed the behavior of rockfill at the topmost layer is totally different from the behavior of sand layers. It can be concluded that defining rockfill layer as if sand layer, by using equivalent strength parameters, in the analysis is not realistic way to define rockfill behavior. Note that the author of this thesis could not access Diaz et. al. [71] paper. He has shared the information covered by this paper via McCullough and Dickenson [72] paper.

McCullough [12] proposed pseudo-cohesion concept to consider the interlocking effect of rockfill in analysis models. The comparative results of centrifuge tests and numerical modeling showed that the use of 15 KPa pseudo-cohesion was the best es-

timate for rockfill and pile interaction modeling. It was also stated that an additional adjustment regarding the interface spring stiffness was required to model near-field interaction of pile and rockfill due to the sloping ground condition of embankment. The best estimate for the ratio of upslope and downslope stiffness for p-y springs represented sloping ground was stated as 10.

Dickenson and McCullough [14] mentioned, maybe for the first time, that discrete element modeling could be a better choice than continuum modeling technique for better representation of pile-rockfill interaction.

Blandon [44] presented the details of full-scale pile-rockfill interaction tests, which was a joint study conducted with other Phd project studied by Kawamata [73]. As a result of this study, the p-y springs predicted for rockfill-pile interaction was softer than the ones measured from the tests [44]. The difference in stiffness and strength properties between the measured responses and the predicted ones was again attributed to interlocking effect of the particles.

Kawamata et. al. [74] showed the difference of p-y curves specified in POLA code [75] and the ones measured from the full-scale tests. Even though upper bound strength of p-y curves seemed similar to measured ones, the initial stiffness of the measured ones was still much larger than the ones proposed in POLA code. Note that these tests were conducted by performing actuator at the deck level, thus, it can be thought that only inertial loading condition (static) was simulated in these tests.

The qualitative observations regarding interlocking mechanism and its components were presented by Kawamata [73]. In addition, the quantitative comparisons for p-y curves used in current practice in US and test results were given. Considerable resistance observed at ground level were in good agreement with Diaz et. al. [71] test results. It was clearly showed that the interlocking of rockfill had significant effect on rockfill-pile interaction. Discrete element modeling (DEM) was proposed for better representation of micro behavior of rockfill [73].

Arulmoli et. al. [45] presented the comparative results of p-y curves for pile-rockfill interaction used for the design of wharves in POLA and POLB with the results of full-scale tests conducted by Kawamata [73].

Dickenson et. al. [76] and Dickenson et. al. [47] used pseudo cohesion concept for rockfill modeling in 2D plane strain analyses to be employed for validation studies. Heidary-Torkamani et. al. [17] and Amirabadi et. al. [18] used pseudo cohesion concept for rockfill modeling in fragility estimation studies for piled wharves. Su et. al. [20], Su et. al. [21], Su et. al. [22], Su et. al. [23] and Su et. al. [24] used pseudo cohesion concept for rockfill modeling in two- and three-dimensional finite element analysis of pile-supported wharf systems.

Centrifuge and full-scale test results are shown that rockfill has additional strength with respect to sand due to the large size of individual particles, so-called interlocking effect of the particles. This effect has been considered in finite element models by adding pseudo-cohesion value of 10-20 kPa in addition to internal friction angle of 42°-45° in general engineering practice.

3.5. Code Procedures

In this chapter, the soil-structure interaction (SSI) analysis procedures given in two seismic design codes, namely, "Turkish Seismic Code for the Design of Marine Structures (TSCDMS-2020)" [77] and "Port of Long Beach Wharf Design Criteria (POLB-WDC-2021)" [58] used in Turkish and American practice will be explained. Although there are several other codes incorporating SSI methods, such as "ASCE 61-14 Seismic Design of Piers and Wharves" [78] used in American practice, those are not given herein on the grounds that they have more or less the same procedures with POLB-WDC-2021. It is intended to present two different SSI analysis trends given in seismic codes for the design of pile-supported wharves, as a supplementary element to the literature review.

3.5.1. Turkish Seismic Code for the Design of Marine Structures (TSCDMS-2020)

TSCDMS-2020 [77] is the second performance-based design code for the seismic analysis and design of marine structures published in Turkey. Unlike the predecessor [61], TSCDMS-2020 code encompasses approximate substructure analysis methods and direct analysis method for SSI analysis. Note that only SSI procedures are summarized herein. The order and/or the way of implementation of these procedures are based on the provisions related to the hazard levels, structure importance classes and performance objectives accordingly and out of the scope of this thesis.

In this code, two stage analysis is proposed for the design of marine structures generally. First stage analysis is carried out for preliminary design purpose and only inertial interaction is considered. The inertial interaction analysis, called KZE-A method, is performed within the context of first stage considering directly design acceleration spectrum since there is no foundation input motion calculated by kinematic interaction analysis.

In the second stage, three different approaches are proposed for SSI analysis depending on the provisions regarding different hazard levels and structure importance class. The first method that can be used in the second stage analysis is called KZE-B method. As per KZE-B method, the free-field site response analyses for the wharf embankment are performed for seven earthquake records and the seismic displacement profile for piles is calculated by taking the average of peak displacements at the pile nodes obtained from each free-field analysis. The site specific acceleration spectrum, which is to be employed in inertial interaction analysis later, is also obtained from the free-field analyses. Then, the calculated seismic displacement profile is imposed to the pile nodes by pushover analysis via the p-y springs attached to the nodes, as the kinematic interaction analysis of KZE-B method. The internal forces and displacements of structural elements are stored. The site specific acceleration spectrum is used for the second pushover analysis considering the deck and pile masses and the internal forces

and displacements are obtained for the inertial interaction as well. Then, the internal forces and displacements obtained from the kinematic interaction and inertial interaction analyses are combined as per the given combinations below and the unfavourable results for each element are used as design response quantities.

- 100% kinematic interaction + 50% inertial interaction
- 50% kinematic interaction + 100% inertial interaction

Other SSI analysis procedure used in the second stage is called KZE-C method. In this method, the displacement responses calculated at the pile node locations from seven earthquake records are not idealized as seismic displacement profile. Instead, these displacements, at each time step, are directly imposed to the pile nodes via the p-y springs attached the nodes in time domain analysis. Then, the structural element responses to be used in design are calculated as directly by taking the average of seven earthquakes.

As an alternative to KZE-C substructure method mentioned above, a direct analysis method is also proposed in TSCDMS-2020. According to this method, non-linear soil elements are defined in three-dimensional finite element or finite difference models, non-linear pile elements are defined as one-dimensional elements with interface elements in the same model. Absorbing boundaries at sides are defined and the boundary conditions at bottom are defined as absorbing or fixed boundaries depending on the soil and rock conditions of the problem considered. Time domain analyses are performed for seven earthquake records and the average response quantities are obtained for the design.

3.5.2. Port of Long Beach Wharf Design Criteria (POLB-WDC-2021)

In American practice, the SSI concept for pile-supported wharf structures are treated by two loading conditions, namely, inertial loading and kinematic loading. Inertial loading represents the effect of vibration due to the masses of wharf system

during ground shaking in accordance with the generic definition of inertial interaction. However, the kinematic loading part of SSI analysis is treated as result of the specific phenomenon that the piles of wharf system is subjected to the liquefaction-induced soil deformation of embankment during or end of ground shaking. Thus, it can be considered as a special case of kinematic interaction concept.

As per POLB-WDC-2021 [58], inertial loading is implemented to structural model by pushover analysis employing the design spectrum for specified three hazard levels, namely, OLE, CLE and DE. Then, the requirement of kinematic loading analysis is examined by several analysis techniques.

It begins with the determination of factor of safety by pseudo-static slope stability analysis. Wharf embankment model without piles are analyzed under the horizontal seismic force considering one half of PGA used in project. If the calculated factor of safety is equal or greater than 1.10, kinematic loading analysis is not required [58]. If it is less than 1.10, it is proceeded with Newmark sliding block displacements.

Newmark sliding displacement curves given in "Port-Wide Ground Motion Study Update, Port of Long Beach" [79] document are used for the first estimates of equivalent sliding block displacements of free-field embankment model for three hazard levels. If the estimated rigid block displacements are less than the given displacement levels in POLB-WDC-2021, kinematic loading analysis is not required. If those are greater than the displacement limits, it is proceeded with Newmark sliding block analysis.

Newmark sliding block analyses are performed under site-specific "within motions" calculated at the base level of rigid blocks by site response analyses for three different hazard levels. If the calculated rigid block displacements are less than the given displacement levels in POLB-WDC-2021, kinematic loading analysis is not required. If those are greater than the displacement limits, it is proceeded with Newmark sliding block analysis considering "pile-pinning" effects.

The geotechnical engineer shares the information regarding the geometry of soil layers and the p-y spring data above or below the weak (sliding) layer with the displacement demands of embankment. The structural engineer establishes a structural analysis model incorporating these p-y springs for single pile and performs a pushover analysis to find the displacement capacities and the pile shear forces at the level of weak soil layer conforming to the limiting strains of cross-section materials for three hazard levels. The calculated pile shears are incorporated as so-called "pile-pinning effects" in pseudo-static slope stability/Newmark sliding block analysis as an additional strength and the reduced pile displacement demands are calculated. If the displacement capacities obtained from pushover analyses are greater than the displacement demands calculated by Newmark analysis, no further kinematic loading evaluation is required. If it is not, a detailed numerical analysis is proposed by POLB-WDC-2021 [58].

According to POLB-WDC-2021 [58], it is expected that inertial loading causes the plastic hinges at the pile deck intersections whereas kinematic loading causes in-ground plastic hinges separately. Thus, no need for further evaluation regarding the coupled behavior of two loading conditions for typical container wharves. It is also stated that it should be evaluated for other types of wharves in project-basis manner [58].

3.6. General Evaluation and Research Objectives

The literature review carried out above can be concluded as follows:

(i) The effect of longitudinal excitation on the seismic response of pile-supported wharf system has never been investigated by direct SSI analysis. There are only a few attempts trying to incorporate longitudinal excitation by substructure methods, but those are based on very crude approximations.

(ii) The seismic response of multi-segmented wharf systems has never been investigated by models incorporating kinematic soil-structure interaction effects.

(iii) Past earthquakes has shown that liquefaction-induced lateral spreading and soil deformation is the main source of damage for pile-supported wharves. For this reason, incorporation of SSI in analysis models, particularly for the situations having loose/soft soil conditions, is inevitable for realistic structural analysis and design.

Based on the findings from literature review, the research objectives of this dissertation are determined as follows:

(i) To understand the effect of longitudinal excitation considering soil liquefaction on the seismic behavior of pile-supported wharf systems. Although soil liquefaction and wharf response have been investigated by many researchers, all studies in the literature, to the best of the author's knowledge, were treated by plane-strain models or three-dimensional models considering only transverse and/or vertical excitation. For this reason, it is important to consider the existence of multiple excitation for both soil and structural response.

(ii) To understand the seismic behavior of multi-segmented wharves. It is important because the current design procedures dealing with the real-life wharf problems

are all based on the solution of single module system and/or two-dimensional plane-strain solutions by considering constant soil stratification. However, wharves are generally very long systems and most likely constructed on changing soil stratigraphy along longitudinal direction. Some crude methods, which are neglecting soil behavior, and some other applications in the literature are not sufficient to understand the realistic behavior of the wharf systems.

(iii) To show the applicability of performance-based seismic evaluation of large-scale soil-structure interaction problems by employing one of the most sophisticated and advanced commercial software currently available.

4. MODELING OF WHARF SYSTEM

In line with the research objectives specified in the previous chapter, a set of analysis cases for a realistic engineering problem, which are given in Chapter-6 and Chapter-7, are investigated by performing soil-structure interaction models. In this chapter, the modeling details of these analysis cases are presented.

4.1. Essentials of Dynamic Modeling

The engineering problem addressed in Chapter-6 and Chapter-7 is defined through soil-structure interaction models. This modeling technique essentially treats the problem as a wave-propagation phenomenon occurring through soil and structural media. The wave propagation phenomenon specifically for the soil-structure interaction problem can be described as follows:

The seismic stress waves, applied to the model boundary at the bottom, propagate through soil layers, reflecting and transmitting at the interfaces of soil layers due to the differences in soil impedances. *The transmitted waves* reach the structure and surface, with some propagating through the structure and reflecting back from its top, while others directly reflect from the soil-structure boundary or surface. These reflected outgoing waves scatter and *damp out* through the soil layers. As the waves, differing from those in the free-field, reach the *free-field (viscous) boundaries* on the side, this difference is absorbed. The remaining waves are eventually absorbed by the *quiet (viscous) boundaries* at the bottom.

The features of the aspects written in *italic* form in the preceding paragraph will be explained in subsequent sections.

4.1.1. Boundary Conditions

Ideally, a very large model with static boundaries can be developed to minimize the artificial wave reflection problem by allowing the dissipation of the waves reflected from the structure via damping [80]. However, performing an analysis of such a large model is not feasible due to its computational cost. The use of viscous boundaries along the sides and the bottom of model helps reduce its size by absorbing outgoing waves, thereby decreasing the runtime of the analysis.

Unlike the rigid or elastic boundaries used in static analysis, dynamic boundary conditions are employed in the dynamic analysis of soil medium. The outer environment of the dynamic analysis model, called far-field, is represented by dynamic boundary conditions defined along the sides and the bottom of the near-field soil zone (Figure 4.1). It is assumed that far-field, which has the same properties as the soil medium at the boundary of the near-field grids, extends infinitely at the bottom and two directions along the sides. Thus, interaction of dynamic analysis model with the surrounding environment is defined.

In FLAC3D, the viscous boundaries developed by Lysmer and Kuhlemeyer [81] are used [80] as quiet and free-field boundaries (Figure 4.1). These boundaries are simply a couple of dashpots defined at the bottom and side boundary joints, which are oriented parallel and perpendicular to the considered plane to absorb outgoing waves (Figure 4.1). However, the absorption at the boundaries may be limited in certain situations. The efficiency of absorption at the boundaries depends on the incidence angle of outgoing waves. If the incidence angle is greater than 30 degree, the absorption at the boundaries is sufficient. If the incidence angle of outgoing waves is less than 30 degree, the energy absorption is limited [80]. For this reason, it might be beneficial to use larger models to enhance the efficiency of viscous boundaries. On the other hand, creating larger models increases runtime undesirably. Thus, it is necessary to optimize the model size through trial and error, considering the accuracy of the results.

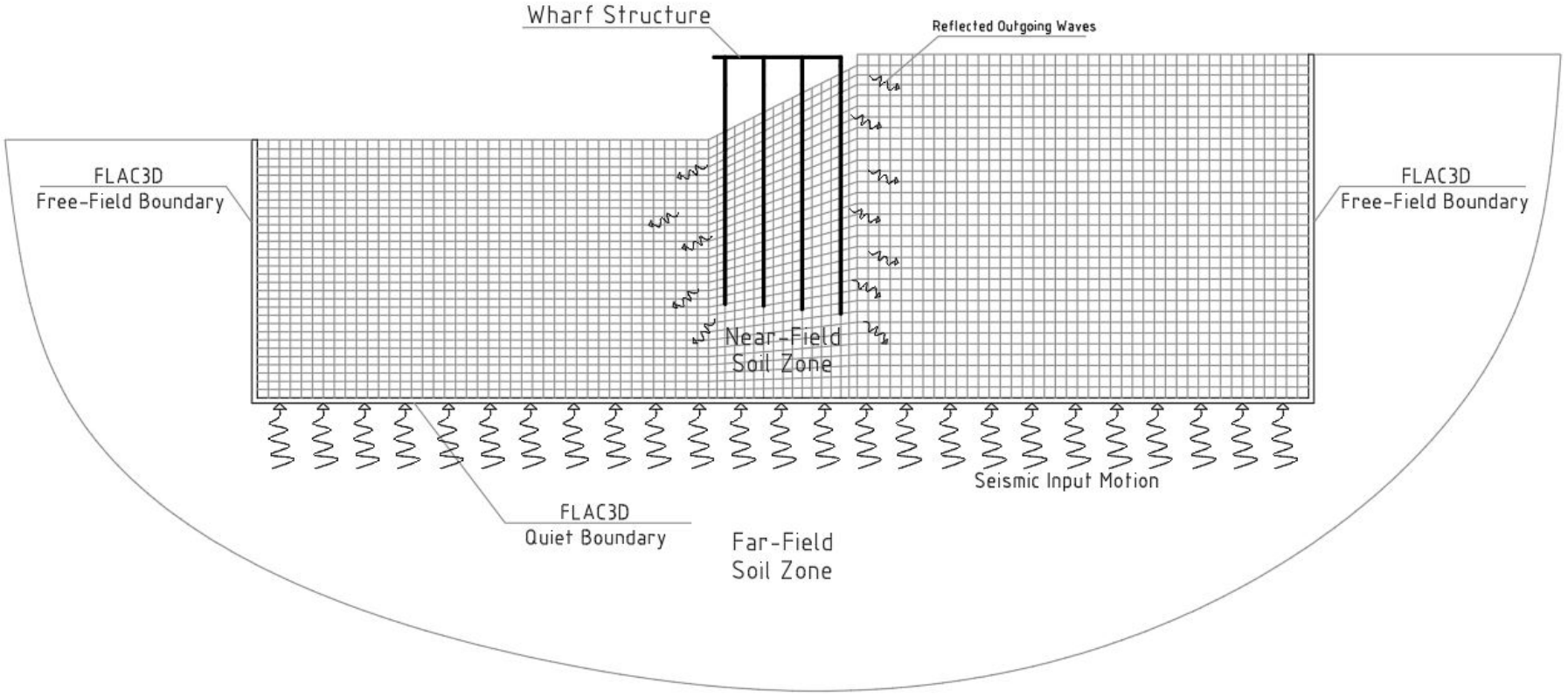

Figure 4.1. Soil-Structure Interaction Model.

4.1.1.1. Quiet Boundaries. The traction vectors, calculated at each time step, at the quiet boundaries for both normal and shear directions, are defined in Equation (4.1) and Equation (4.2).

$$t_n = -\rho C_p v_n \tag{4.1}$$

$$t_s = -\rho C_s v_s \tag{4.2}$$

Where, ρ is mass density, C_p is p-wave velocity of medium, v_n is input particle velocity in normal direction, C_s is s-wave velocity of medium, v_s is input particle velocity in shear direction. The definitions of C_p and C_s are given in Equation (4.3) and Equation (4.4), respectively.

$$C_p = \sqrt{\frac{K + 4G/3}{\rho}} \tag{4.3}$$

$$C_s = \sqrt{\frac{G}{\rho}} \tag{4.4}$$

4.1.1.2. Free-Field Boundaries. As mentioned, the far-field properties are identical to those of the adjacent near-field grids of the model. It implies that the free-field site response of each soil column at the sides of the model is identical to that of corresponding grids at the near-field. In this condition, if the model did not include any structure and its surface was flat, there would be no interaction between the far-field and the near-field grids, as the response of the near-field grids would be identical to that of far-field. However, the radiating waves from the structure located on the model alter the response of near-field grids. These waves must propagate away from the structure and eventually fade out, as they would in reality. Thus, these must be absorbed by the free-field boundaries in the model. In this regard, FLAC3D runs a simultaneous parallel analysis of the main soil-structure interaction model and the free-field model and, the difference in response between the near-field grids and the

far-field is absorbed by the free-field boundaries at sides. This phenomenon is defined by the following Equations (4.5), (4.6) and (4.7). Note that the forces (F_x, F_y, F_z) at the near-field grids near sides and those (F_x^{ff}, F_y^{ff}, F_z^{ff}) at the free-field are equal to each other when the net velocities are zero at the interface of free-field and near-field grids.

$$F_x = -\rho C_p(v_x^m - v_x^{ff})A + F_x^{ff} \tag{4.5}$$

$$F_y = -\rho C_s(v_y^m - v_y^{ff})A + F_y^{ff} \tag{4.6}$$

$$F_z = -\rho C_s(v_z^m - v_z^{ff})A + F_z^{ff} \tag{4.7}$$

Where, v_x^m, v_y^m and v_z^m are the particle velocities of nodes in near-field grids near the side boundaries, in X, Y and Z directions, respectively. v_x^{ff}, v_y^{ff} and v_z^{ff} are the particle velocities of nodes in free-field, in X, Y and Z directions, respectively. F_x^{ff}, F_y^{ff} and F_z^{ff} are the free-field forces at the nodes in X, Y and Z directions, respectively. F_x, F_y and F_z are the forces at the nodes of near-field grids in X, Y and Z directions, respectively.

4.1.2. Application of Seismic Motion

The seismic ground motions, obtained from the deconvolution analysis presented in Section 5.3, are applied to the analysis model in three directions as stress wave histories via the quiet boundaries at the bottom. The stress wave histories are converted from the ground velocity histories and are multiplied by 2 (Equations (4.8) and (4.9)). This adjustment accounts for the fact that half of the motion is directly absorbed by the quiet boundaries, allowing the remaining half to propagate through the soil medium [80].

$$\sigma_n = -2\rho C_p v_n \tag{4.8}$$

$$\sigma_s = -2\rho C_s v_s \tag{4.9}$$

Where, σ_n is applied stress in normal direction, σ_s is applied stress in shear direction.

4.1.3. Wave Transmission and Maximum Grid Size

Wave transmission through a soil medium depends on the wave propagation velocity of the soil layers, the frequency content of ground motion and the discretization of the soil medium. Considering the shear wave velocity (182m/s) of the least stiff soil layer (Table 6.4) and the highest frequency (9Hz) of the ground motion (Section 5.2) the upper bound of element size is calculated as 2.02m. Therefore, the maximum grid size used in the analyses is selected as 2m. The formulation for calculating the maximum element size as one-tenth of the wavelength to ensure correct wave transmission [80] is given as follows Equation (4.10):

$$10h \leqslant \frac{V_{s-min}}{f_{max}} \tag{4.10}$$

Note that the other important criterion in selecting the upper limit of soil element size is ensuring the accurate interaction between soil and pile elements, achieved by linking at appropriate intervals. The adopted upper limit in this study is considered appropriate given the large analysis models.

4.1.4. Damping

Energy absorption in dynamic systems can be treated in two parts. The first part, called damping, involves various mechanisms typically occurring at a micro-level, such as internal friction within material [80]. Approaches used to account for damping in dynamic analysis are based on mathematical assumptions rather than reflecting physical realities.

The second source of energy absorption is related to the inelastic strain energy of dynamic systems. As a matter of fact, for systems prone to large-strain behavior under seismic excitation, a significant portion of the absorbed energy occurs through

this mechanism. Thus, damping does not significantly affect the seismic response of such systems. It is typically used to absorb the high frequency oscillations [80].

Rayleigh damping, based on the combination of mass and stiffness proportional damping, is common in practice. In FLAC3D, Rayleigh damping procedure is characterized by a central frequency (f_{min}) and a damping ratio (ξ_{min}) corresponding to that frequency. f_{min} and ξ_{min} are assumed as 1Hz and 0.15%, respectively, for the soil media in this study.

In explicit analysis, stiffness-proportional damping leads to considerable decrease in time-step for media generating high frequency vibrations, thereby resulting in significant increase in runtime [80]. Therefore, the use of Rayleigh damping for the structural elements is not recommended. In fact, the response of the structural systems in this study are mainly governed by low frequency excitations and the most of the energy will be absorbed by the plastic hinges. Consequently, damping is not defined for the structural elements in this study.

4.1.5. Time-step and Run-time

Managing time-step size in a soil-structure interaction analysis is crucial for improving the runtime performance of analysis. For a feasible runtime performance, specifically for large-scale analysis models, optimizing certain aspects is essential. The main factors affecting time-step size in FLAC3D include:

- Stiffness property of medium or element,
- Element size,
- Frequency content of motion,
- Rotational mass definition of structural elements,
- Damping procedure.

As a matter of fact, aspects such as small element size and/or rigid medium or element, high frequency content of ground motion or the phenomena generating oscillations rich high frequency content necessitate reducing the time-step size. This ensures that the effects are accurately captured through the element nodes without causing numerical instability. Equation (4.11) gives the calculation of critical time-step used in FLAC3D [80].

$$\Delta t_{crit} = min(\frac{V}{C_p A^f_{max}}) \tag{4.11}$$

Where, V is the tetrahedral subzone volume, A^f_{max} is the face area associated with the tetrahedral subzone. Then, a factor of safety is used, since the calculated time-step is based on an estimation, to calculate the time-step size, Δt_d, used in the analysis given in Equation (4.12) [80].

$$\Delta t_d = \frac{\Delta t_{crit}}{2} \tag{4.12}$$

4.1.5.1. Time-step for Stiffness Proportional Damping. When stiffness proportional damping is employed, Equation (4.13) is used to calculate the critical time-step to maintain numerical stability [80].

$$\Delta t_\beta = (\frac{2}{\omega_{max}})(\sqrt{1+\lambda^2} - \lambda) \tag{4.13}$$

Where, Δt_β is the critical time-step in case of stiffness proportional damping is used, ω_{max} is the highest frequency of the system, λ is the fraction of critical damping at this frequency. Equation (4.14), Equation (4.15) and Equation (4.16) give ω_{max}, λ and β, respectively [80].

$$\omega_{max} = (\frac{2}{\Delta t_d}) \tag{4.14}$$

$$\lambda = (\frac{0.4\beta}{\Delta t_d}) \tag{4.15}$$

$$\beta = \frac{\xi_{min}}{\omega_{min}} \tag{4.16}$$

Where, ξ_{min} is the damping ratio specified in Rayleigh damping, ω_{min} is the central (angular) frequency specified in Rayleigh damping.

4.1.5.2. Effect of Rotational Mass Definition on Time-step Size. In FLAC3D, users can choose between fully dynamic mode and partially dynamic mode for defining the rotational mass of structural elements. Fully dynamic mode includes both translational and rotational masses. In this study, partially dynamic mode option is chosen due to its advantage regarding time-step size. In partially dynamic mode, the stable time-step is calculated considering only translational masses. Then, angular vibration frequencies are bounded for the selected time-step size. Consequently, rotational masses that do not create higher vibration frequencies than the bounded frequencies are included in the mass matrix of structural elements. In other words, rotational masses that produces higher frequency vibrations compared to translational masses are disregarded, allowing for the selection of a larger time-step size.

Note that the calculated time-step size by FLAC3D for the analyses in this study is $9.74x10^{-5}$ seconds. The corresponding runtime for the largest dynamic analysis (8-Module System) is approximately 41 hours on a HP Z4 Workstation with Intel Xeon Gold 5218R 2.10GHz processor, which has 20 physical cores and 27.5MB of L3 cache size.

4.2. Modeling of Geotechnical System

In this section, details regarding the modeling of geotechnical components, namely, embankment, soil and rockfill layers are presented.

4.2.1. Embankment Dimensions

The dimensions of embankment used in this study is given in Figure 4.2. The length of embankment is different for each analysis case, as given in Table 6.5.

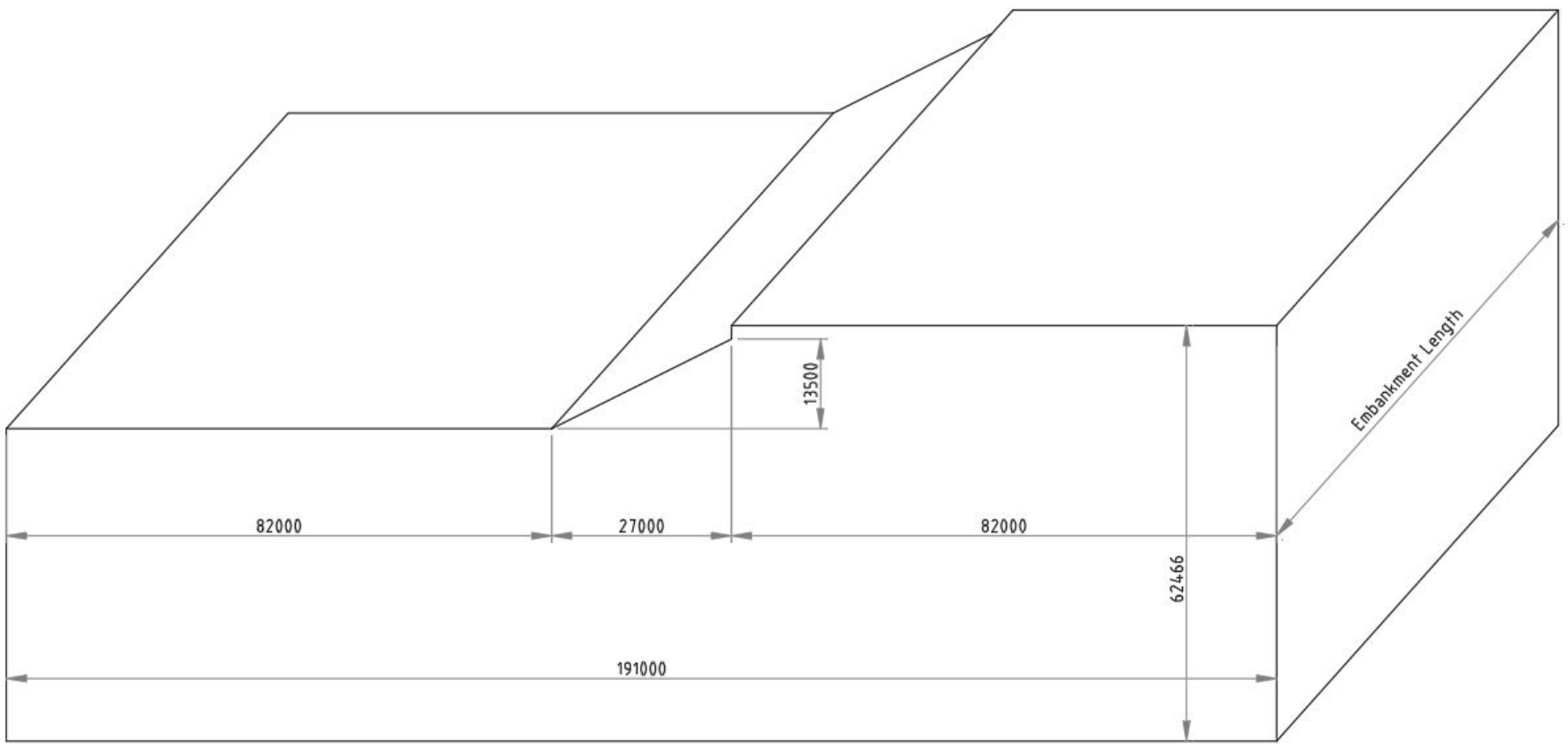

Figure 4.2. Embankment Dimensions.

Due to the embankment geometry and pile locations, it is not possible to create elements of the same size given in Section 4.1.3. Therefore, the element sizes are selected between 1.5-2.0m based on the geometric criteria in the model. The element sizes in X and Z directions for all elements are shown in Figure 4.3. The size of the all elements is determined as 1.75m in the Y direction in line with the pile spacing in the same direction.

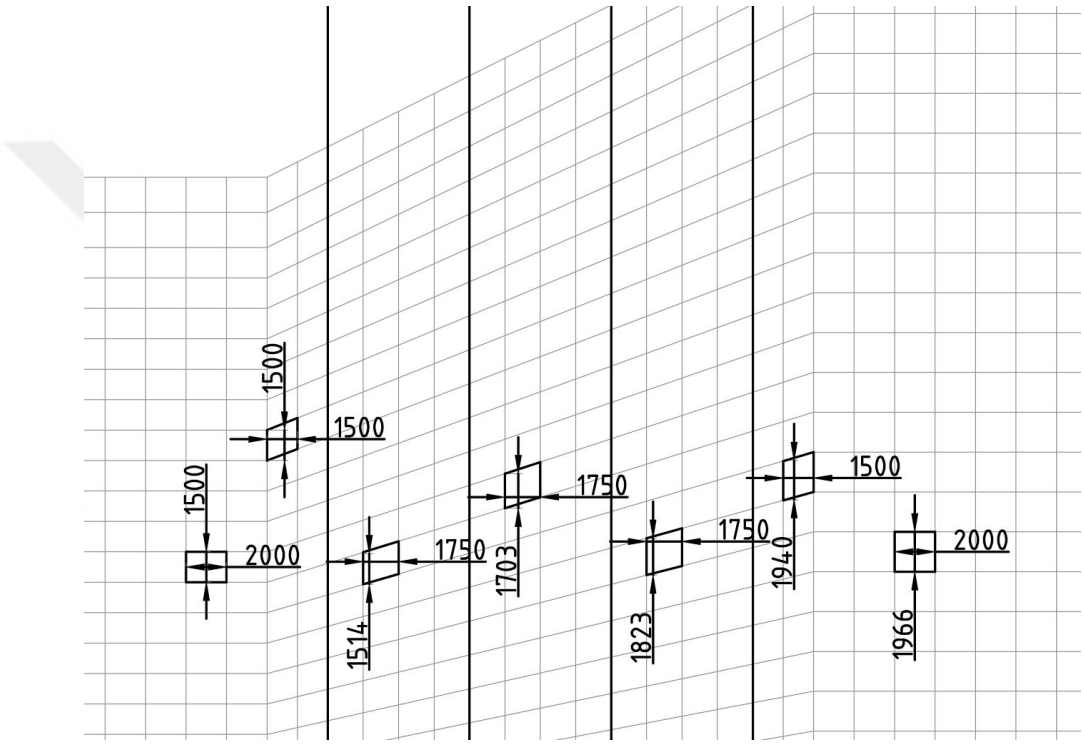

Figure 4.3. Soil Element Sizes Used in Analysis (X-Z Plane).

4.2.2. Modeling of Rockfill and Soil Layers

The soil and rockfill layers, whose stratification and properties are defined in Section 6.2, defined by Mohr-Coulomb constitutive model (except MDS layer) during seismic analysis case. Note that masses of rockfill and soil medium are automatically assigned to the corresponding grid nodes.

4.2.3. Modeling of Liquefiable Soil Layers

Liquefaction is a phenomenon that must be considered when analyzing wharf structures due to typically loose and fully-saturated conditions in marine environment. In this study, P2PSand model [82], a practice-oriented two-surface plasticity sand model available in FLAC3D, is used to simulate liquefaction.

P2PSand constitutive model, a modified extension of Dafalias and Manzari (2004) model [83], has been developed to model liquefaction by simply reducing the input parameters to only a relative density parameter (D_r) or $(N_1)_{60}$ value Equation (4.17). This model can be used in three-dimensional geotechnical engineering problems.

$$D_r = \sqrt{\frac{(N_1)_{60}}{46}} \tag{4.17}$$

In liquefaction analysis, it is assumed that seawater is trapped inside MDS layers (undrained condition), leading to an increase in pore pressure with changes in the volumetric strain of sand medium. The formulation regarding this phenomenon is given in Equation (4.18) [80].

$$\Delta_p = -K_w \Delta\varepsilon_v \tag{4.18}$$

Where, K_w is the water bulk modulus, which is assumed as 2.10^6 kN/m^2 in this study, $\Delta\varepsilon_v$ is the change in volumetric strain of an element. P2PSand constitutive model calculates the stress-strain relationships of soil elements, accounting for stiffness and strength reductions due to changes in effective stresses caused by the increase in pore pressure. Thus, the effect of liquefaction is incorporated in the analysis, resulting in potentially excessive soil deformations.

4.3. Modeling of Structural System

In this section, details regarding the modeling of structural components are presented.

4.3.1. Modeling of Piles

In this study, the 1-D Euler-Bernoulli beam element is used to model pile elements [80]. Details regarding the dimensional and material properties of these pile elements are presented in Section 6.3. The inelastic behavior of the pile elements is modeled by plastic beam hinges. Figure 4.4 illustrates the components of the pile element and the corresponding elastic and inelastic modeling conditions. The properties and assumptions regarding pile interface elements are presented in Section 4.4.1, 4.4.2 and 4.4.3.

The pile element used in this study consists of an RC plug section, a composite section and a steel section. Reinforced concrete properties are used to define the plug section since the pile is connected to the pile cap via dowel bars that extend through the pile plug, while the steel pipe is not fixed to the pile cap. In fact, plastic deformation is expected at the pile-deck interface, thus, the ideal plasticity model would be the zero-length plastic hinge element (non-linear rotation springs in FLAC3D terms). However, non-linear rotation springs can be defined as uncoupled in two ortohogonal directions. Therefore, classical beam plastic hinge elements, which exhibit elastic-perfectly plastic hysteretic behavior, are adopted to model the inelastic behavior at the pile-deck interface. The same plasticity model is used for the steel pipe section as well. No plasticity model is defined for composite section since inelastic behavior is not expected for it. The plastic moment capacities for the RC plug and steel pile hinges are calculated in Section 6.3.

The hydrodynamic water mass (added mass) around the composite and steel pile sections and the trapped water mass inside the steel pile above the seabed level is

defined by lumping the masses to the corresponding pile nodes. Equation (4.19) is used to define the hydrodynamic water mass.

$$m_A = \rho_w \pi r^2 \tag{4.19}$$

Where, ρ is water density, r is the radius of pipe section.

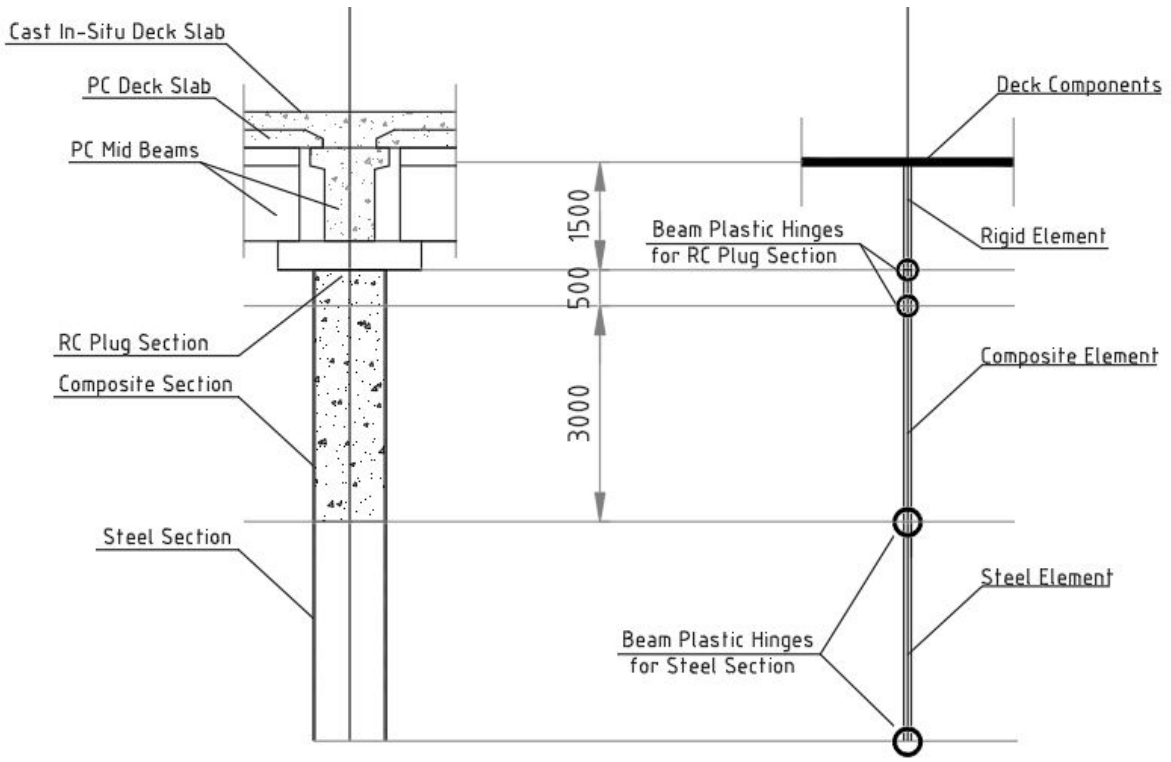

Figure 4.4. Modeling of Piles.

4.3.2. Modeling of Deck Beams

The 1-D Euler-Bernoulli beam element is used to model deck beam elements [80]. Details regarding the dimensional and material properties of these beam elements are presented in Section 6.3. Plasticity models are not assigned to the beam elements because these elements are assumed to be capacity-protected members in marine structural engineering practice.

4.3.3. Modeling of Deck Slabs

The shell-type structural elements are used to model deck slab elements [80]. Details regarding the dimensional and material properties of these elements are presented in Section 6.3. Plasticity models are not assigned to the deck slab elements because these elements are assumed to be capacity-protected members in marine structural engineering practice. The masses related to superimposed dead loads and live loads are lumped at the corresponding deck nodes.

4.3.4. Modeling of Deck Shear Keys

Three linear rigid springs are defined between the modules at the shear key locations to represent linked behavior of wharf modules in the transverse direction.

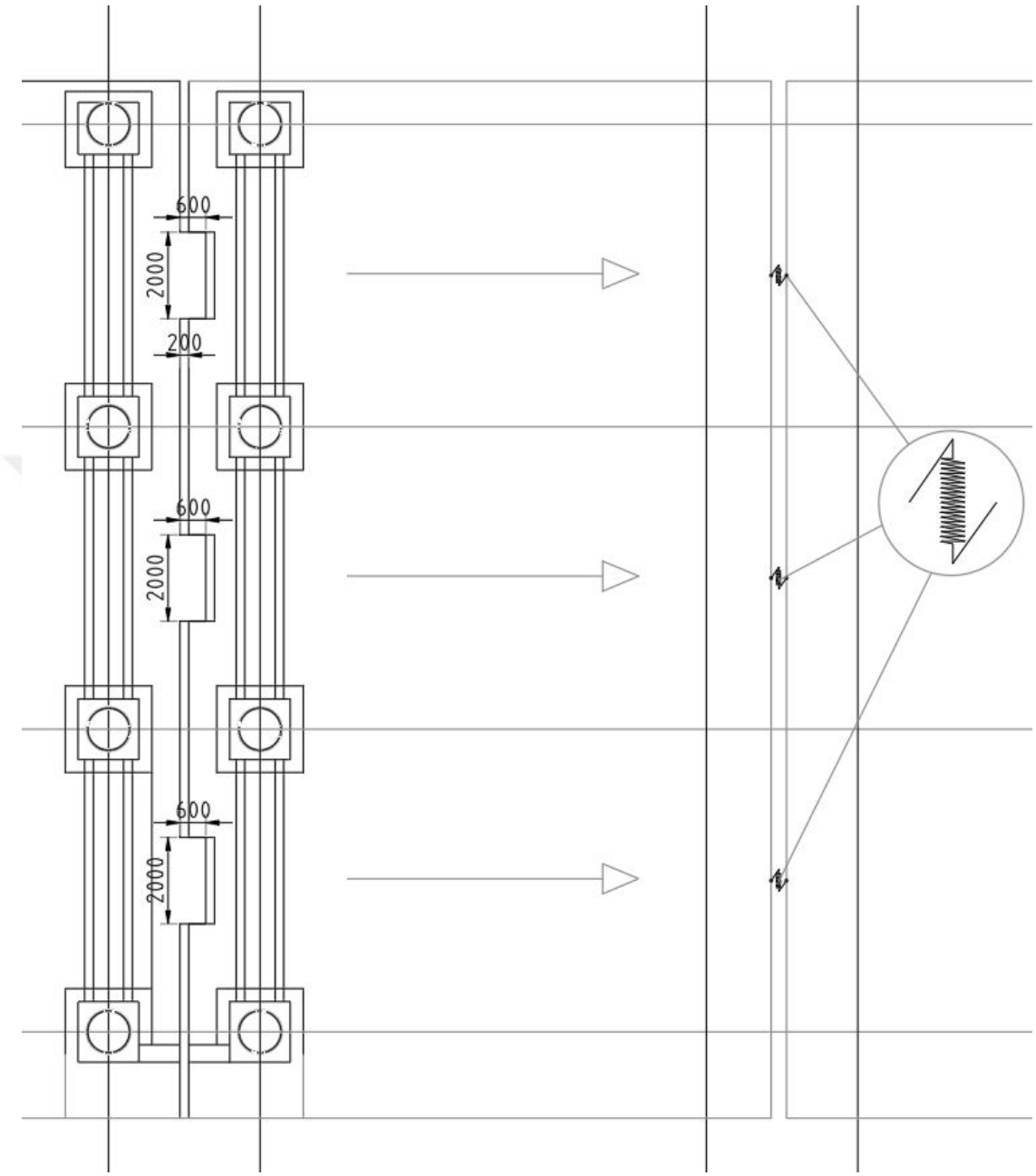

Figure 4.5. Modeling of Shear Keys.

4.3.5. Modeling of Retaining Wall

The liner-type structural elements are used to model the retaining wall elements. Details regarding the dimensional and material properties of these elements are presented in Section 6.3. The friction angle at wall-rockfill interface is assumed as 38°.

4.4. Modeling of Interface Elements

4.4.1. Vertical Interface Elements

Vertical interface elements are used to represent the friction and slip mechanism between the pile-soil interface. Zero-length 1-D spring elements are automatically defined between the nodes of soil elements and the nodes of pile elements. These elements have an elastic-perfectly plastic force-displacement relationship, as illustrated in Figure 4.6 (a).

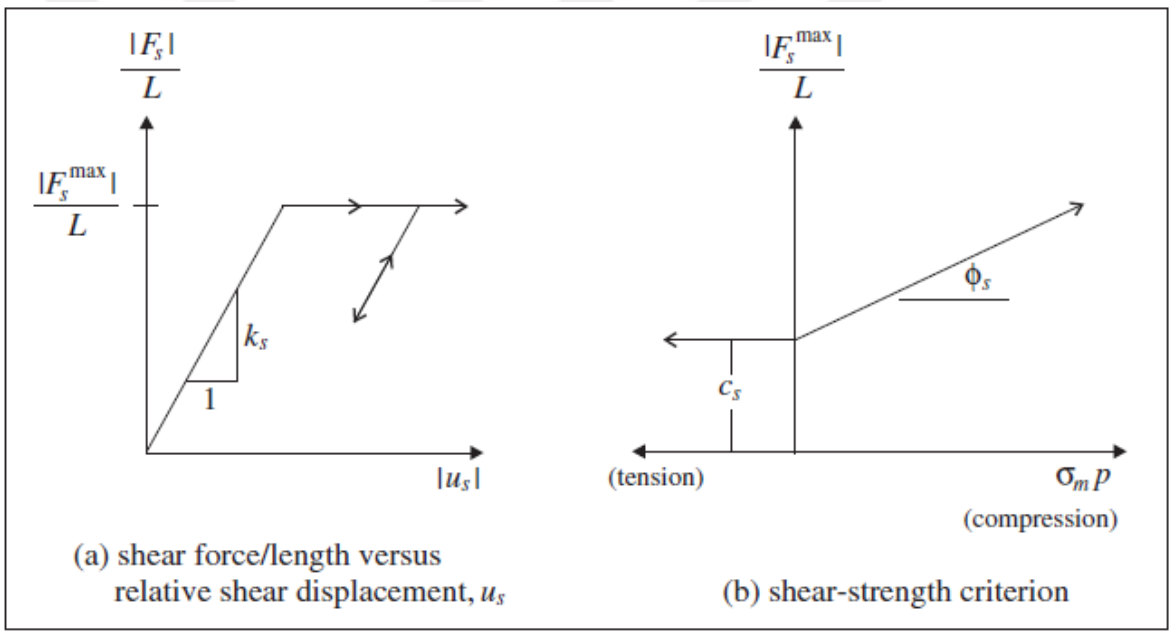

Figure 4.6. Vertical interface element properties in FLAC3D (FLAC3D Manual [80]).

Figure 4.6 (b) shows the shear strength definition based on Mohr-Coulomb failure criterion with strength properties c_s and ϕ_s for the vertical interface elements. ϕ_s is defined as the friction angle at pile-soil interface. It is taken as 0.67 times the internal friction angle (ϕ) for non-cohesive soils in contact with steel piles [84]. c_s is the adhesion factor, defined as the ratio of the adhesion at the pile-soil interface to the undrained shear strength of the adjacent soil layer. In this study, a value of 1.0 is adopted for cohesive soils, considering the properties of soil stratification [84]. Note that the friction between rockfill and pile is neglected. The details regarding rockfill and pile interaction will be given in "Loading Stages" Section. Since there is no friction defined between

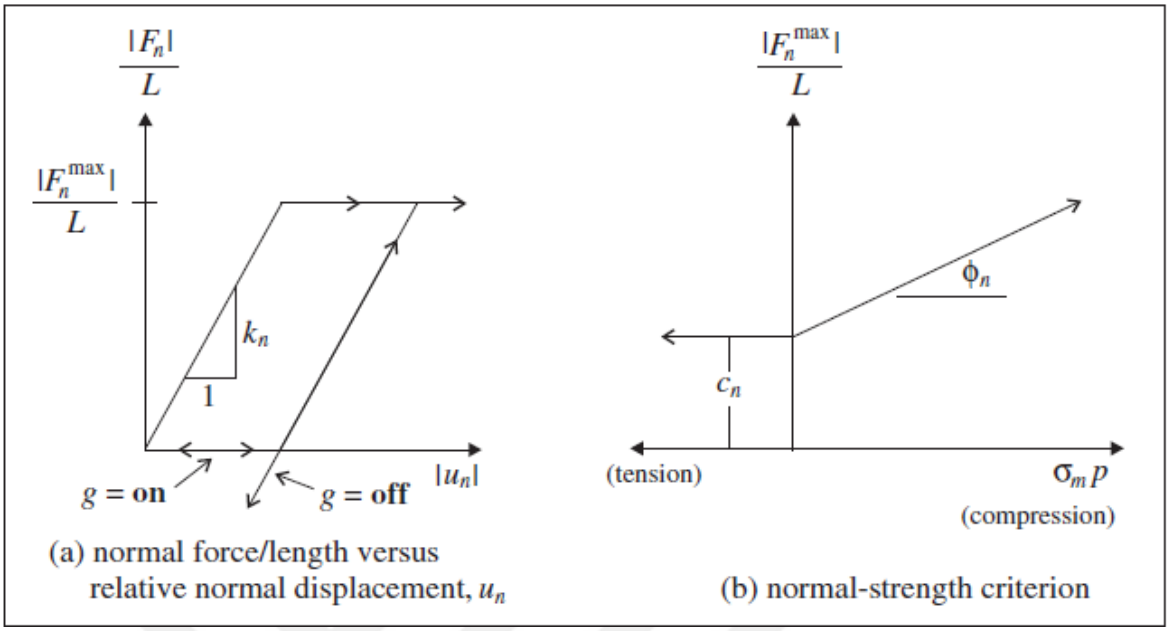

Figure 4.7. Lateral interface element properties in FLAC3D (FLAC3D Manual [80]).

rockfill and pile, there will not be force transmission due to vertical excitation through this interface.

Note that c_s and ϕ_s parameters are assigned to the soil layers considering drained and undrained conditions for static and seismic cases, respectively.

4.4.2. Lateral Interface Elements

The lateral interface element used in FLAC3D represents the load transfer between the pile and soil in the direction normal to the pile. It is a zero-length 1-D spring element with an elastic-perfectly plastic force-displacement relationship. The strength of lateral interface element is determined by the shear strength properties, c_n and ϕ_n, at the pile-soil interface. The gap property, which represents relative movement between pile and soil at pile-soil interface, can be assigned to the element according to the adopted soil behavior in the analysis. Details regarding the properties of the lateral interface element is given in Figure 4.7.

As seen in Figure 4.7b, the compression strength is associated with both c_n and ϕ_n, while the tensile strength is only related to c_n. It implies that the tension-free interface springs are defined in the normal direction for non-cohesive soils, whereas only cohesive soils exhibit tensile strength at the pile-soil interface.

The stiffness of the lateral interface springs is assumed as infinitely rigid (10^6 kN/m^2) for both cohesive and non-cohesive soil layers. Thus, it is ensured that the force at the pile node is directly transmitted to the adjacent zone element node (representing soil), or vice versa, if the contact force is in compression. If the contact force is in tension, there will not be any interaction between pile and soil for non-cohesive layers. However, for cohesive soils, if the contact force is in tension, the interface spring will resist with the same stiffness until the force reaches c_n level.

The shear strength properties are taken in different manner for different soil types. The ϕ_n is taken considerably larger than the internal friction angle of adjacent soil layer for non-cohesive soils both in drained and undrained conditions. By doing this, it is assumed that the shear strength in compression at the pile-soil interface is significantly greater than the shear strength of adjacent soil layer. This ensures that non-linear deformation occurs primarily within the zone element rather than at the interface spring. If non-linear deformation occurs initially at the pile-soil interface before the yielding of surrounding zone element, the force transfer between the pile and soil will be constrained by the strength level of the interface element.

Note that c_n and ϕ_n parameters are assigned considering drained and undrained conditions for static and seismic cases respectively.

4.4.3. Modeling of Pile Tip Bearing

The load transfer from pile to soil at the tip of pile is defined by a tension-free 1D structural link element. It is assumed that driving of each pile ends when the tip of pile reaches the very dense sand (VDS) layer (Figure 6.2) and soil plug naturally

forms. In this regard, the compression force at the tip of pile is transferred to the soil below using the area calculated by the outer diameter of pile instead of steel pipe cross section area. The stiffness of the link element is assumed to be 10^6 kN/m^2 with infinite strength in the compression and zero strength in the tension.

4.5. Large Displacement Theory

Large displacement theory (or large strain analysis, as termed in FLAC3D) is applied in all analyses performed in this study unless otherwise stated. Large displacement theory is based on the assumption that the coordinates of element nodes are adjusted after each analysis step, or at intervals, to account for the deformations occured during the analysis.

4.6. Loading

4.6.1. Static Loads

Static loading conditions are summarized in this chapter. The live load levels specified below is taken in accordance with the realistic operational requirements that would likely prevail during an earthquake with a large magnitude.

- Dead Load: The self-weight of all elements considered automatically by FLAC3D.
- Superimposed Dead Load: The weight of covering material on deck, 2.5 kN/m^2.
- Live Load on Deck: The operational load on deck, 2.5 kN/m^2.
- Live Load on New Backyard: The operational load on the new backyard, 5.0 kN/m^2.
- Live Load on Existing Backyard: The operational load on the existing backyard, 50.0 kN/m^2.

The static loads given above are applied to the system prior to conducting dynamic analysis of wharf system.

4.6.2. Loading Stages

The loading stages of wharf systems considered in this study are divided into two parts, namely, static and seismic loading stages. Static loading stages cover the analysis of the embankment and the wharf system under static loading condition. Seismic loading stage includes the seismic analysis of the wharf system.

4.6.2.1. Static Embankment Analysis. In local (Turkish) practice, steel piles are driven through natural soil layers while the backyard filling operation continues. Subsequently, rock armour and filter layers are carefully placed between the piles. Unlike natural soil layers, which have completed their consolidation over a long period, significant settlement is expected for rockfill layer for some time after its placement. Therefore, vertical bearing of piles through rockfill will not occur. Instead, negative skin friction between the fill and the piles expected, leading to down-drag forces acting on the piles. The strength of vertical interaction springs used for rockfill and pile interface is taken zero to exclude the vertical bearing of piles through rockfill layers. However, the anticipated down-drag forces on the piles are not considered in the analyses. It is thought that the effect of down-drag forces on the seismic response of the systems is minimal.

The static analysis of embankment includes its own weight and the live load acting on the backyard.

4.6.2.2. Static Wharf System Analysis. In the second stage analysis, the wharf system including structural components is analyzed under static loads.

4.6.2.3. Seismic Analysis. After completing the static analyses, seismic analysis begins. The stress wave histories (Section 4.1.2) calculated by the deconvolution analysis in Section 5.3 are applied through the quiet boundaries of the models.

5. SEISMIC GROUND MOTION

5.1. Ground Motion Selection

The effect of ground motion variability falls outside the scope of this study. Only one ground motion record set with three components is used for the analyses: "1999 Kocaeli Earthquake - Yarimca Record" is classified as no-pulse near-field record according to FEMA P-695 [85]. Ground conditions of the record well match with the soil profile of the proposed wharf model and the recording station in close proximity to the potential wharf systems to be located in the Marmara Region, Turkey.

The acceleration, velocity and displacement time histories of ground motions are given in Figures 5.1, 5.2 and 5.3 for three components, respectively. The response spectra of ground motions are given in Figure 5.4. The properties of earthquake and the ground motion records, which are retrieved from PEER Ground Motion Database NGA-West-2 [86], are itemized as follows:

- Event Name: Kocaeli Earthquake
- Station Name: Yarimca
- Magnitude (Mw): 7.4
- Fault Mechanism: Strike-slip
- Vs30: 297m/s
- PGA(YPT060): 0.23g
- PGA(YPT150): 0.32g
- PGA(YPT-UP): 0.24g
- Time Step: 0.005s
- Number of Data Points: 7000

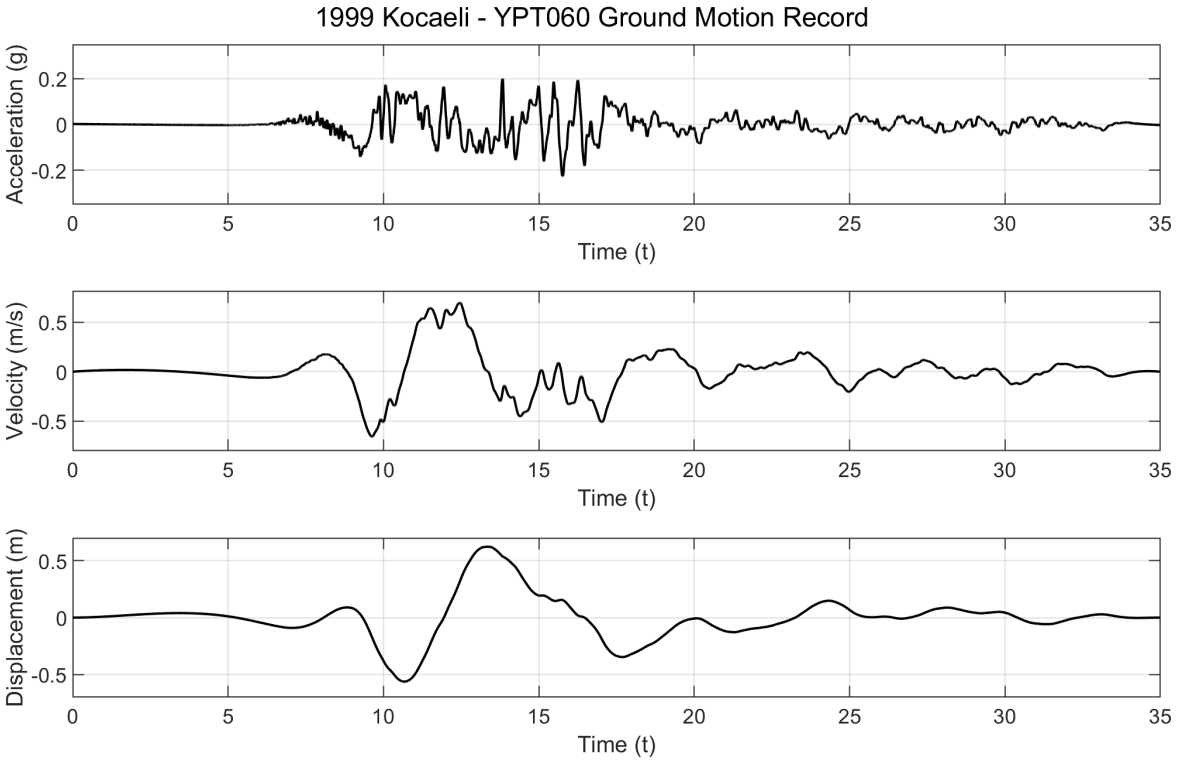

Figure 5.1. 1999 Kocaeli Earthquake, Yarimca Record (YPT060).

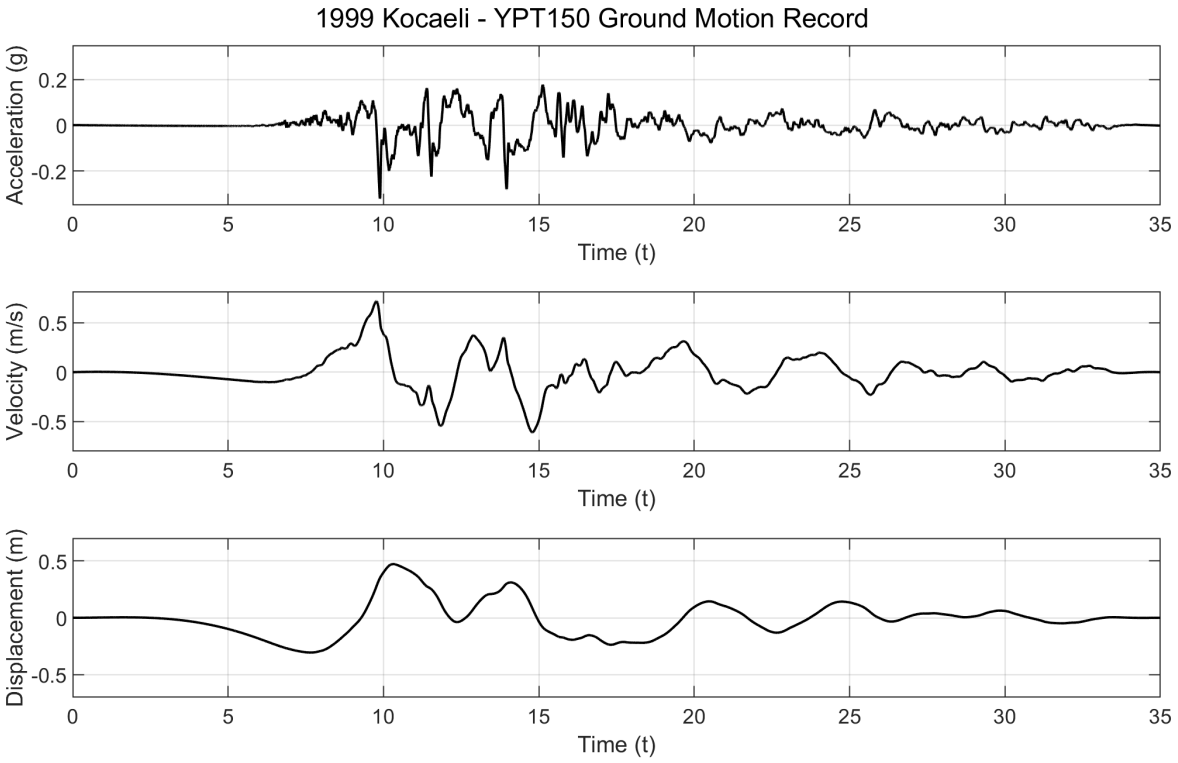

Figure 5.2. 1999 Kocaeli Earthquake, Yarimca Record (YPT150).

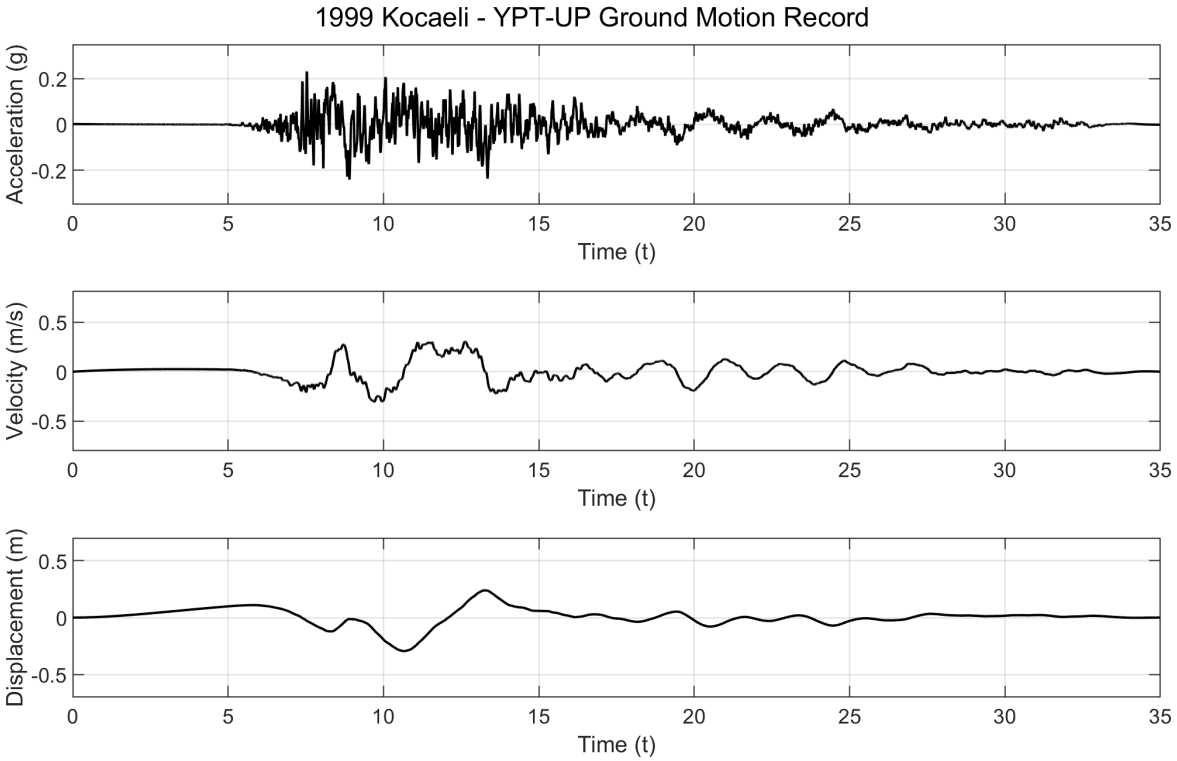

Figure 5.3. 1999 Kocaeli Earthquake, Yarimca Record (YPT-UP).

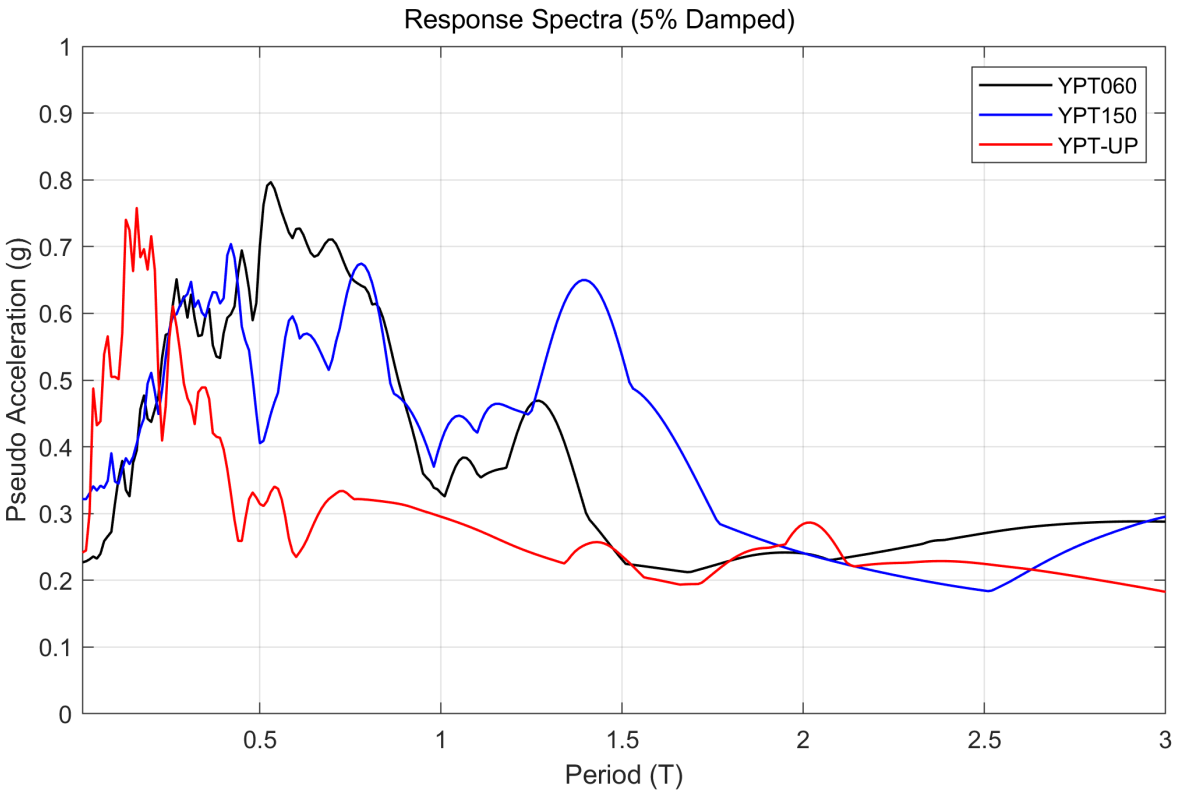

Figure 5.4. Response Spectra of Yarimca Records.

5.2. Filtering

As it is mentioned in Chapter 4, the selection of element size for an analysis model is directly related to the frequency content of the ground motion. The allowable highest frequency consistent with the allowable maximum size of element was determined as 9Hz. In this respect, the ground motion records are filtered using a low-pass filter with a corner frequency of 9Hz. The raw and filtered ground motion data for three components are presented in Figures 5.5, 5.6 and 5.7 respectively. The Fourier amplitude spectra for raw and filtered ground motions are given in Figures 5.8, 5.9 and 5.10, respectively. It appears that the change in the filtered data is insignificant for horizontal components whereas it is significant for the vertical component. The Arias intensity plots for ground motion components are illustrated in Figures 5.11, 5.12 and 5.13 respectively. The energy loss is around 2-3% for the horizontal components whereas it is approximately 15% for the vertical component since the vertical motion is considerably rich in high frequency content. Assuming that vertical motion has a limited impact on seismic response, the energy loss level for the vertical component is deemed acceptable.

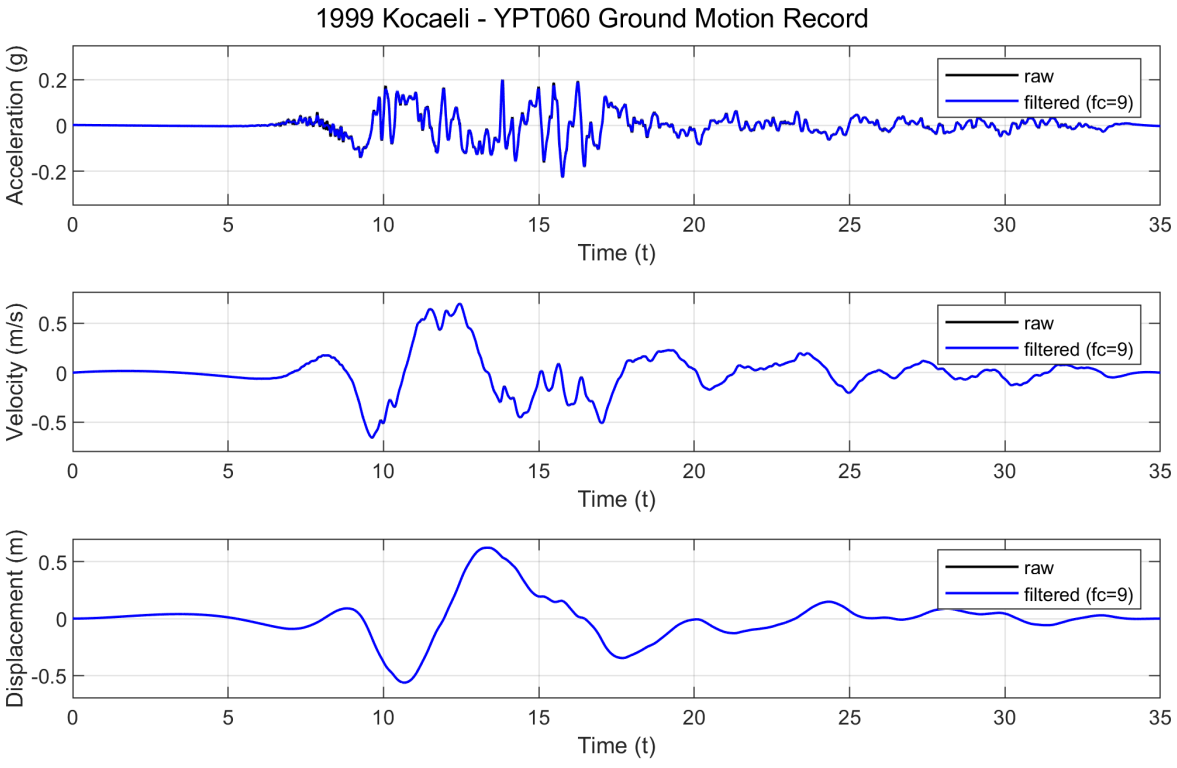

Figure 5.5. 1999 Kocaeli Earthquake, Filtered Yarimca Record (YPT060).

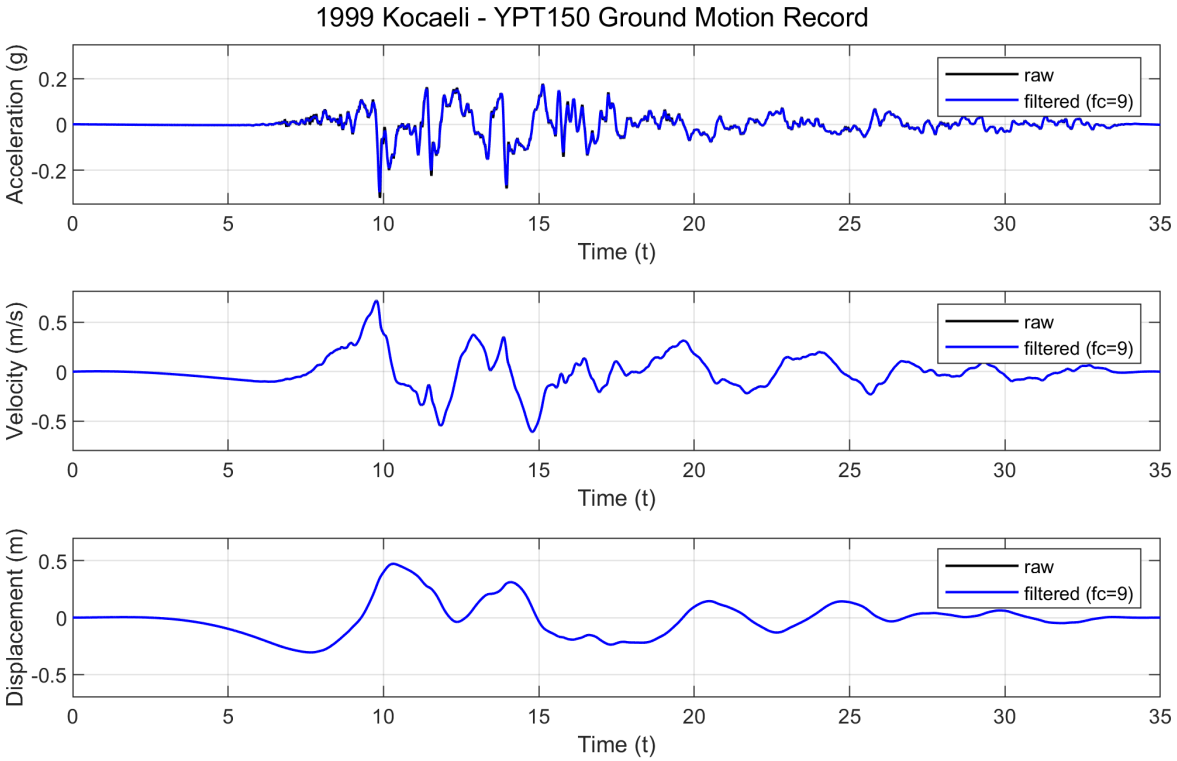

Figure 5.6. 1999 Kocaeli Earthquake, Filtered Yarimca Record (YPT150).

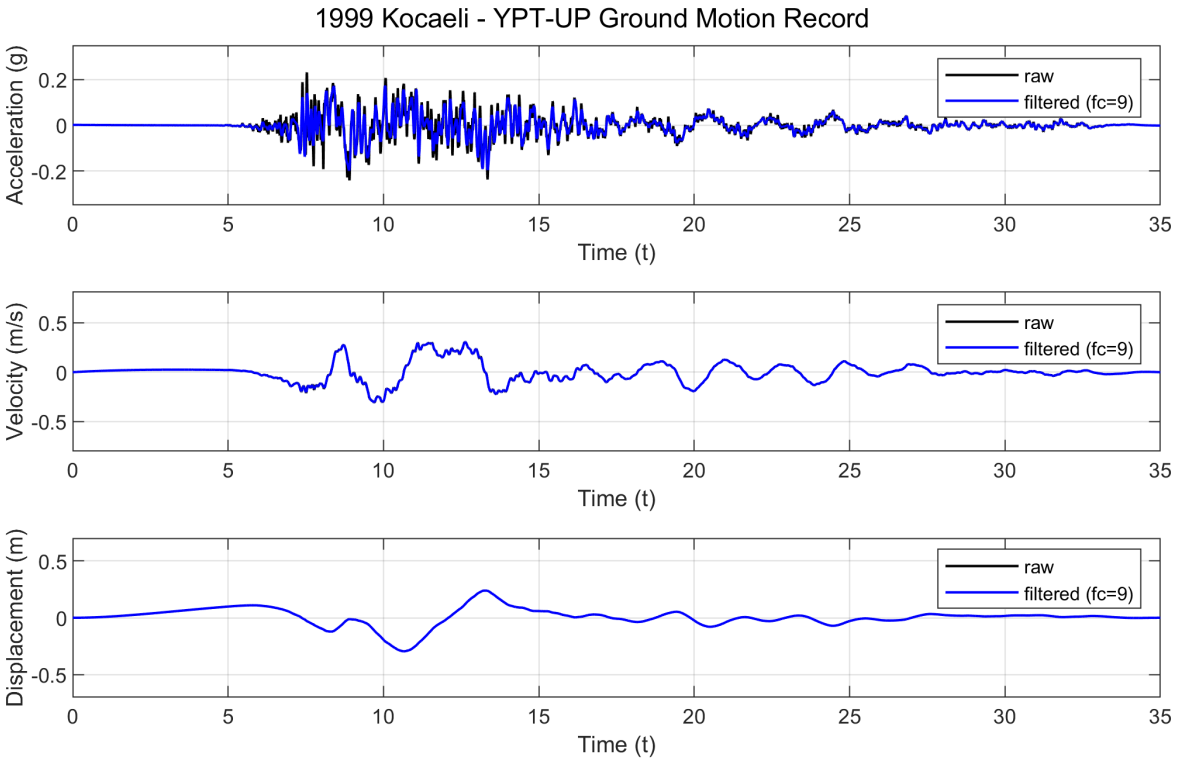

Figure 5.7. 1999 Kocaeli Earthquake, Filtered Yarimca Record (YPT-UP).

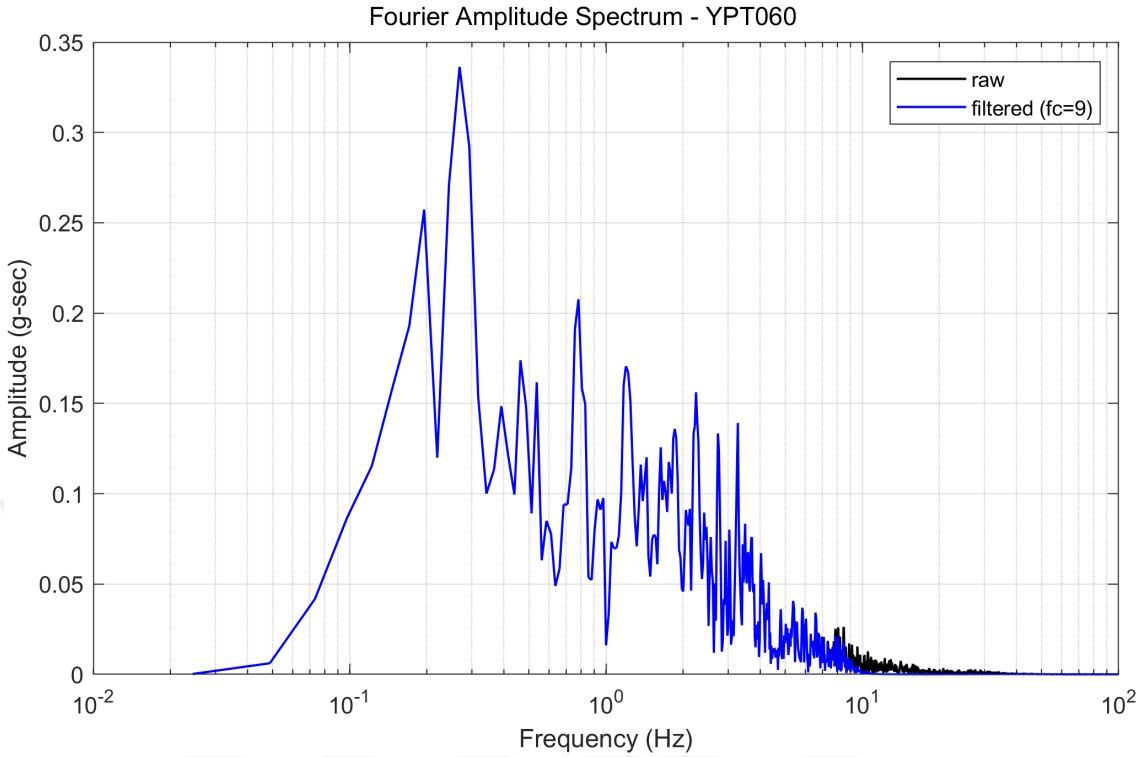

Figure 5.8. Yarimca Record (YPT060) Fourier Amplitude Spectra.

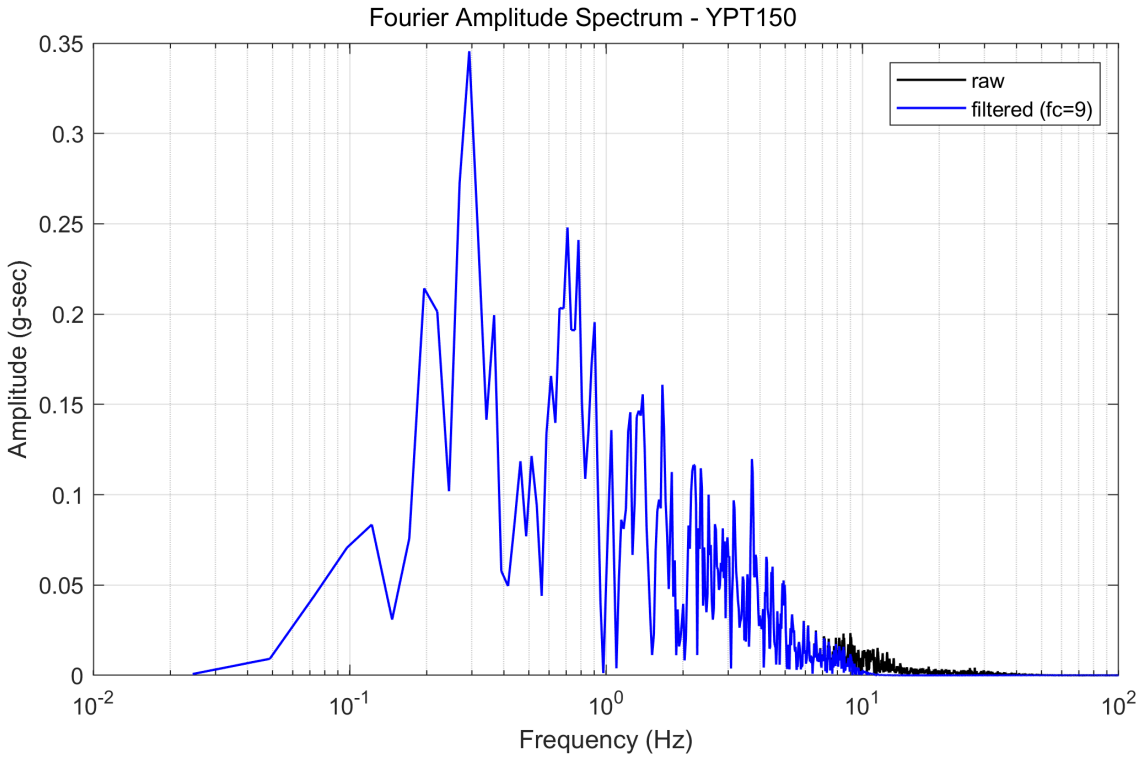

Figure 5.9. Yarimca Record (YPT150) Fourier Amplitude Spectra.

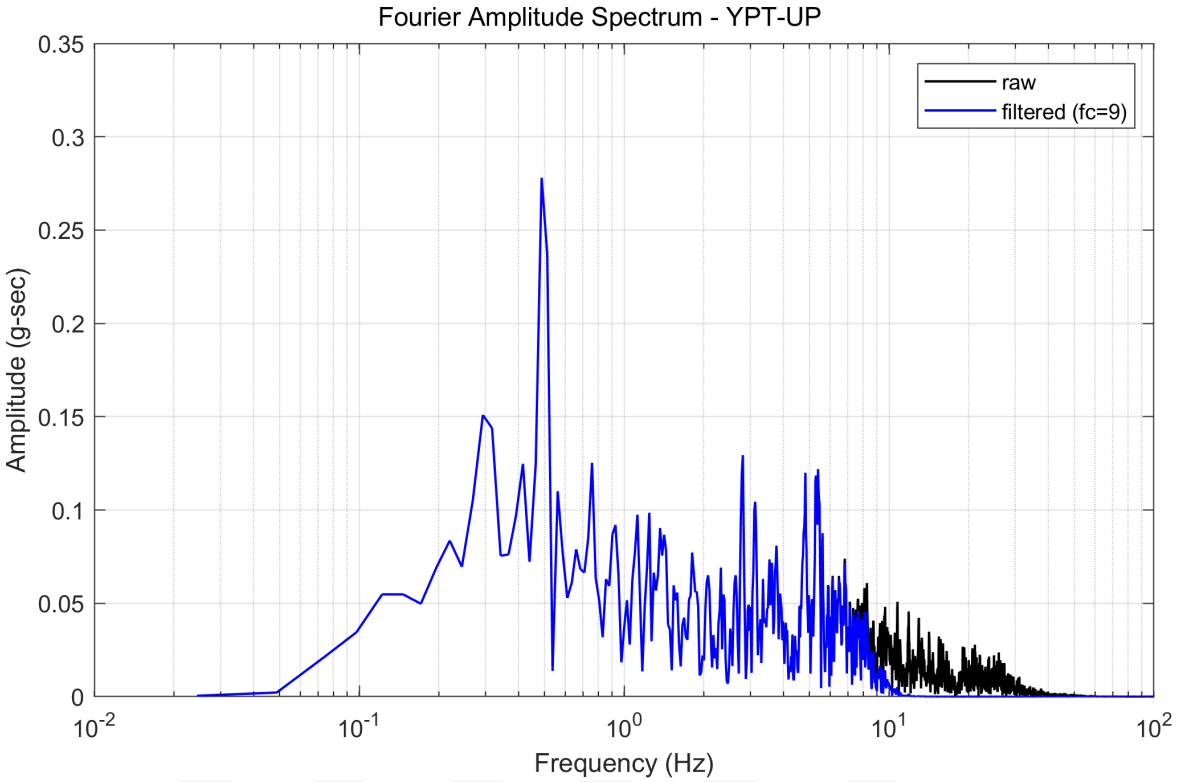

Figure 5.10. Yarimca Record (YPT-UP) Fourier Amplitude Spectra.

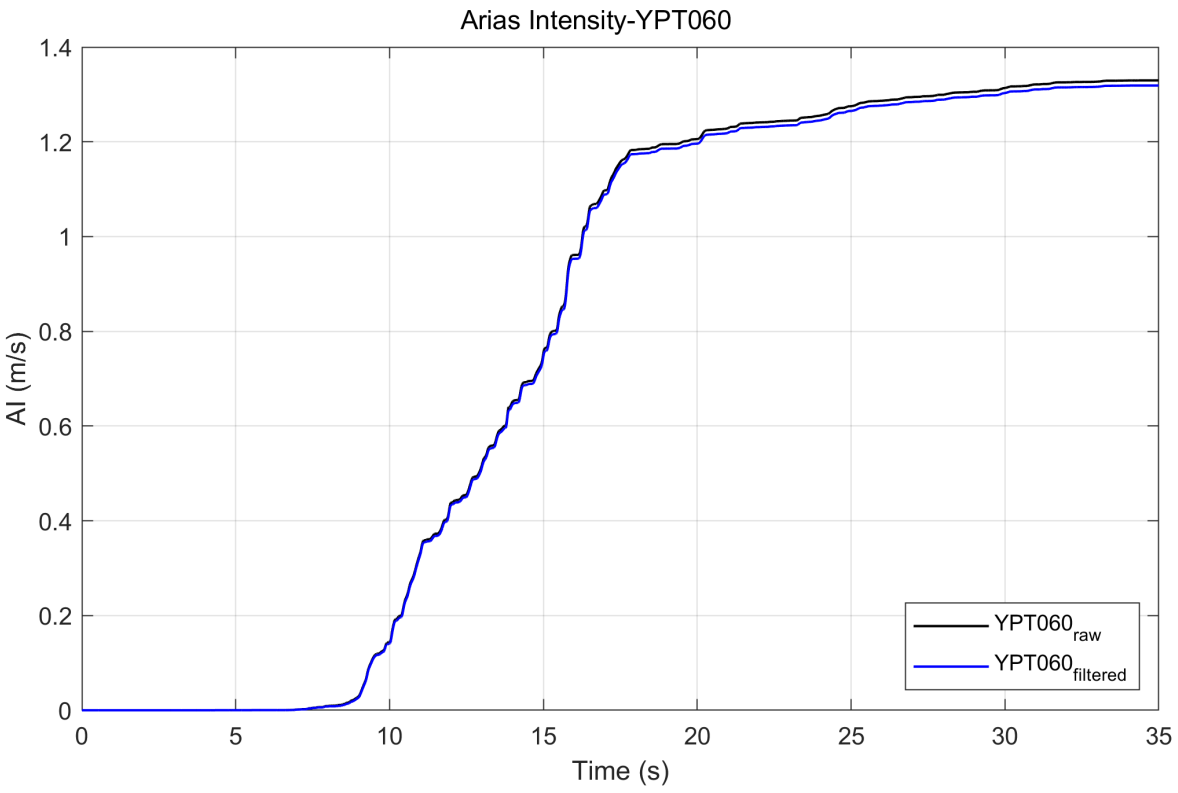

Figure 5.11. Yarimca Record (YPT060) Arias Intensities.

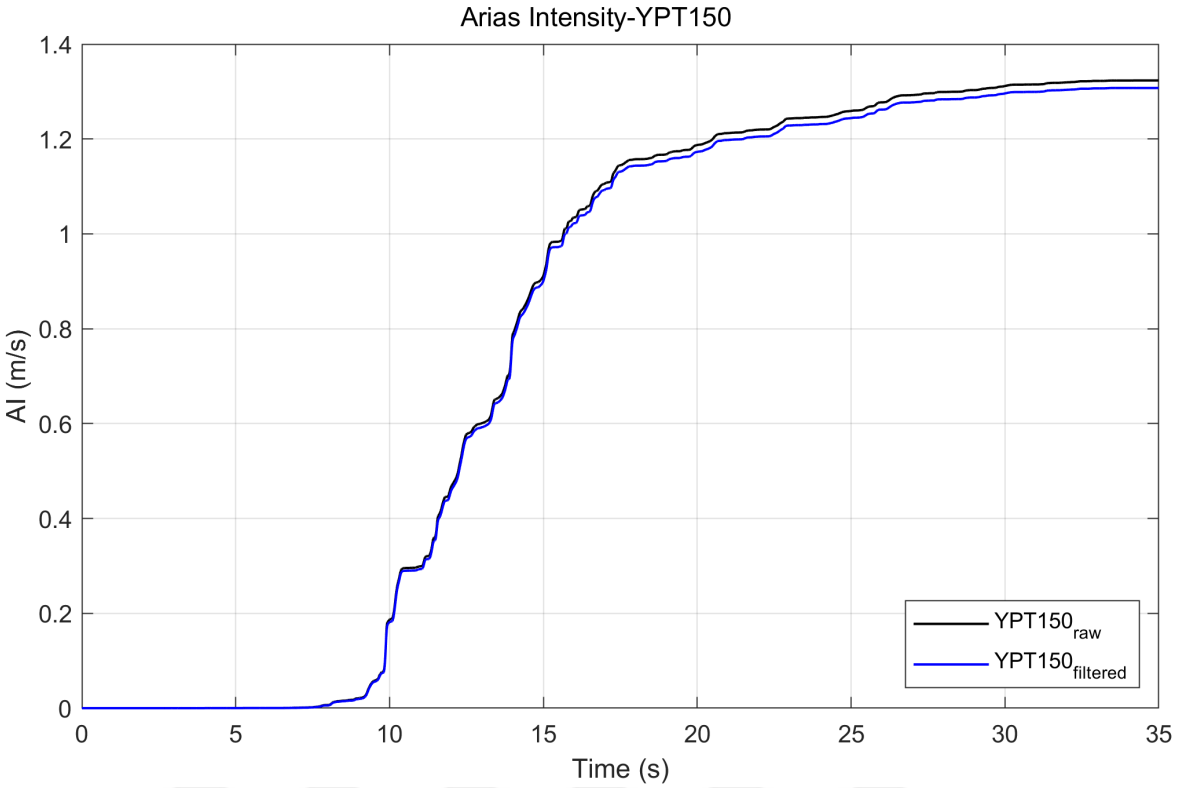

Figure 5.12. Yarimca Record (YPT150) Arias Intensities.

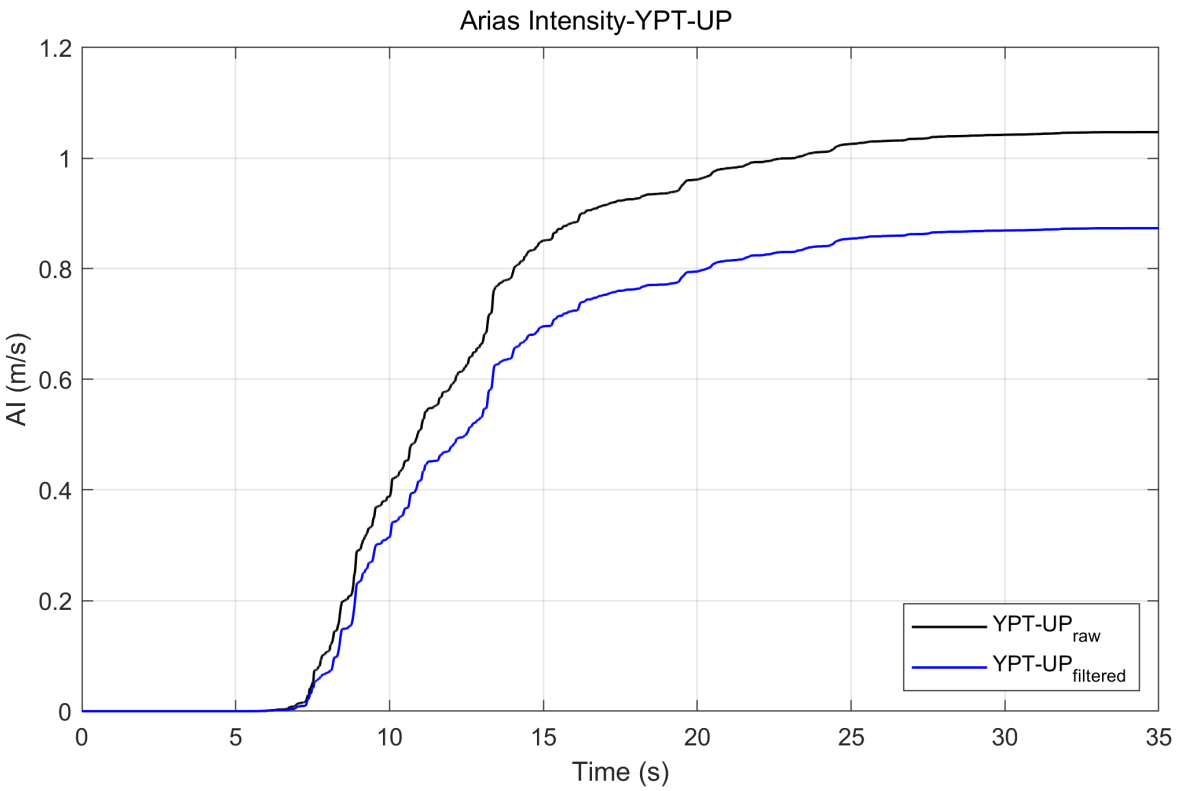

Figure 5.13. Yarimca Record (YPT-UP) Arias Intensities.

5.3. Deconvolution

As it is mentioned in Chapter 4, the seismic motion is imposed to the wharf system via the absorbing boundaries defined along the bottom surface of the model. However, the selected ground motion is recorded at a surface station. Therefore, a simple conversion is required to determine the incident motion at the bottom level of the soil model from the recorded surface motion.

The presence of absorbing boundaries implies that the half-space has similar properties with those of the deepest soil layer (VDS) of the model. In fact, the site of the selected ground motion satisfies this requirement such that its average Vs value is very close to that of the deepest layer of the soil model. It is assumed that the half-space possesses an anonymous soil layer with v_s=297m/s and the depth equal to the total depth of all soil layers, which is 47m (Figure 5.14). Then, deconvolution analysis is performed for the recorded ground motion to determine the incident motion at the soil-halfspace interface. Seismosoil software [87] is used for deconvolution analysis. The incident motions to be applied through the absorbing boundaries of FLAC3D model for the transverse and longitudinal directions are given in Figures 5.15 and 5.16, respectively.

It is assumed that the vertical motion is unaffected by the soil layers and remains the same as in the recorded version at surface [88]. Therefore, the vertical motion given in Figure 5.3 is used directly without any modification.

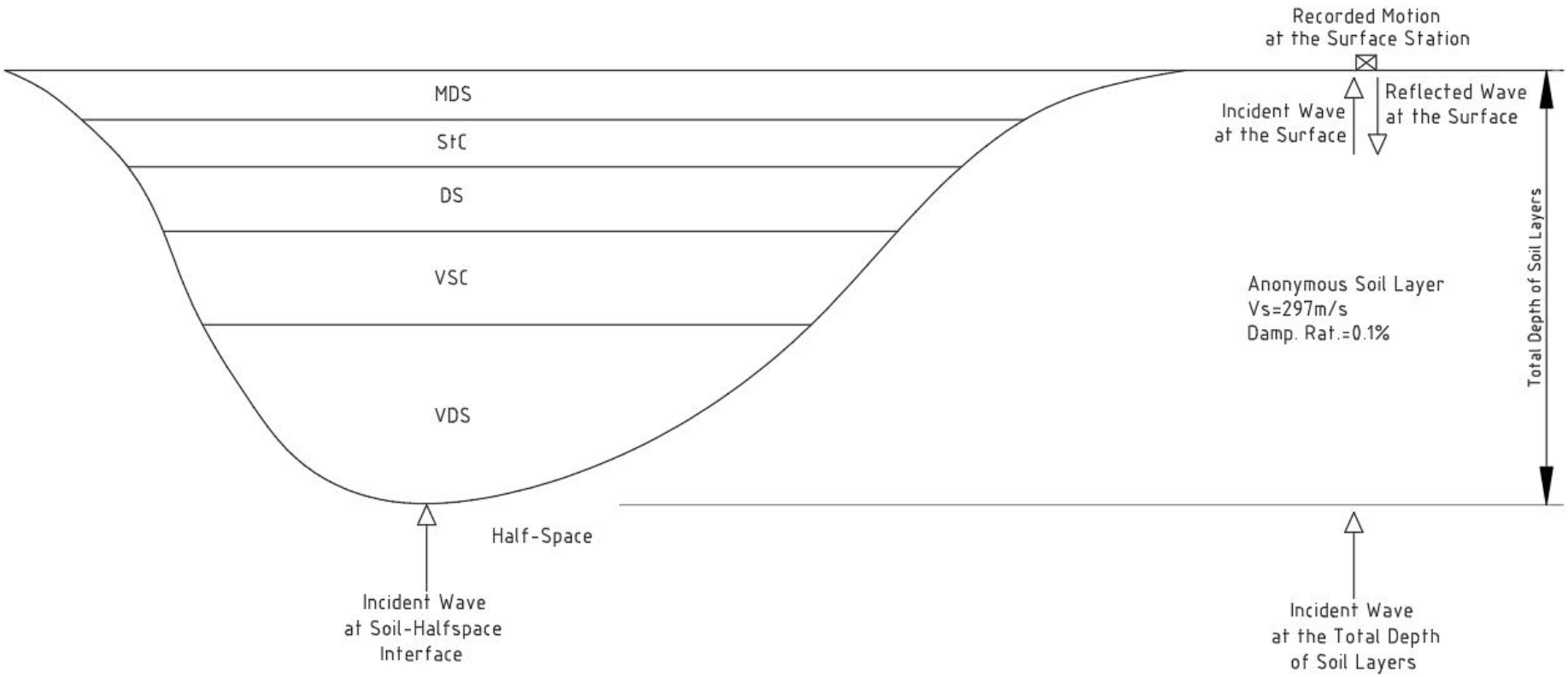

Figure 5.14. Deconvolution.

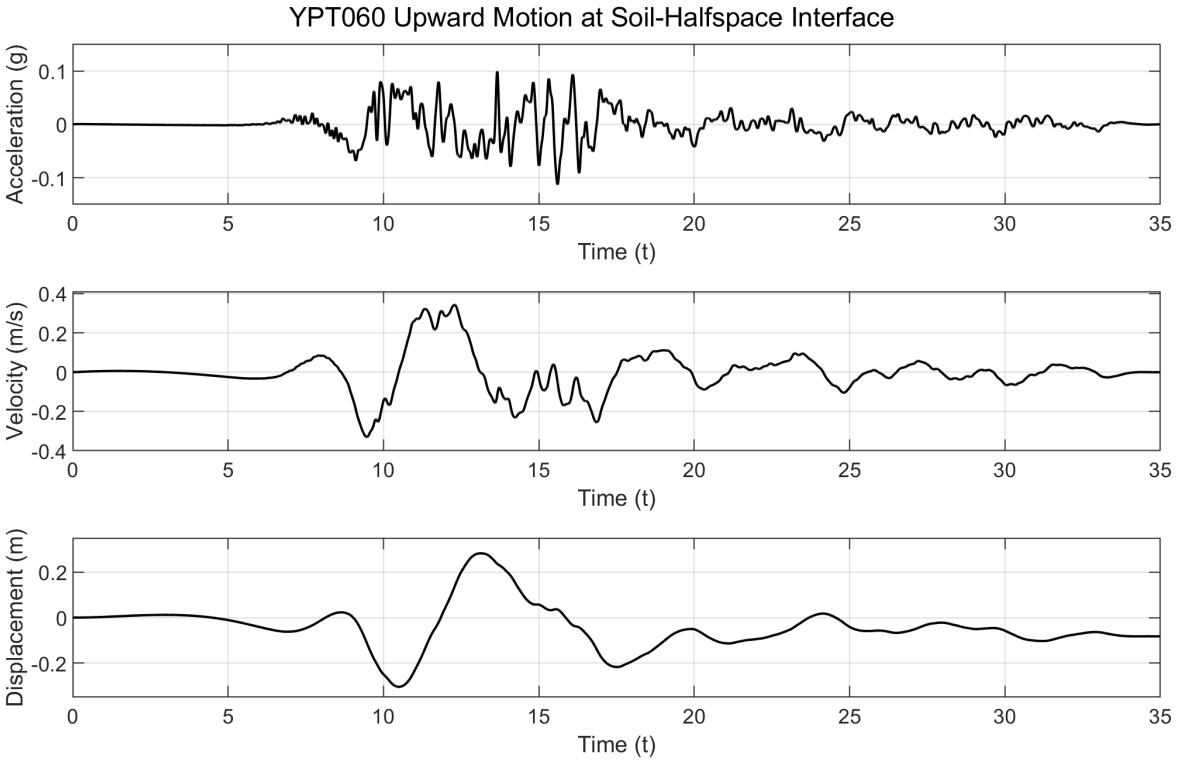

Figure 5.15. Yarimca Incident Motion at Soil-Halfspace Interface (YPT060).

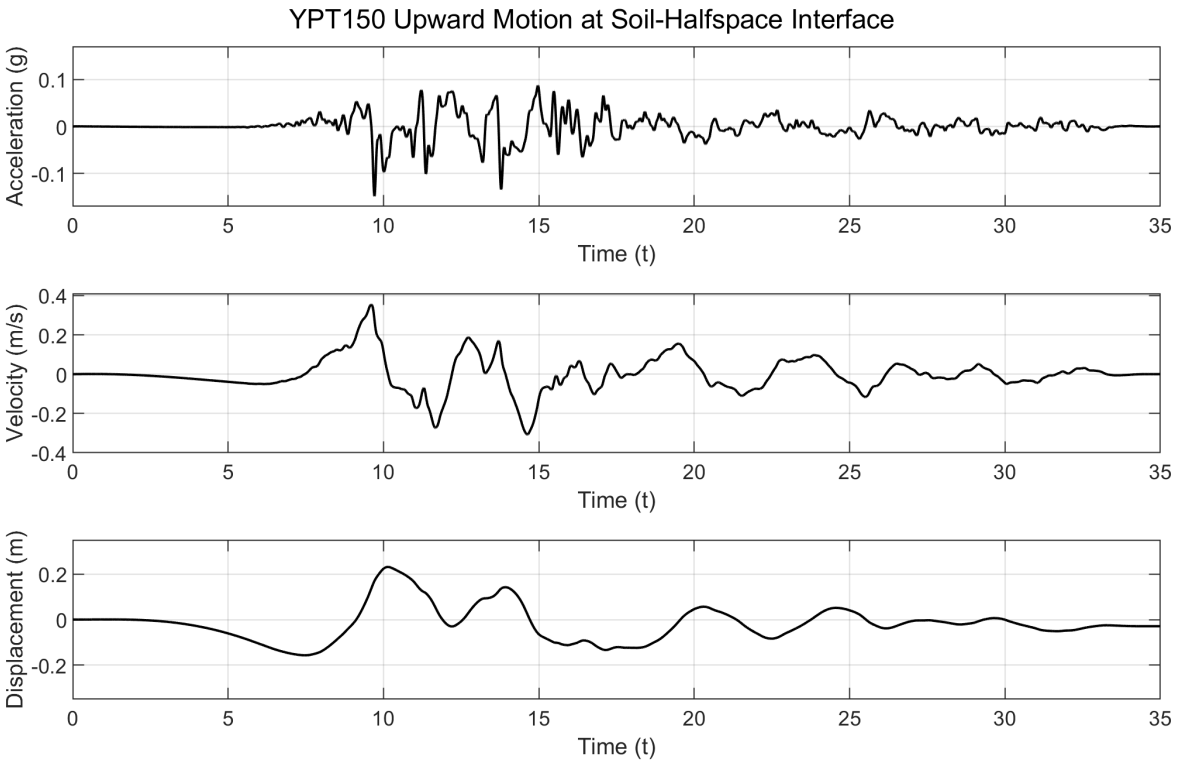

Figure 5.16. Yarimca Incident Motion at Soil-Halfspace Interface (YPT150).

6. WHARF SYSTEMS USED IN ANALYSIS CASES

The wharf systems investigated in this thesis are presented in this chapter. Firstly, information regarding the general arrangement and geometric criteria for the wharf systems are given. Then, the properties of geotechnical and structural systems are presented.

6.1. General Arrangement

A typical general arrangement plan for the embankment and wharf system is given in Figure 6.1. There is an existing facility behind the new reclamation fill, on which a new wharf system constructed. In study, the new wharf system is investigated. The existing reclamation fill shown in Figure 6.1 accommodates the existing facility, enabling the operations related to the transportation of goods. The new reclamation fill will be made on the existing reclamation fill as it is seen from Section A-A (Figure 6.2). The slope line (1/2) dividing the existing fill and the new fill is shown in the same figure. The top level of existing reclamation fill (FGL), the new reclamation fill (FGL) and the wharf deck (DTL) is +3.00m CD (Chart Datum). Seabed level (DL) is constant along the embankment and it is -13.00m CD. Mean sea level (MSL) is taken as ±0.00m CD.

6.2. Geotechnical System

Figure 6.2 illustrates the typical soil stratification used for the analysis of wharf systems. Considering the previous overloading at the existing facility, the properties of sand layer (MDS-3) beneath the existing fill is assumed to have been enhanced over the years due to consolidation. The same applies to sand layer MDS-2. Thus, it is assumed that MDS-3 layer is stiffer than MDS-2 layer and MDS-2 layer is stiffer than MDS-1 layer.

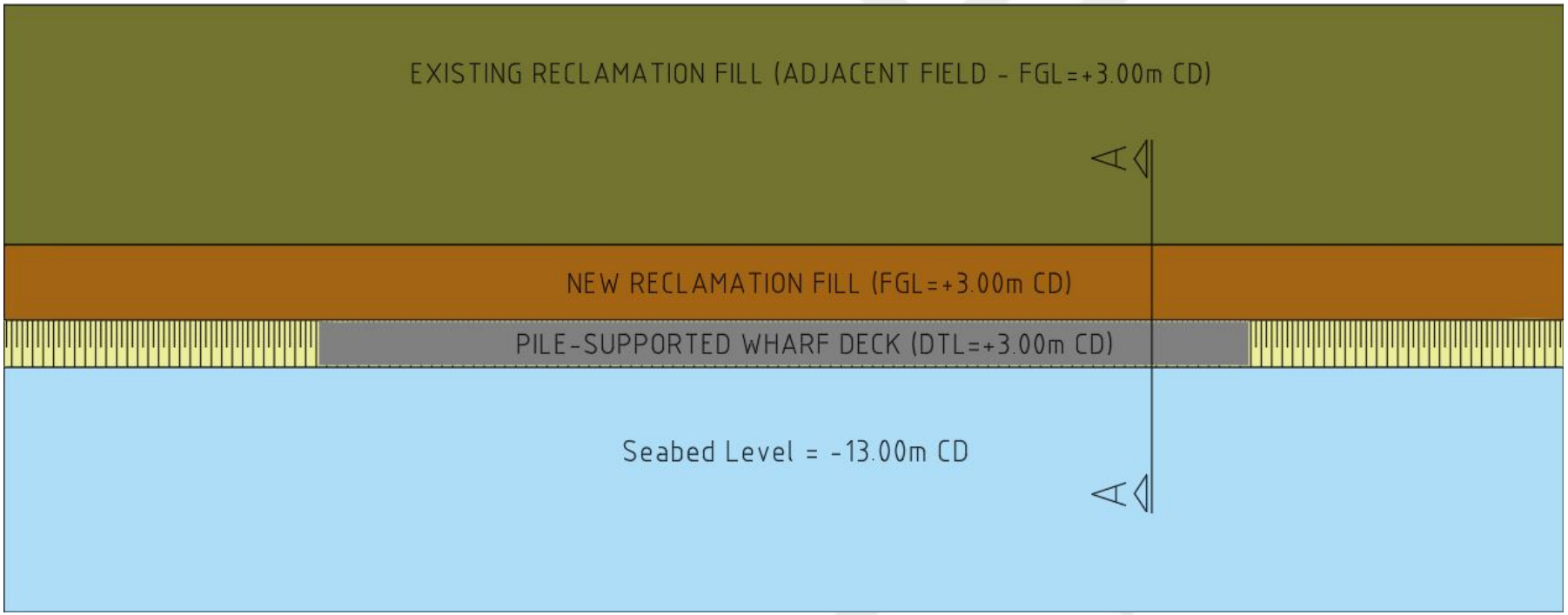

Figure 6.1. General Arrangement Plan.

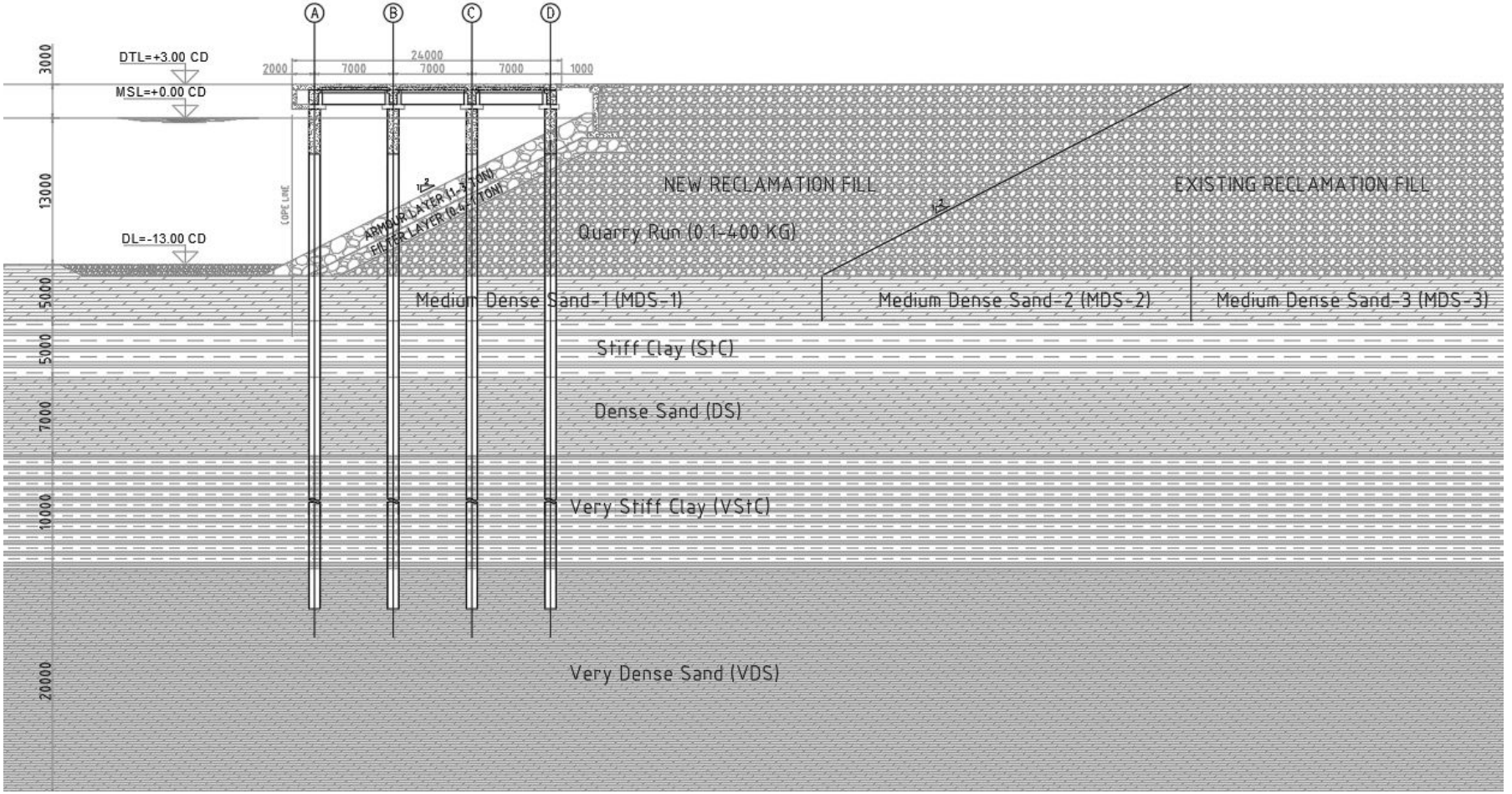

Figure 6.2. Wharf Section (A-A).

The soil layers, dimensions, densities, porosities, relative densities, strength and stiffness properties are tabulated in Tables 6.1, 6.2, 6.3 and 6.4.

Table 6.1. Soil Layers and Dimensions.

Soil Layer	Depth(m)	Thickness(m)
Armour&Filter	(+2.50) - (-13.00)	3.1
Quarry Run	(+2.50) - (-13.00)	0.0 - 15.5
MDS-Par1*	(-13.00) - (-18.00)	5.0
MDS-1	(-13.00) - (-18.00)	5.0
MDS-2	(-13.00) - (-18.00)	5.0
MDS-3	(-13.00) - (-18.00)	5.0
MDS-Par2*	(-13.00) - (-18.00)	5.0
Stiff Clay	(-18.00) - (-23.00)	5.0
Dense Sand	(-23.00) - (-30.00)	7.0
Very Stiff Clay	(-30.00) - (-40.00)	10.0
Very Dense Sand	(-40.00) - (-60.00)	20.0

Table 6.2. Soil Layers and Properties.

Soil Layer	$\rho_d(t/m^3)$	n	$\rho_{sat}(t/m^3)$	Dr
Armour&Filter	1.66	0.36	2.02	-
Quarry Run	1.74	0.33	2.07	-
MDS-Par1*	1.46	0.44	1.90	0.47
MDS-1	1.51	0.42	1.93	0.51
MDS-2	1.56	0.40	1.96	0.59
MDS-3	1.61	0.38	1.99	0.66
MDS-Par2*	1.66	0.36	2.02	0.72
Stiff Clay	1.56	0.40	1.90	-
Dense Sand	1.82	0.30	2.12	0.78
Very Stiff Clay	1.61	0.38	1.93	-
Very Dense Sand	1.87	0.28	2.15	0.85

**This layer is used only in the parametric study mentioned in Section 8.1.3*

Table 6.3. Soil Layers and Strength Properties.

Soil Layer	$\phi'(degree)$	c'(kPa)	cu(kPa)
Armour&Filter	45	15	-
Quarry Run	38	5	-
MDS-Par1*	31	-	-
MDS-1	32	-	-
MDS-2	33	-	-
MDS-3	34	-	-
MDS-Par2*	35	-	-
Stiff Clay	23	12	85
Dense Sand	36	-	-
Very Stiff Clay	25	18	110
Very Dense Sand	37	-	-

Table 6.4. Soil Layers and Stiffness Properties.

Soil Layer	G(kPa)	K(kPa)	$v_s(m/s)$
Armour&Filter	140000	212593	290
Quarry Run	130000	252121	273
MDS-Par1*	40000	91930	166
MDS-1	50000	122222	182
MDS-2	70000	182549	212
MDS-3	90000	251250	236
MDS-Par2*	110000	330000	257
Stiff Clay	100000	966667	253
Dense Sand	133000	620667	270
Very Stiff Clay	150000	1200000	305
Very Dense Sand	158000	737333	291

**This layer is used only in the parametric study mentioned in Section 8.1.3*

Note that the static analyses are conducted using the drained parameters, while the undrained parameters are utilized for seismic analysis.

6.3. Structural System

Conventional deck-on-pile system, which is one of the most preferred structural system in marine construction practice, is used as the structural system in this study. The structural system is composed of the following elements:

- Tubular steel driven piles;
- Cast-in-situ concrete plugs at pile tops with sufficient lengths of dowel bars to provide monolithic connection between piles and the concrete deck;
- Cast-in-situ concrete pile caps at pile tops to provide support for the precast concrete (PC) deck girders;
- Pile-beam joints formed by cast-in-situ concrete;
- Precast concrete (PC) slabs placed onto girders;
- Cast-in-situ concrete topping to complete the deck construction.

The plan view of a typical interior(int) module deck and a typical section are given in Figures 6.3 and 6.4, respectively.

A typical pile section is illustrated in Figure 6.5. The steel pipe pile diameter is 1016mm, the pipe wall thickness is taken as 18mm, and accordingly, the RC plug diameter is 980mm. Note that the dimensions given in the figures are in "mm" unless otherwise stated.

The typical int-module length is 66.3m, the width is 24m and the height of deck system is 2.2m from the pile cap soffit and 1.8m from the beam soffit. The axis to axis span of each beam is 7m in both orthogonal directions. The dimensions of PC int-beam are 700x1800mm and those of PC exterior(ext) beam are 840x1800mm. The total thickness of the deck slab is 500mm, consisting of a 250mm thick PC slab and a 250mm thick cast-in-situ topping (Figures 6.3 and 6.4). These slabs are assembled using shear connector rebars left exposed on the PC slabs.

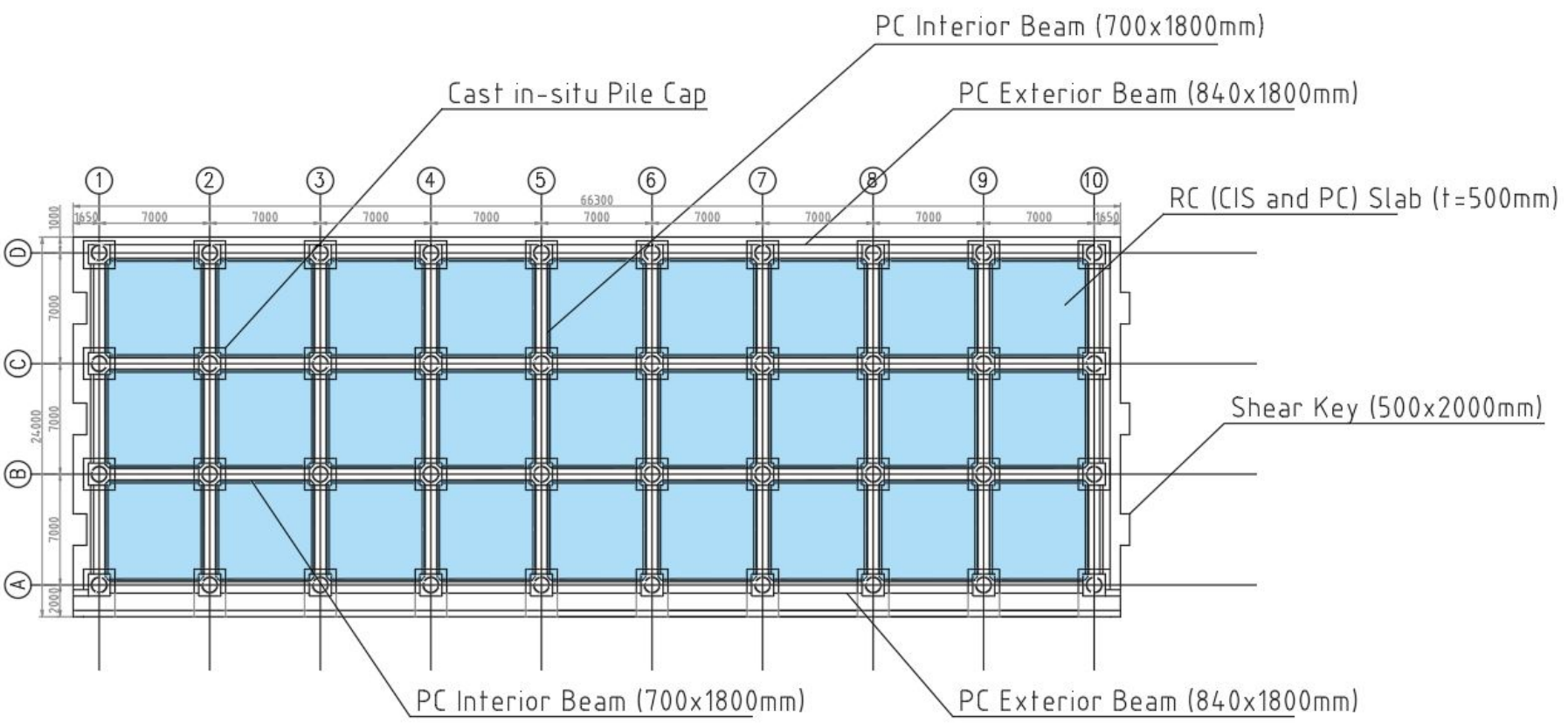

Figure 6.3. RC Deck System Plan of a Typical Interior Module.

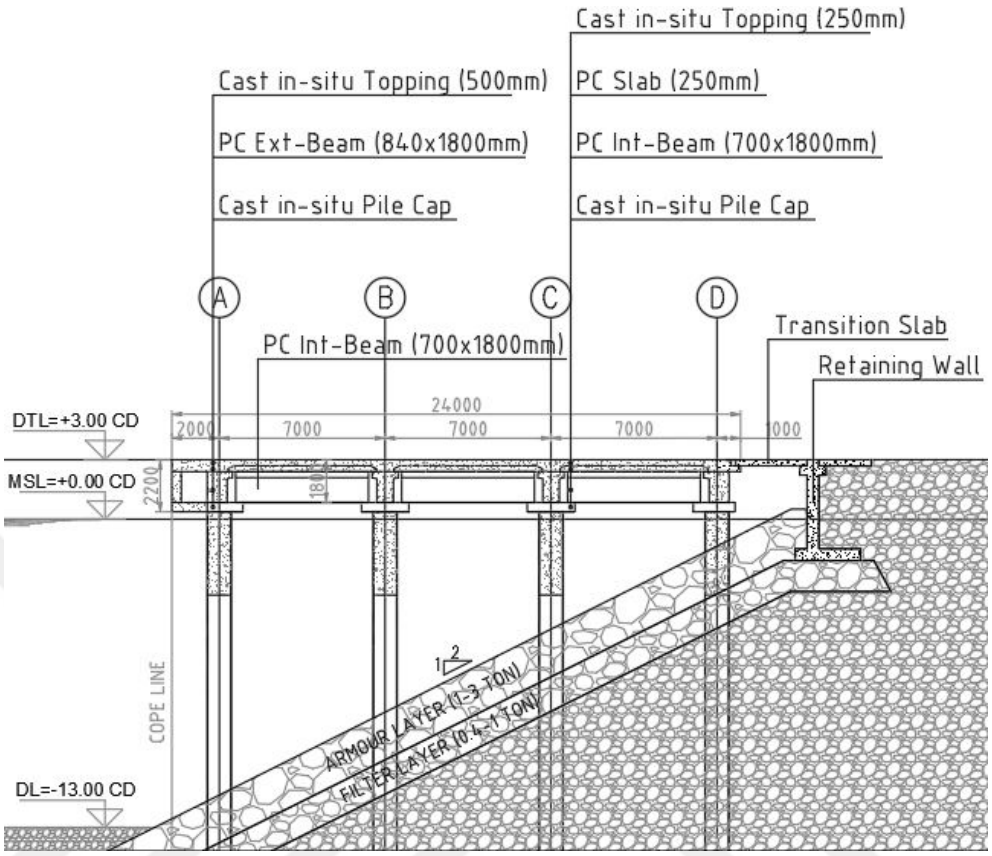

Figure 6.4. Typical Structural System Section.

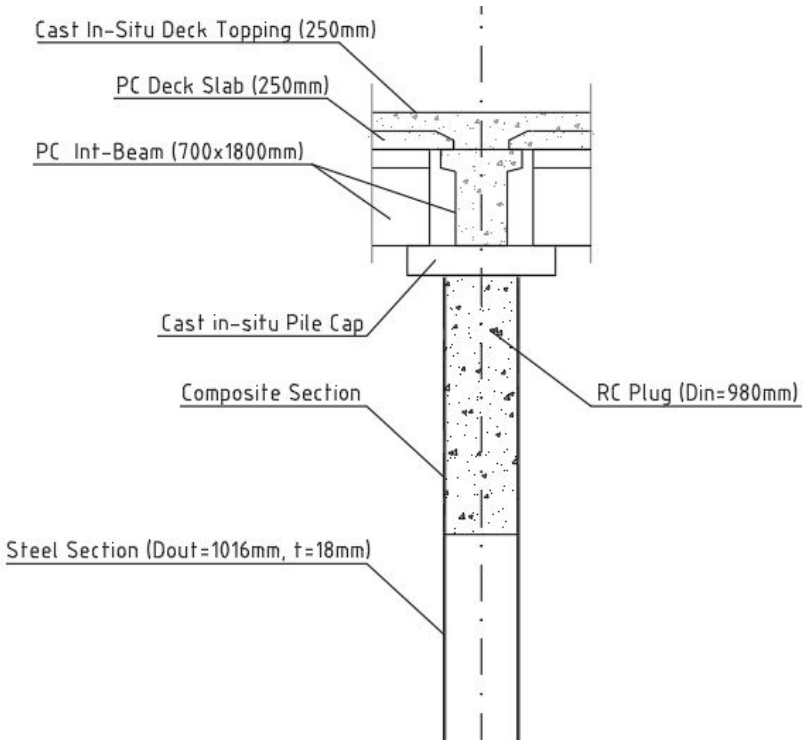

Figure 6.5. Typical Pile Section.

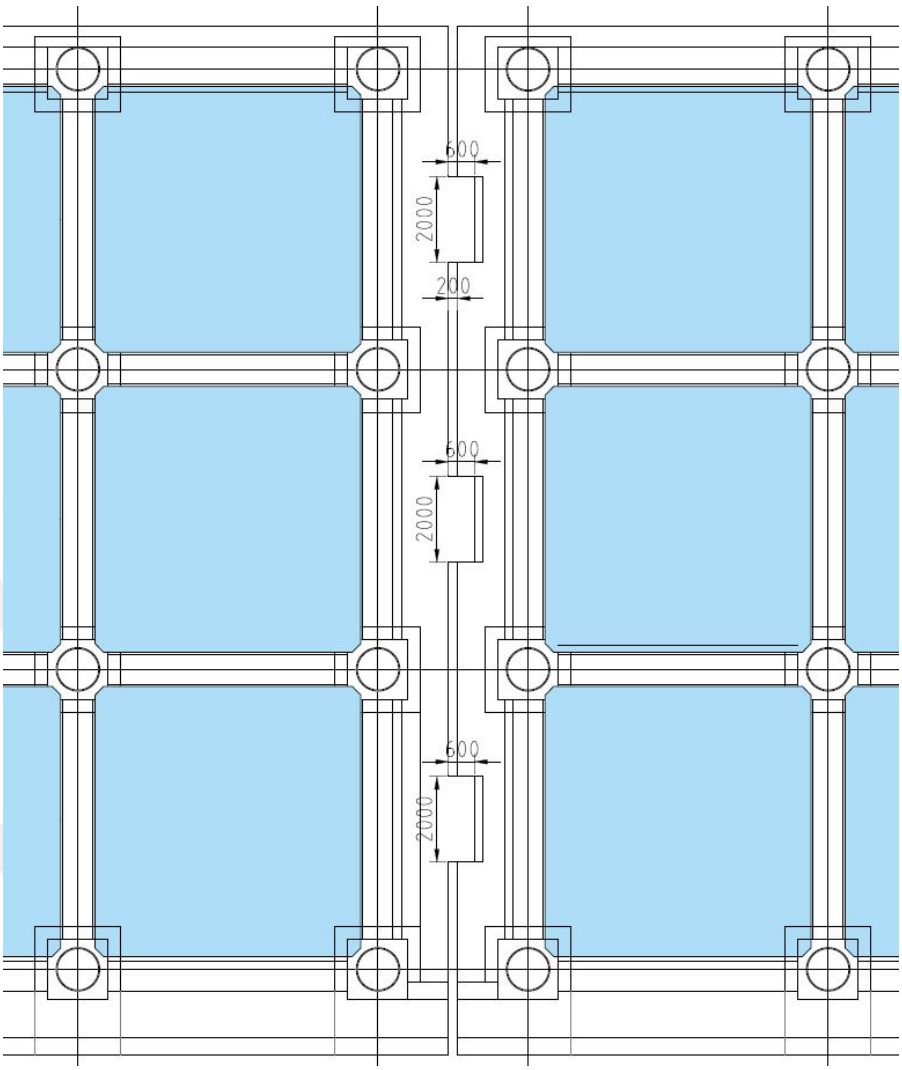

Figure 6.6. Shear Key Dimensions.

Table 6.5. Deck and Embankment Lengths for the Wharf Systems.

Wharf System	Total Deck Length (m)	Total Embankment Length (m)
1-Module-Wharf	65.0	224.0
2-Modules-Wharf	131.5	290.5
3-Modules-Wharf	198.0	357.0
4-Modules-Wharf	264.5	423.5
5-Modules-Wharf	331.0	490.0
6-Modules-Wharf	397.5	556.5
7-Modules-Wharf	464.0	623.0
8-Modules-Wharf	530.5	689.5

Wharf modules are linked each other via shear keys. The expansion joint gap between two adjacent modules is 200mm. The plan dimensions of shear keys are 600x2000mm in plan (Figure 6.6) and the depth is 500mm (Figure 6.3). The wharf systems with different number of modules, up to eight, are modeled in this study. The total deck lengths and the embankment lengths of the wharf systems are given in Table 6.5.

The retaining wall section and its dimensions are given in Figure 6.7. Note that the transition slab linking the wharf deck to the retaining wall (Figure 6.3) is not modeled. Because the sufficient distance at the expansion joint is provided to tolerate the relative movement of wharf deck and retaining wall, an interaction between them is not expected.

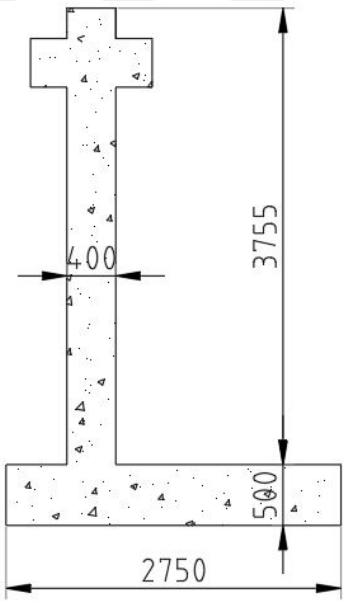

Figure 6.7. Retaining Wall Dimensions.

6.3.1. Material Properties of Structural Elements

6.3.1.1. Concrete. The concrete class and its properties used in this study are given as follows based on Turkish Standard TS-500 [89]:

- Class : C40
- E_c : 34000 Mpa
- f_{co} : 40 Mpa
- γ_c : 25 kN/m^3
- ν_c : 0.2

The stress-strain relationships for unconfined and confined concrete are given in Figure 6.8 according to TSCDMS-2020 [77],

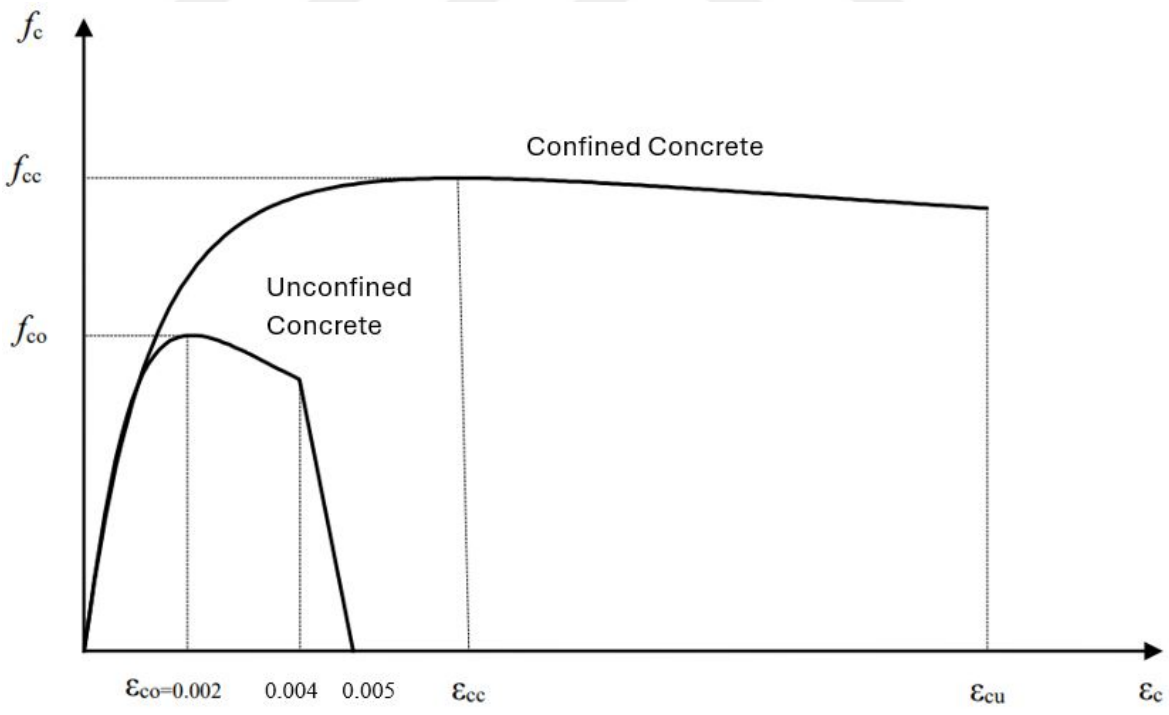

Figure 6.8. Stress-Strain Relationships for Unconfined and Confined Concrete (from TSCDMS-2020 [77]).

The strain values indicated in Figure 6.8 is given as follows:

- ε_{co} : 0.002
- ε_{cs} : 0.004
- ε_{ss} : 0.005

6.3.1.2. Reinforcing Steel. The reinforcing steel class and its properties, which are taken from Turkish Standard TS-708 [90] and TS-500 [89], are given as follows:

- Class : B420C
- E_s : 200000 Mpa
- f_{sy} : 420 Mpa
- f_{su} : 550 Mpa

The stress-strain relationship for reinforcing steel are given in Figure 6.9 according to TSCDMS-2020 [77],

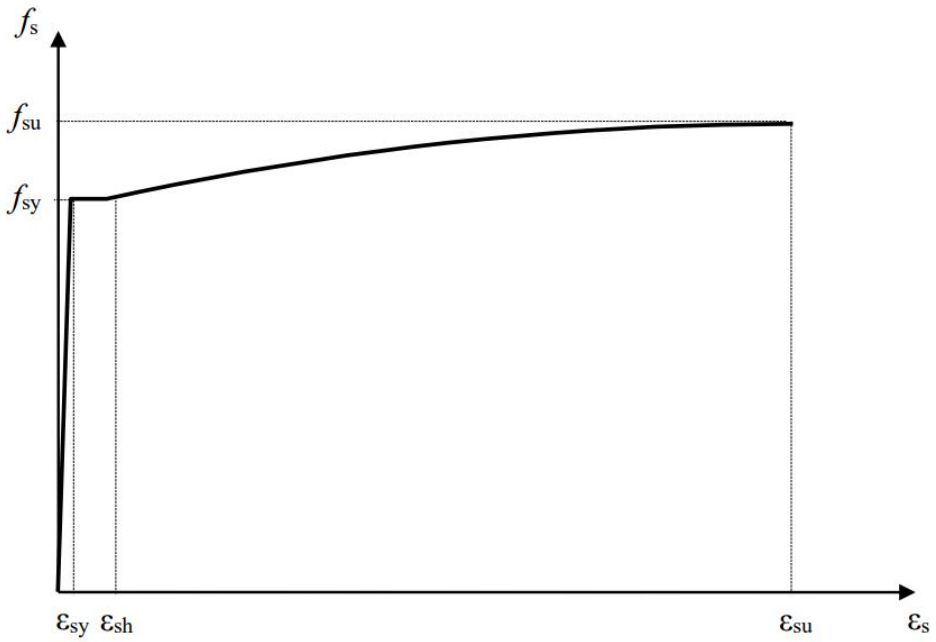

Figure 6.9. Stress-Strain Relationship for Reinforcing Steel (from TSCDMS-2020 [77]).

The strain values for reinforcing steel indicated in Figure 6.9 is given as follows:

- ε_{sy} : 0.0021
- ε_{sh} : 0.008
- ε_{su} : 0.08

6.3.1.3. Structural Steel. The structural steel class and its properties, which are taken from Eurocode-3 [91], are given as follows:

- Class : S355 H
- E_{ss} : 210000 Mpa
- f_{ssy} : 355 Mpa
- f_{ssu} : 490 Mpa
- ρ_{ss} : 7.85 t/m^3
- ν_{ss} : 0.3

6.3.1.4. Expected Material Strengths. The strength values given in class definitions (i.e. C40, S355 etc.) are the characteristic values of materials. The expected (mean) strengths of materials are used in the analyses. The coefficients for the expected (mean) strengths of materials, which are taken from TSCDMS-2020 [77] and TSDCB-2018 [92], are given as follows:

- f_{ce} : $1.3f_{ck}$
- $f_{ye,r}$: $1.2f_{yk,r}$
- $f_{ye,s}$: $1.1f_{yk,s}$

6.3.2. Steel Pipe Compactness

Compactness ratio (D/t) is a parameter associated with the local buckling phenomenon in steel sections. If a sufficiently tough circular hollow section is not selected for a wharf pile, the pipe pile may lose its stability before it reaches the cross-sectional yield strength. For this reason, the compactness ratio is a critical parameter in selecting of the steel pipe used as a wharf pile.

The steel pipe compactness criterion given in TSCDMS-2020 [77] is adopted for the selection of steel pipe thickness. The formulation is given in Equation (6.1),

$$\frac{D}{t} \leqslant c\frac{E_{ss}}{f_{ssy}} \leqslant 80 \tag{6.1}$$

where, "D" is the outside diameter of pipe, "t" is the wall thickness of pipe and "c" is a coefficient related to the filling material to be possibly used. As per TSCDMS-2020 [77], "c" is taken as 0.10 if the pipe is not filled with any material, 0.12 if the pipe is filled with granular soil or naturally filled with soil and 0.14 if it is filled with lean concrete. D/t upper limit for an unfilled section is calculated as 59.2 from Equation (6.1). D/t is 56.4 for the steel pipe section used in this study.

The other compactness criteria considered in this study are given in Eurocode-3 [91]. Four classes are defined in Eurocode-3, namely, Class-1, Class-2, Class-3 and Class-4. Class-1 represents the toughest class, Class-4 represents the most slender class. Class-3 is defined as the compactness class that elastic section modulus can be used for the design of steel sections. The formulation of compactness ratio upper limit for Class-3 is given in Equations (6.2) and (6.3),

$$\frac{d}{t} \leqslant 90\epsilon^2 \tag{6.2}$$

$$\epsilon^2 = \frac{235}{f_y} \tag{6.3}$$

where, "d" is the outside diameter of pipe, "t" is the wall thickness of pipe, "f_y" is the characteristic yield strength of steel. Therefore, the d/t upper limit for Class-3 is calculated as 59.4 per Eurocode-3 [91].

The formulations in TSCDMS-2020 and Eurocode-3 are presented to warrant the level of strength only and do not include any information regarding the deformation capacity of steel section after yielding. which is an essential parameter for deformation-based design. Gardner and Nethercot [93] shares a figure that qualitatively demonstrates the inelastic behavior of cross sections of different compactness classes (Figure 6.10).

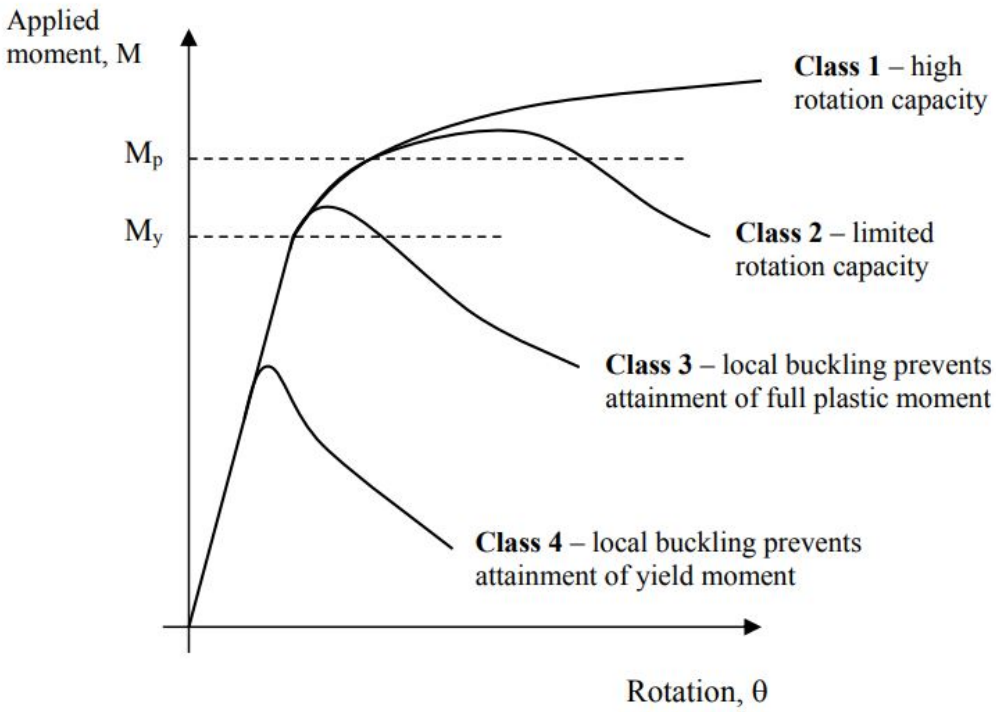

Figure 6.10. Inelastic Behavior of Steel Section from the Compactness Classes Defined by Eurocode-3 (Gardner and Nethercot [93]).

According to Figure 6.10, although the steel section in Class-3 reaches the yield strength capacity, it doesn't have a sufficient ductility capacity. It implies that if a steel section belonging to Class-3 is selected, it should be considered as a capacity-protected member in design. Nevertheless, none of the seismic design codes for marine

structures considers the effect of local-buckling failure on the limit deformation criteria. In this regard, Harn et. al. [94] proposed a new strain criterion for steel pipes to be used for marine structures incorporating the compactness ratio for the first time. It is stated that the limit strain levels in ASCE 61-14 [78] must be reduced drastically when considering the compactness ratio of pipe sections [94]. This issue is likely to be incorporated into future versions of ASCE codes.

A collection of the test results for the relationship of compactness ratio and the local buckling strain of pipe pile is presented in Figure 6.11, by Harn et.al. [94].

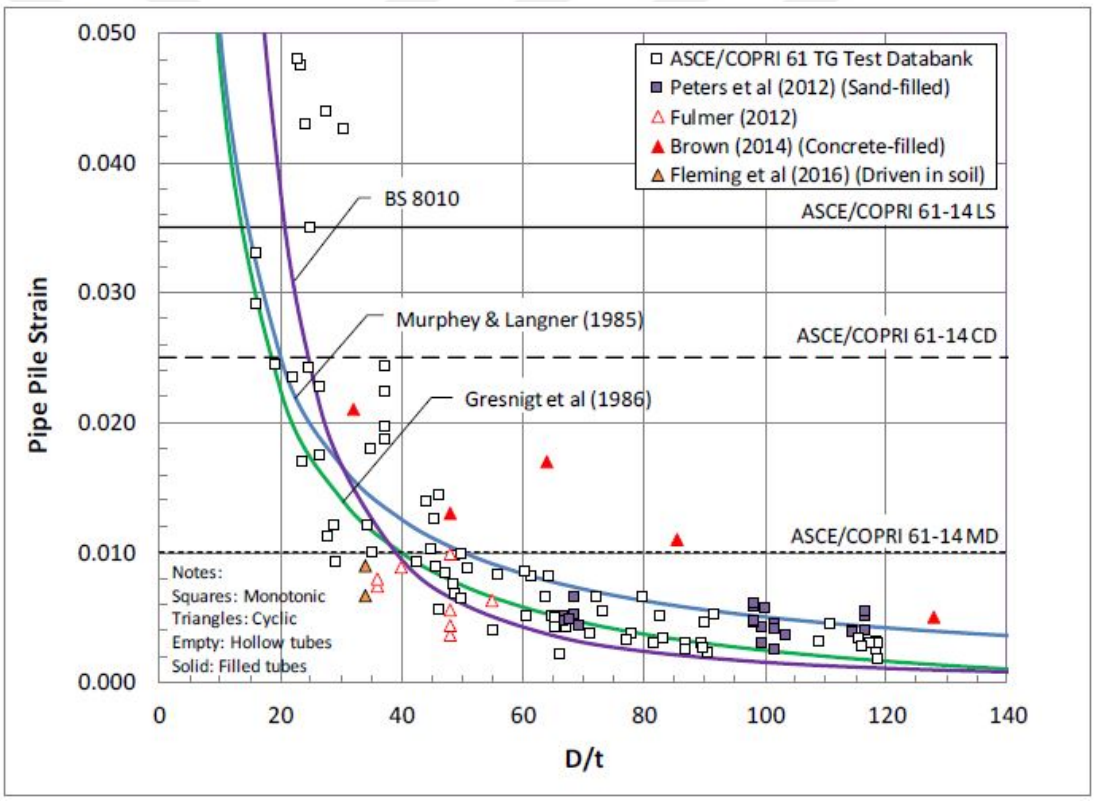

Figure 6.11. Local Buckling Strain vs. Compactness Ratio (Harn et.al. [94])

6.3.3. Cross-Section Analysis of Piles

The cross-section fiber analyses for RC plug and steel sections are performed to determine the plastic moment capacities to be used in the analyses. The material properties given in Section 6.3.1 are used.

6.3.3.1. Moment Capacity of RC Plug. The RC plug diameter is 980mm and the concrete cover for the RC plug section is taken as 75mm. The longitudinal reinforcement is 16Φ32 and the spiral transverse reinforcement is Φ16/75mm.

Mander confined concrete model [95] is employed to find the confined concrete properties. The confined concrete strength is calculated as 71Mpa, the yield and crushing strains for the confined concrete section are calculated as 0.004 and 0.015 respectively.

The axial forces acting on the RC plugs are classified in two groups. The first group covers A,B,C axes piles and the second group covers D axis piles (Landside). The average axial load level for the first group is 1033 kN and that of the second group is 616kN. Considering the axial load levels, the moment-curvature analyses are performed for two groups and the results are illustrated with the idealized bi-linear curves in Figures 6.12 and 6.13. The moment capacities of RC Plug sections to be used in the analyses are calculated as 2635 kNm and 2518 kNm for the first and second group piles respectively.

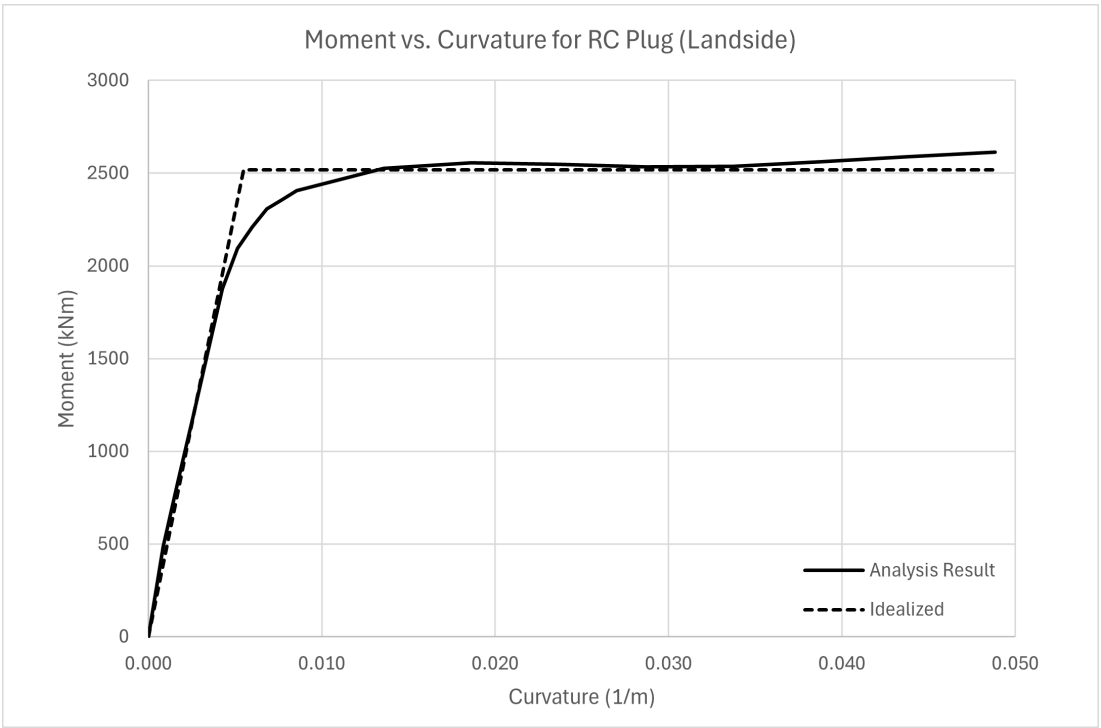

Figure 6.12. Moment vs. Curvature for Landside RC Plug.

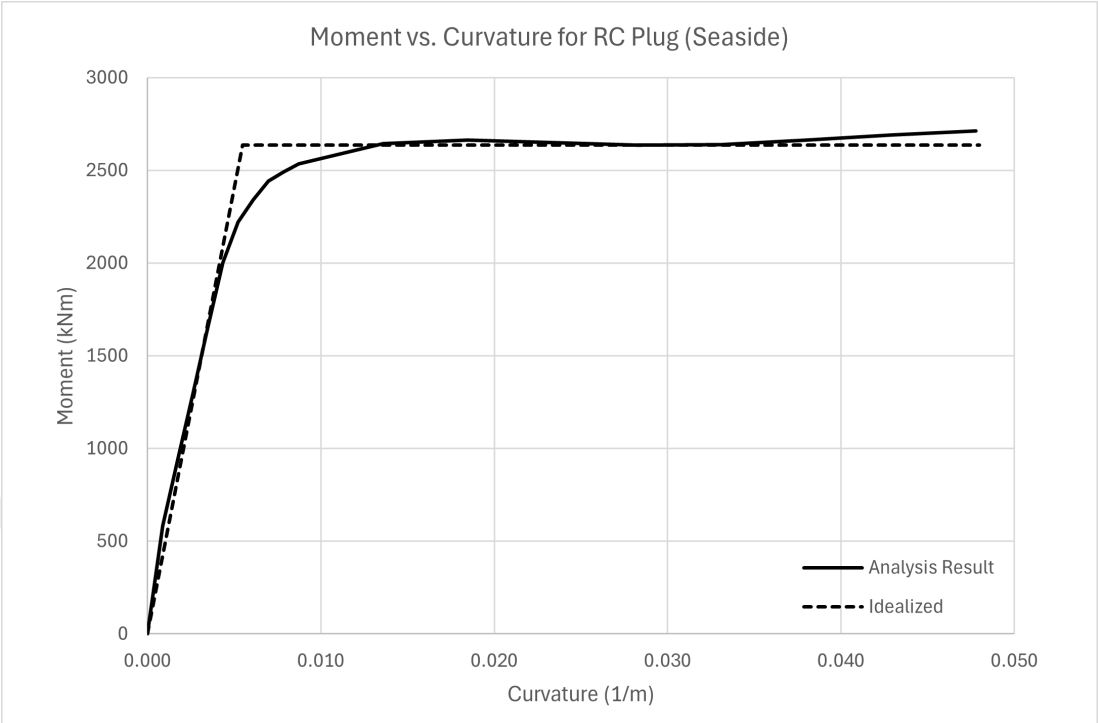

Figure 6.13. Moment vs. Curvature for Seaside RC Plug.

6.3.3.2. Moment Capacity of Steel Pile. The dimensions of steel pipe section are D= 1016mm with t=18mm and D/t ratio is 56.4. Then, it is assumed that the pile local buckling strain is 0.0064 based on Figure 6.11. The average axial force acting on the steel sections, at which the in-ground plastic hinges will probably occur, is taken as 1046kN. The results of cross section analysis for the steel pipe section are given in Table 6.6.

Figure 6.14 shows the moment and steel strain relationships. The black curve indicates the relation obtained directly by the fiber analysis. The point that the blue curve ended corresponds the buckling strain level. Note that the red curve plotted after that point is plotted only for illustrative purpose. The dashed black curve indicates the idealized relation. Therefore, the moment capacity of the steel section is taken as 6547 kNm.

Table 6.6. Steel Section Analysis Results.

Curvature (1/m)	Moment (kNm)	Steel Strain
0	0	0.0001
0.0009	1291	0.0005
0.0022	3226	0.0012
0.0039	5704	0.0021
0.0061	6513	0.0032
0.0087	6789	0.0048
0.0118	**6840**	**0.0064**
0.0153	6840	0.0082
0.0192	6840	0.0101
0.0236	6840	0.0123
0.0284	6840	0.0147
0.0337	6875	0.0173
0.0394	6992	0.0201
0.0455	7136	0.0232
0.0520	7289	0.0265
0.0590	7455	0.0300

The limited inelastic deformation capacity of the section can be seen clearly from Figure 6.14. The ductility character of the pipe piles is related to the cases of sand-filling or filling with soil plug occurred during the driving process naturally. The deformation behavior of pipe piles after yielding due to local buckling is a topic that is still open to improvement. Many wharf systems, which have been designed over the years without considering the inelastic deformation behavior of pile local buckling phenomenon, exist. Thus, it is particularly important for the existing systems.

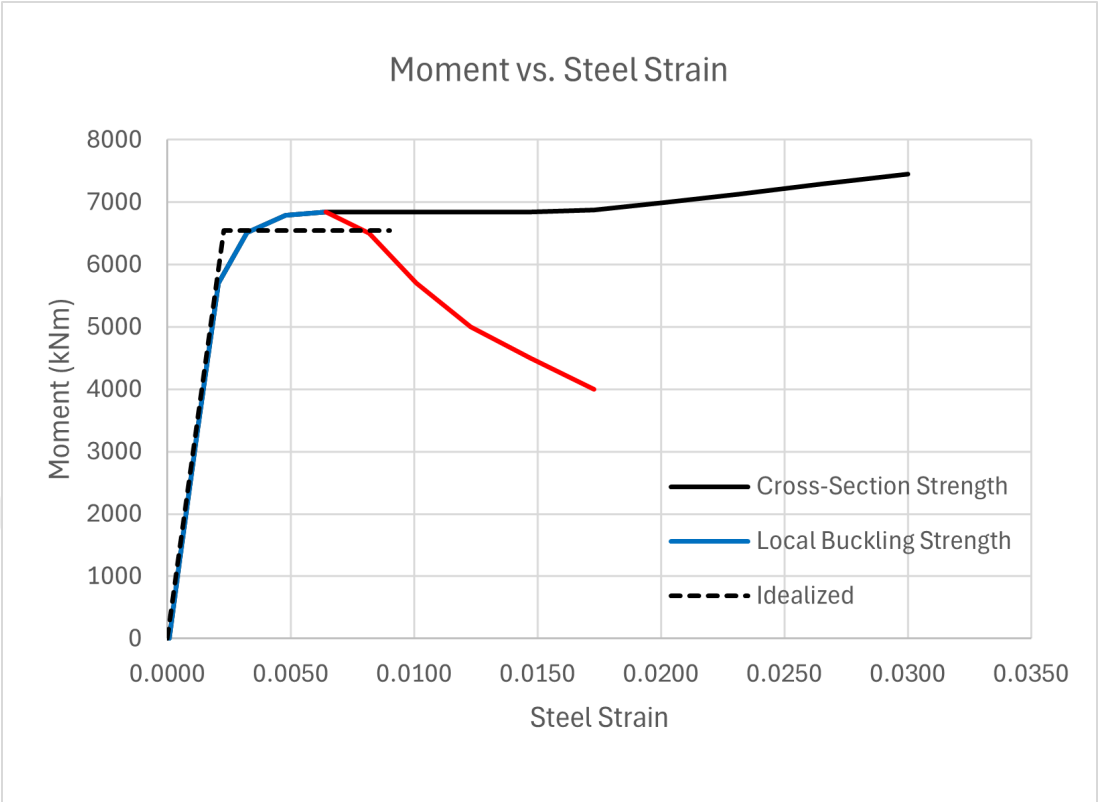

Figure 6.14. Steel Strain vs. Moment.

6.4. Processing of Output Data

The analysis models used in this study are generally quite large in size and contain many elements. Consequently all of the output response quantities of these elements are drastically large. The number of output data to be processed after analysis is relatively very small. In this regard, only the data to be processed are saved and sorted as text files by FISH (FLAC programming language) coding. Then, the data in these files are processed in MATLAB environment [96] to visualize in graphic form as figures.

The data stored in FLAC3D are consisting of coordinates, pile internal forces, pile total displacements and total rotations, total displacements and total accelerations at some deck nodes, shear key forces, pore pressures, effective stresses, shear strains, shear stresses and soil displacements at some soil nodes.

In this section, the locations of nodes at which the data taken is presented so that the reader can follow the output figures easily. The eight deck nodes at which the displacement and acceleration data read and processed are illustrated in Figure 6.15. The three shear key nodes at which the shear force data read and processed are illustrated in Figure 6.16.

Figure 6.17 shows the soil nodes at which the response data are taken. Figure 6.18 shows the soil axes in longitudinal direction. Each soil axis has 18 soil nodes seen in Figure 6.17. Soil Axis No:0, passes through approximately 30m away from 1st axis of structural system. It is assumed that it corresponds to the free-field soil response. Soil Axis No:1 passes through 1st axis of structural system. Soil Axis No:2 passes through 4th axis of structural system. Soil Axis No:3 passes between 4th and 5th axes of structural system.

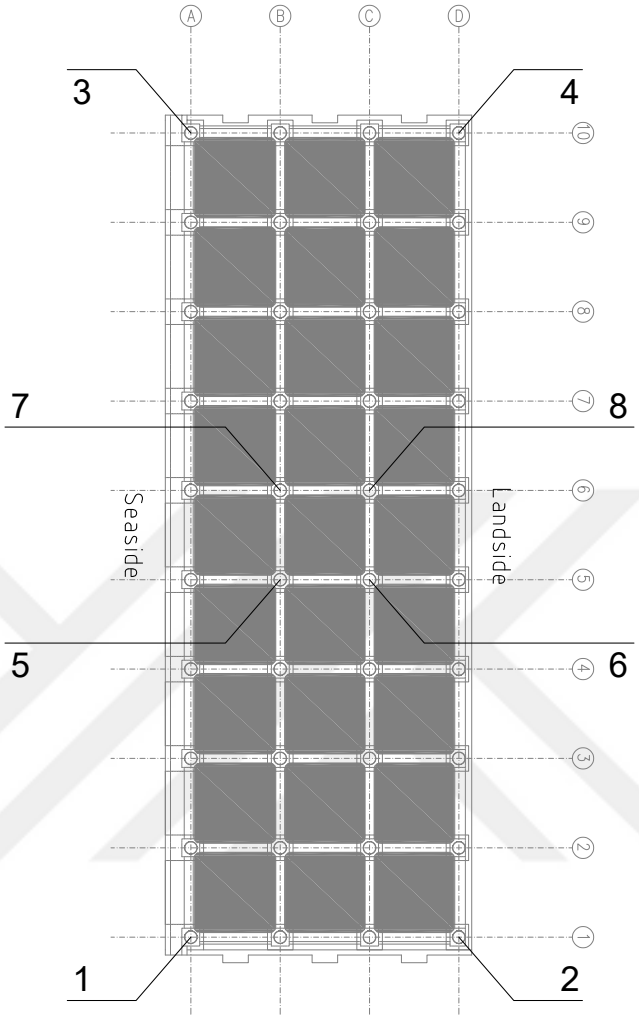

Figure 6.15. Deck Node Numbers.

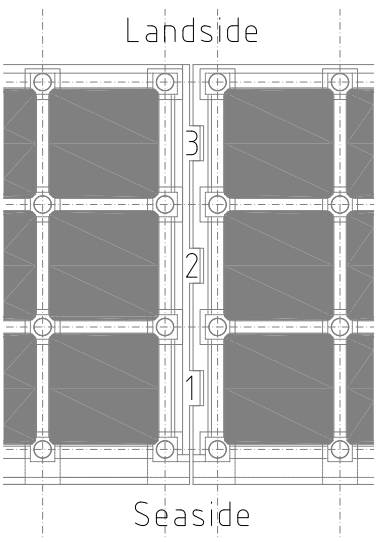

Figure 6.16. Shear Key Node Numbers.

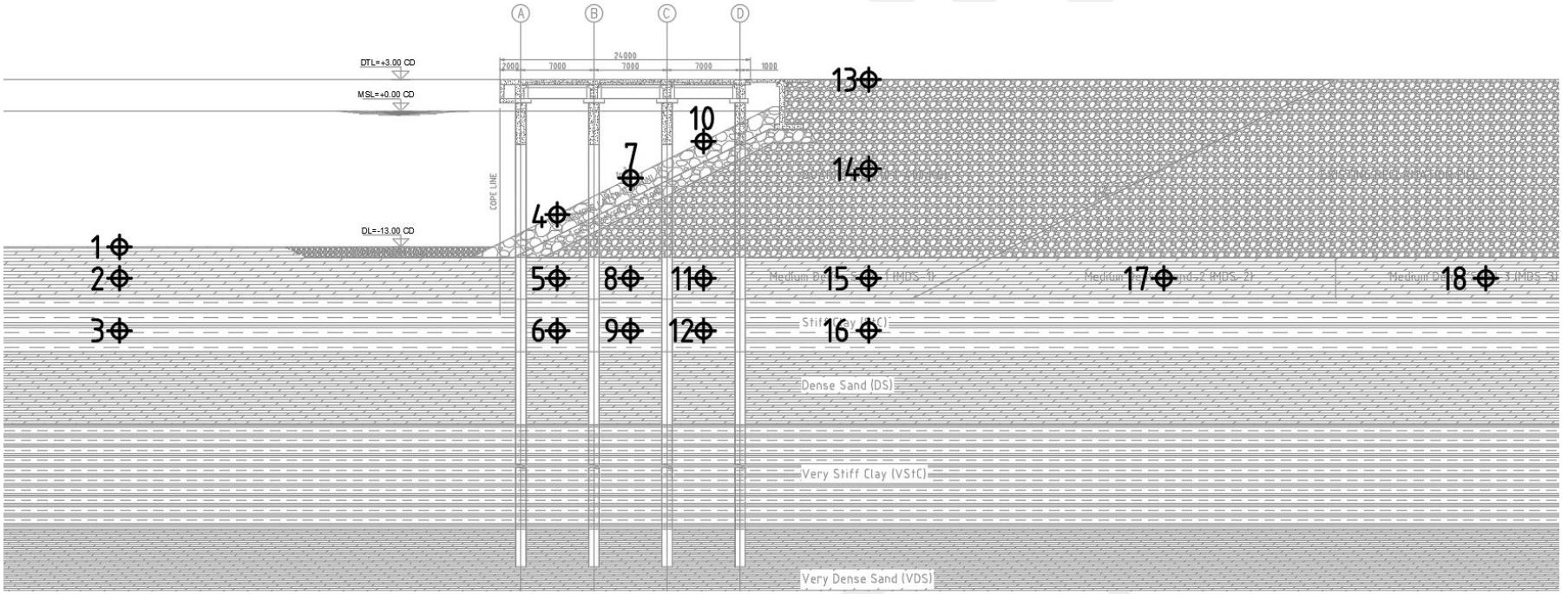

Figure 6.17. Soil Nodes in XZ plane.

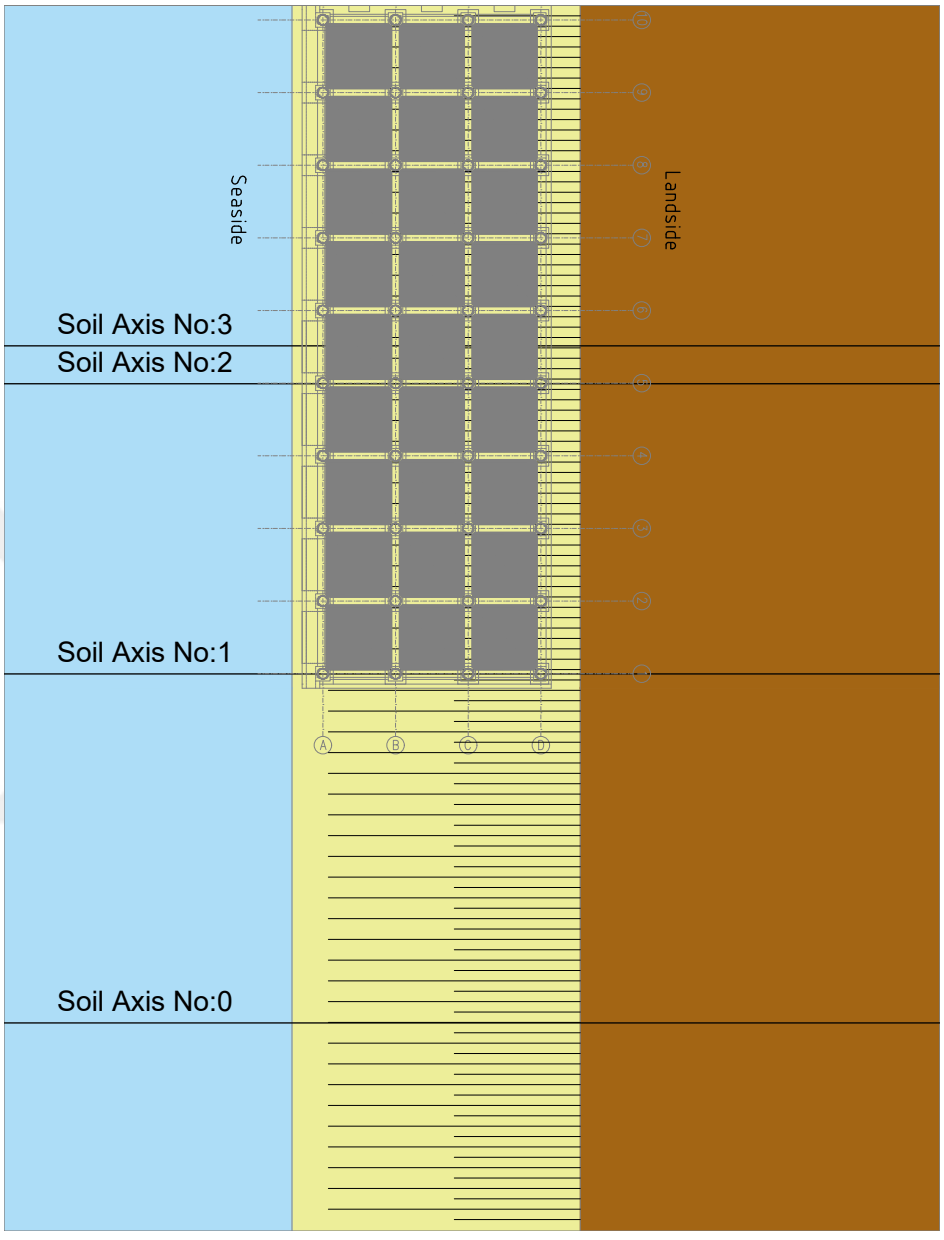

Figure 6.18. Soil Axes in Plan.

7. ANALYSIS CASES

7.1. Wharf Strip Analysis (STRP)

Wharf strip analysis actually resembles plane-strain model for zone elements with one span (7m) thickness in out-of-plane (longitudinal) direction. It includes pile elements, which are located at the middle of the thickness of the strip, defined as frame elements (Figure 7.1). Thus, the pile elements are modeled more rationally than compared to the ones in 2D plane strain model, which is very common in practice. Wharf strip modeling may be particularly important in cases where highly nonlinear soil behaviour is expected, such as in liquefiable soil conditions. Since the piles are modeled as wall elements in plane-strain model, the lateral spreading around piles is not allowed in plane-strain model. It may increase the pile response unnecessarily high levels. Therefore, wharf strip model is employed to represent "two dimensional" character of the wharf systems in this study although the model is actually three-dimensional. Note that this model is analyzed under transverse excitation (T) only. The effect of vertical excitation will be treated in the following sections.

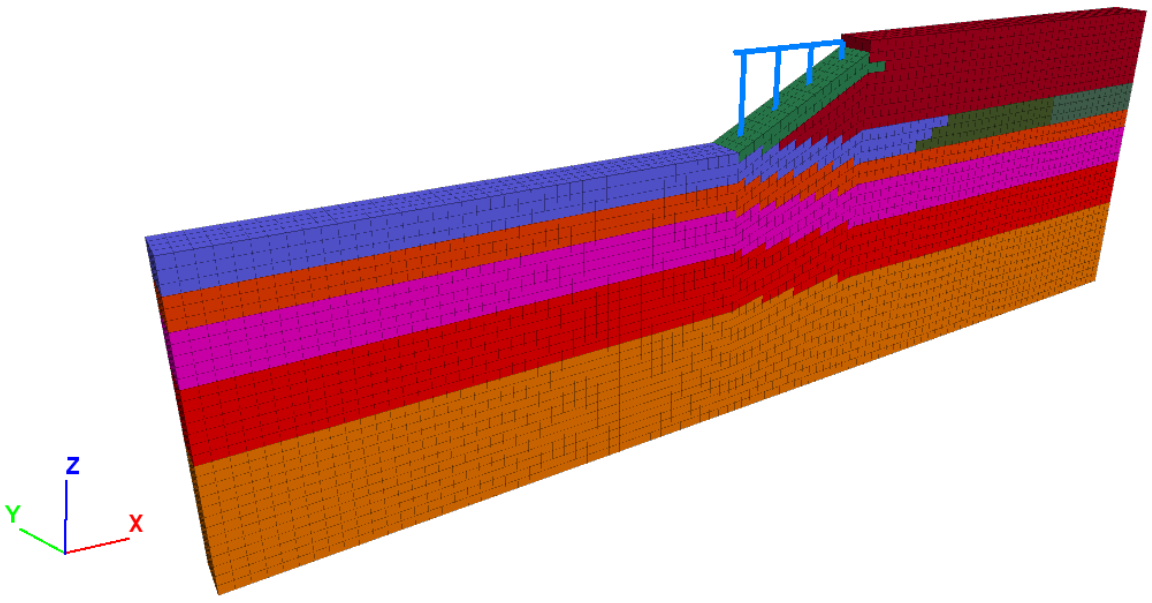

Figure 7.1. Wharf Strip Model.

7.2. Single Module Wharf Analysis with Constant Soil Stratification (1-mod)

Single module wharf system with constant soil stratification is analyzed under four different seismic excitations, namely, transverse excitation only (1-mod-T), longitudinal excitation only (1-mod-L), simultaneous transverse and longitudinal excitation (1-mod-TL), simultaneous transverse, longitudinal and vertical excitation (1-mod-TLV). FLAC3D model of single module wharf system is given in Figure 7.2.

7.3. Multi-Modules Wharf Analysis with Constant Soil Stratification (X-mod)

Two, four and eight-modules wharf systems with constant soil stratification are analyzed under four different seismic excitations, namely, transverse excitation only (X-mod-T), longitudinal excitation only (X-mod-L), simultaneous transverse and longitudinal excitation (X-mod-TL), simultaneous transverse, longitudinal and vertical excitation (X-mod-TLV). FLAC3D models of 2-modules, 4-modules and 8-modules wharf systems are given in Figures 7.3, 7.4 and 7.5 respectively.

Three, five, six and seven-modules wharf systems with constant soil stratification are analyzed under only simultaneous transverse, longitudinal and vertical excitation (X-mod-TLV). For the sake of brevity, FLAC3D model views are not shared herein.

7.4. 8-Modules Wharf Analysis with Changing Soil Stratification (8-mod-LCS)

Eight-modules wharf system with longitudinally changing soil stratification is analyzed under only simultaneous transverse, longitudinal and vertical excitation (8-mod-LCS-TLV). FLAC3D model of 8-modules wharf system is given in Figures 7.6 and 7.7 from two different perspectives in order to depict the changing soil stratification along the embankment clearly. The liquefiable MDS layer starts at zero thickness at the

beginning of embankment and increases to 10 meters thickness at the end. Conversely, StC layer starts with 10m thickness at the beginning of embankment and decreases to zero thickness at the end. The rest of layers remain the same as in the models with constant stratification.

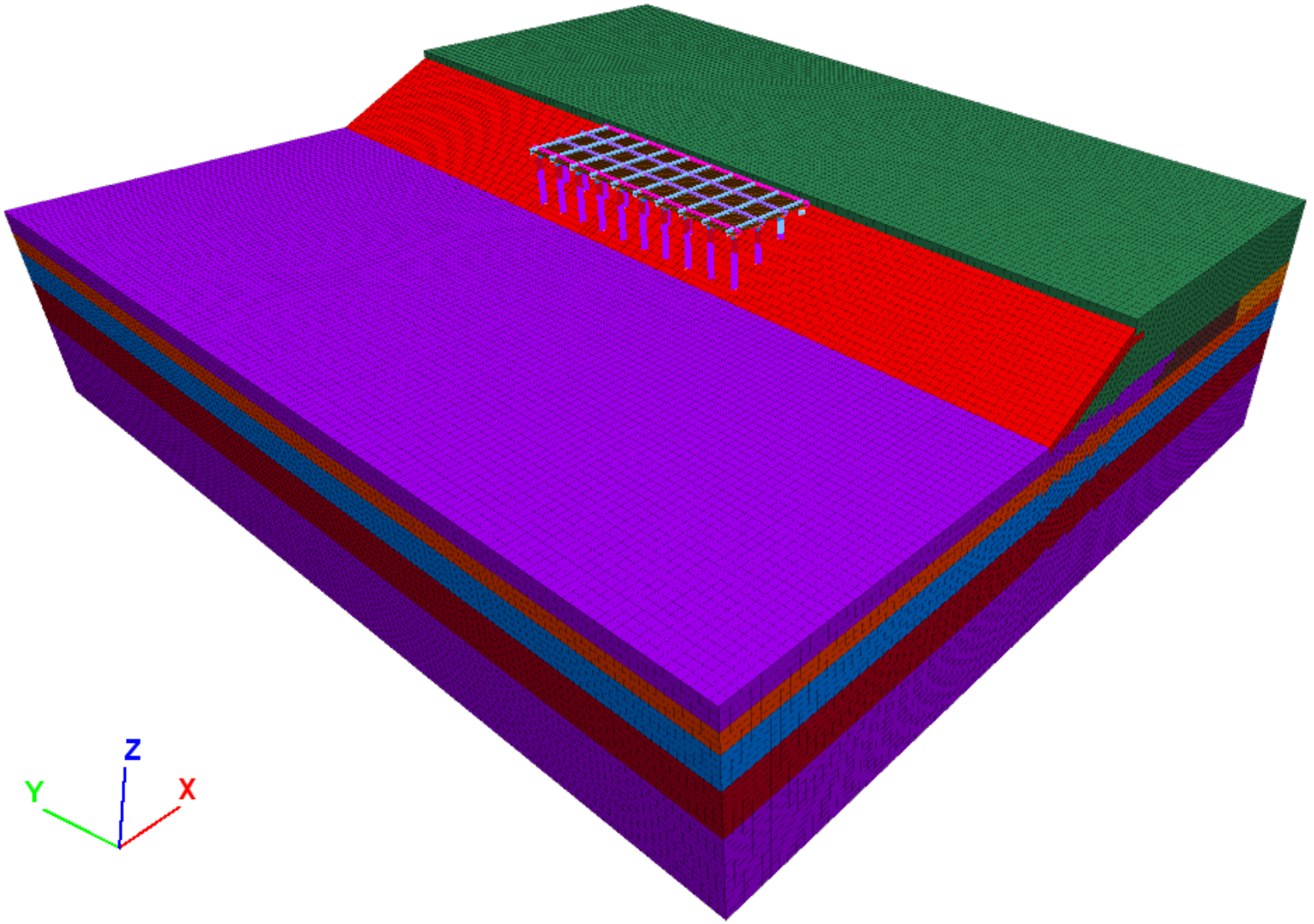

Figure 7.2. 1-Modules Wharf System with Constant Soil Stratification.

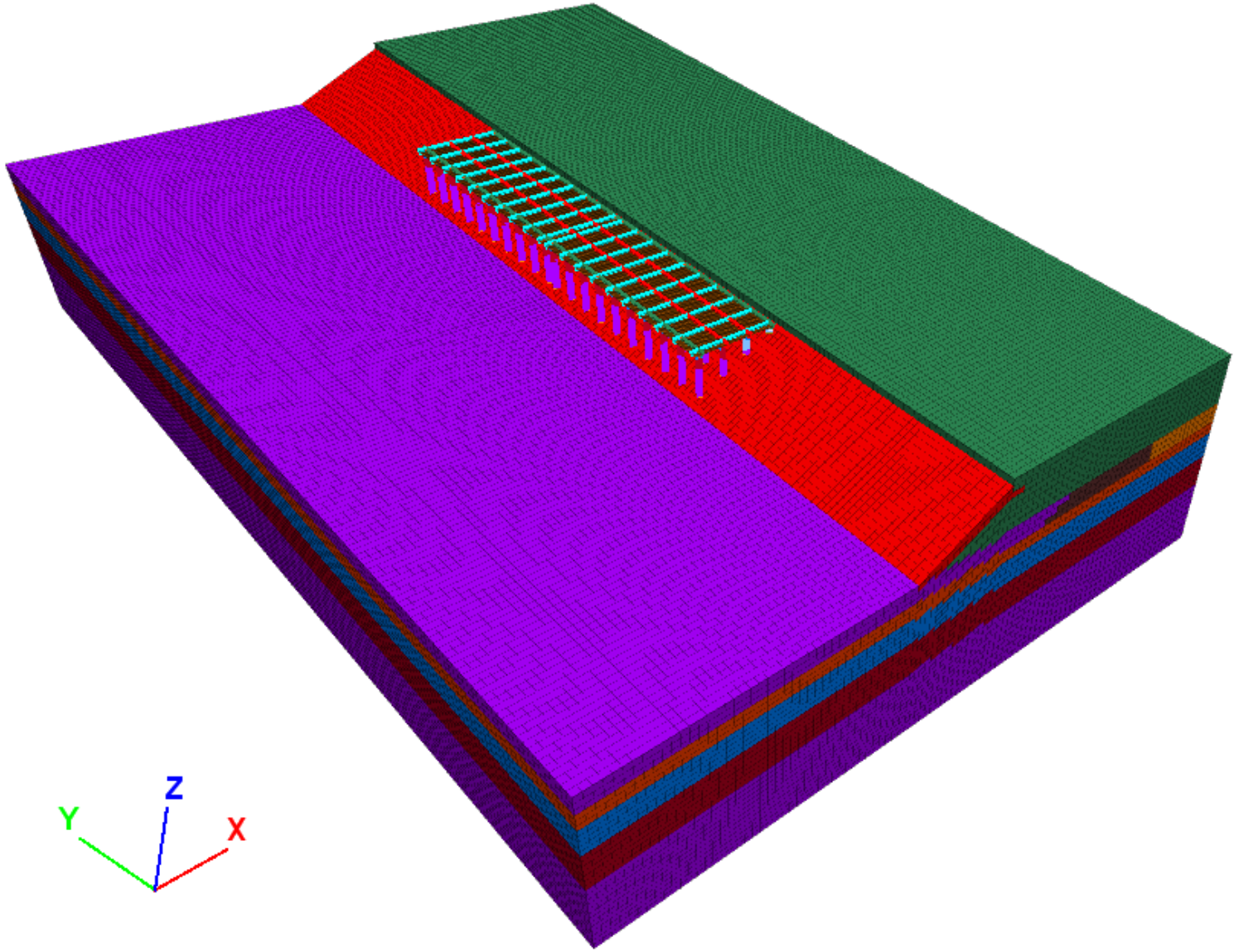

Figure 7.3. 2-Modules Wharf System with Constant Soil Stratification.

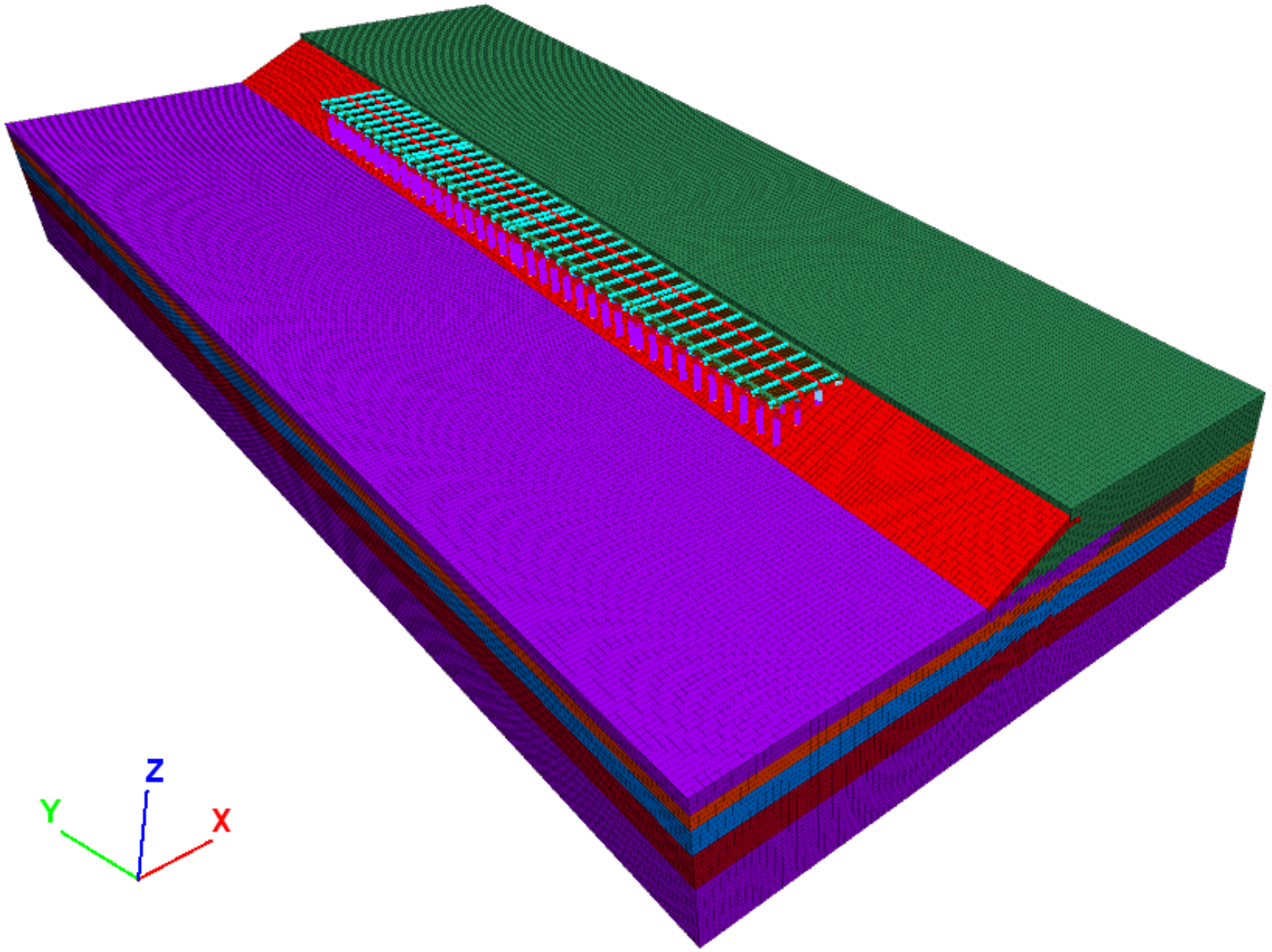

Figure 7.4. 4-Modules Wharf System with Constant Soil Stratification.

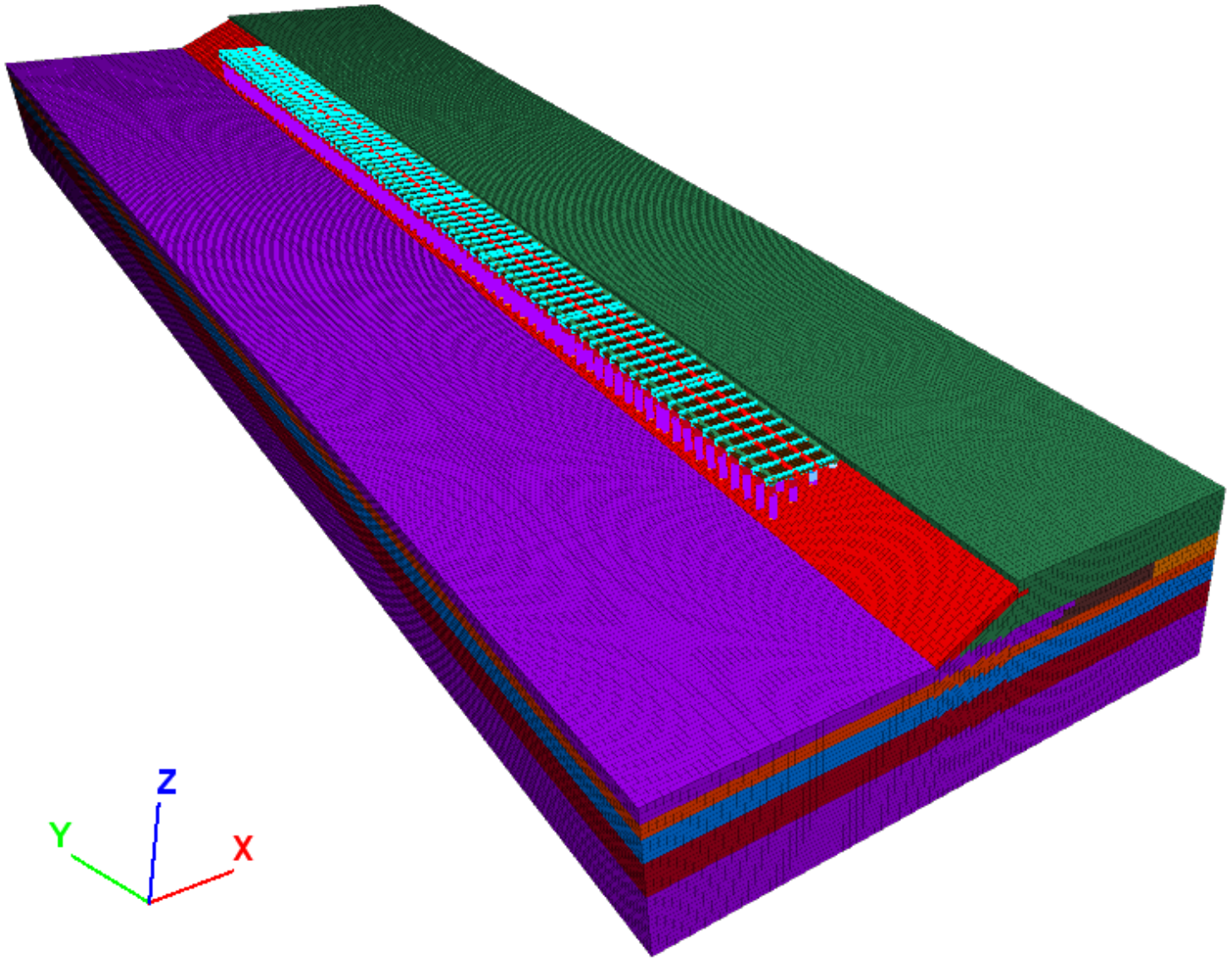

Figure 7.5. 8-Modules Wharf System with Constant Soil Stratification.

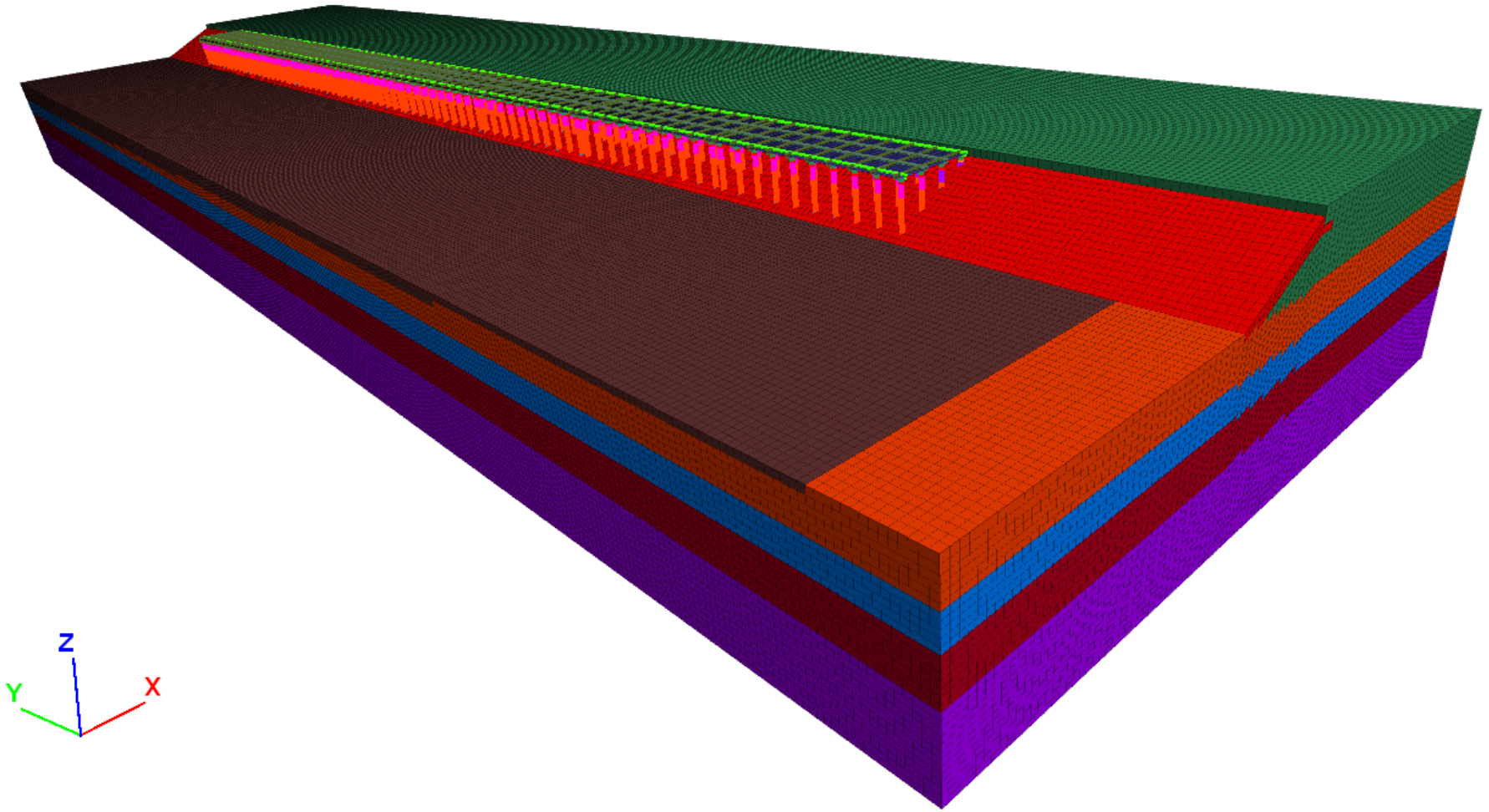

Figure 7.6. 8-Modules Wharf System with Longitudinally Changing Soil Stratification (From 1st Module Towards Last Module).

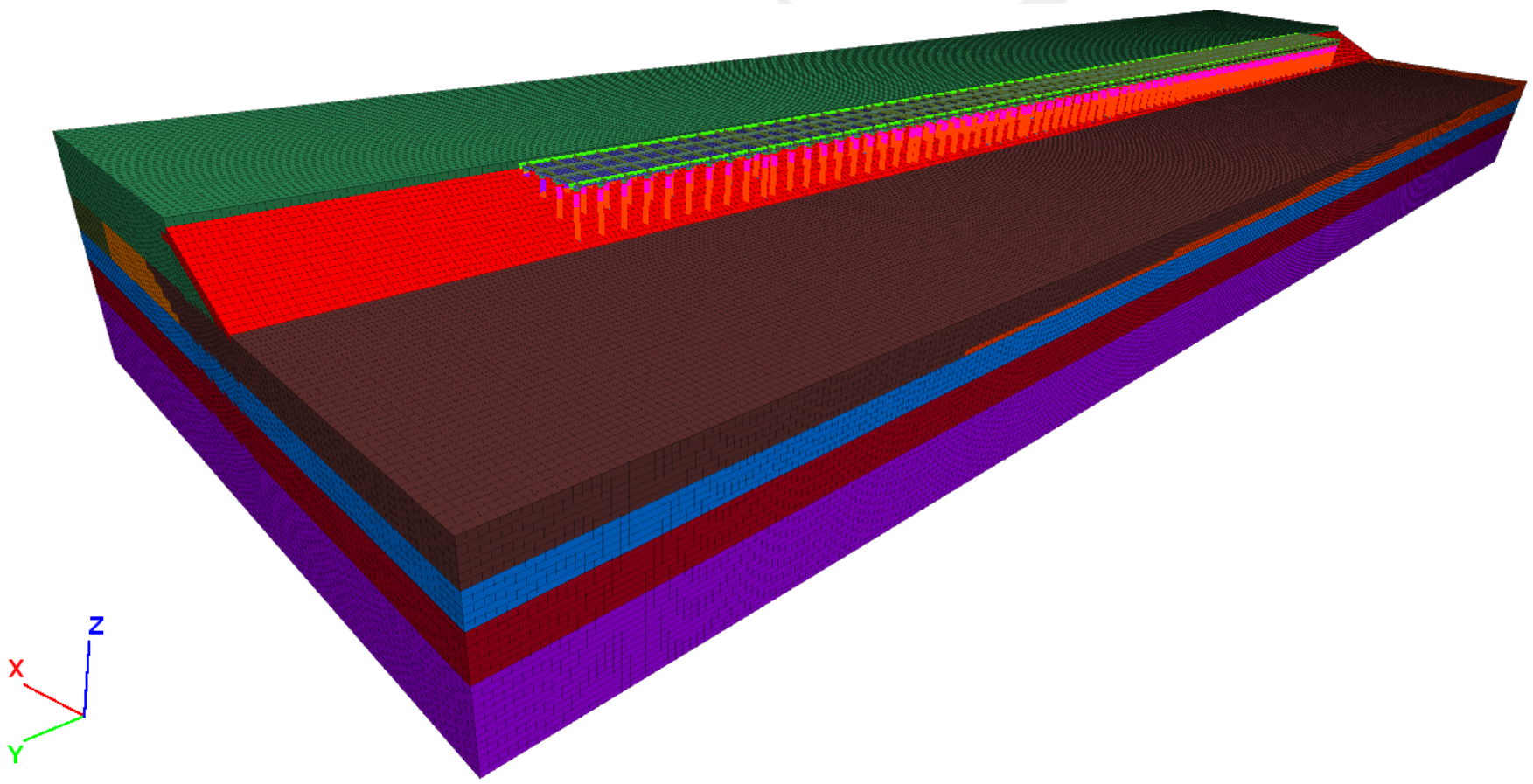

Figure 7.7. 8-Modules Wharf System with Longitudinally Changing Soil Stratification (From Last Module Towards 1st Module).

8. RESPONSE EVALUATIONS AND DISCUSSIONS

This chapter includes evaluations and discussions of the findings obtained through the analysis of the cases.

8.1. Evaluation of Seismic Response for the Wharf Systems with Longitudinally Constant Soil Stratification

In this section, some important aspects are evaluated focusing on the single and multi-segmented wharf systems with constant soil stratification in the longitudinal direction, as detailed in Section 7.2 and Section 7.3.

8.1.1. Importance of Longitudinal Excitation in Liquefiable Soil Condition

The effect of longitudinal excitation is considered in the structural analysis of the wharves but it has not been taken into account in geotechnical engineering practice. Probably because of the obvious failure mechanism of a slope, it is thought that the wharf embankment would mobilize in the sloped (transverse) direction due to the seismic excitation and the deformation occurred in that direction would be much larger than that occurred in the longitudinal direction. Thus, the contribution of longitudinal effects is deemed negligible.

The premise explained above would be correct if the seismic excitation was directionally independent. In other words, if two independent analyses were performed for a wharf system in two orthogonal directions, independent response of the system under transverse excitation could be much larger than that obtained under longitudinal excitation. However, the seismic excitation is not a directionally independent effect. It is the effect happened in all directions simultaneously. Thus, neglecting longitudinal excitation means reducing the efficiency of excitation at the failure surface of embankment.

Figures 8.1, 8.2 and 8.3 illustrate the pore pressure, the effective stress, the shear strain time histories and the shear strain-shear stress relationship respectively for three different excitations, namely, longitudinal (L), transverse (T), simultaneous transverse and longitudinal excitation (TL). Note that these figures are obtained from the 1-mod system analysis results. The response quantities are taken from Soil Axis-2 and Node-15 (Figure 6.17 and 6.18).

The reduction in effective stress (Figure 8.2) due to the pore pressure development (Figure 8.1) and the increase in shear strain (Figure 8.3) consistent with the effective stress reduction clearly demonstrate the effect of soil liquefaction in MDS layer under T, L and TL excitation.

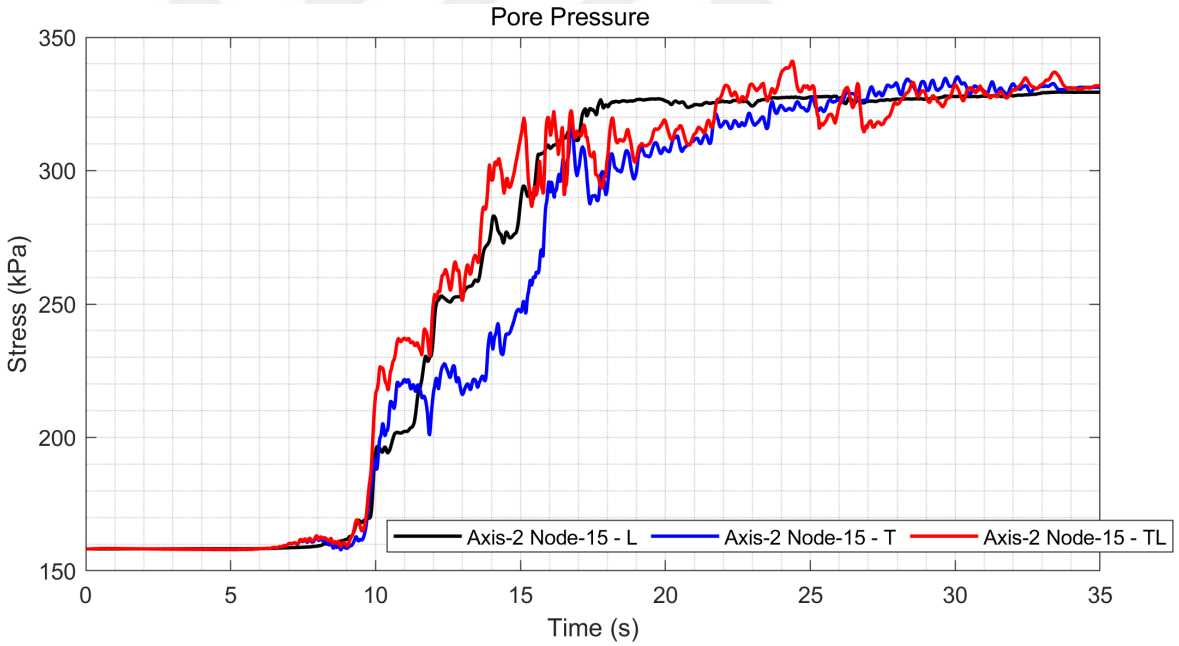

Figure 8.1. Effect of Longitudinal Excitation on Pore Pressure (Soil Axis-2 Node-15).

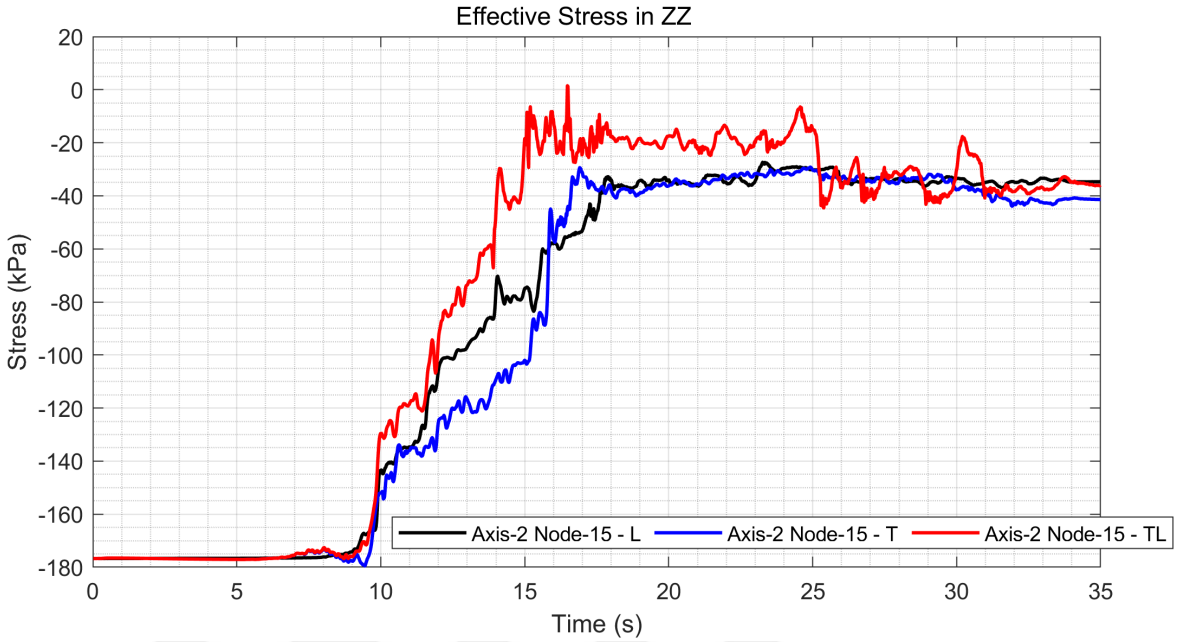

Figure 8.2. Effect of Longitudinal Excitation on Effective Stress (Soil Axis-2 Node-15).

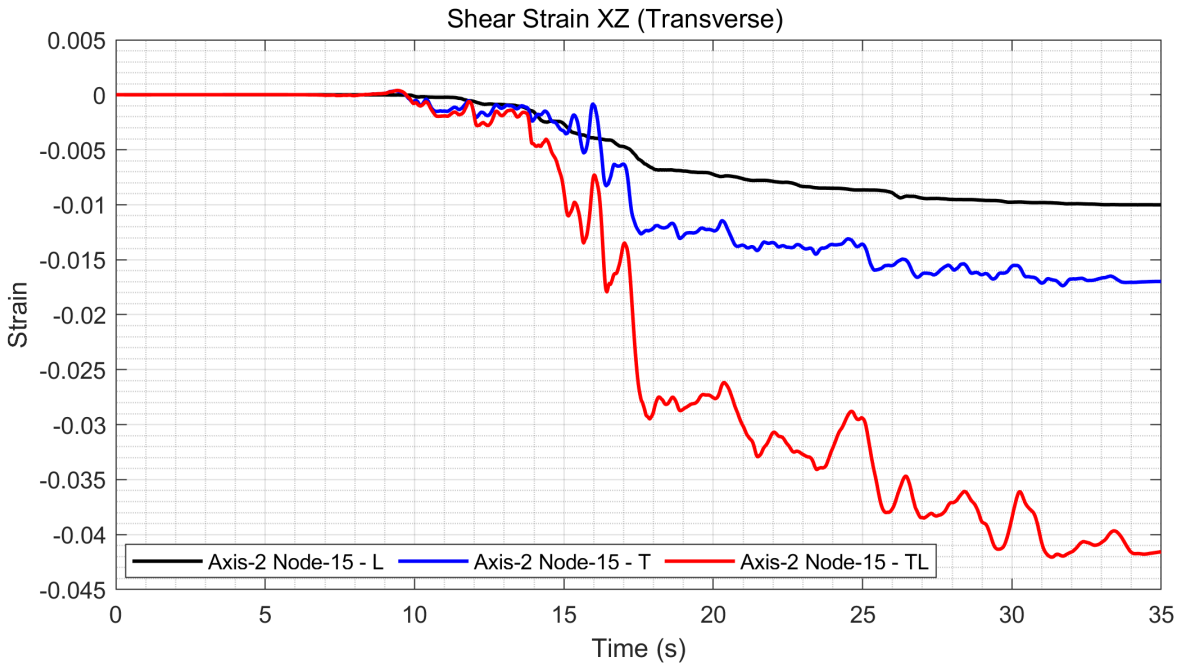

Figure 8.3. Effect of Longitudinal Excitation on Soil Shear Strain (Soil Axis-2 Node-15).

It is seen from Figures 8.1 and 8.2 that the longitudinal excitation and transverse excitation contribute equally to the pore pressure development and the effective stress reduction. The black curve in Figure 8.3 shows that the quasi-static soil deformation, which reaches 1% shear strain in transverse direction at the end of ground shaking, is occurred under the only longitudinal excitation. In other words, the slope is mobilized in transverse direction without any transverse excitation. Since the direction of excitation and the direction of mobilization is perpendicular to each other, the inertia of soil is not effective in the transverse direction, thereby resulting in quasi-static deformation. Similar trend can also be observed from the black curve in Figure 8.5, which shows the displacement response of the embankment crest.

The blue curve in Figure 8.3 shows the shear strain increase in transverse direction due to the transverse excitation. Although the longitudinal excitation has a similar influence on pore pressure generation as the transverse excitation (Figure 8.1), the shear strain level reaches a greater value, 1.7%, than that obtained from the longitudinal excitation. The reason is that the inertia of soil contributes the mobilization of embankment in transverse direction since the excitation direction is the same with the mobilization direction.

The red curve in Figure 8.3 demonstrates the increase in shear strain under simultaneous transverse and longitudinal excitation. It reaches 4.2% shear strain, which is considerably larger than that obtained from the transverse excitation at the end of ground shaking. It clearly shows the contribution of longitudinal excitation on the soil deformation. The simultaneous application of transverse and longitudinal excitation causes to reduce the shear strength at the failure surface earlier than that caused by transverse excitation only (between t=14-18s). The embankment with reduced shear strength of soil at the failure surface is exposed to ground shaking for a longer duration, making it more vulnerable to excessive deformation. A sudden leap of shear strain (red curve) from 1% to 3% corresponding to t=14-18s can be observed in Figures 8.3 and 8.4.

The crest displacement of embankment in transverse direction is calculated as 0.45m at the end of ground shaking under transverse excitation only whereas it is calculated as 0.65m under simultaneous transverse and longitudinal excitation. Note that these displacements are total displacements (Figure 8.5).

Figures 8.6 and 8.7 show the relative displacement plots of Axis-01 piles in transverse and longitudinal direction respectively for three excitation types. Note that A-axis represents seaside pile and D-axis represents landside pile.

The displacement response trend of piles is consistent with the soil deformation as expected. Again, the displacement of piles in the transverse direction due to longitudinal excitation is clearly observed. The transverse displacement response of pile at the top level under simultaneous transverse and longitudinal excitation is around 0.45m. Corresponding transverse displacement under only transverse excitation is 0.22m (Figure 8.6).

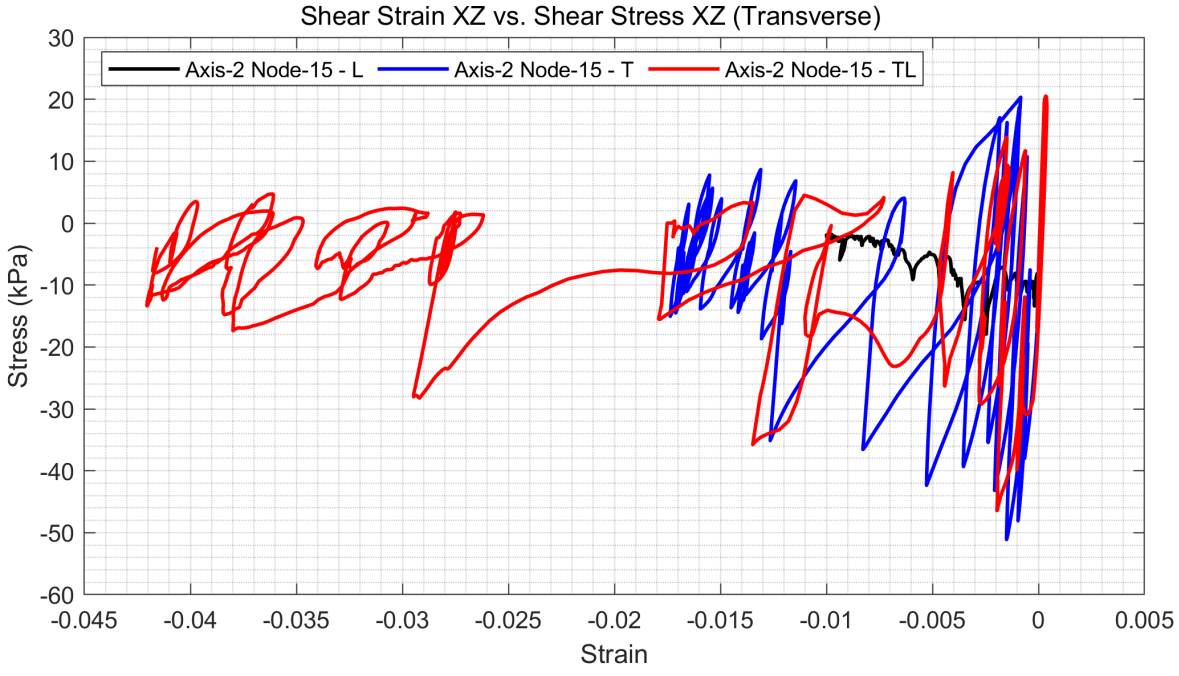

Figure 8.4. Effect of Longitudinal Excitation on Soil Shear Strain (Soil Axis-2 Node-15).

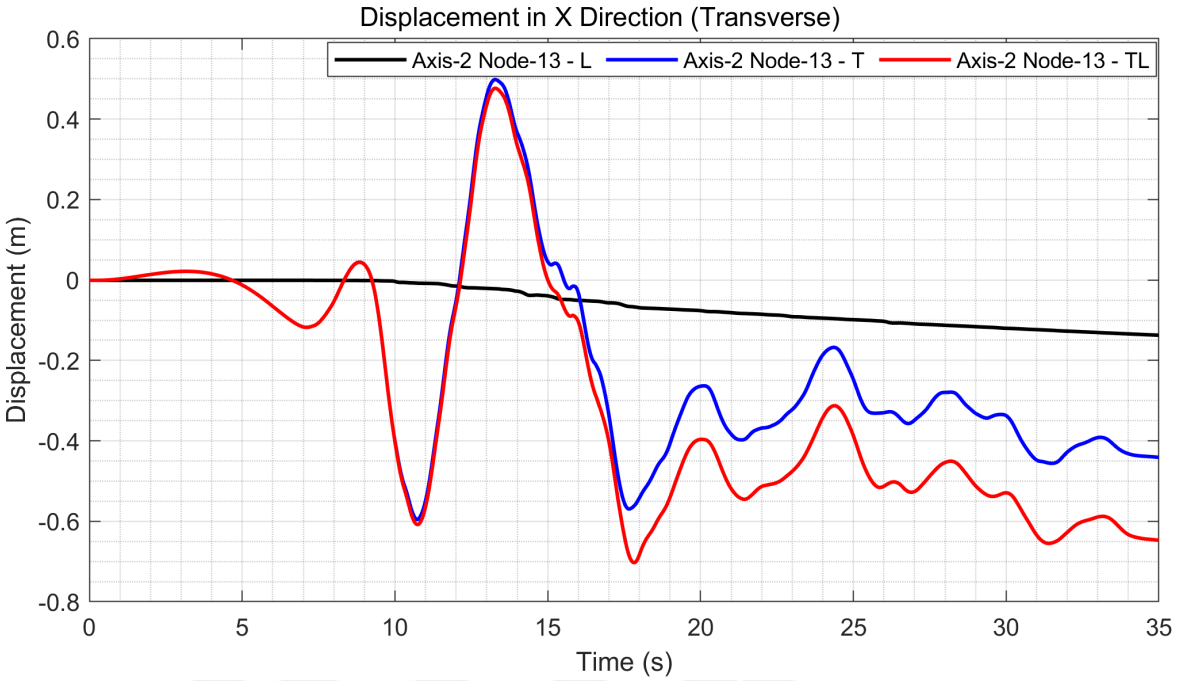

Figure 8.5. Effect of Longitudinal Excitation on Soil Displacement in Transverse Direction (Soil Axis-2 Node-13).

Figures 8.7 shows the displacement response plot in longitudinal direction under three excitation types. It is observed that the top relative displacement of piles in longitudinal direction due to simultaneous transverse and longitudinal excitation is approximately 0.09m. It is considerably larger than that obtained under only longitudinal excitation (0.02m). It proves the importance of bi-directional excitation.

The plastic hinge locations occurred under T and TL excitation is illustrated in Figures 8.8. The plastic hinge occurrence is not observed under L excitation.

The relative rotation plots in transverse and longitudinal direction are given in Figures 8.9 and 8.10 respectively. They demonstrate the similar response trend with the soil deformation. Note that the abrupt changes at the RC plugs indicate plastic hinge occurrences. The effect of longitudinal excitation on the plastification is clearly observed at the RC plugs. The rotations at the seaside (Axis-A and Axis-B) plug hinges are notably greater than those of the landside (Axis-C and Axis-D) plug hinges.

Figures 8.11, 8.12, 8.13 and 8.14 show the moment and shear diagrams for the piles in both transverse and longitudinal direction under three types of excitation. Similar trend can be seen for the internal forces as well.

Figures 8.15 and 8.16 show the SRSS envelopes of internal forces. These quantities are important for the design of piles. The moments of piles can reach 1.5 times of those obtained under only transverse excitation in StC layer when TL excitation is imposed. Those can reach 2.0 times inside the rockfill and RC plugs.

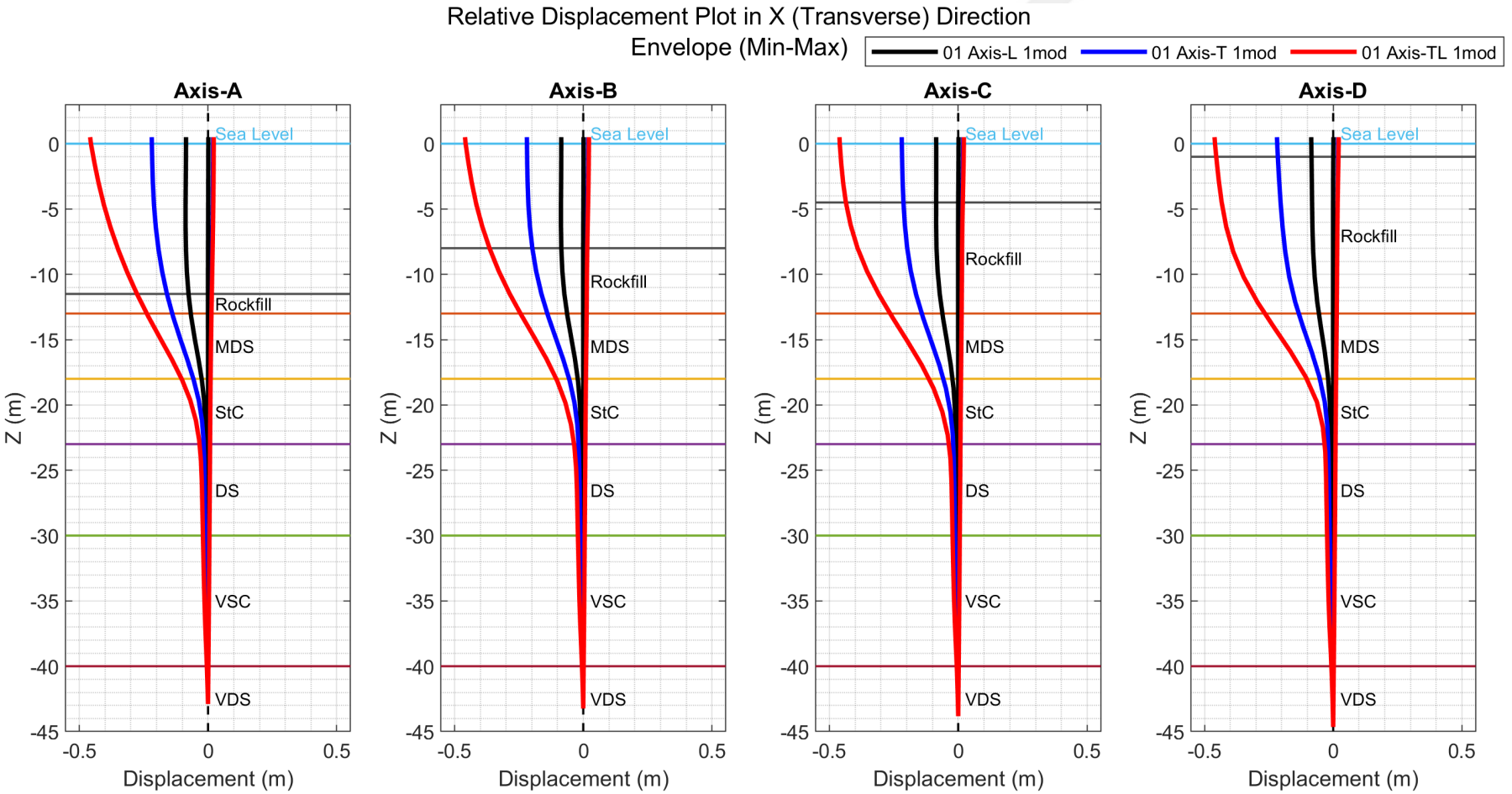

Figure 8.6. Effect of Longitudinal Excitation on Pile Relative Displacements in Transverse Direction.

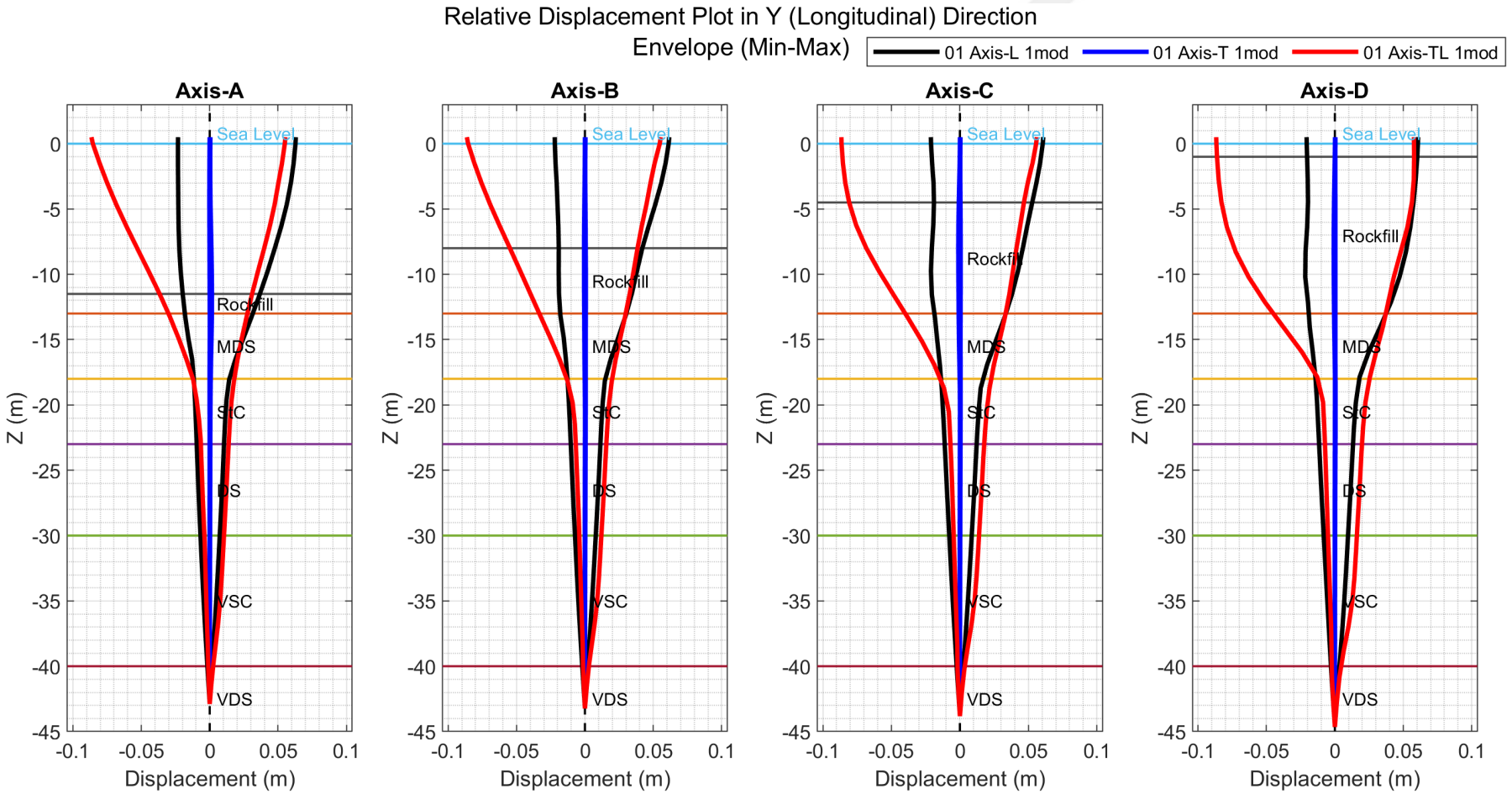

Figure 8.7. Effect of Longitudinal Excitation on Pile Relative Displacements in Longitudinal Direction.

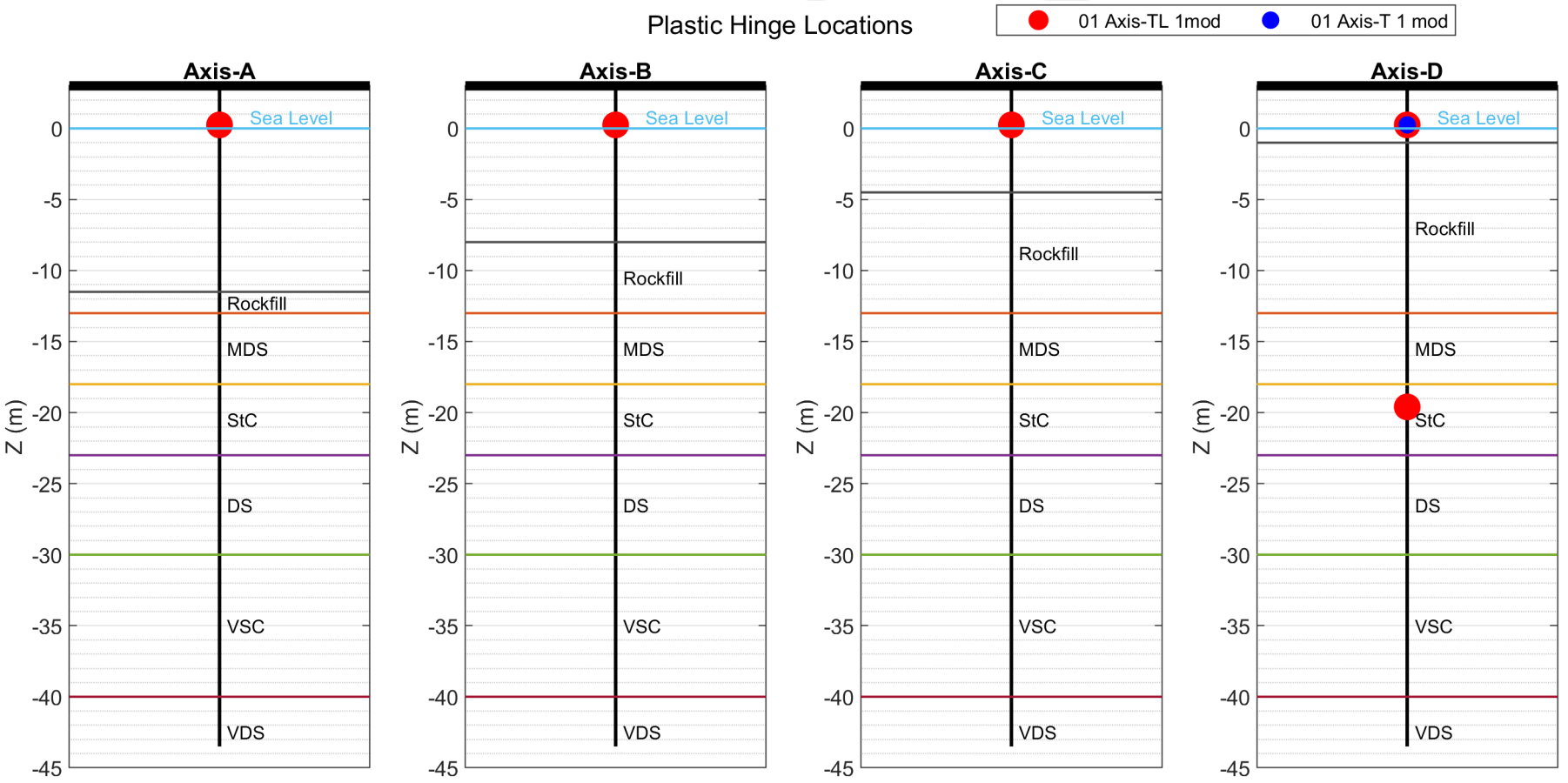

Figure 8.8. Plastic Hinge Locations.

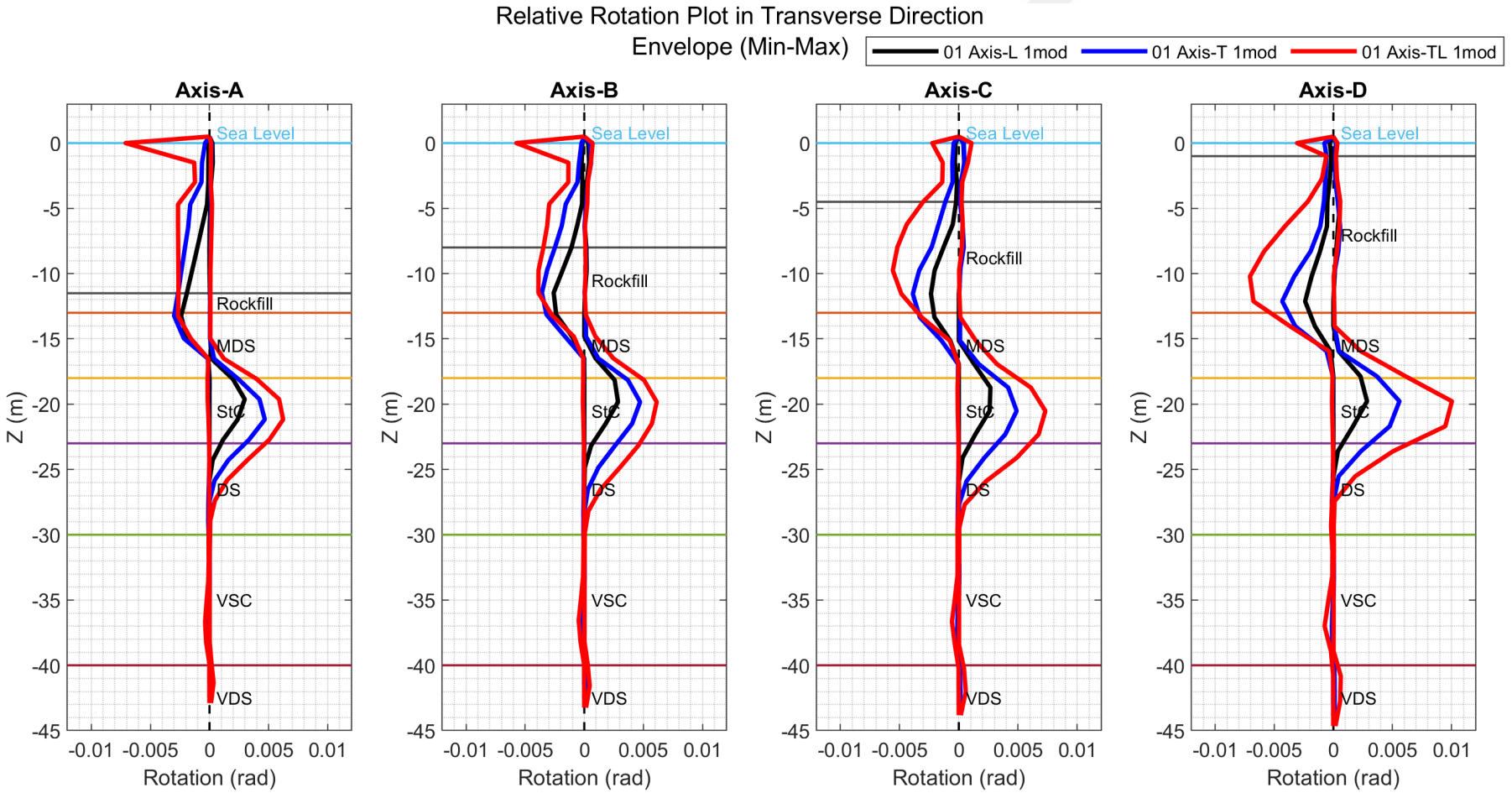

Figure 8.9. Effect of Longitudinal Excitation on Pile Relative Rotations in Transverse Direction.

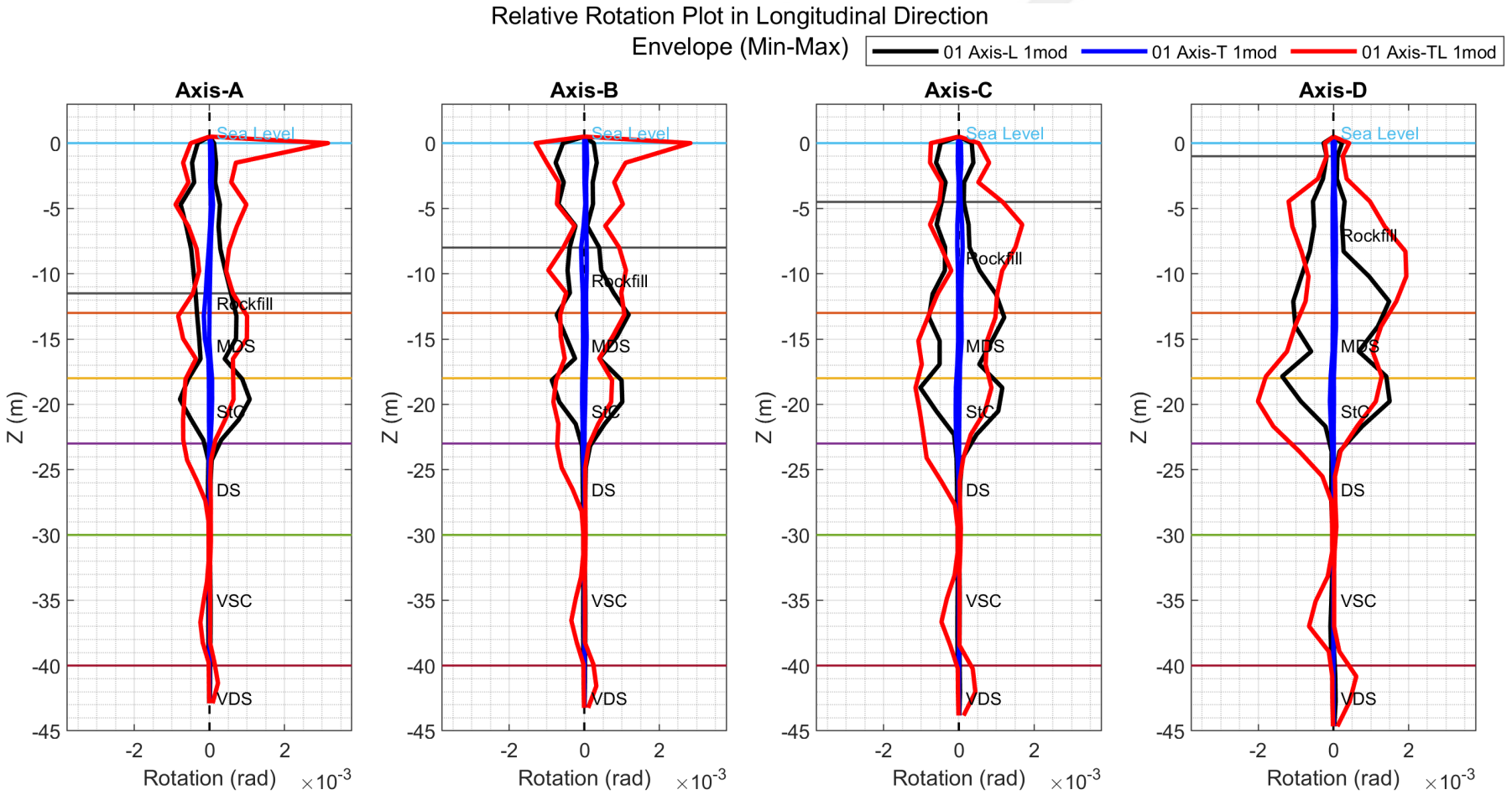

Figure 8.10. Effect of Longitudinal Excitation on Pile Relative Rotations in Longitudinal Direction.

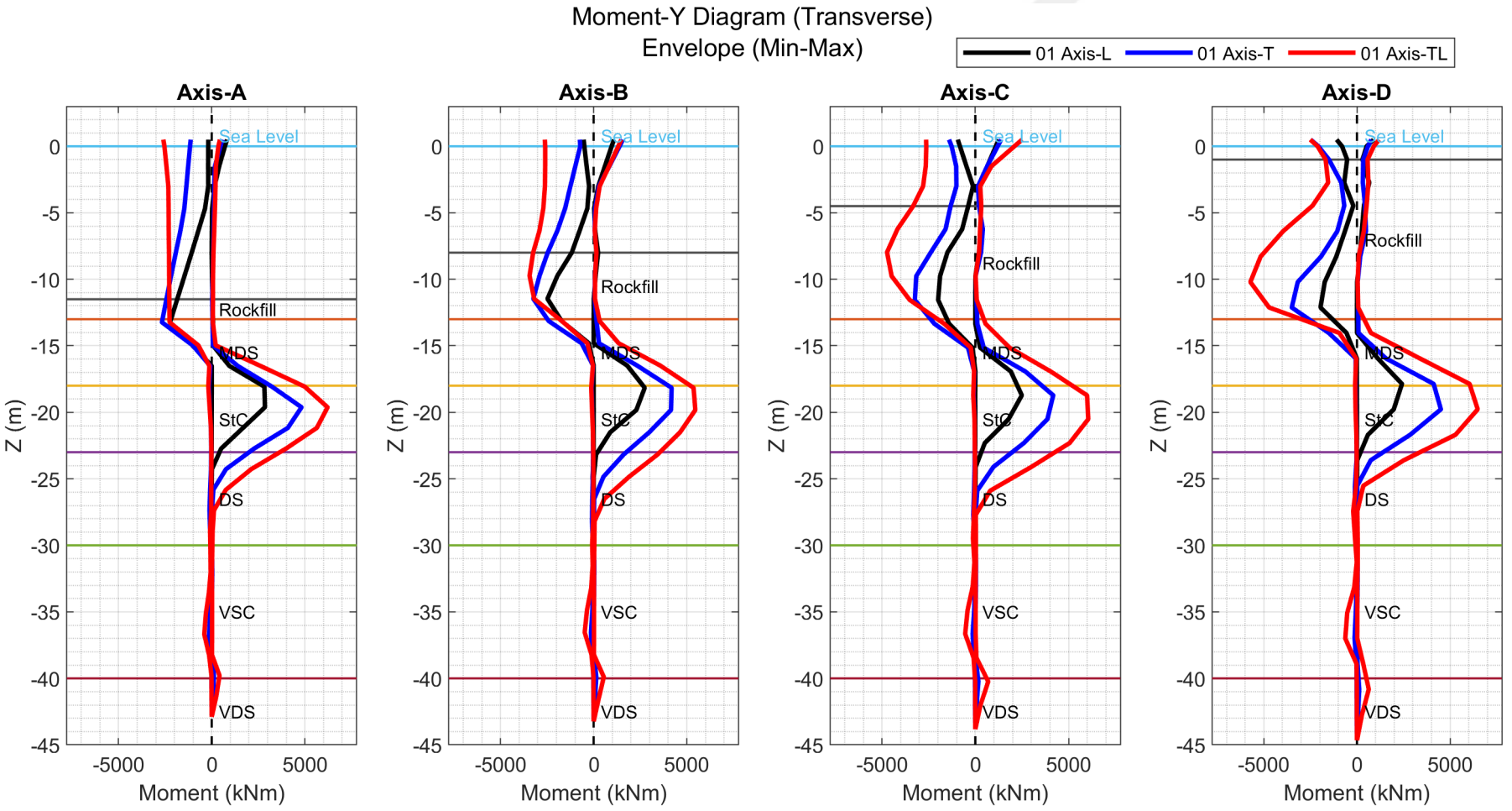

Figure 8.11. Effect of Longitudinal Excitation on Pile Moments in Transverse Direction.

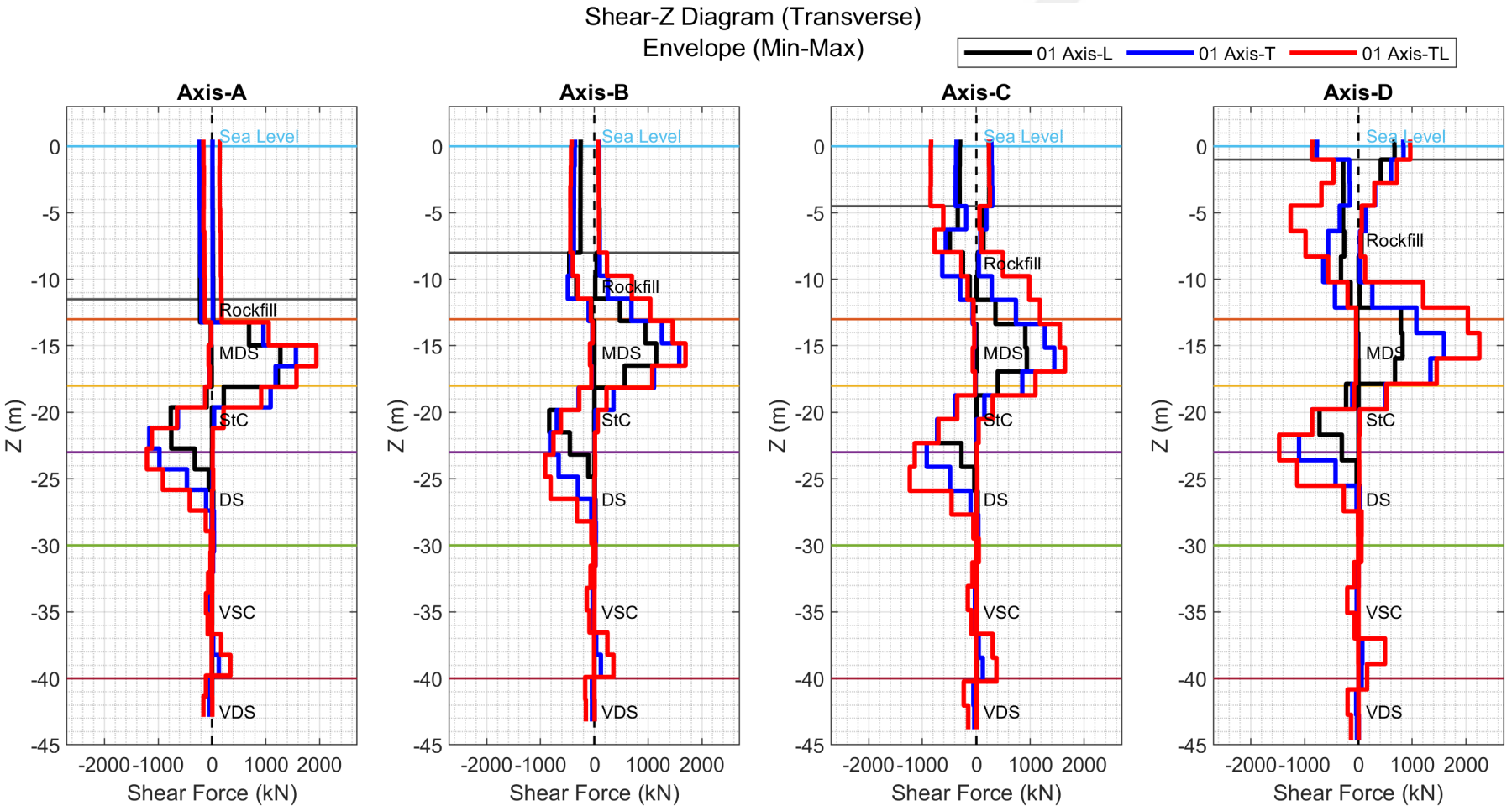

Figure 8.12. Effect of Longitudinal Excitation on Pile Shear Forces in Transverse Direction.

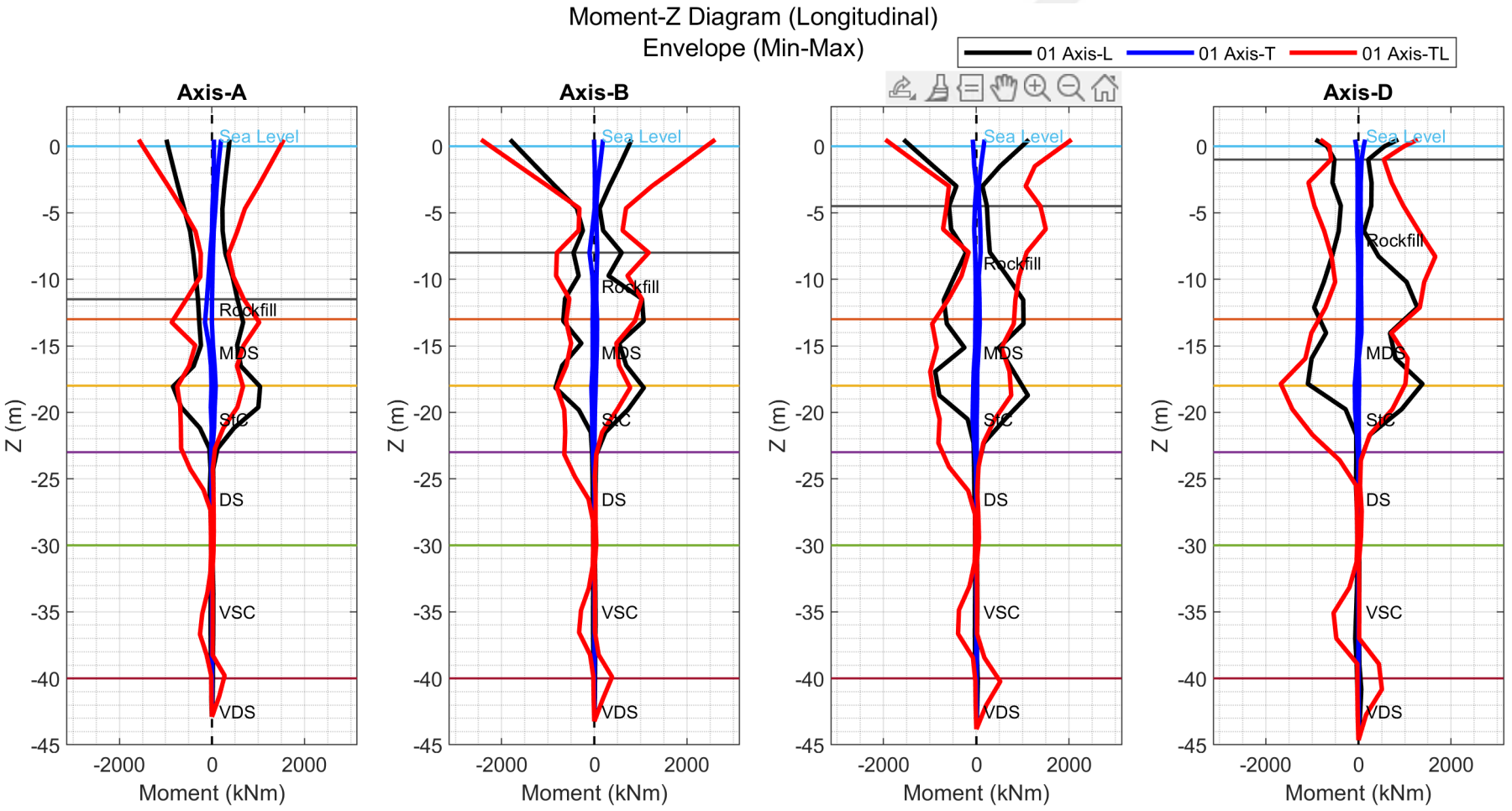

Figure 8.13. Effect of Longitudinal Excitation on Pile Moments in Longitudinal Direction.

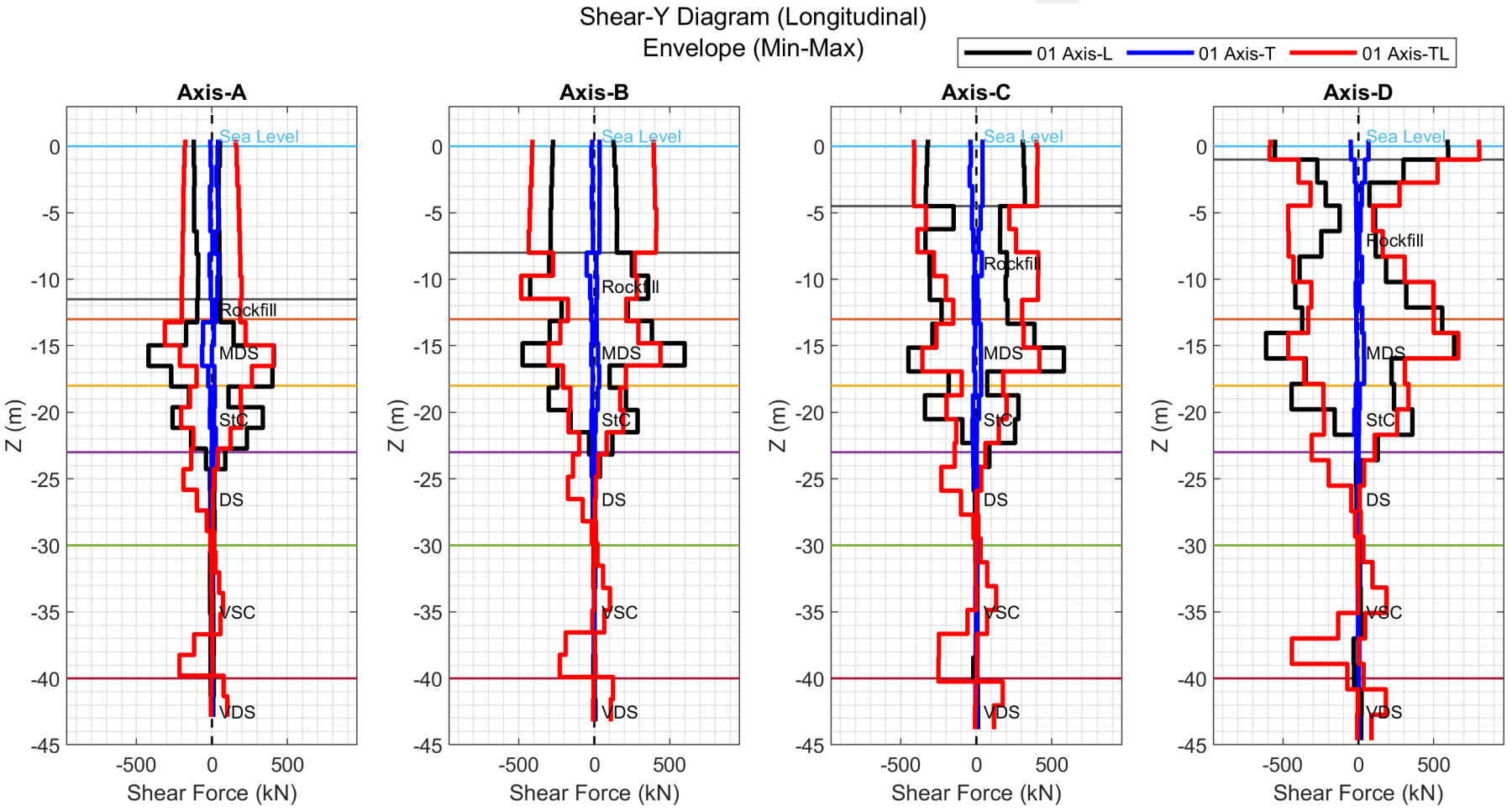

Figure 8.14. Effect of Longitudinal Excitation on Pile Shear Forces in Longitudinal Direction.

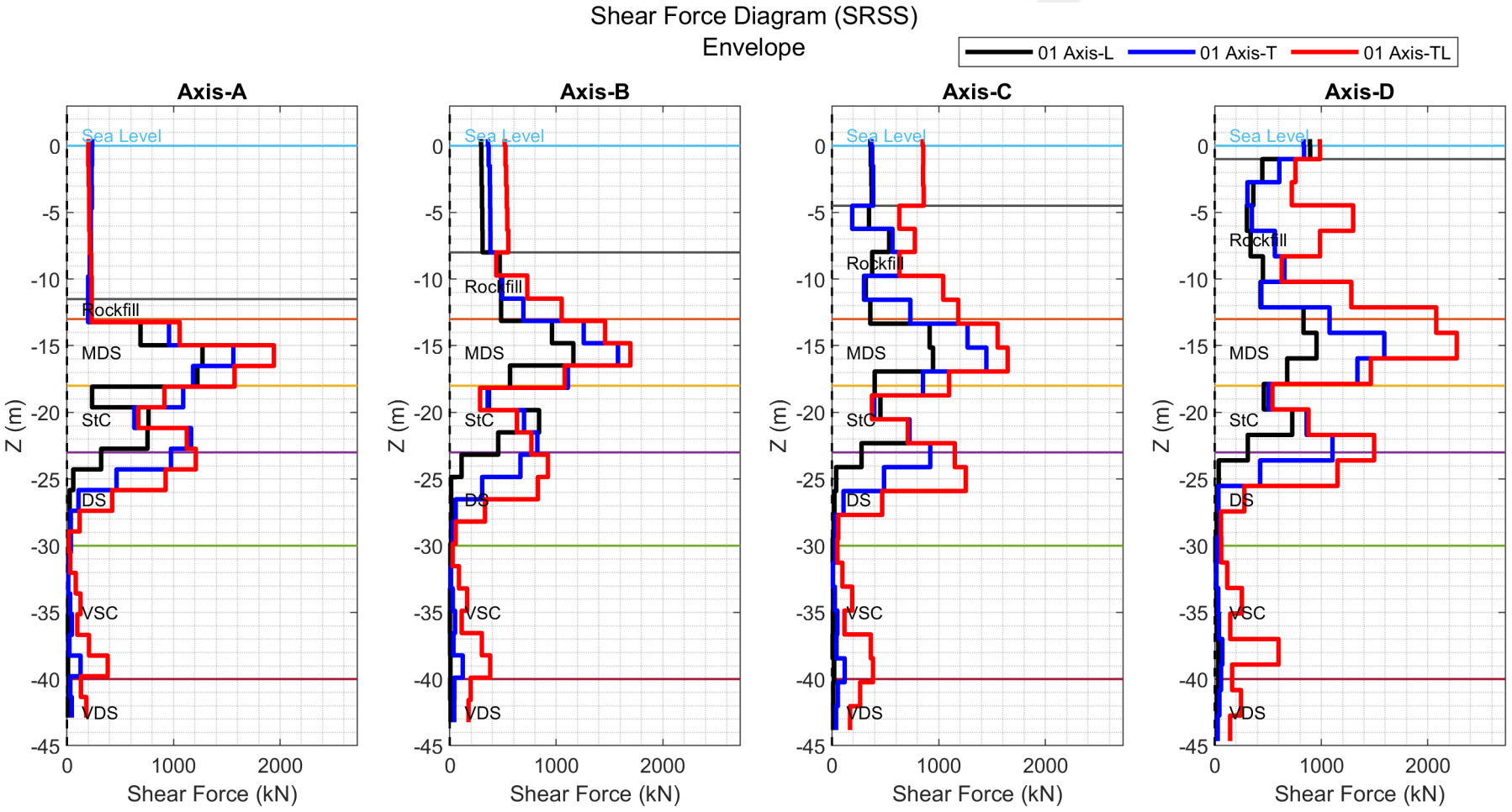

Figure 8.15. Effect of Longitudinal Excitation on Pile Shear Forces (SRSS).

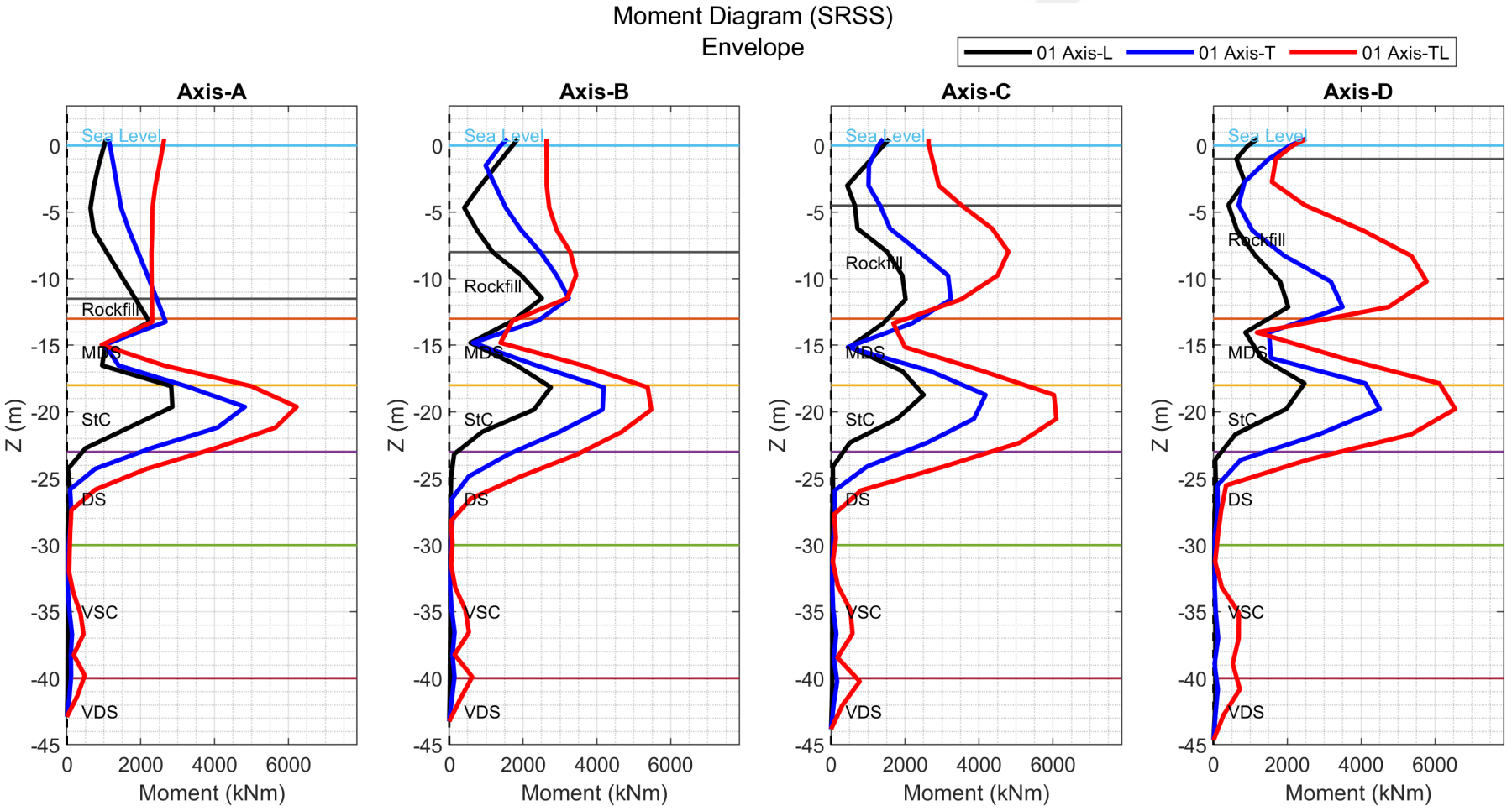

Figure 8.16. Effect of Longitudinal Excitation on Pile Moments (SRSS).

8.1.2. Dynamic Magnification Factors Incorporating Soil Behavior and SSI

The so-called "Dynamic Magnification Factor" (DMF) concept, which refers to a simplified method in traditional design practice, is developed to estimate the three-dimensional response of wharf decks from the calculated deck response of a two-dimensional structural analysis model by directly multiplying it with a predefined coefficient. In other words, this concept attempts for an easy estimation of three-dimensional response of a wharf system without actually performing a three-dimensional analysis.

DMF is essentially a concept that estimates the effect of longitudinal excitation on a specific response quantity (deck displacement), without considering soil behavior and soil-structure interaction (SSI). However, as mentioned in Section 9.1.1, the soil behavior, particularly in liquefiable soils, has a considerable influence on the structural response. Considering those effects, DMF values are calculated for the cases defined in this thesis. The wharf strip model is employed corresponding to two dimensional analysis models of the traditional design practice.

Figure 8.17 illustrates the DMF values incorporating soil behavior and SSI. The presence of longitudinal excitation causes the deck displacements to increase 2.25 (in average) times compared to those obtained from wharf strip analysis solved under transverse excitation only. DMF values in the literature is given as 1.1 for inner modules and it can reach to 1.5 for outer modules [58]. The effect of soil behavior and SSI is significant that cannot be ignored for the cases defined in this study. Secondly, the DMF values are almost constant for all modules of wharf systems having different number of modules. It demonstrates that torsional behavior, which can increase the relative movements of modules, is not significant.

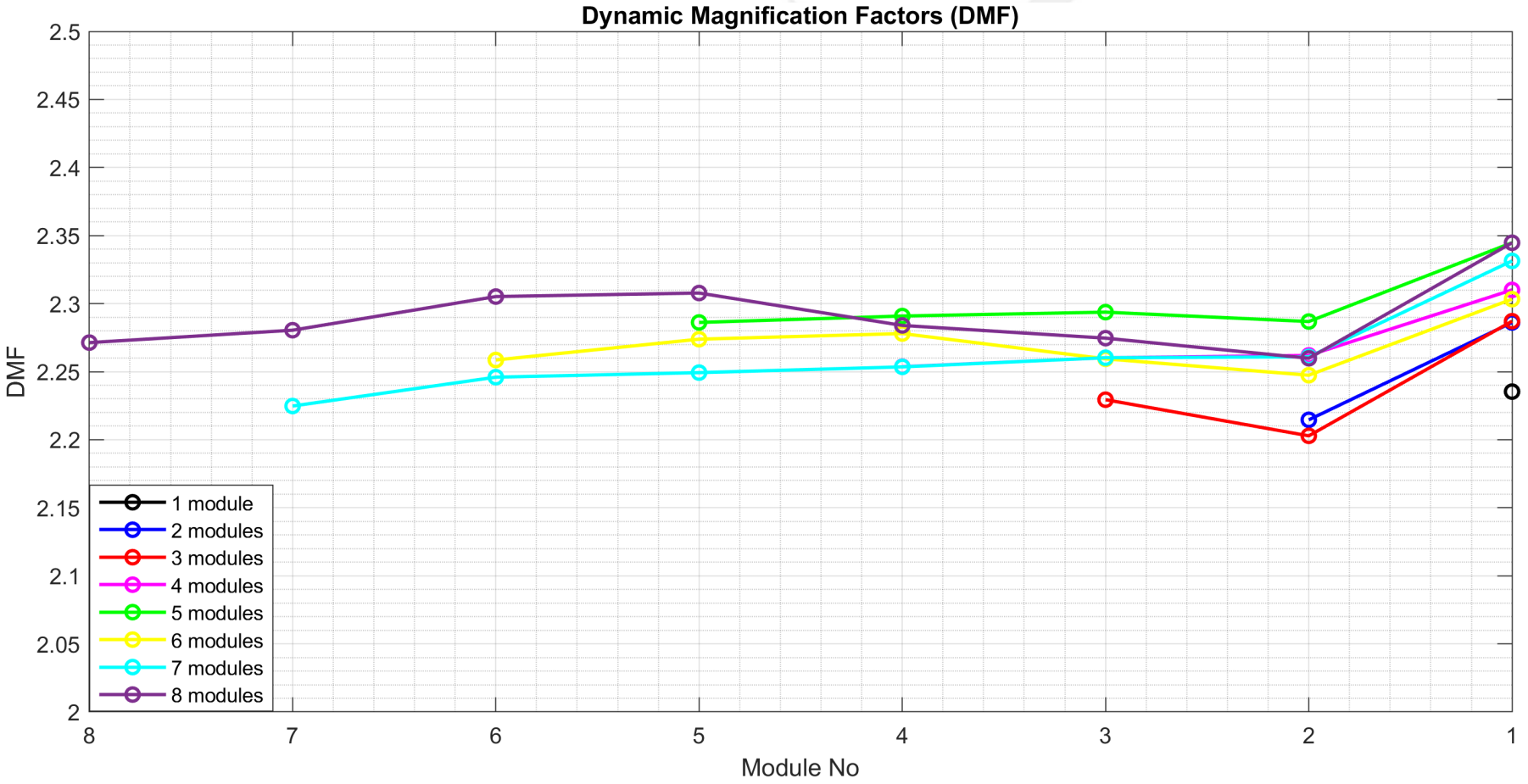

Figure 8.17. Dynamic Magnification Factors Incorporating Soil Behavior and SSI.

8.1.3. Effect of Liquefaction on Seismic Response

The importance of liquefaction on the soil and structural response was clearly demonstrated in the previous section. In this section, the level of soil deformations due to liquefaction is treated through a parametric study. In this regard, the liquefiable MDS layer, which is the critical layer for the seismic response of wharf system, is defined by five different group of relative densities (Dr). As it is mentioned in Section 6.2, the MDS layer is consisting of three different sections, namely, MDS-1, MDS-2 and MDS-3 (Figure 6.2). The relative densities assigned to the layers within the context of the parametric study is tabulated in Table 8.1. The other soil parameters used in the analyses are not given herein for the sake of the brevity. Those are taken from Tables 6.1, 6.2, 6.3 and 6.4 in accordance with the given relative densities. Note that the analyses in this section are performed for single module wharf system.

Table 8.1. Relative Densities (Dr) for MDS layers.

Layer No	Analysis-1	Analysis-2	Analysis-3	Analysis-4	Analysis-5
MDS-1	0.47	0.51	0.59	0.66	0.72
MDS-2	0.51	0.59	0.66	0.72	0.78
MDS-3	0.59	0.66	0.72	0.78	0.85

Figures 8.18 and 8.19 demonstrate the pore pressure and effective stress time histories for five different analysis. The pore pressures increase with increasing relative densities, the effective stresses decrease with increasing relative densities as expected. As a result, the soil deformations are increasing in time drastically with decreasing relative densities (Figures 8.20 and 8.21), The soil displacements at embankment crest increase in line with the measured strain levels at soil nodes (Figures 8.22 and 8.23).

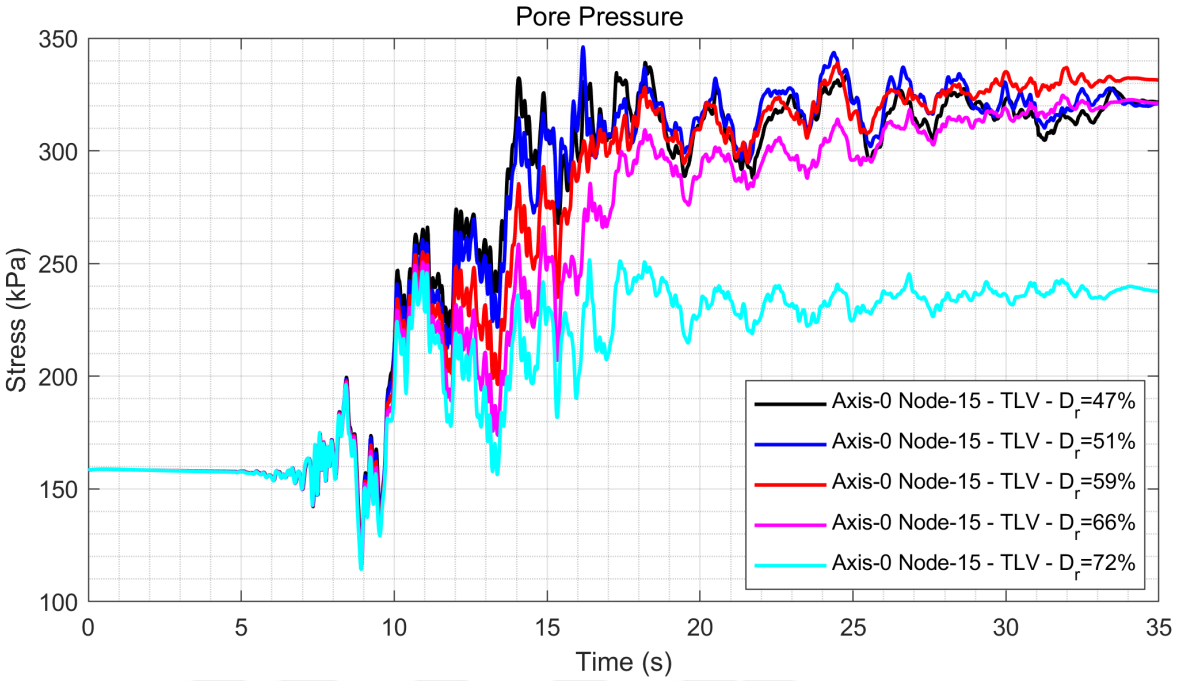

Figure 8.18. Effect of Liquefaction Potential on Pore Pressure (Soil Axis-0 Node-15).

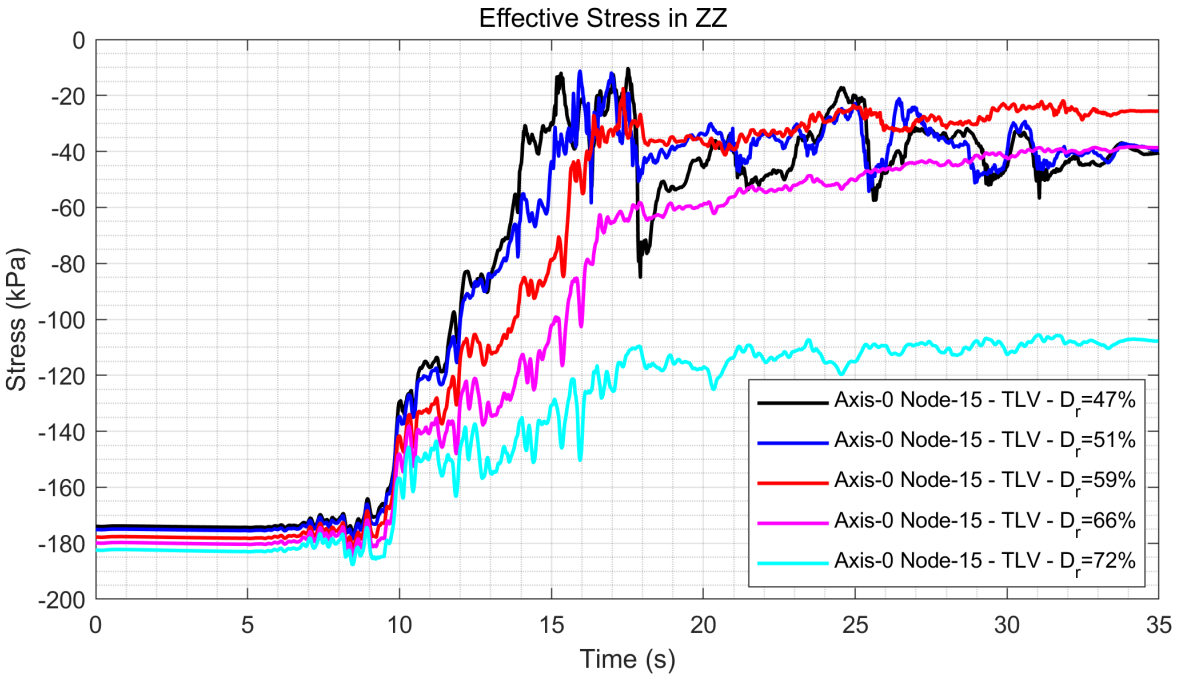

Figure 8.19. Effect of Liquefaction Potential on Effective Stress (Soil Axis-0 Node-15).

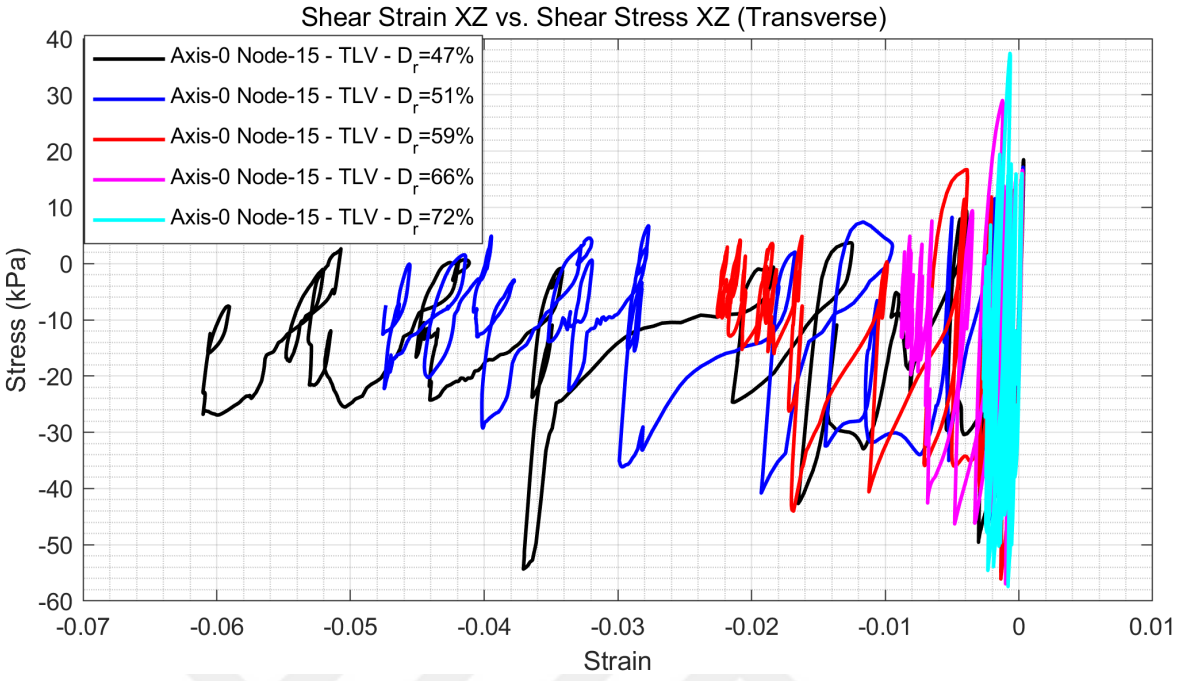

Figure 8.20. Effect of Liquefaction Potential on Stress-Strain in Transverse Direction (Soil Axis-0 Node-15).

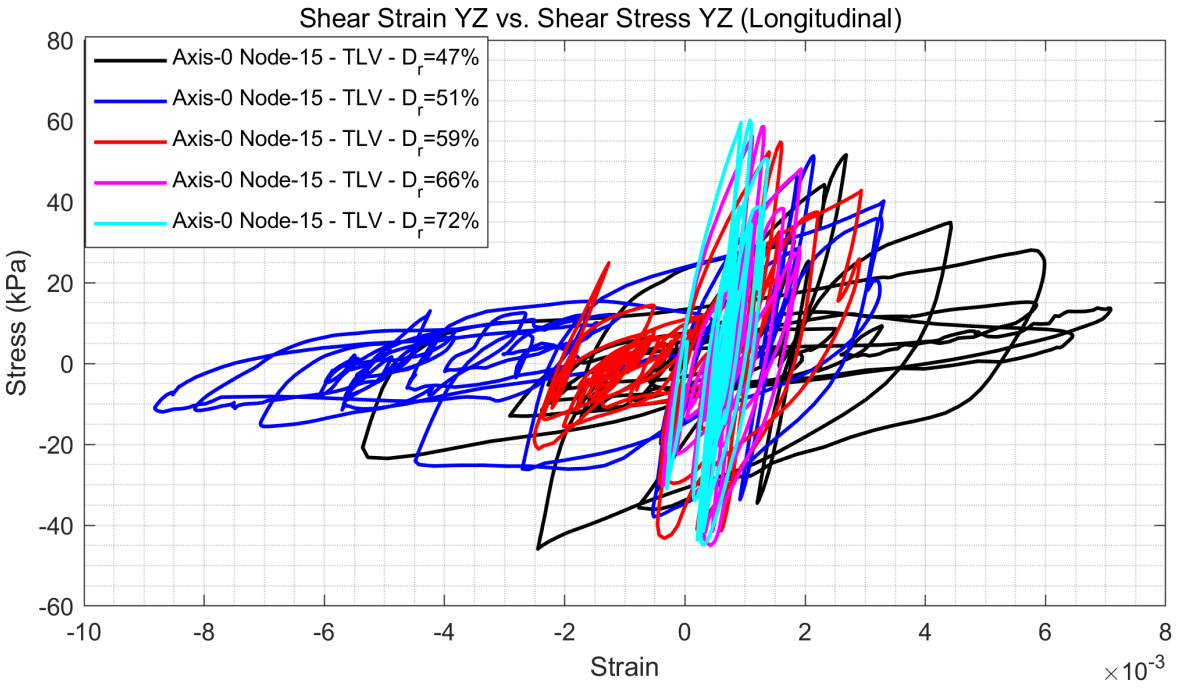

Figure 8.21. Effect of Liquefaction Potential on Stress-Strain in Longitudinal Direction (Soil Axis-0 Node-15).

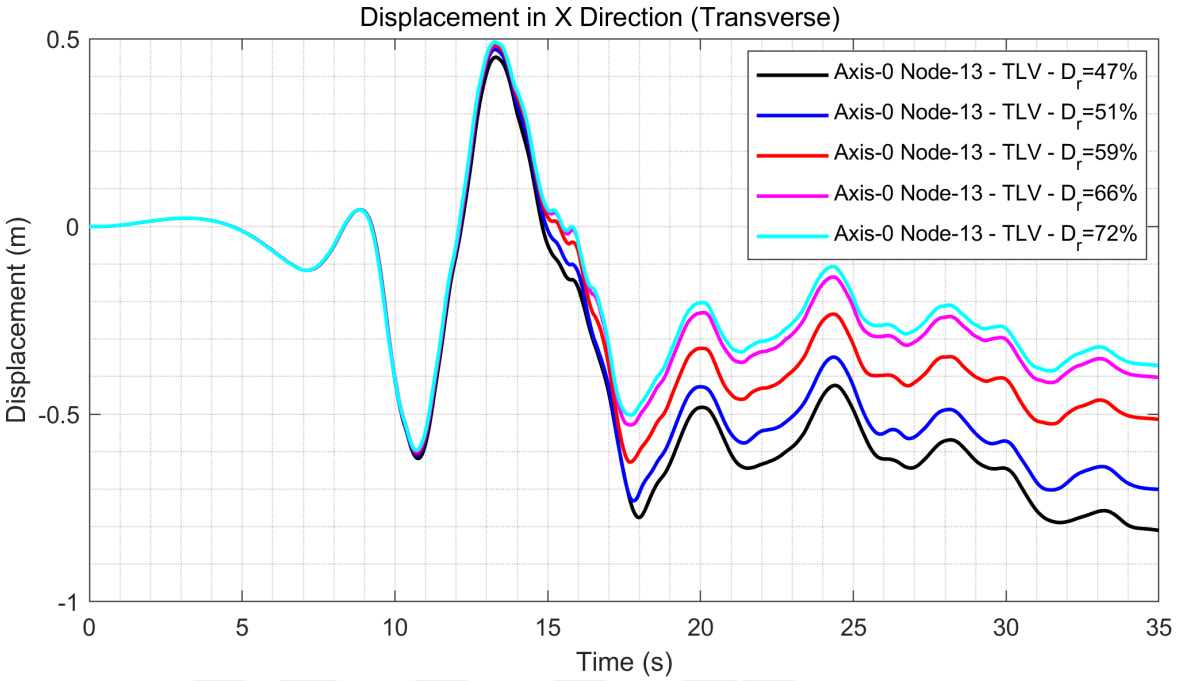

Figure 8.22. Effect of Liquefaction Potential on Displacement in Transverse Direction (Soil Axis-0 Node-15).

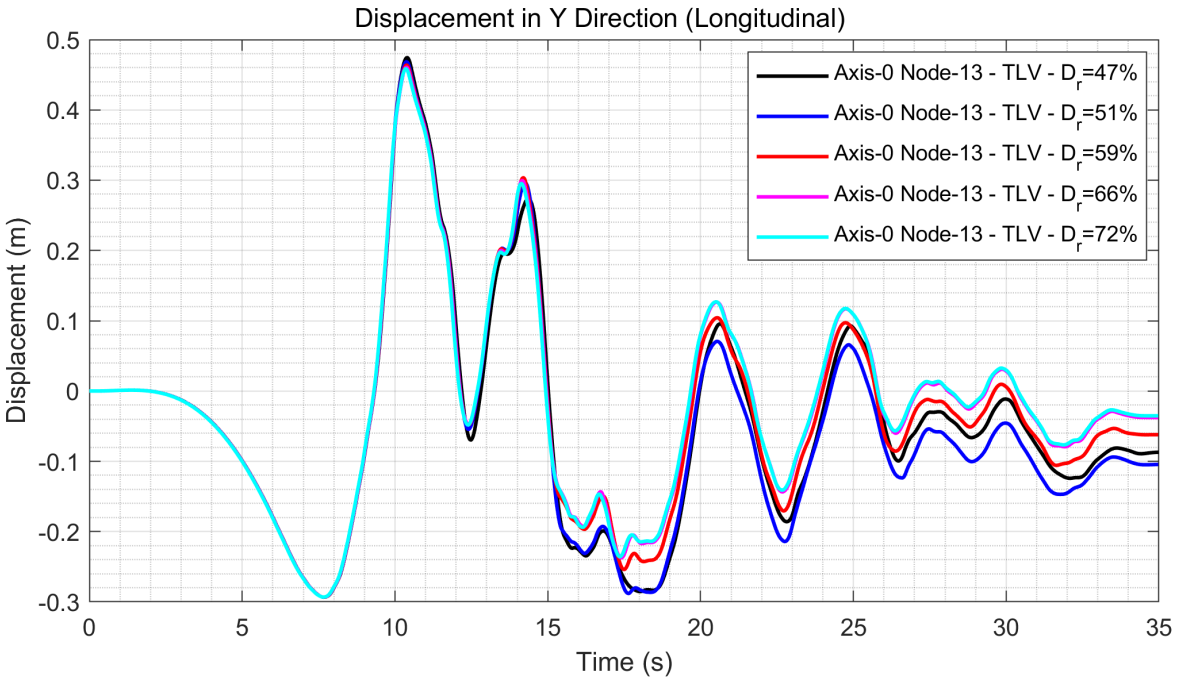

Figure 8.23. Effect of Liquefaction Potential on Displacement in Longitudinal Direction (Soil Axis-0 Node-15).

The pile relative displacements and relative rotations have a consistent trend with soil deformation (Figures 8.24, 8.25, 8.27 and 8.28). The distribution of plastic hinges are illustrated in Figure 8.26. The increase in plastification at the pile plugs can be observed qualitatively (Figures 8.27 and 8.28) along with the rising trend in the number of plastic hinges with liquefaction (Figure 8.26). The increase in internal forces with similar trend can be seen in Figures 8.29, 8.30, 8.31, 8.32, and 8.33. It can be observed that the shear forces and moments are not increasing at the pile hinge locations.

Although the torsional behavior of wharf systems will be treated in Section 8.1.4, the effect of liquefaction on the torsional response of 1-mod wharf systems is evaluated herein. Figure 8.34 shows the peak in-plane rotations for 1-mod wharf decks, with respect to relative densities of the MDS-1 layer associated with liquefaction potential. It is observed that liquefaction does not affect the torsional response of wharf decks.

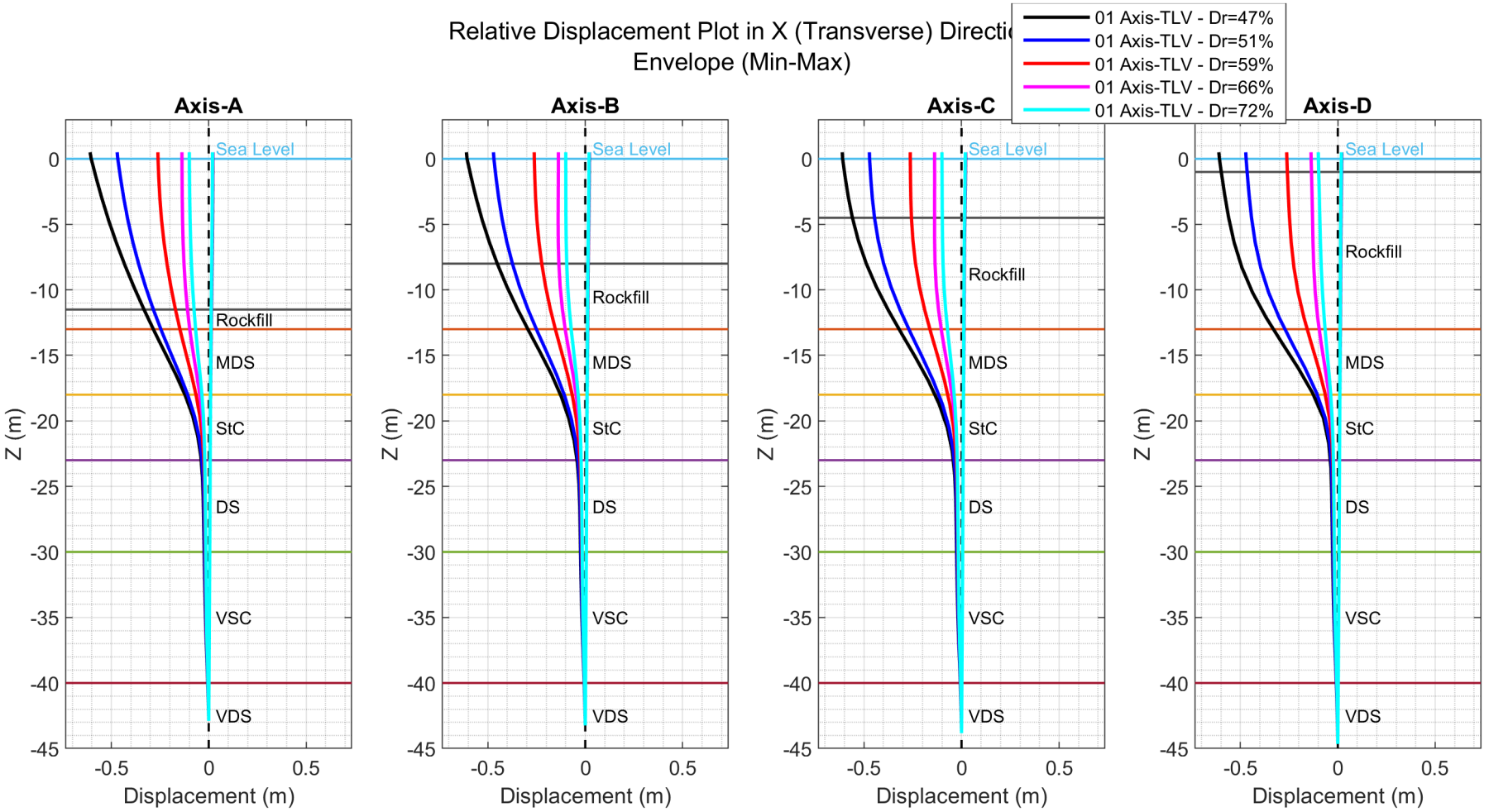

Figure 8.24. Effect of Liquefaction Potential on Pile Relative Displacements in Transverse Direction.

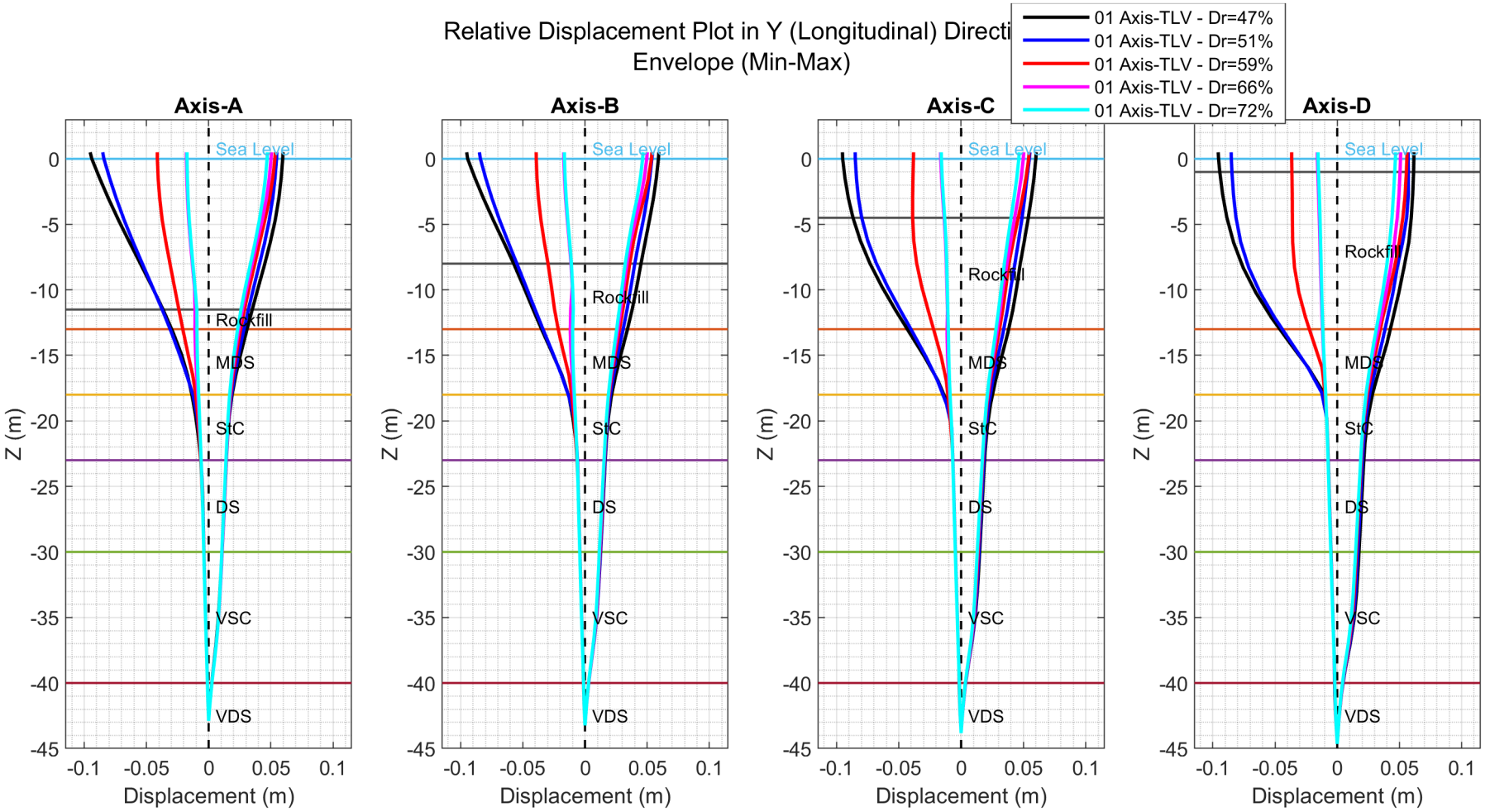

Figure 8.25. Effect of Liquefaction Potential on Pile Relative Displacements in Longitudinal Direction.

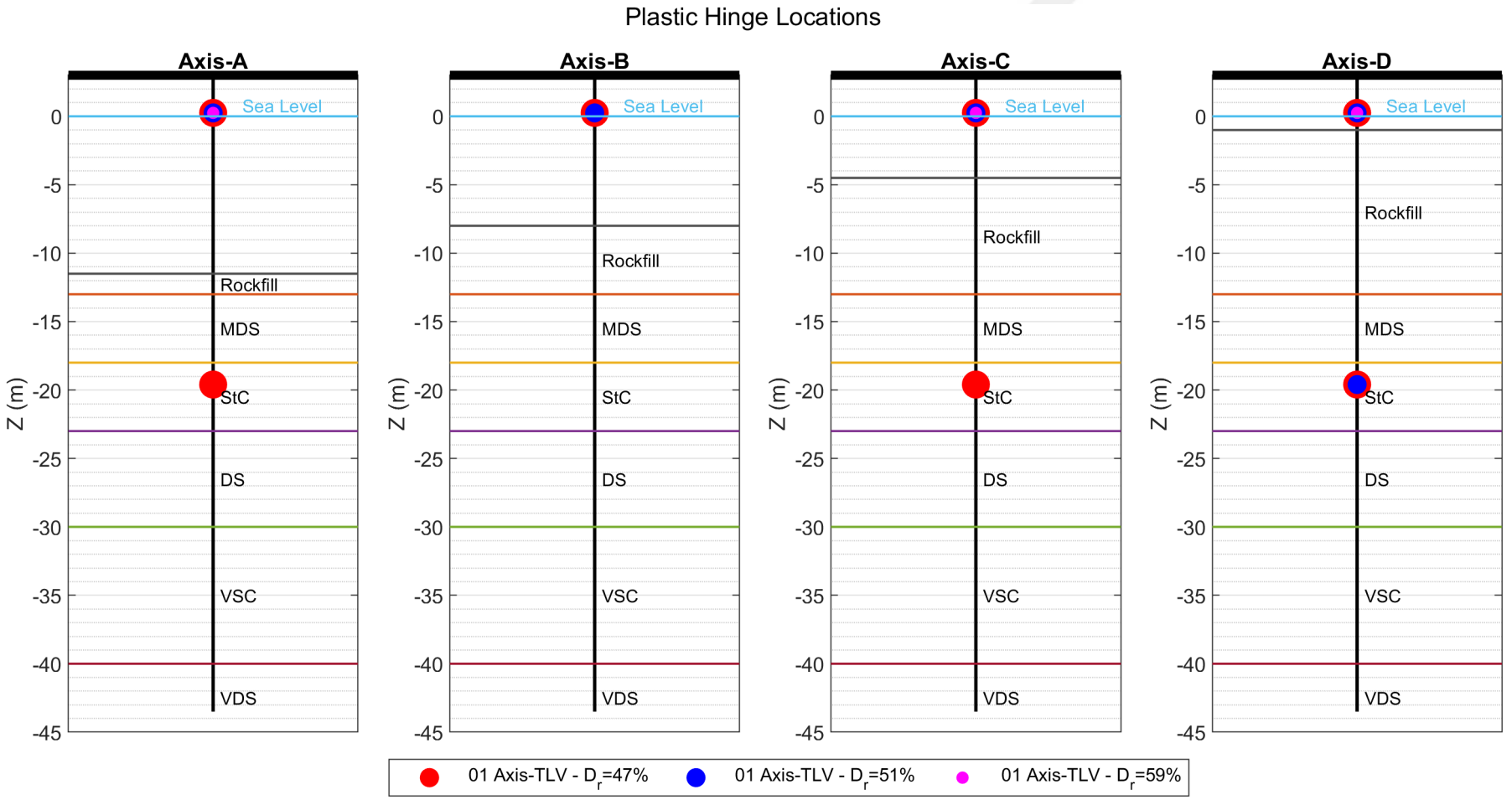

Figure 8.26. Effect of Liquefaction Potential on Plastic Hinge Occurrences.

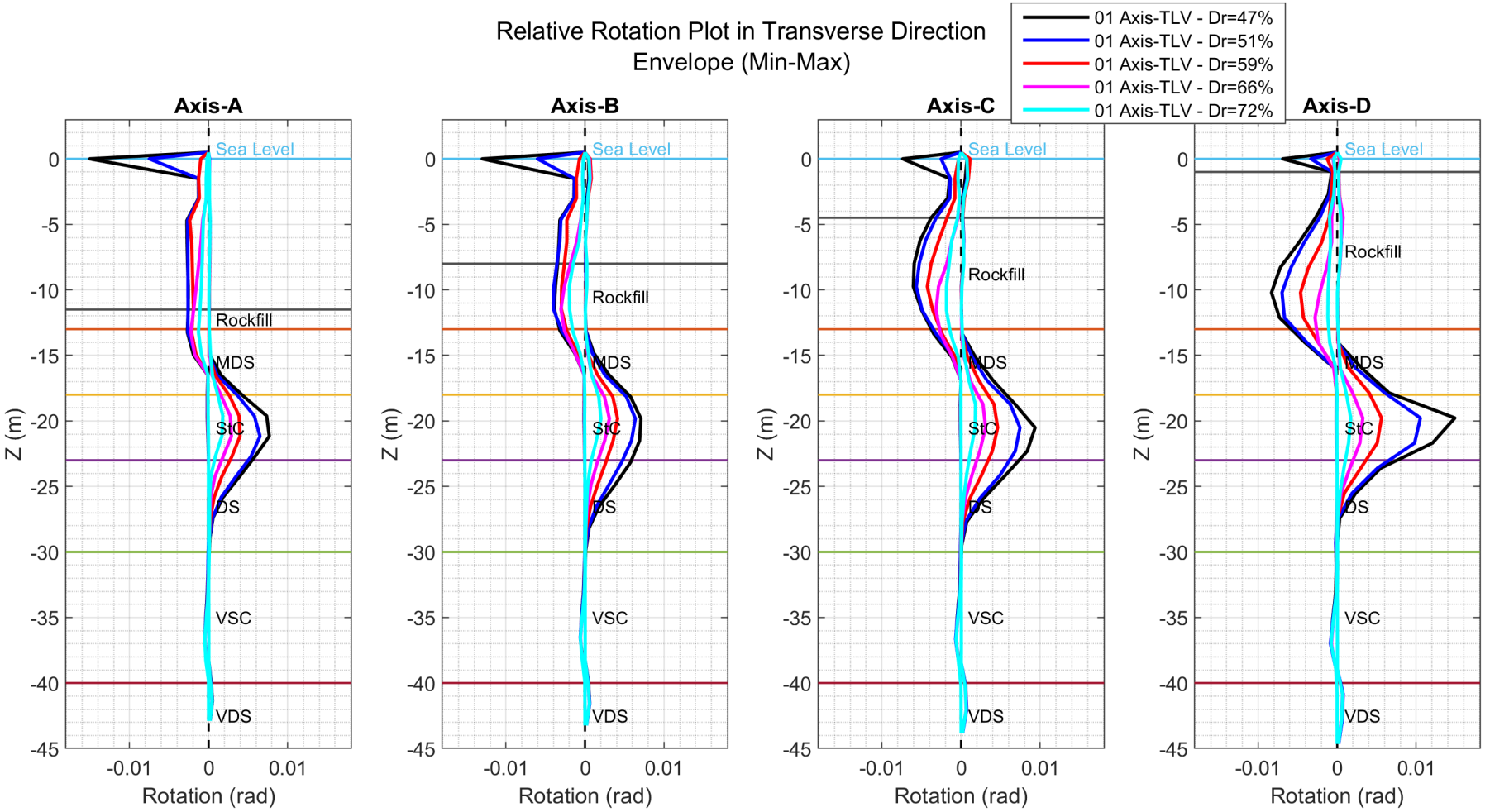

Figure 8.27. Effect of Liquefaction Potential on Pile Relative Rotations in Transverse Direction.

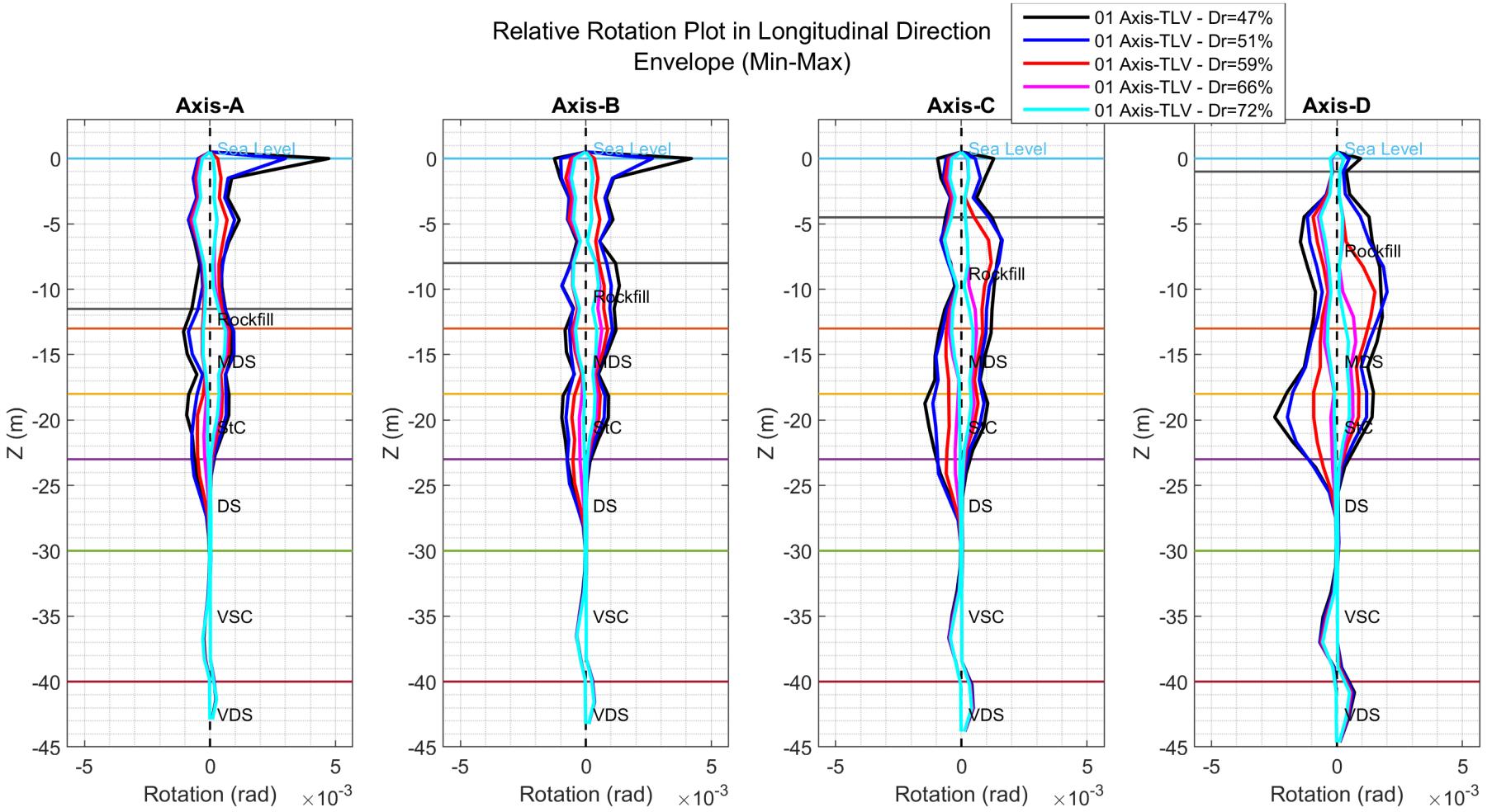

Figure 8.28. Effect of Liquefaction Potential on Pile Relative Rotations in Longitudinal Direction.

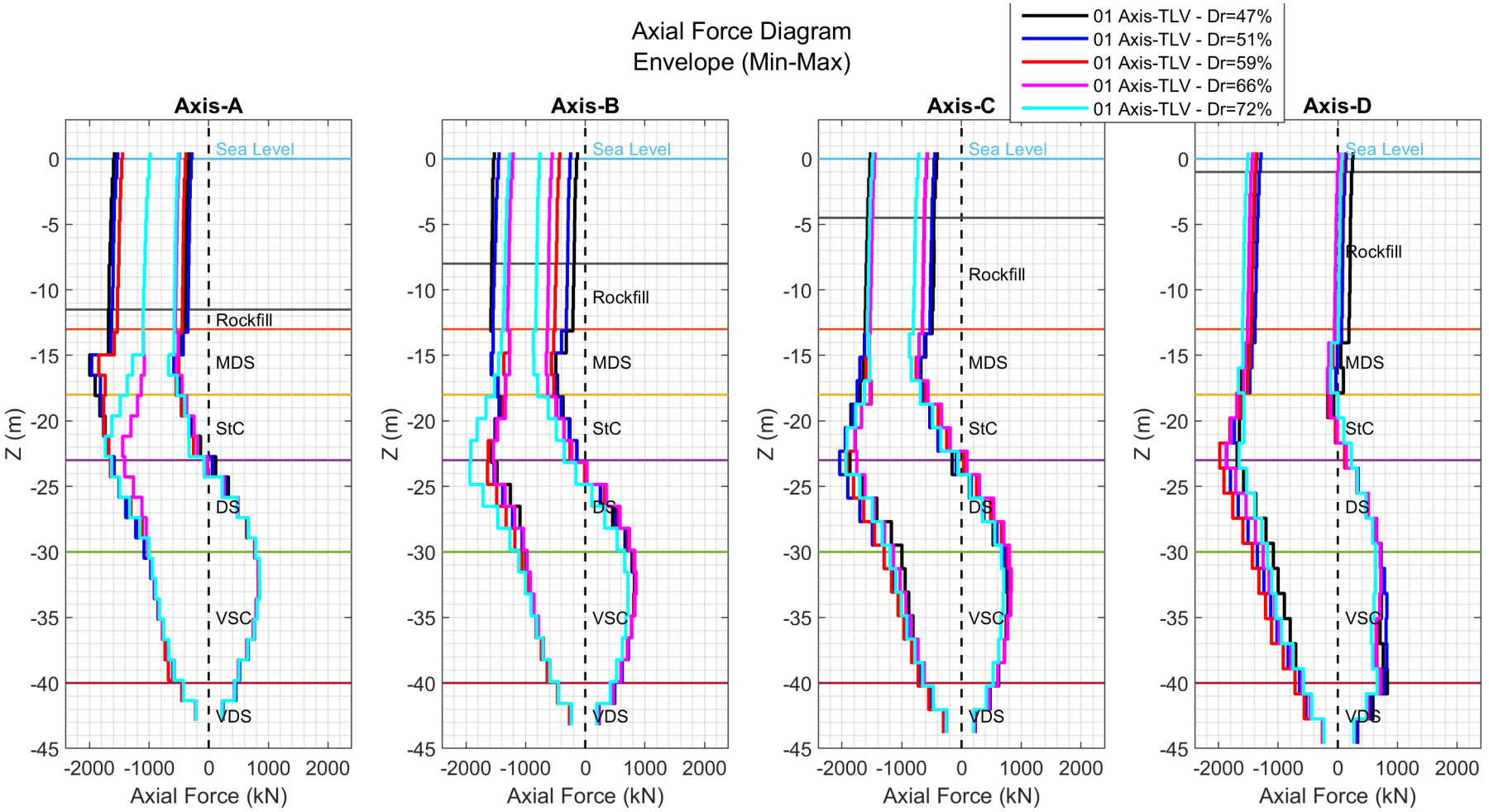

Figure 8.29. Effect of Liquefaction on Pile Axial Forces.

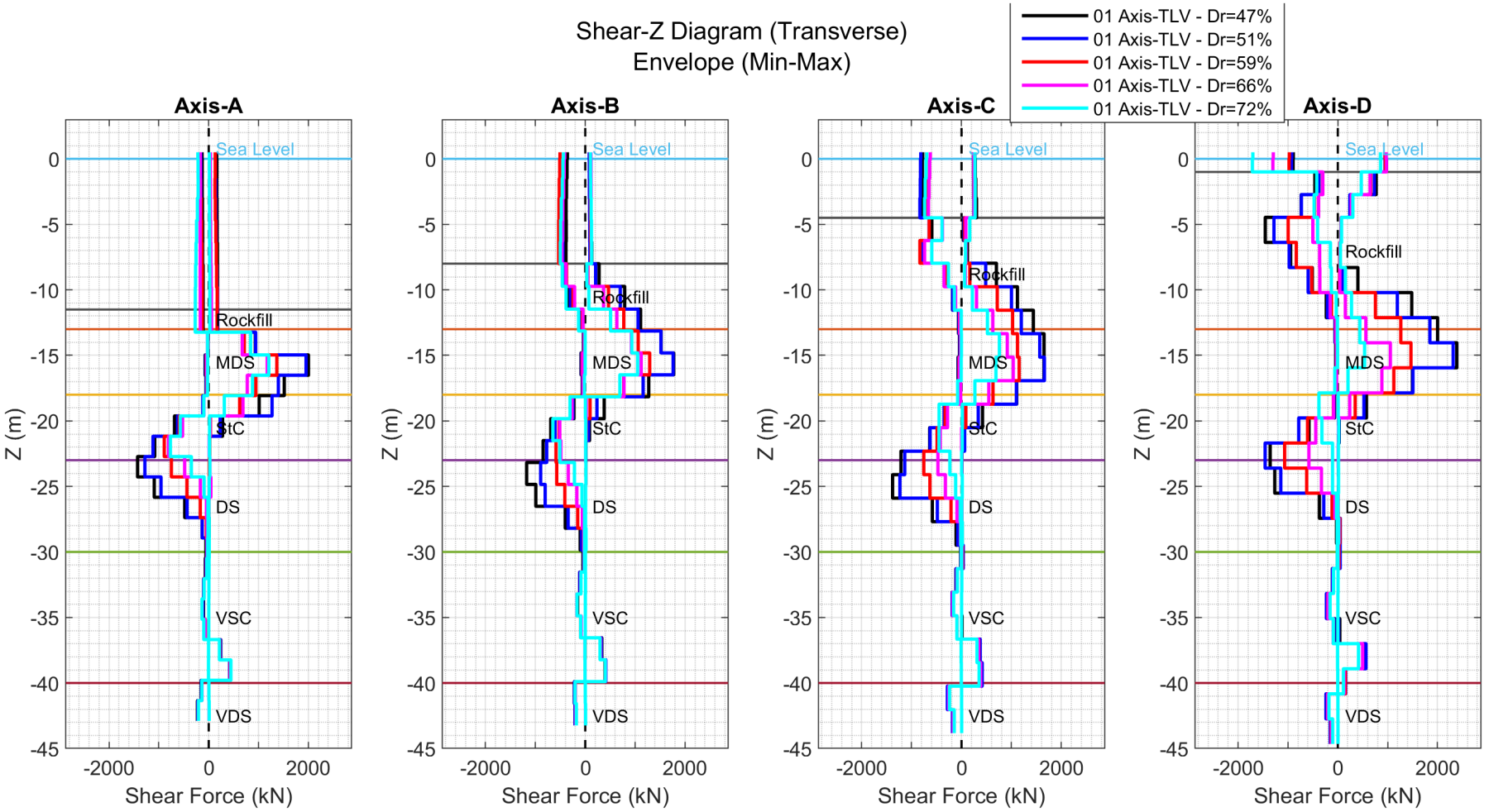

Figure 8.30. Effect of Liquefaction on Pile Shear Forces in Transverse Direction.

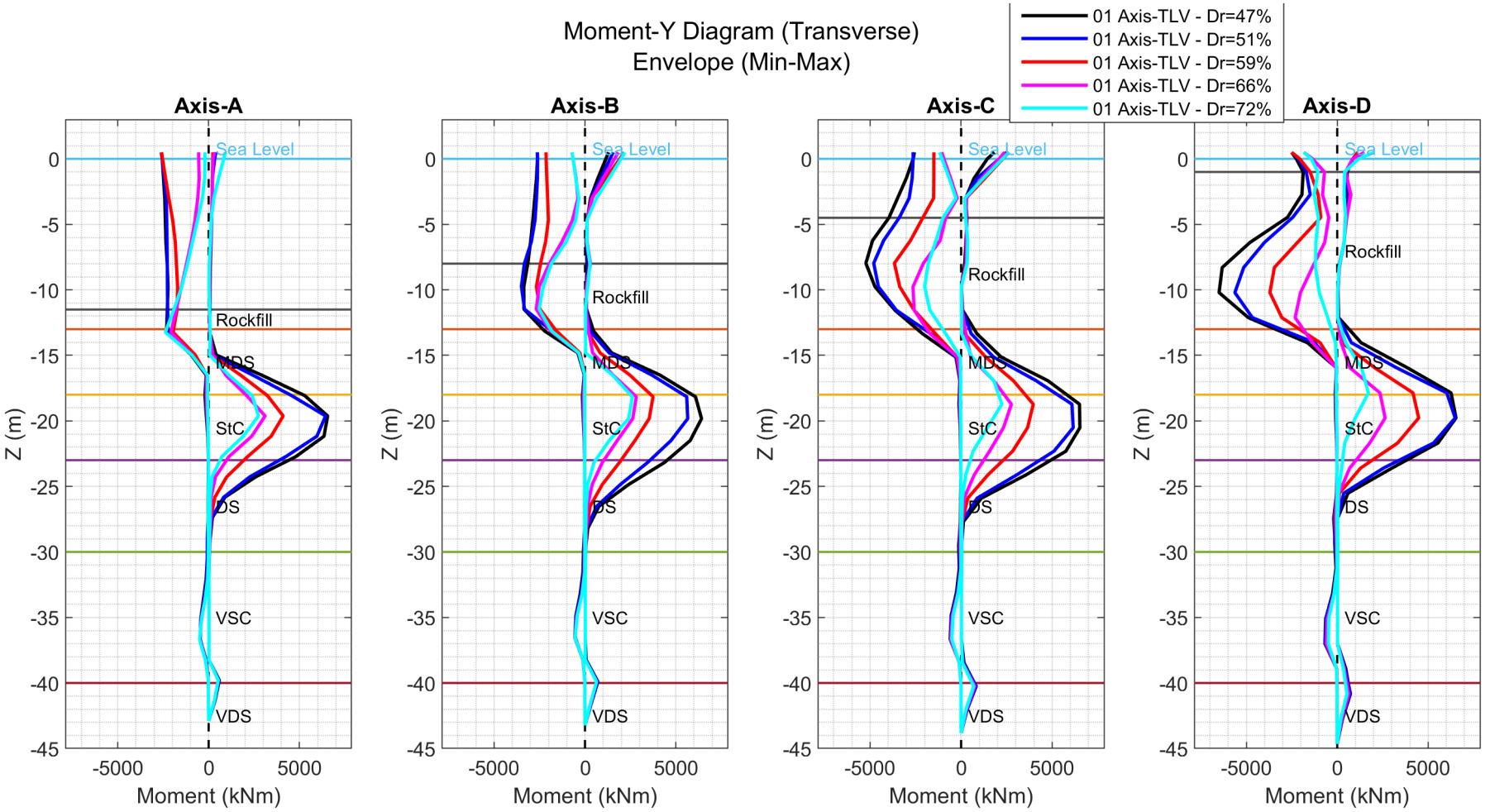

Figure 8.31. Effect of Liquefaction on Pile Moments in Transverse Direction.

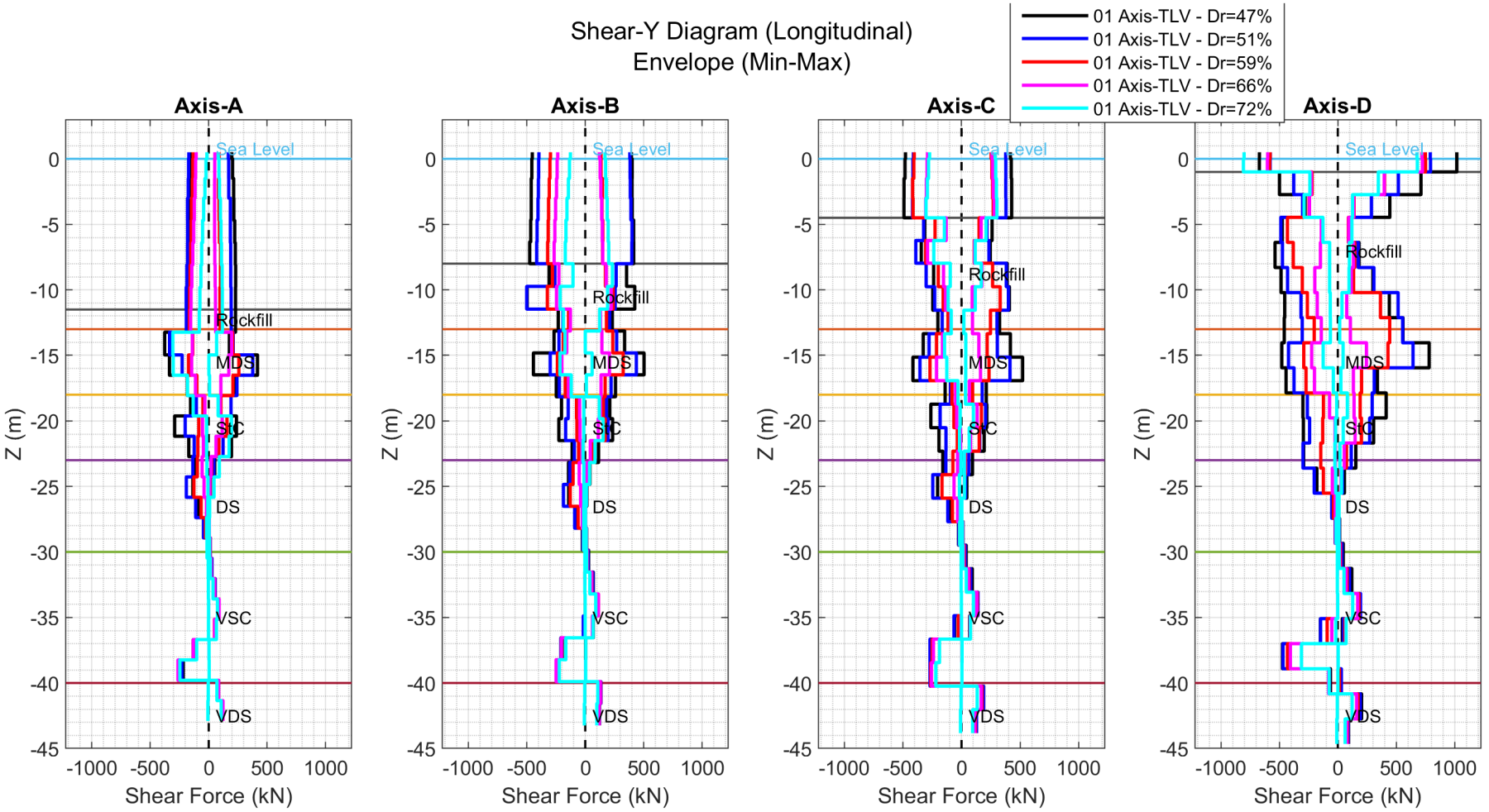

Figure 8.32. Effect of Liquefaction on Pile Shear Forces in Longitudinal Direction.

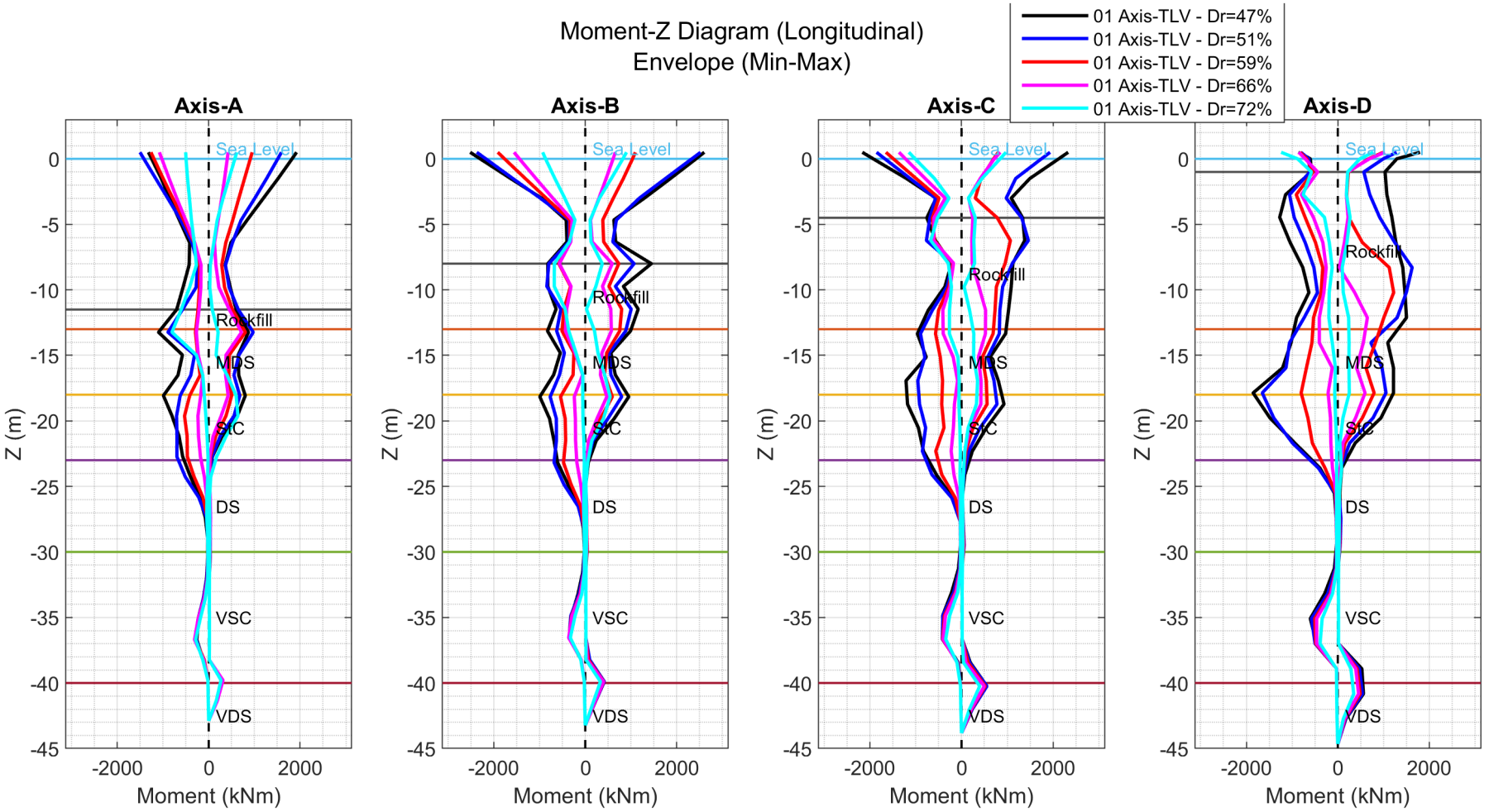

Figure 8.33. Effect of Liquefaction on Pile Moments in Longitudinal Direction.

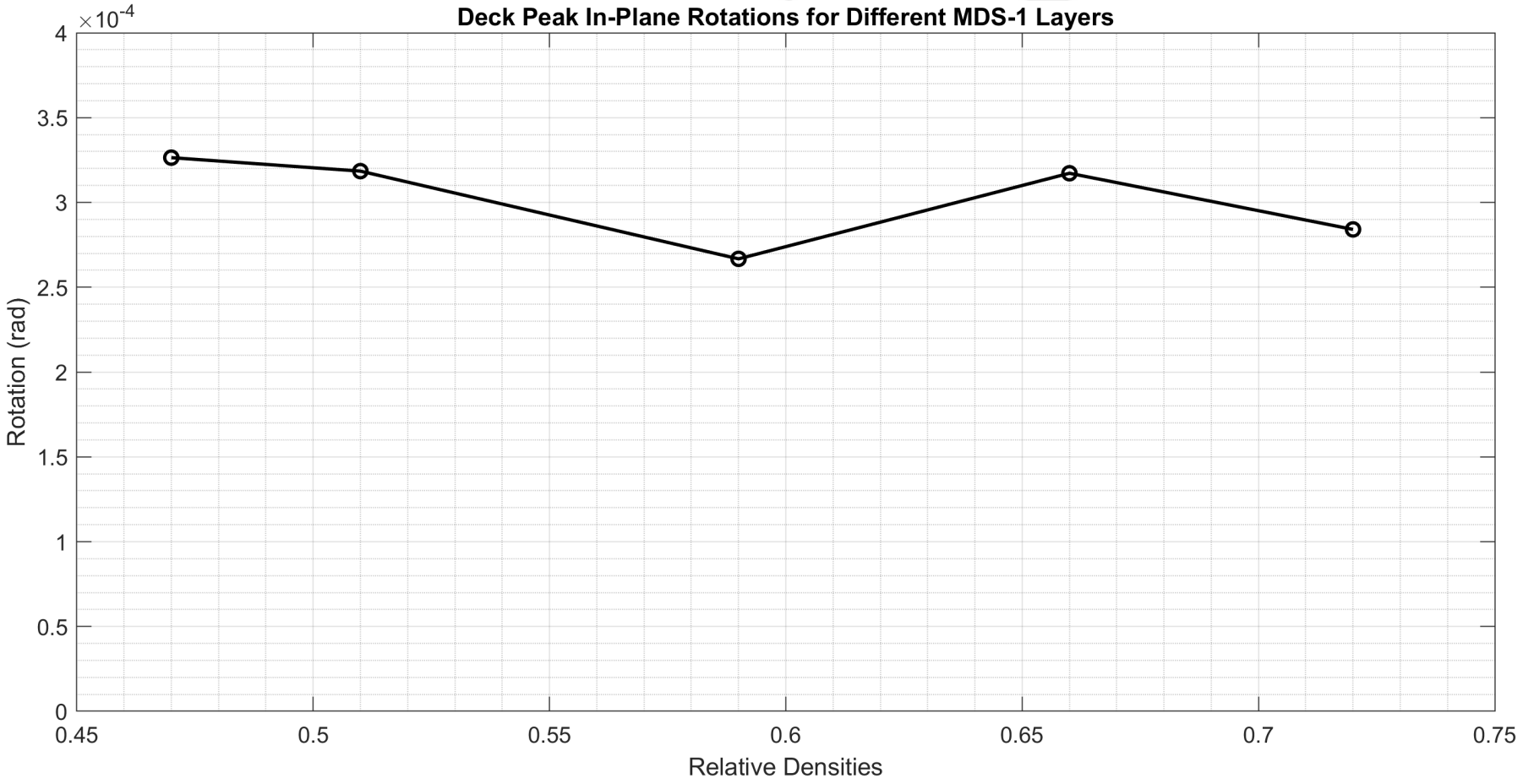

Figure 8.34. Effect of Liquefaction Potential on Deck In-plane Rotations.

8.1.4. Evaluation of Multi-Segmented Wharf Systems and Torsional Behavior of Wharf Decks

Although multi-segmented wharf systems are widely constructed all over the world, the seismic behavior of these systems incorporating soil-structure interaction has not been investigated. A detailed investigation for multi-segmented systems is required for a better understanding of these systems under seismic excitation. It would also be useful to shed light on design-related issues.

Figures 8.35 and 8.37 show the total displacement time histories in the X and Y directions, respectively, for the 1st module decks of 1-module to 8-module systems under TLV excitation. The response histories are taken from the deck node number 1 given in Figure 6.15. Figures 8.36 and 8.38 show the enlarged view of last seconds to see the difference between the module responses. The maximum displacement difference between two modules is 22mm in X direction and 10mm in Y direction.

Figures 8.39, 8.40, 8.41, 8.42, and 8.43 show the exaggerated (multiplied by 1500) displacement views of decks in plan for 1-module to 8-module systems for the several time instants. The first time instant considered is 10.89s. It is seen from Figure 8.3 that the excessive soil deformation has not been started at that time instant yet. It indicates that the main source of the deck in-plane rotations in Figure 8.39 is inertial effects. The eccentric forces, due to the longitudinal seismic excitation, acting on the deck mass center cause torsion. Since the torsional stiffness of 1-module system is less than the others, the in-plane rotation of that system is greater than the others.

As the time progresses, soil deformations increase due to soil liquefaction, leading to greater in-plane rotations of the end modules in multi-segmented systems. The relatively higher rotations of end modules compared to the 1-module system are due to the free-field deformations of soils at both sides. Pile-pinning effects impede the soil deformation through the mid-modules. Therefore, the movement of one side of end module is restricted by the mid-modules, while the other side is forced to move due to

the free-field soil deformation.

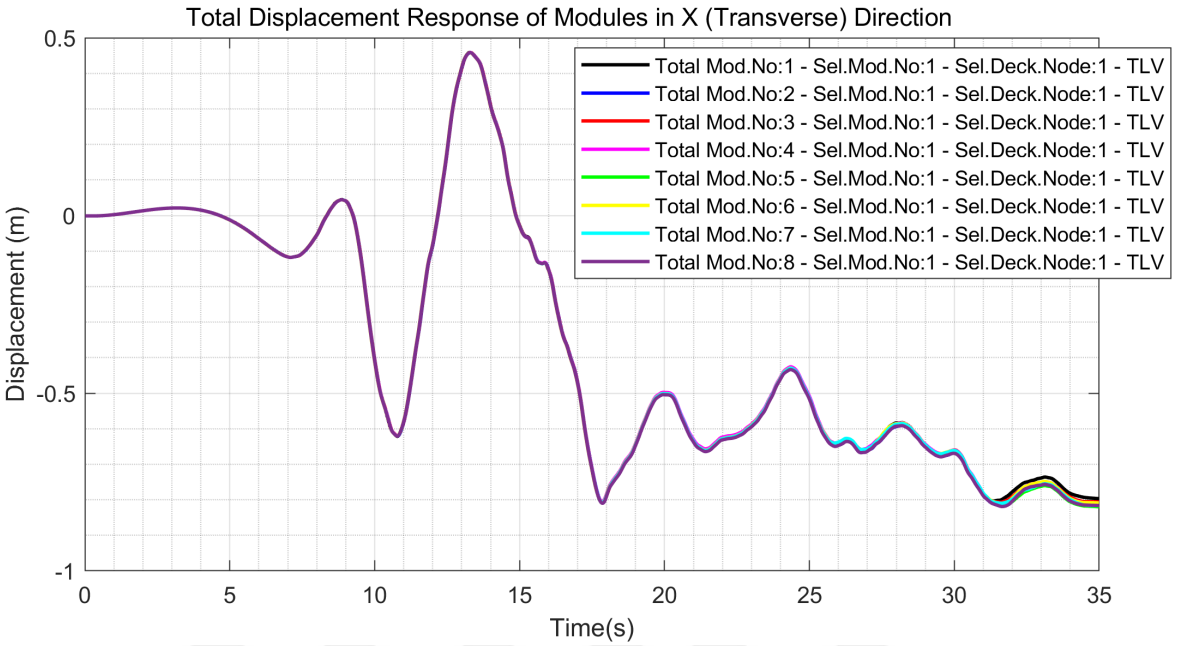

Figure 8.35. Displacement Response of Different Modules in X direction (1st Modules).

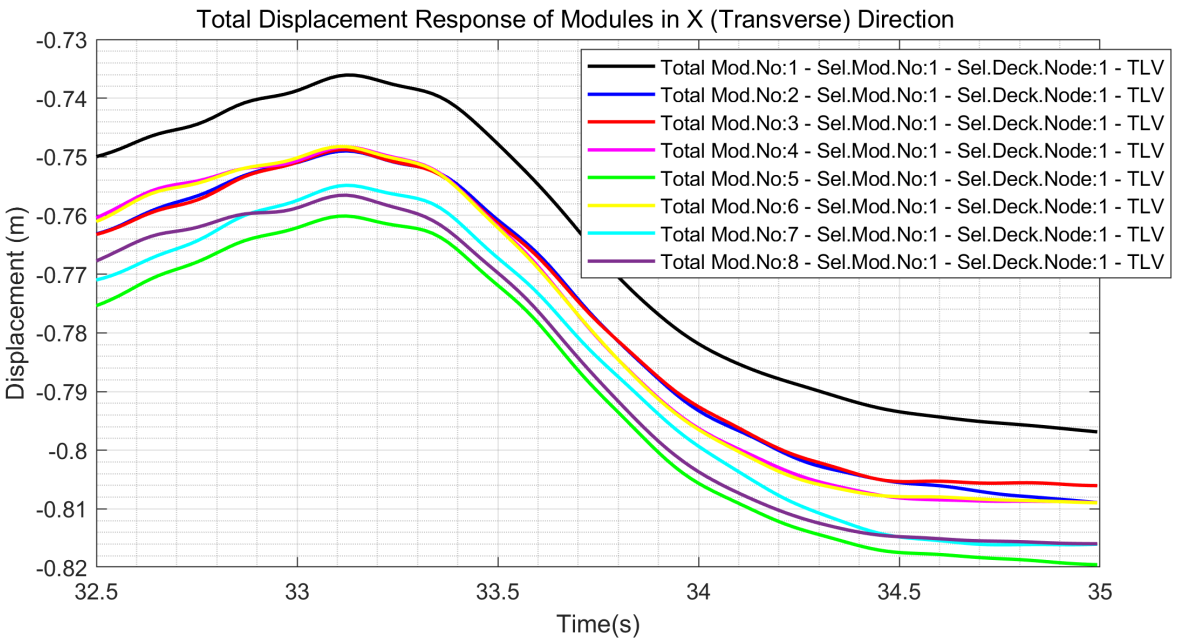

Figure 8.36. Displacement Response of Different Modules in X direction (Close-up t=32.5-35s).

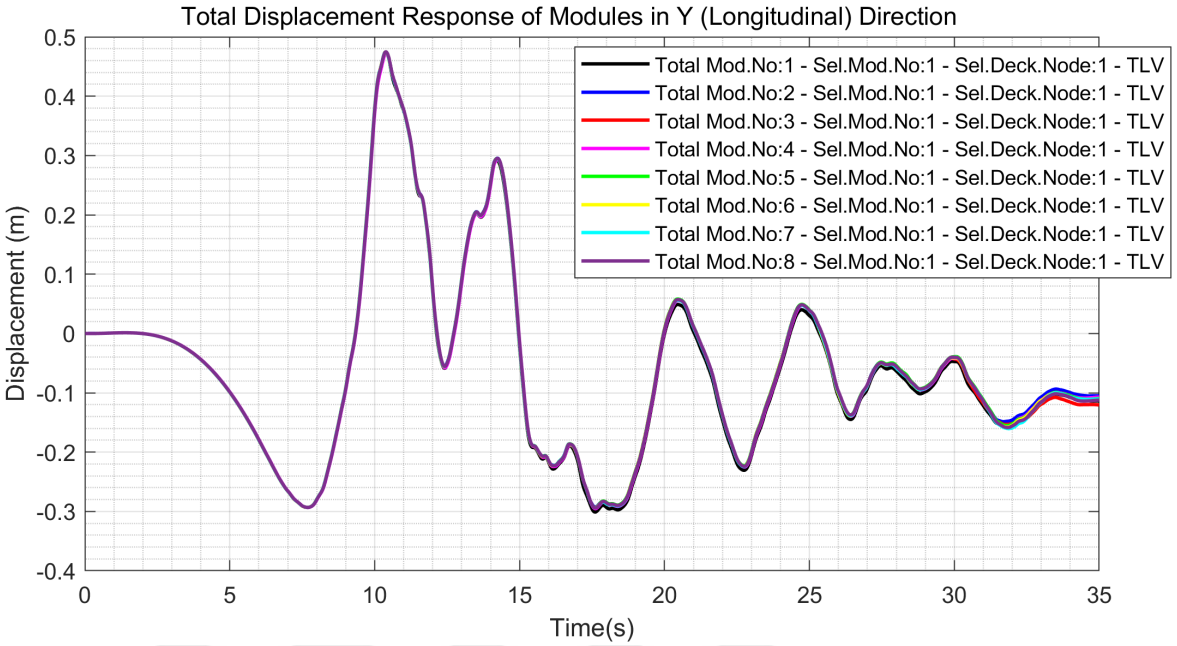

Figure 8.37. Displacement Response of Different Modules in Y direction (1st Modules).

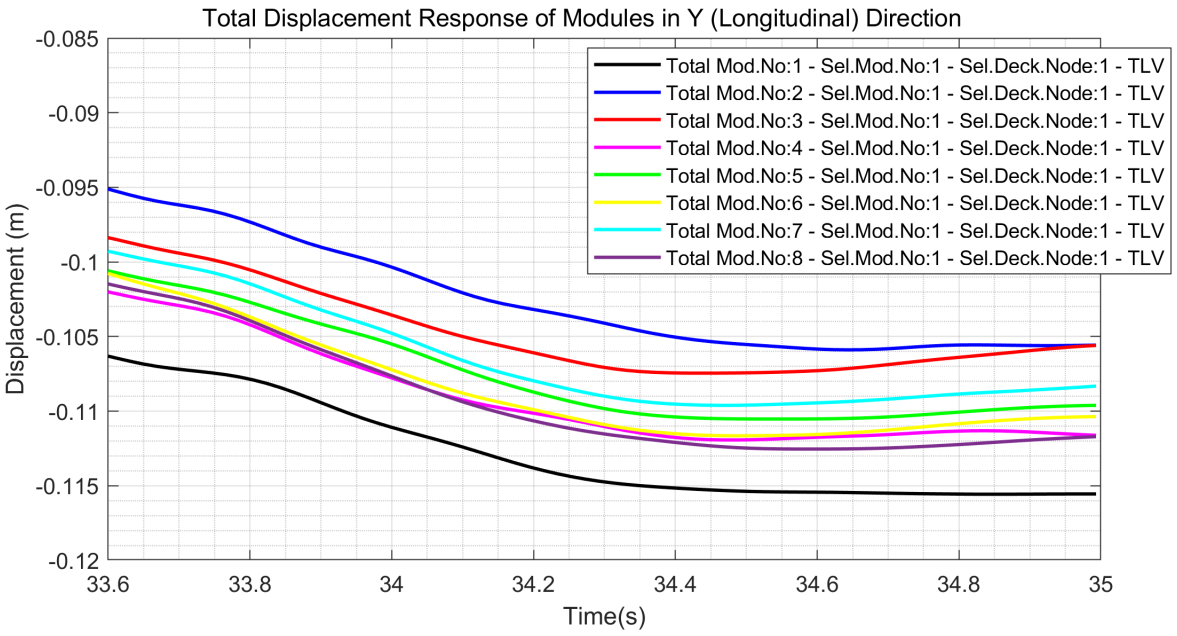

Figure 8.38. Displacement Response of Different Modules in Y direction (Close-up t=33.6-35s).

Even though the level of these in-plane rotations are not very important in terms of structural design, it is interesting to note that the excessive soil deformation changes the torsional character of multi-segmented structural systems. From structural point of view, it is not expected that the in-plane rotations of end modules in multi-segmented wharf systems, which is torsionally more resistant than 1-module system, would be greater than 1-module system under horizontal excitation.

The peak in-plane rotations of modules are illustrated in Figure 8.44. The trend consistently show that the in-plane rotations of end-modules are greater than those of inner-modules. As the number of modules increases, the inner-module rotations are getting smaller and remain constant.

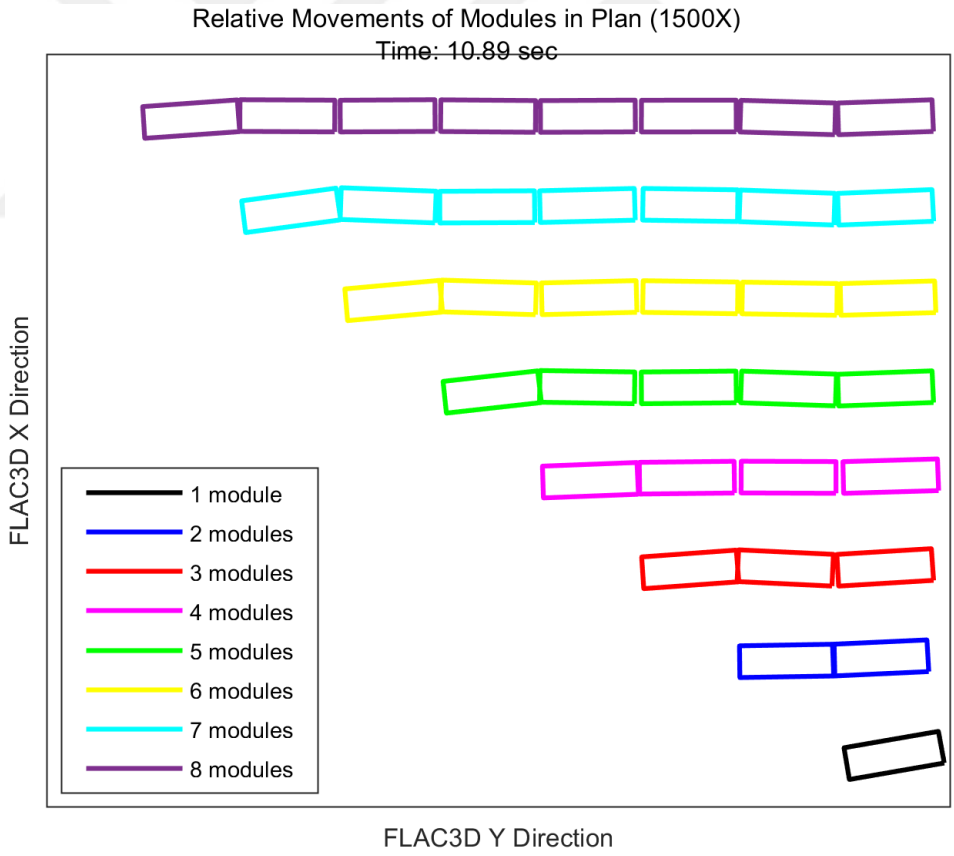

Figure 8.39. Relative Movements of Modules in Plan (Time:10.89s).

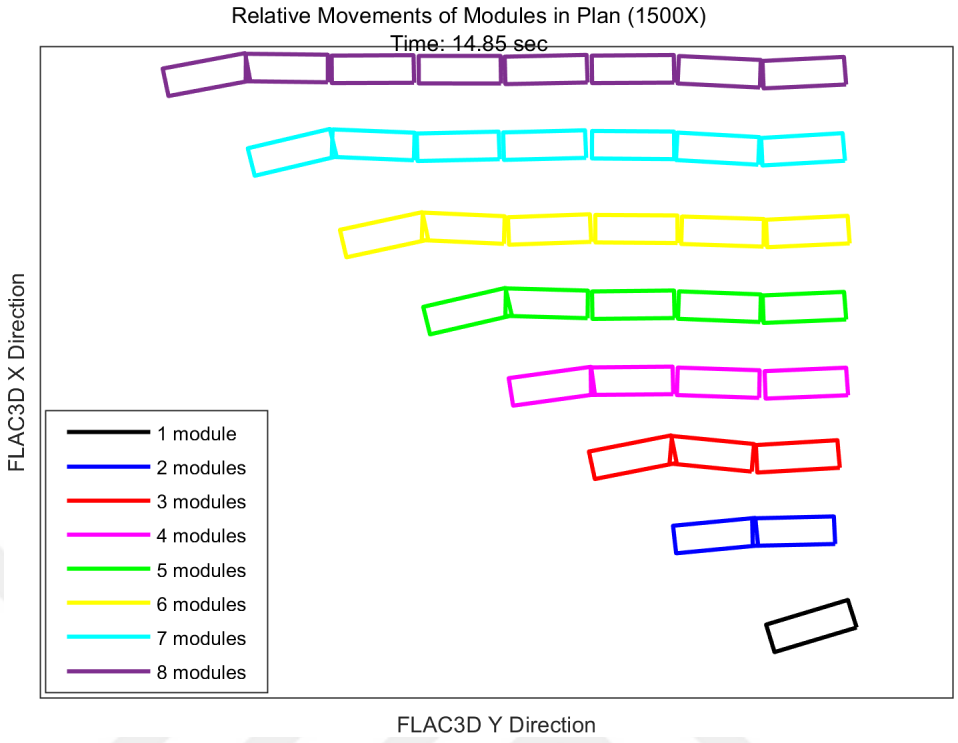

Figure 8.40. Relative Movements of Modules in Plan (Time:14.85s).

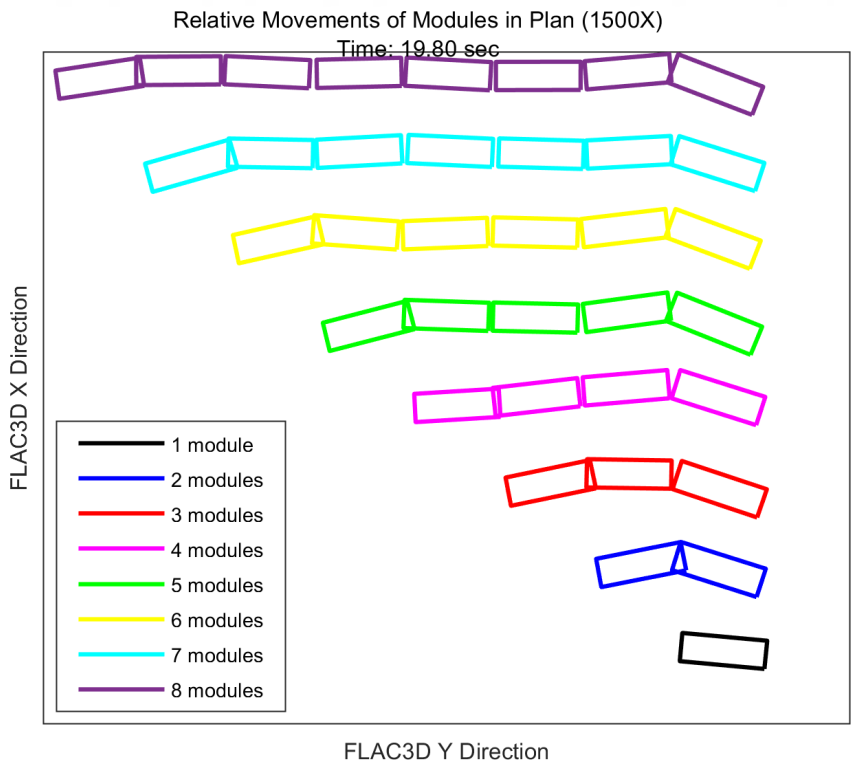

Figure 8.41. Relative Movements of Modules in Plan (Time:19.80s).

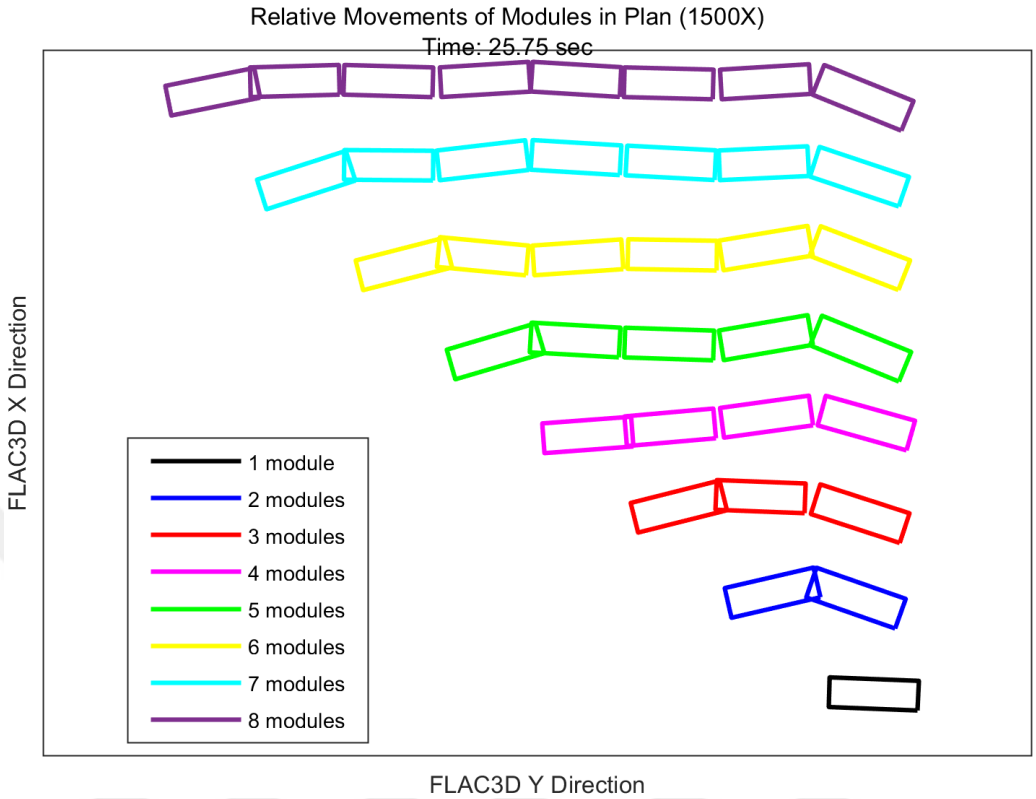

Figure 8.42. Relative Movements of Modules in Plan (Time:25.75s).

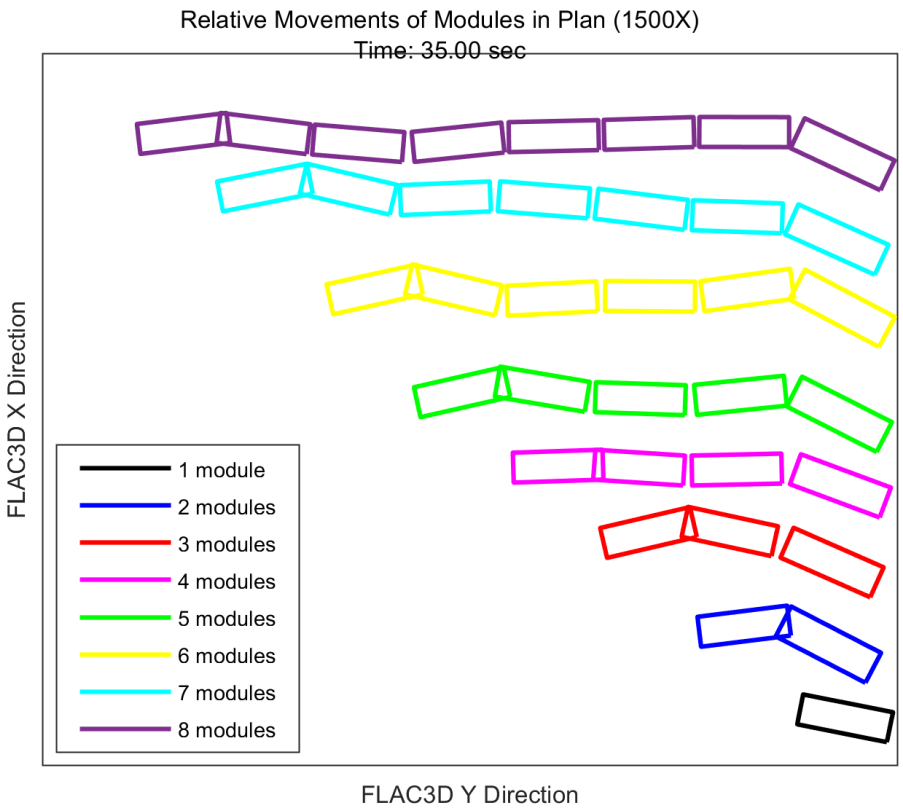

Figure 8.43. Relative Movements of Modules in Plan (Time:35.00s).

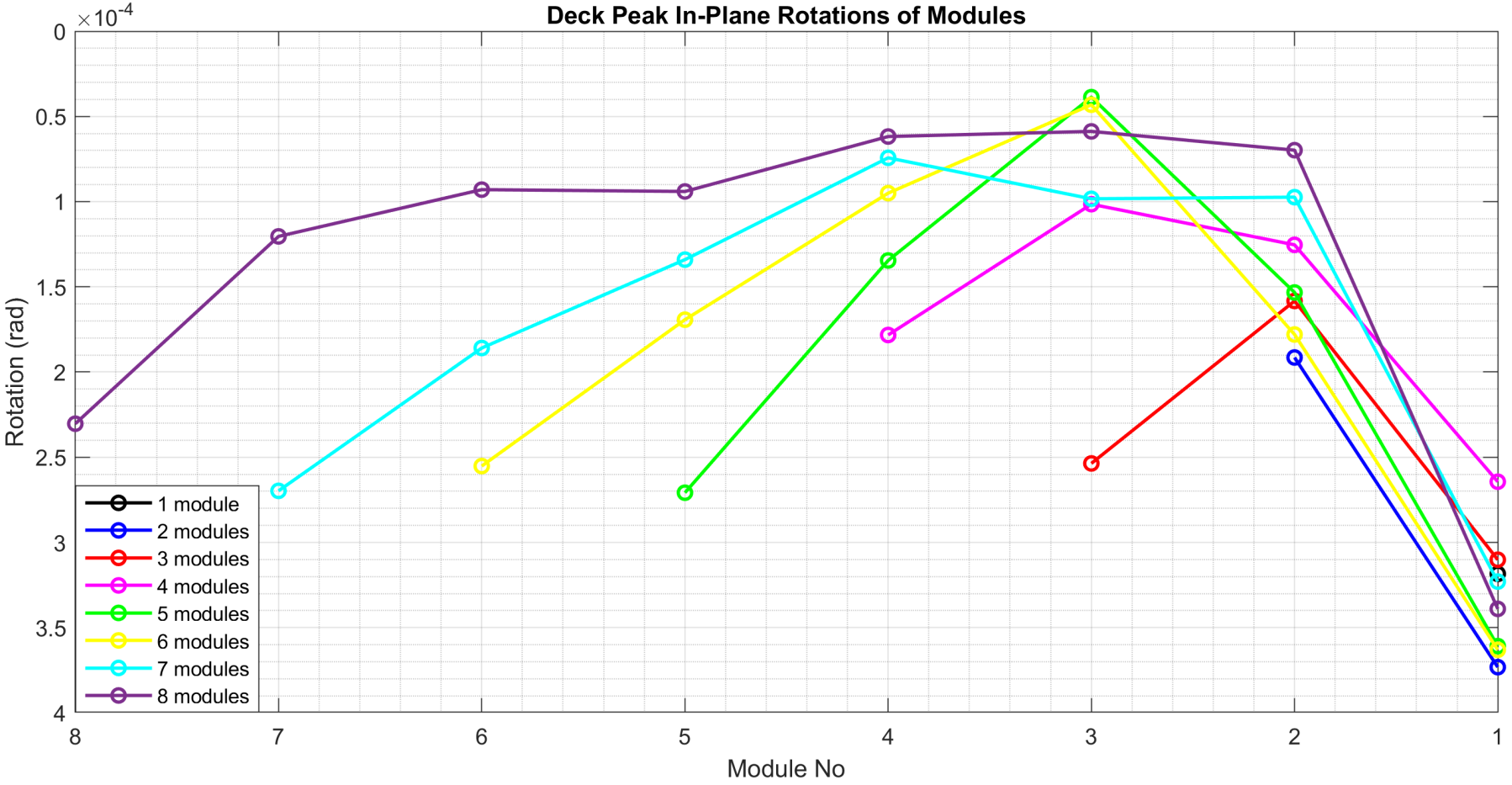

Figure 8.44. Deck Peak In-Plane Rotations of Modules.

The pore pressure, effective stress, stress-strain relationships in two directions and the soil displacement at embankment crest time histories are given in Figures 8.45, 8.46, 8.47 and 8.48. For the sake of the clarity in figures, only 1mod, 2mod, 4mod and 8mod graphics are plotted. It is seen that all quantities have the similar trend during the ground shaking. It is proven that the soil responses are not affected much by the increasing numbers of modules.

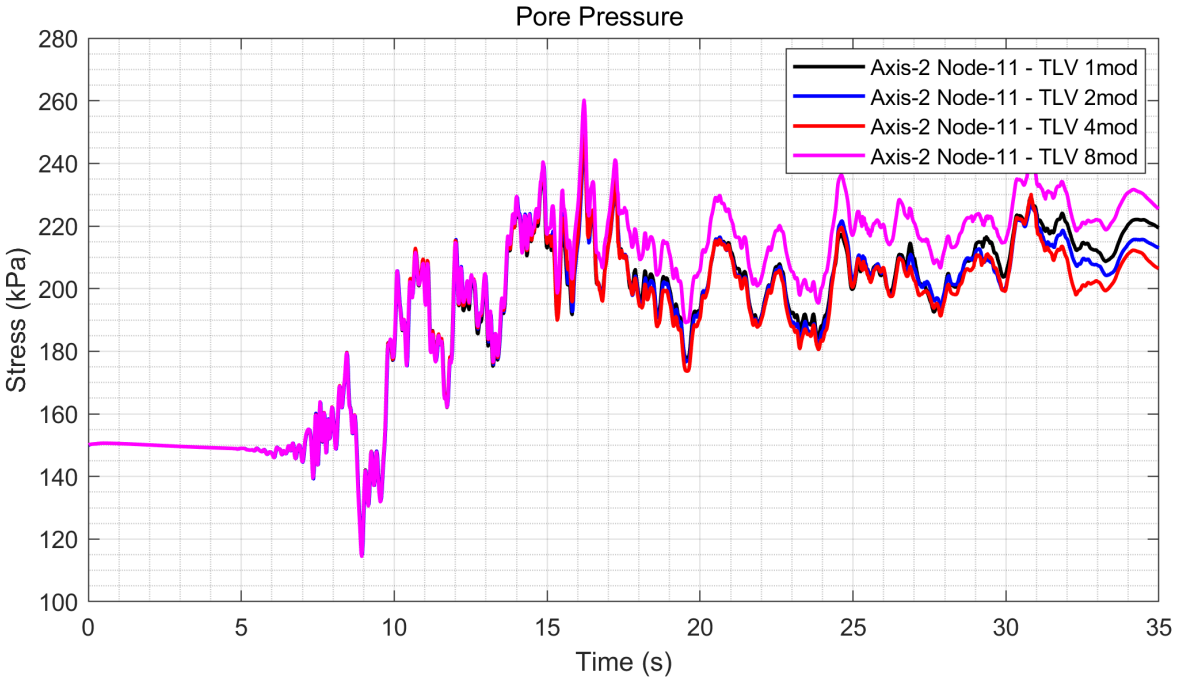

Figure 8.45. Pore Pressure Comparison for 1mod, 2mod, 4mod and 8mod Systems under TLV Excitation (Soil Axis-2 Node-11).

In a similar manner, pile internal force results are identical for the systems having different number of modules. It can be seen from Figures 8.50, 8.51, 8.52, 8.53, 8.51 and 8.54. For the sake of brevity, the results are given only for Axis-01 herein.

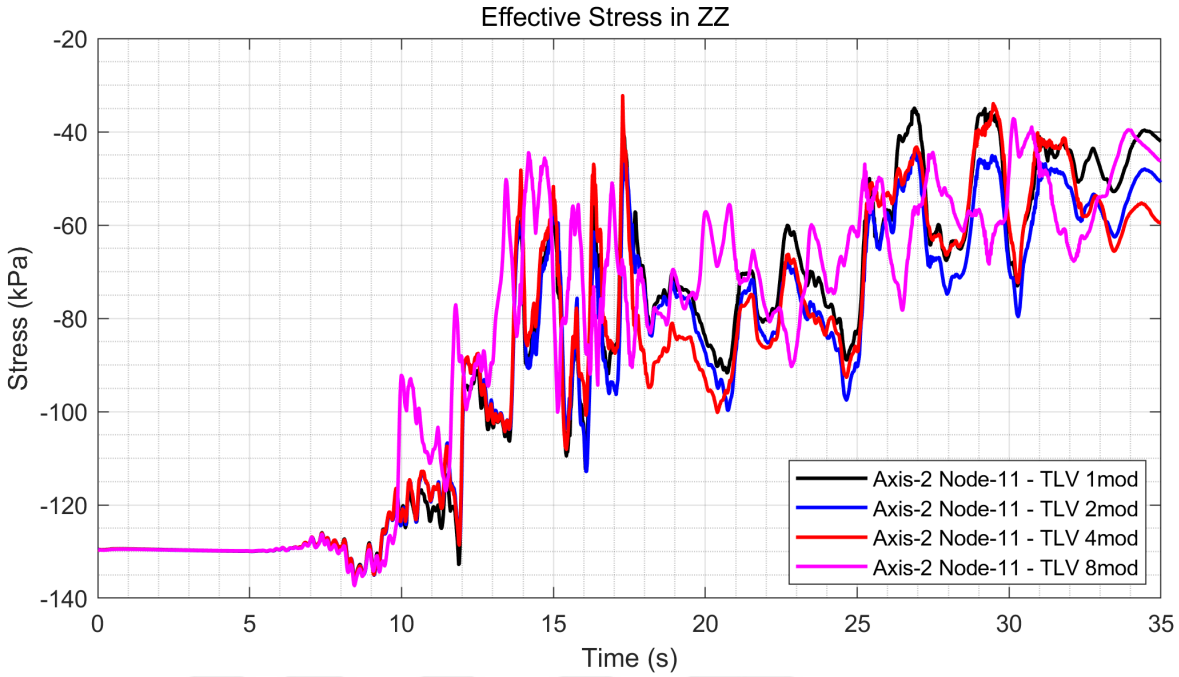

Figure 8.46. Effective Stress Comparison for 1mod, 2mod, 4mod and 8mod Systems under TLV Excitation (Soil Axis-2 Node-11).

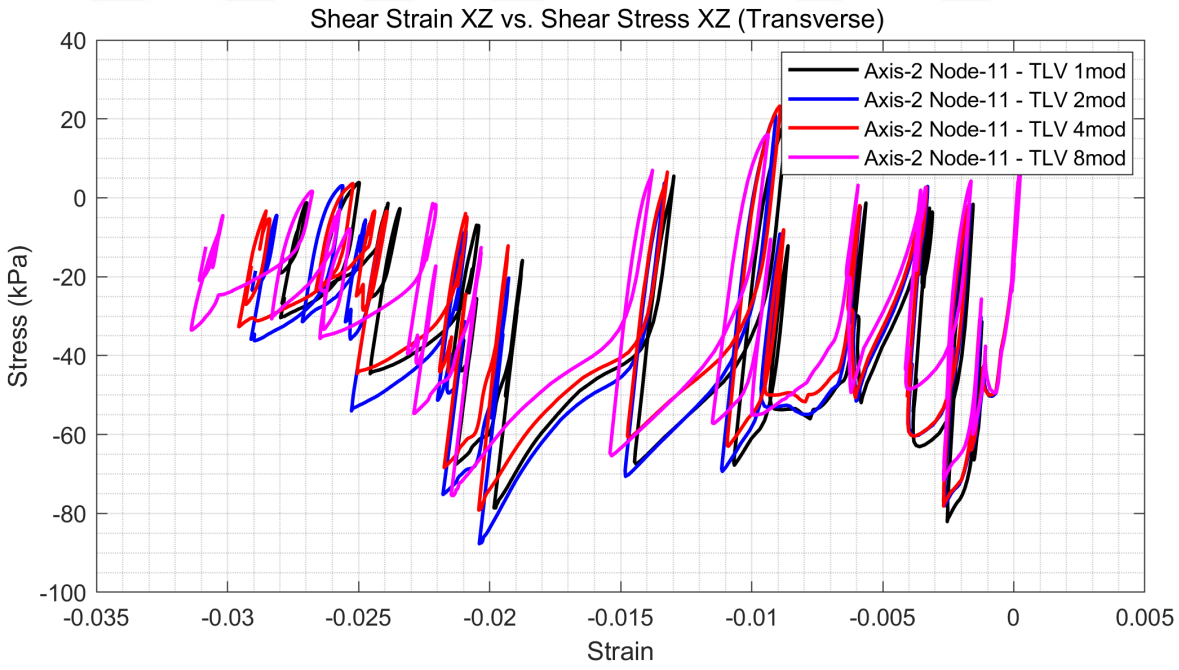

Figure 8.47. Stress-Strain Relationship in Transverse Direction for 1mod, 2mod, 4mod and 8mod Systems under TLV Excitation (Soil Axis-2 Node-11).

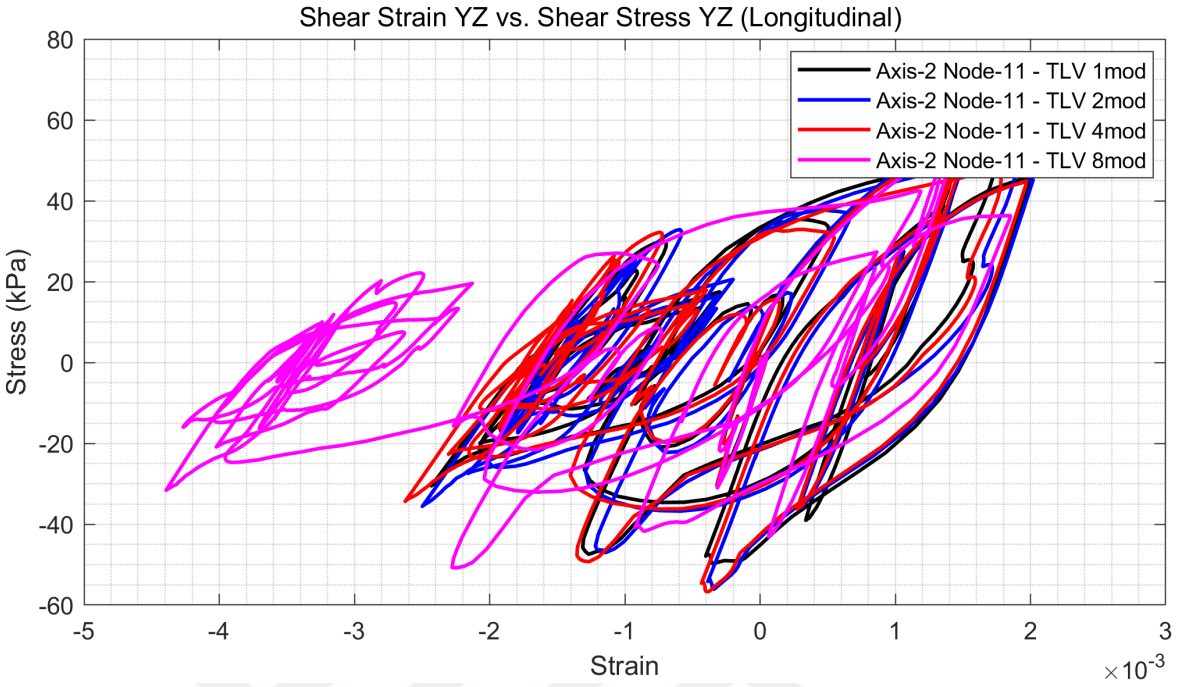

Figure 8.48. Stress-Strain Relationship in Longitudinal Direction for 1mod, 2mod, 4mod and 8mod Systems under TLV Excitation (Soil Axis-2 Node-11).

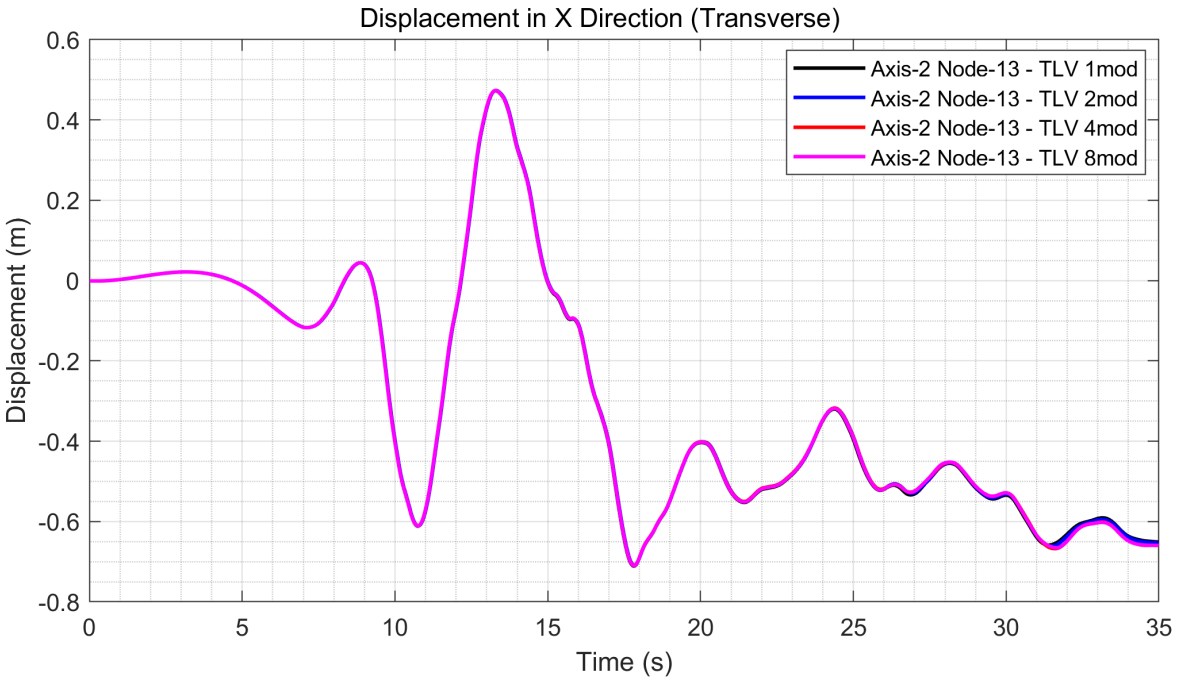

Figure 8.49. Soil Displacement Comparison in Transverse Direction at Embankment Crest for 1mod, 2mod, 4mod and 8mod Systems under TLV Excitation (Soil Axis-2 Node-13).

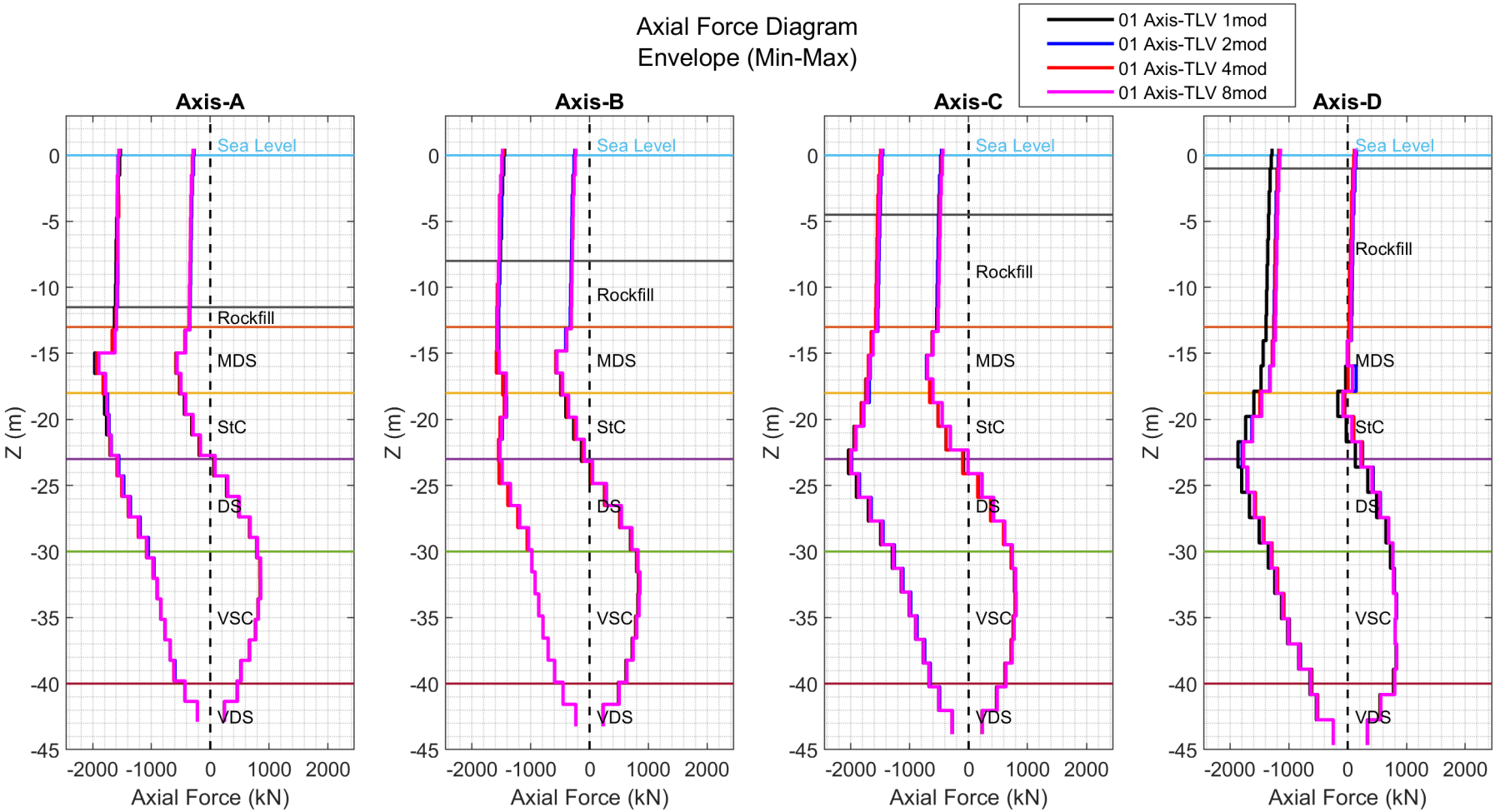

Figure 8.50. Axial Force Comparison for 1mod, 2mod, 4mod and 8mod Systems under TLV Excitation (1st Axes).

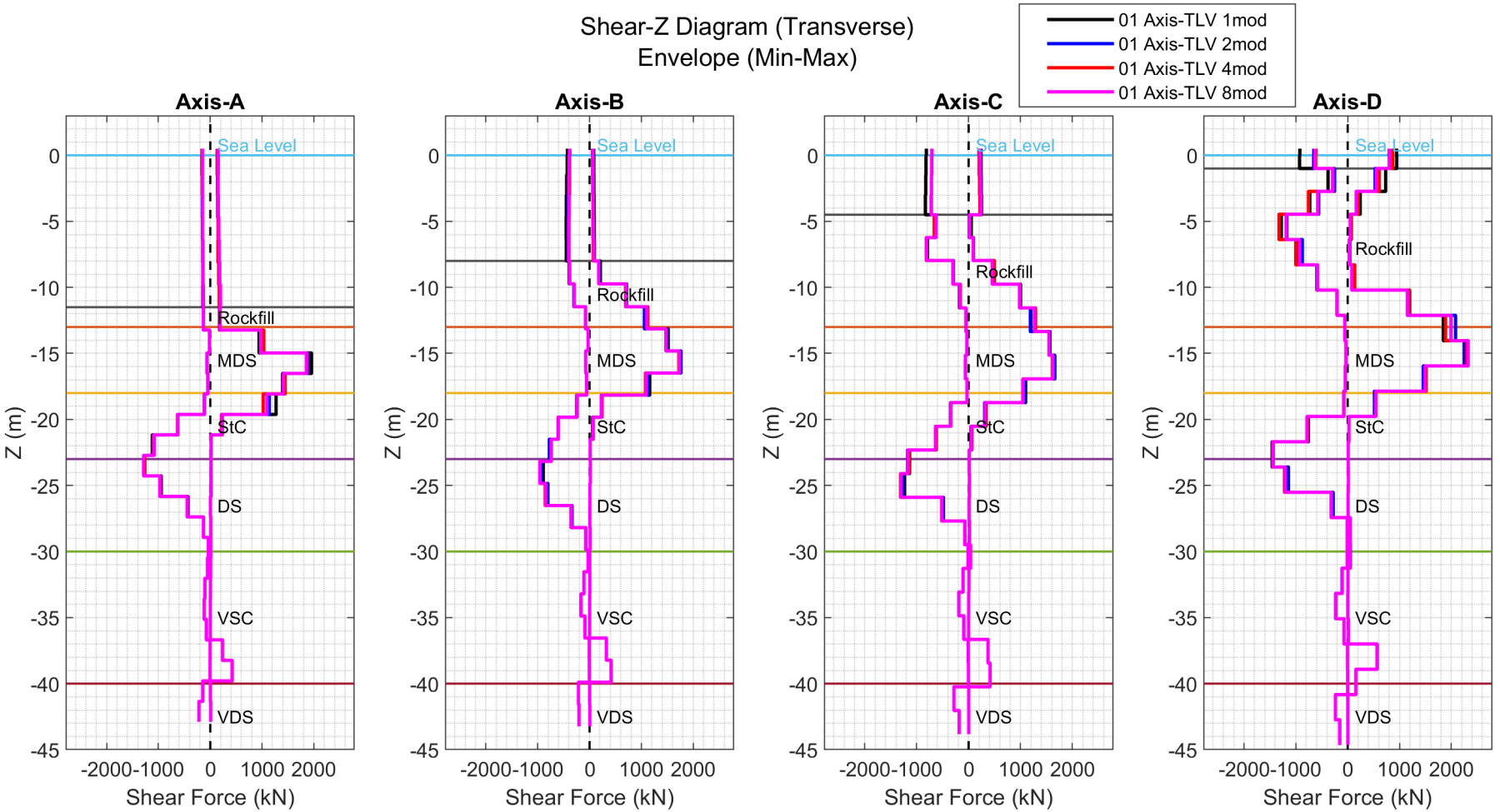

Figure 8.51. Shear Force (Transverse) Comparison for 1mod, 2mod, 4mod and 8mod Systems under TLV Excitation (1st Axes).

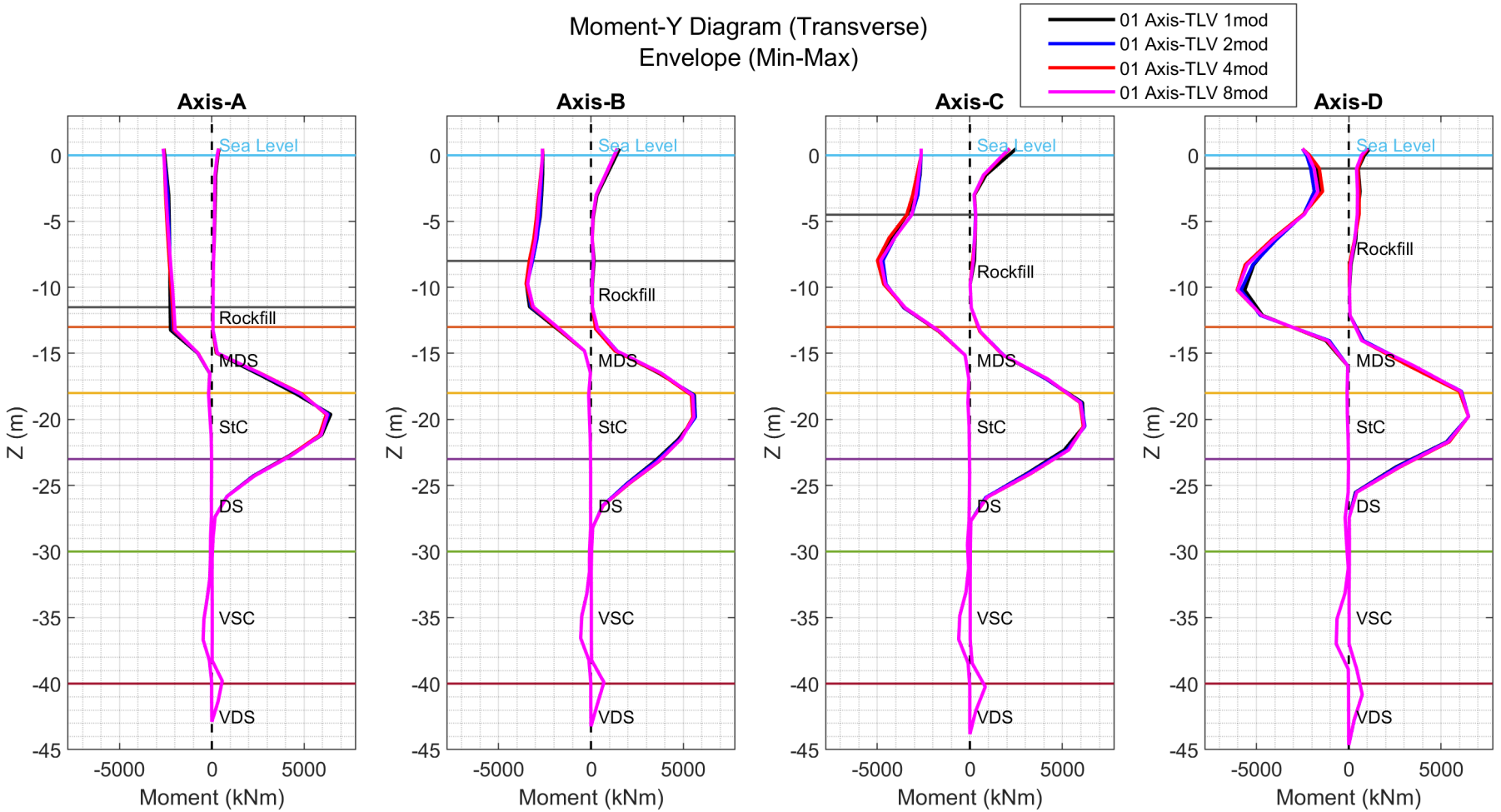

Figure 8.52. Moment (Transverse) Comparison for 1mod, 2mod, 4mod and 8mod Systems under TLV Excitation (1st Axes).

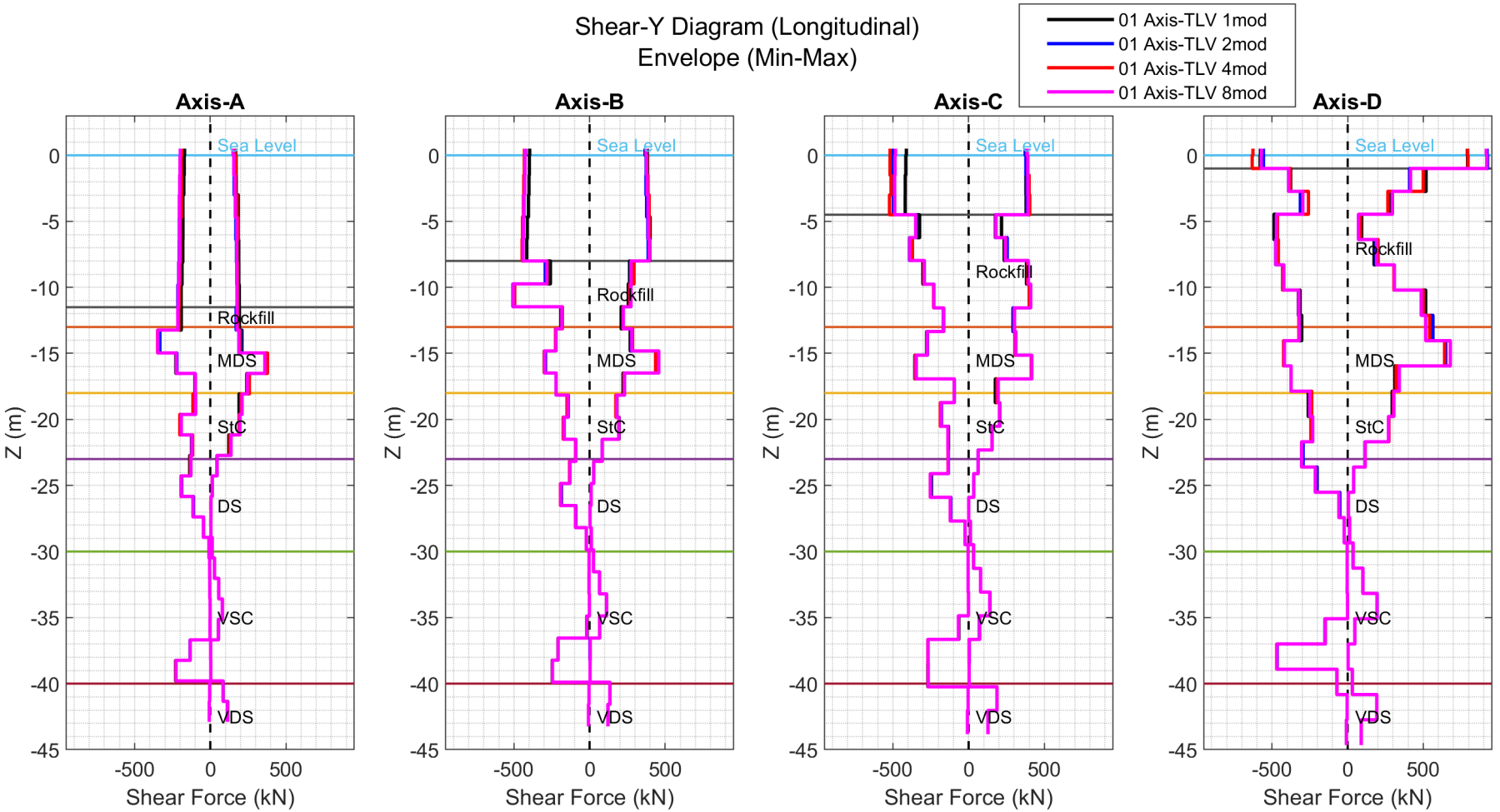

Figure 8.53. Shear Force (Longitudinal) Comparison for 1mod, 2mod, 4mod and 8mod Systems under TLV Excitation (1st Axes).

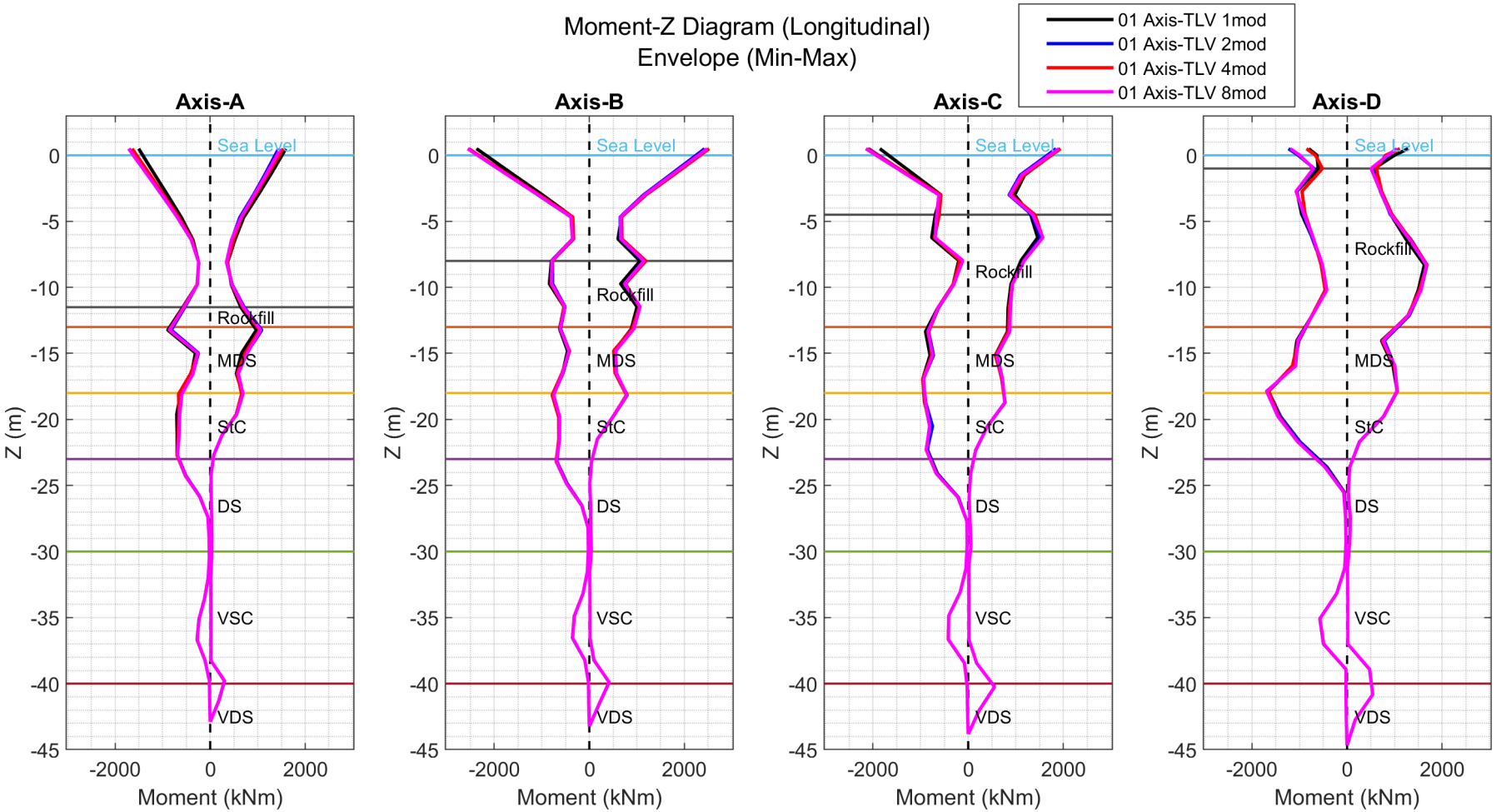

Figure 8.54. Moment (Longitudinal) Comparison for 1mod, 2mod, 4mod and 8mod Systems under TLV Excitation (1st Axes).

8.1.5. Evaluation of Shear Key Forces

Shear key force calculation is not very common in design practice since wharf systems are not modeled as multi-segmented. The calculation methods in literature based on very crude approximations and do not incorporate soil-structure interaction. This is probably the first attempt to calculate the shear forces at the shear keys between the wharf modules by a multi-segmented wharf system model incorporating soil-structure interaction properly.

Figure 8.55 shows the shear key forces between the modules for the systems having different number of modules. It is understood that the shear key force is around 570-670kN for one inner key, it is around 700-800kN for one key located at the end modules generally. 2-module system has the largest shear key force, which is about 900kN. It can be stated that the shear key forces at this level can be resisted solely by the concrete capital without requiring additional shear reinforcement. However, it should not be forgotten that the geotechnical system adopted in these analyses has constant stratification along the embankment.

Note that the shear key forces illustrated in Figure 8.55 belong to shear key no:3 (Figure 6.16). Figures 8.56 and 8.57 show the shear key force distribution for the keys located along the interface of two modules. It is seen that the shear key forces gradually decrease from landside to seaside. The reason is that the most of the transverse shear forces in deck plane is stored towards landside since the landside piles have larger shear forces due to their higher stiffnesses.

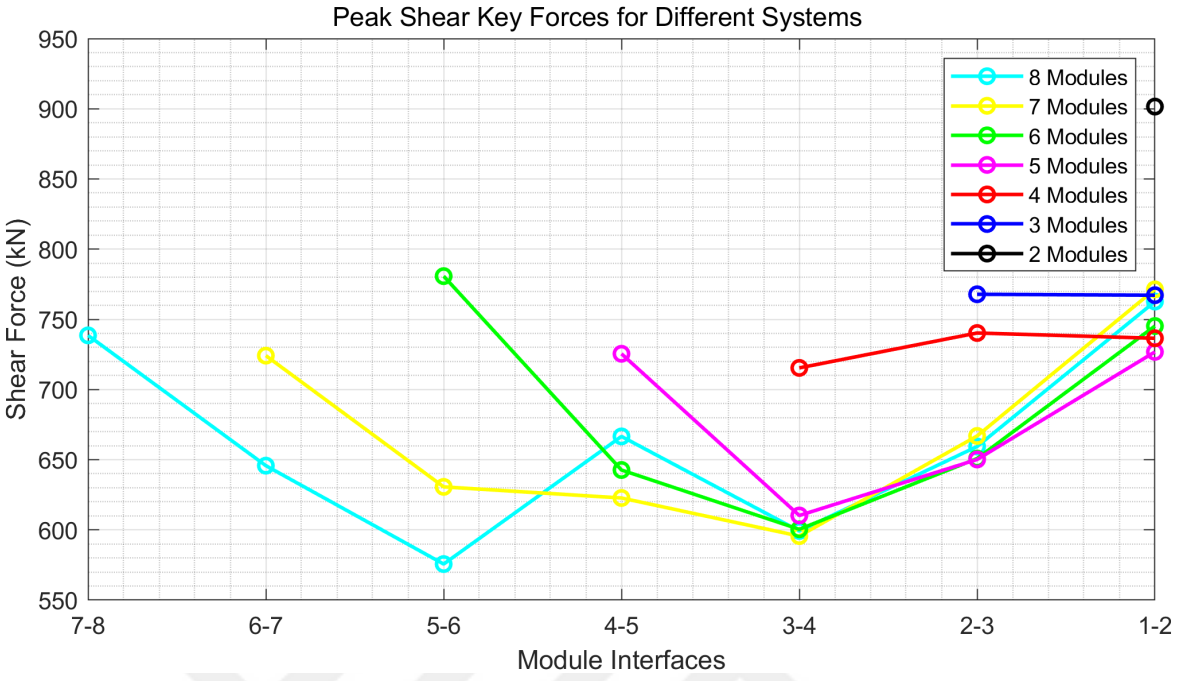

Figure 8.55. Peak Shear Key Forces for Different Systems (Shear Key No:3).

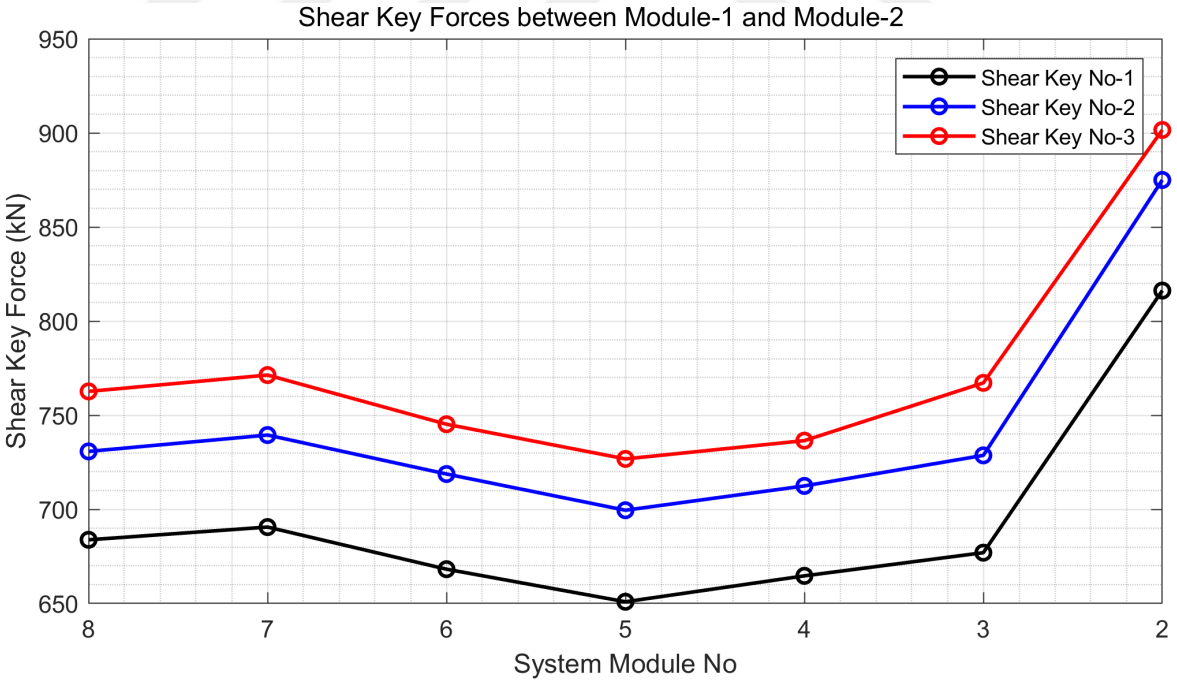

Figure 8.56. Peak Shear Key Forces between Module-1 and Module-2.

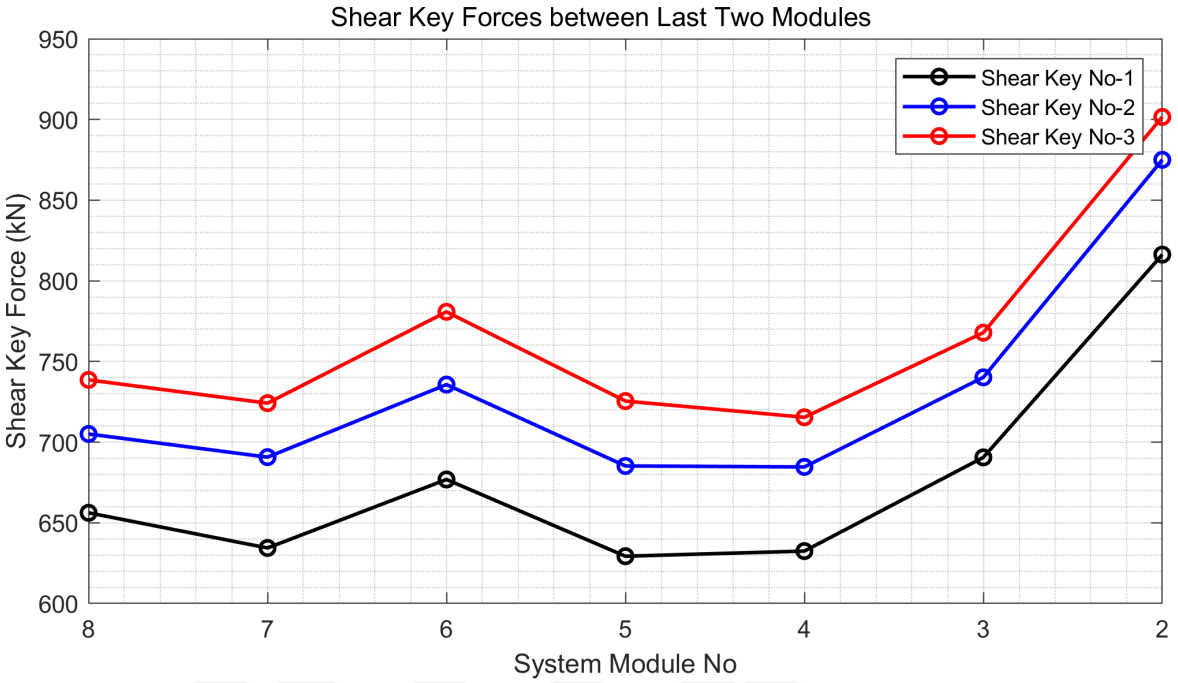

Figure 8.57. Peak Shear Key Forces between Last Two Modules.

8.1.6. Effect of Vertical Excitation

In this section, the model of single module wharf system is solved under TL and TLC excitation to demonstrate the effect of vertical excitation on the seismic response of elements. The results show that there is no notable effect of vertical excitation on the seismic response. It should be noted that the results do not cover the effect of vertical excitation on the inelastic behavior of piles since the adopted procedure for the plasticity modeling is based on simple beam hinge theory.

Figures 8.58 and 8.59 show the pore pressure and effective stress time histories under TL and TLV excitation. The high frequency content in the responses, incorporating vertical excitation is prominent as expected. The high frequency content slightly affects the stress-strain responses and the soil displacement, as can be seen in Figures 8.60, 8.61, 8.62. Note that the node at which the responses illustrated is taken from free-field (Figure 6.18).

The effect of vertical excitation on the internal forces of piles can be seen in Figures 8.64, 8.65, 8.66 and 8.67.

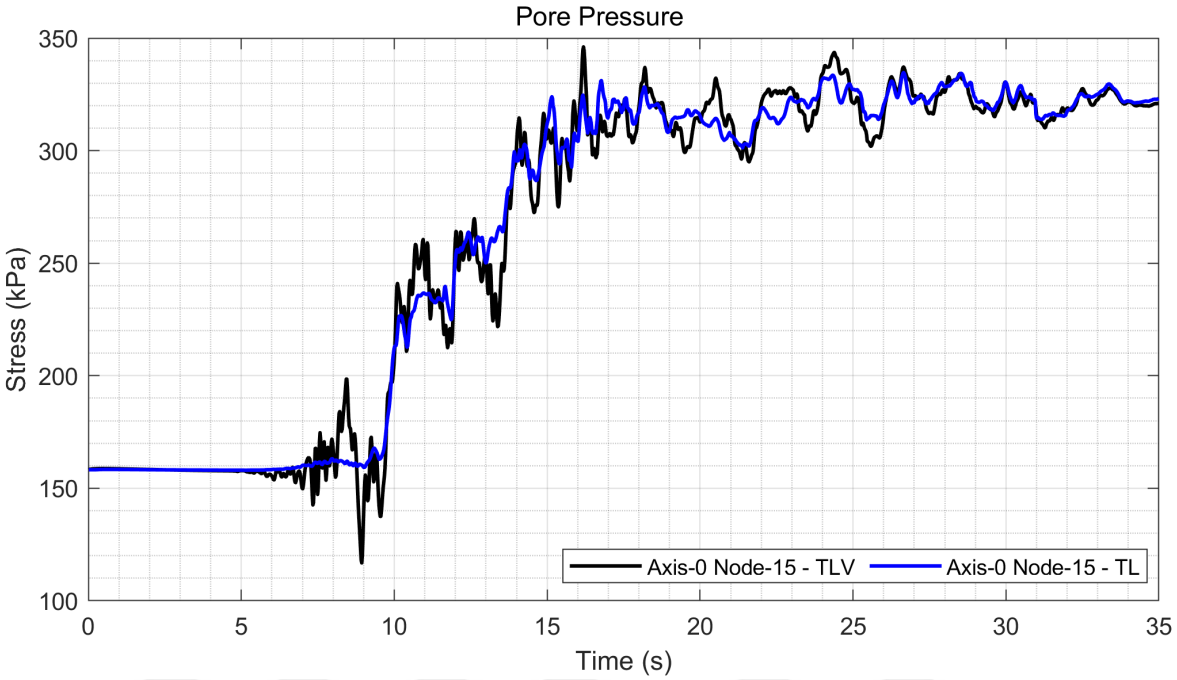

Figure 8.58. Effect of Vertical Excitation on Pore Pressure (Soil Axis-0 Node-15).

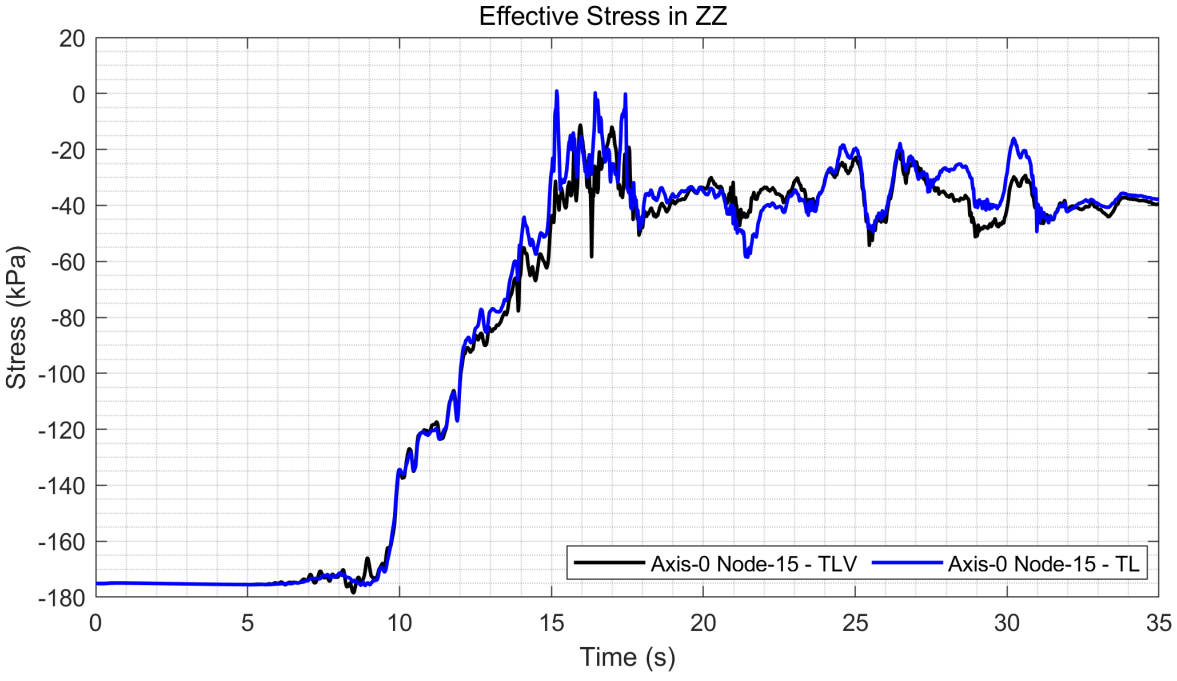

Figure 8.59. Effect of Vertical Excitation on Effective Stress (Soil Axis-0 Node-15).

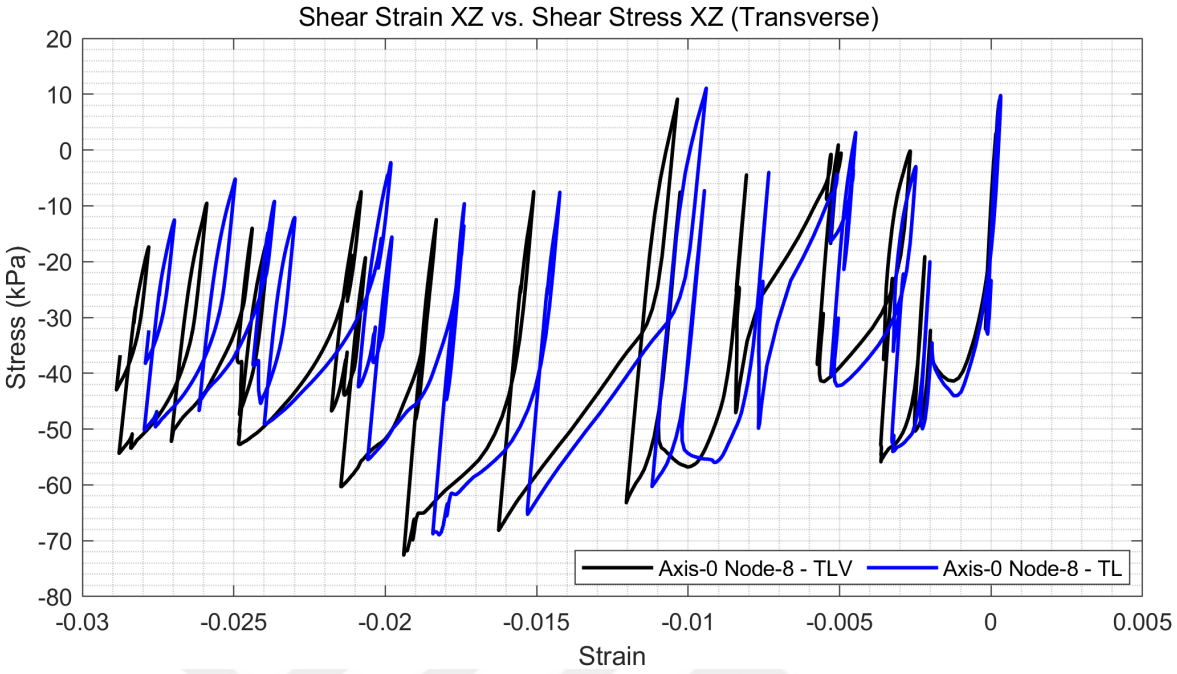

Figure 8.60. Effect of Vertical Excitation on Stress-Strain in Transverse Direction (Soil Axis-0 Node-8).

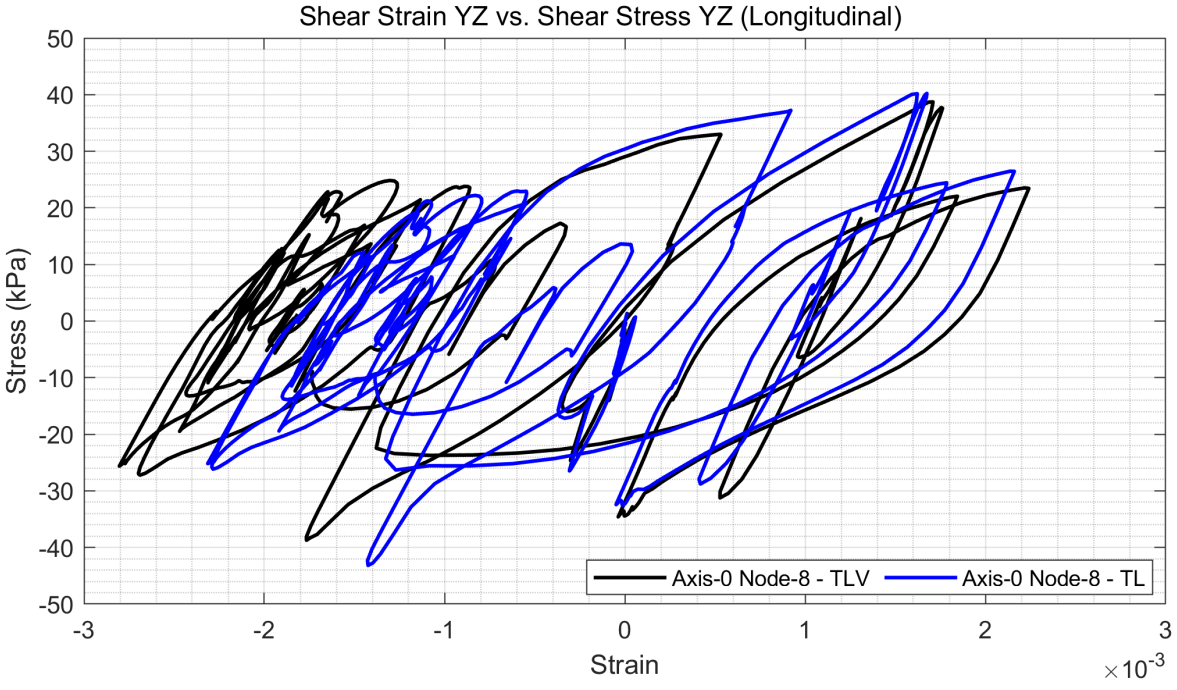

Figure 8.61. Effect of Vertical Excitation on Stress-Strain in Longitudinal Direction (Soil Axis-0 Node-8).

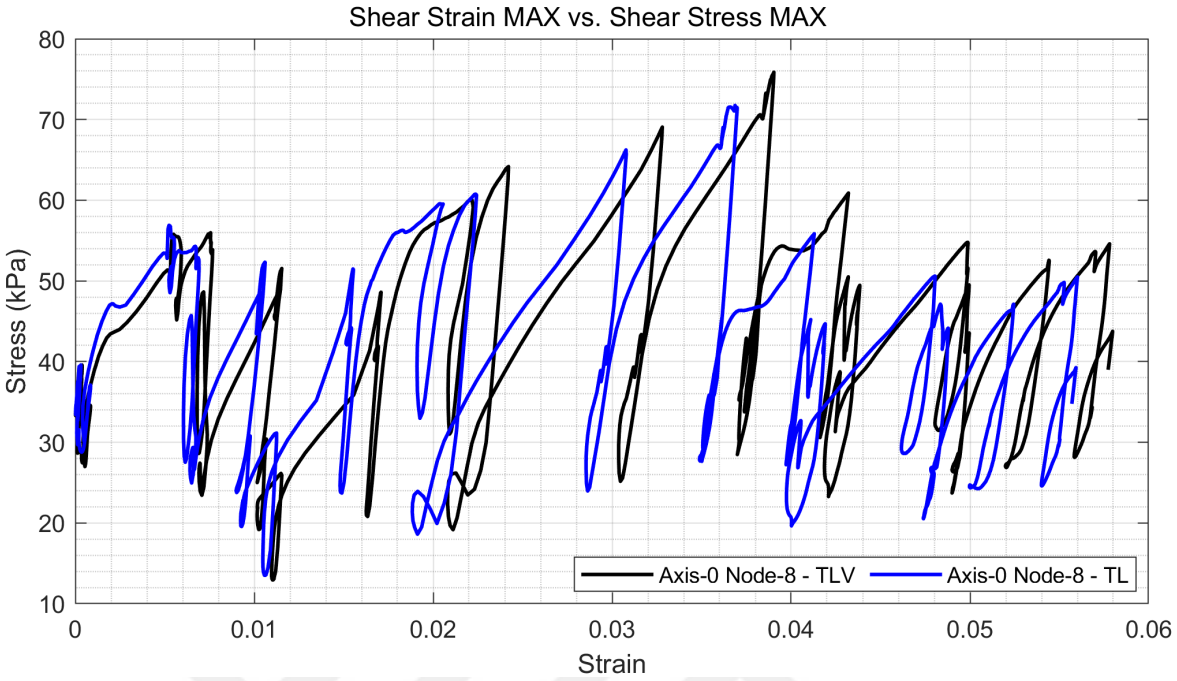

Figure 8.62. Effect of Vertical Excitation on Maximum Stress-Strain (Soil Axis-0 Node-8).

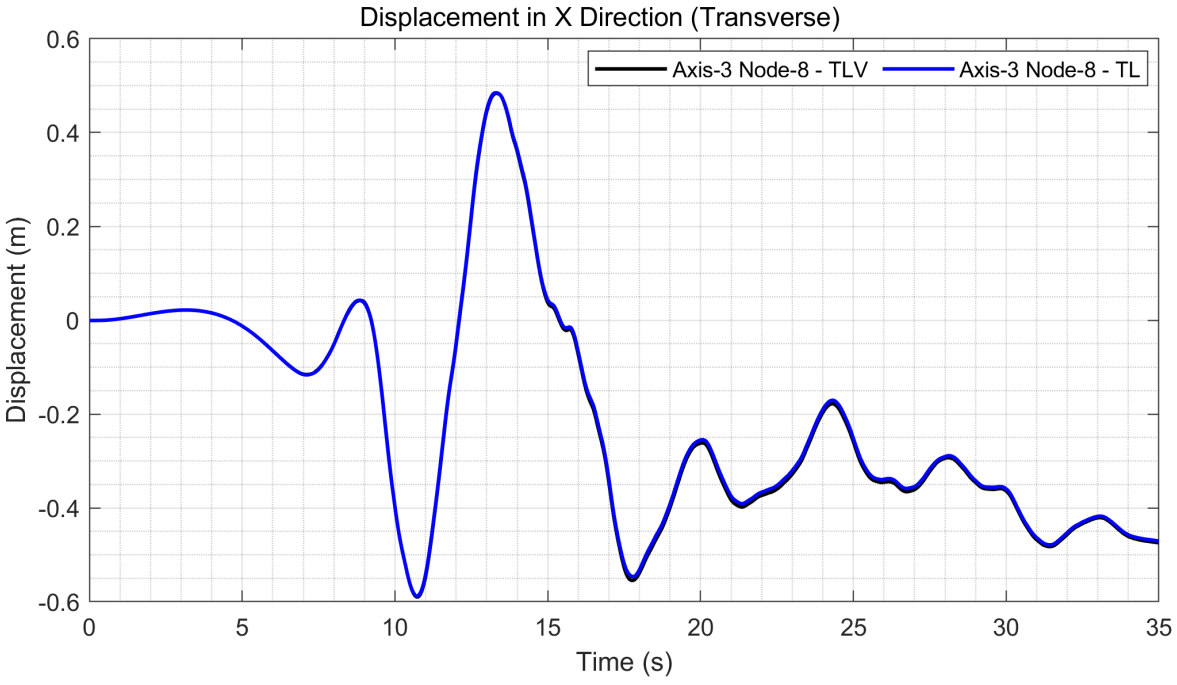

Figure 8.63. Effect of Vertical Excitation on Displacement in X Direction (Soil Axis-0 Node-8).

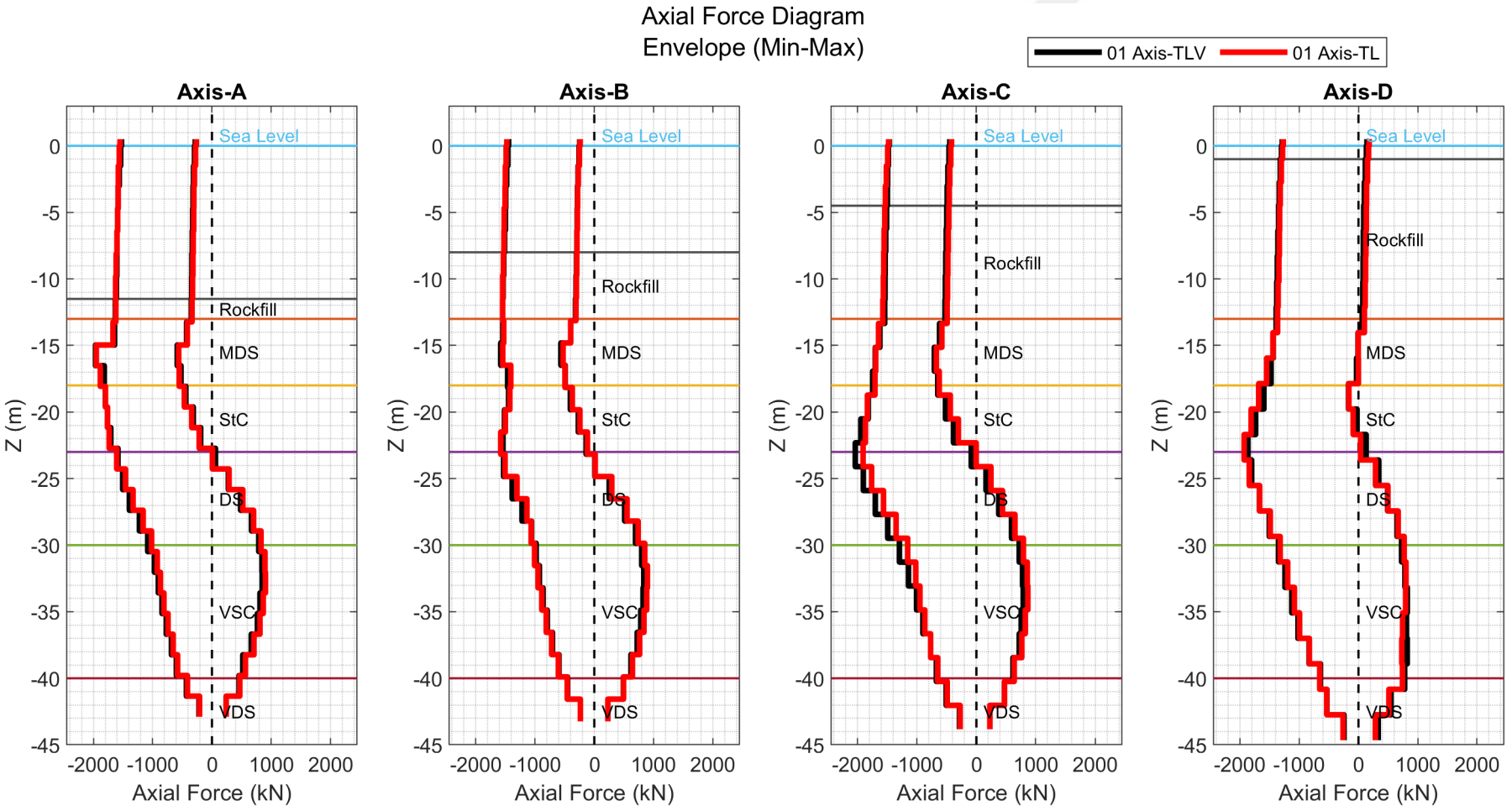

Figure 8.64. Effect of Vertical Excitation on Pile Axial Forces.

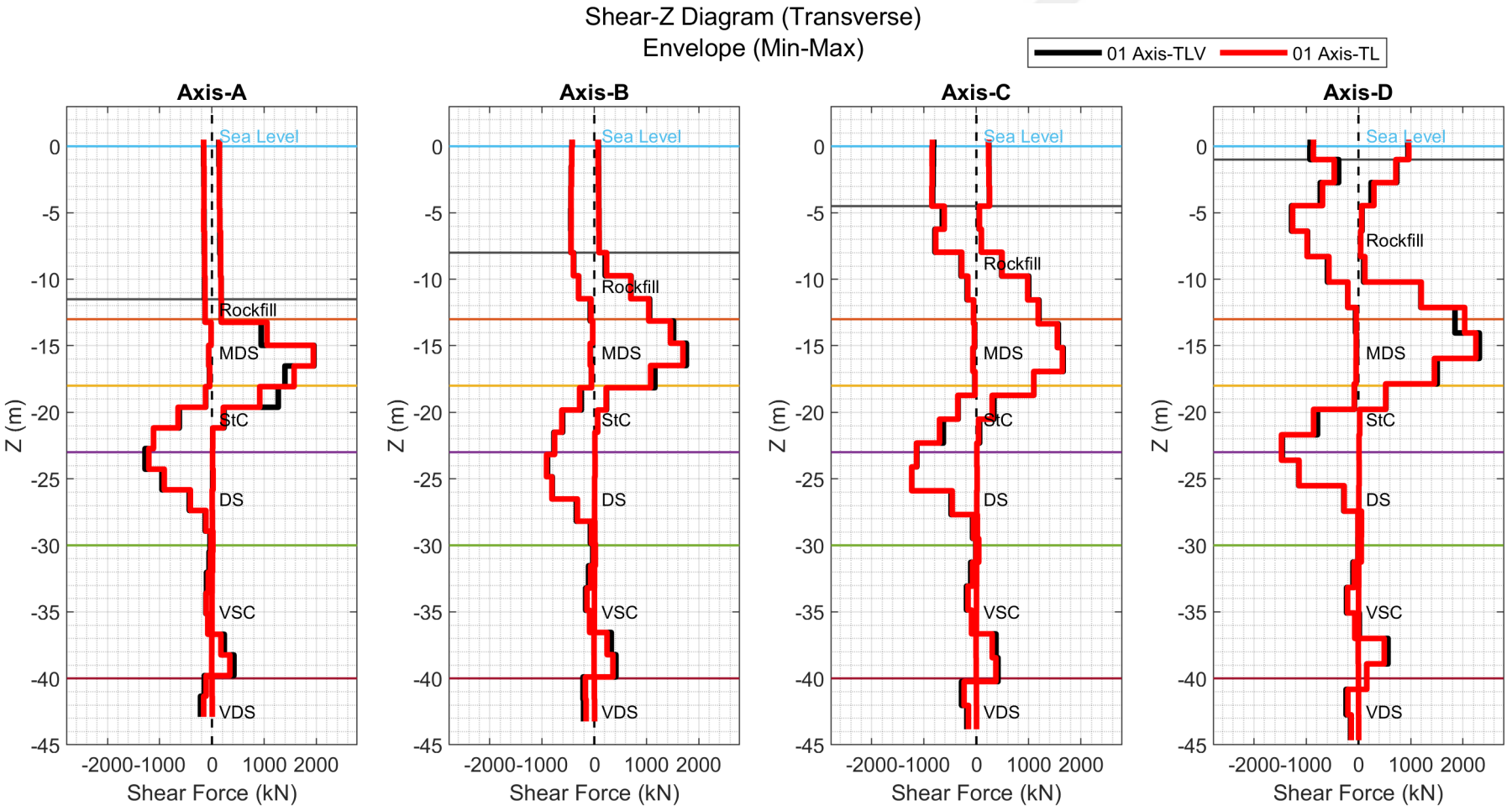

Figure 8.65. Effect of Vertical Excitation on Pile Shear Forces in Transverse Direction.

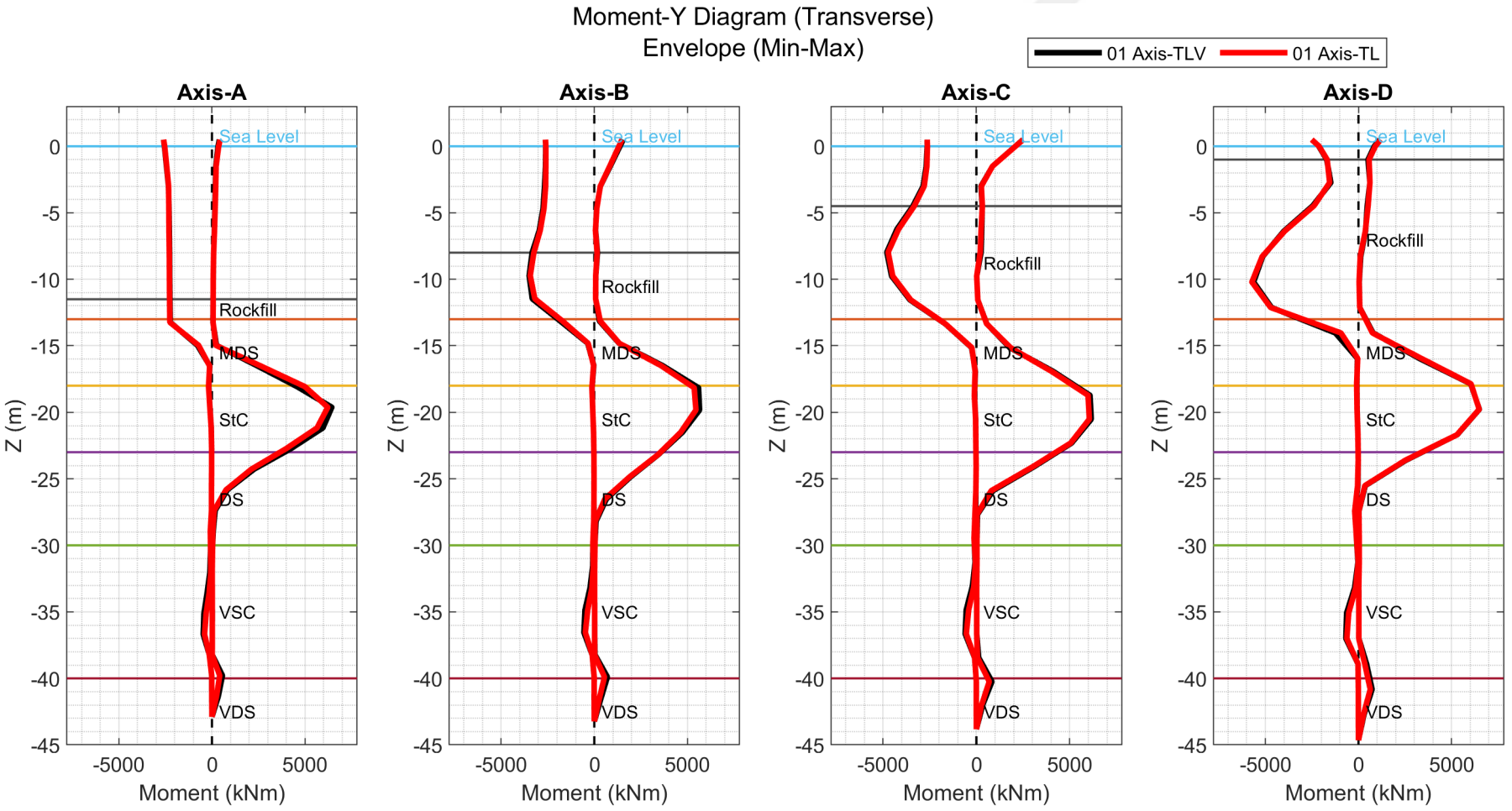

Figure 8.66. Effect of Vertical Excitation on Pile Moments in Transverse Direction.

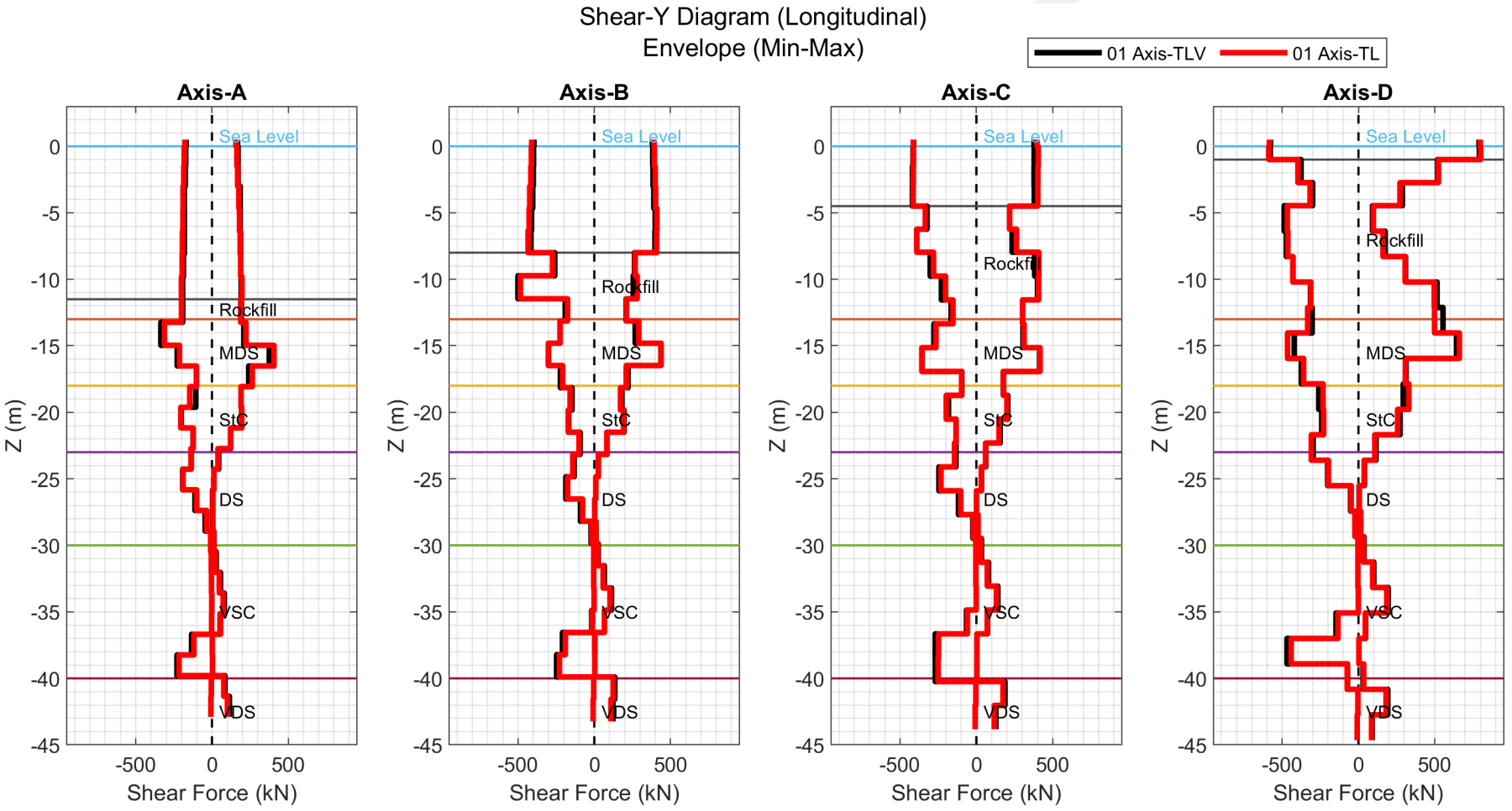

Figure 8.67. Effect of Vertical Excitation on Pile Shear Forces in Longitudinal Direction.

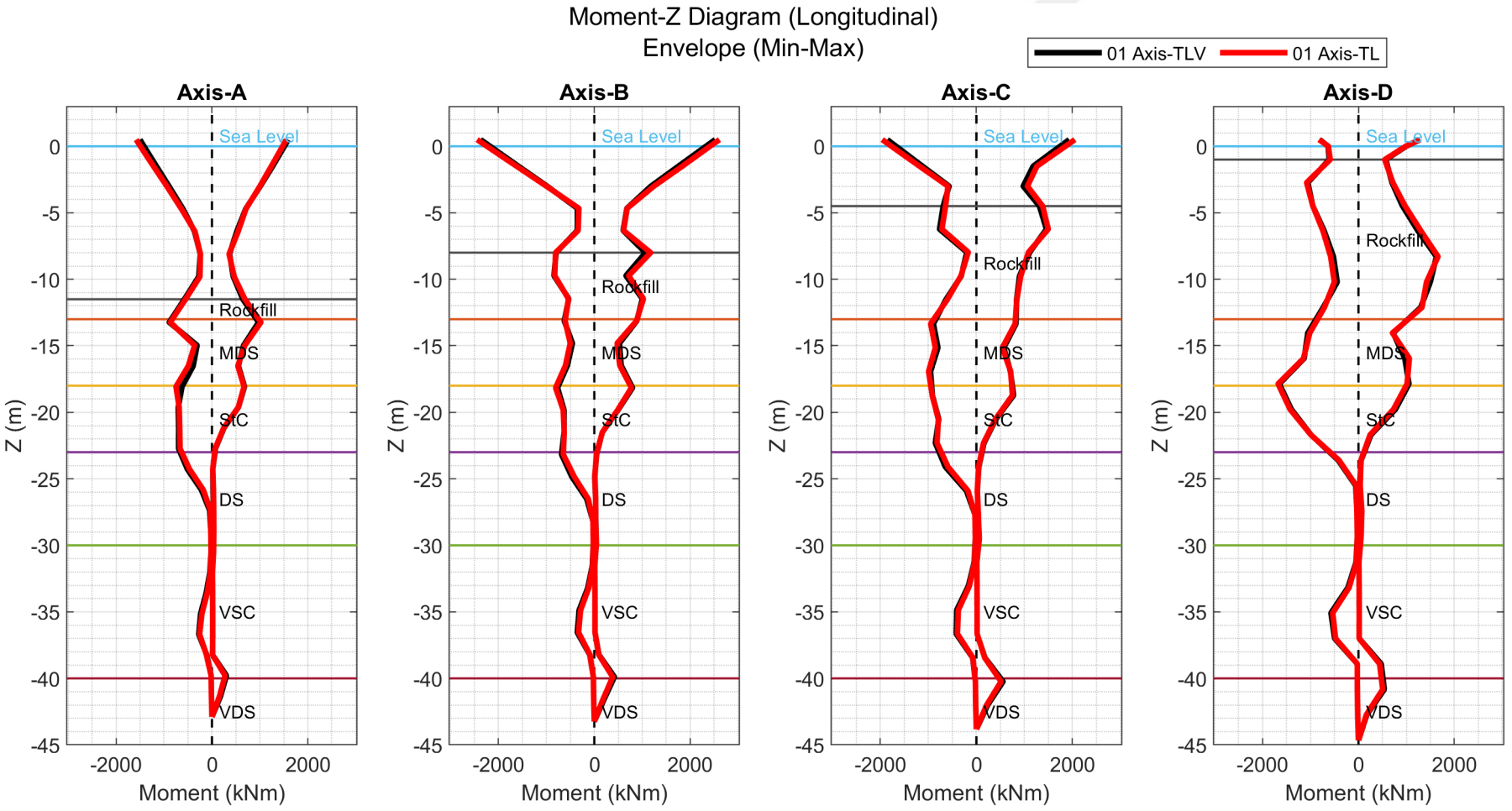

Figure 8.68. Effect of Vertical Excitation on Pile Moments in Longitudinal Direction.

8.2. Evaluation of Seismic Response for 8-Modules Wharf System with Longitudinally Changing Soil Stratification

One of the main aims of this study is to model realistic wharf systems incorporating the important aspects as much as possible. Wharf systems can be very long in general, therefore, it is probable to have changing soil stratification along the embankment and it may affect the seismic response of structural elements considerably. In this regard, a wharf system is modeled to account for varying soil stratification along its longitudinal direction. In reality, such a long embankment may exhibit very complex soil stratification. However, for this study, a model is adopted where the thicknesses of first two layers along the wharf embankment change linearly to simplify the demonstration of the effect of changing soil stratification (Section 7.4).

Figures 8.69 and 8.70 shows the transverse displacement of wharf system in two different perspectives, the first view is from the beginning of the embankment towards the end, the second view is vice versa. Gradually increasing liquefaction-induced deformation is observed clearly towards the end of embankment clearly. Figure 8.71 shows the plan view of embankment. The rotation of wharf decks in plan can be noticeable with the 30 times magnified model view. The transverse displacement measured at the slope is 1.2m at the end of embankment whereas it is around 0.4m at the beginning of embankment.

Figure 8.72 shows the excessive deformation at the piles towards the end of the embankment. Similar to the soil deformation trend as mentioned above, the plastic hinge formation at the piles can be observed at Figures 8.73 and 8.74. While the plastic hinges are observed only at the RC plugs at the beginning of embankment, those are also occurred inside the rockfill and soil layers towards the end of system because of the liquefaction induced soil deformations.

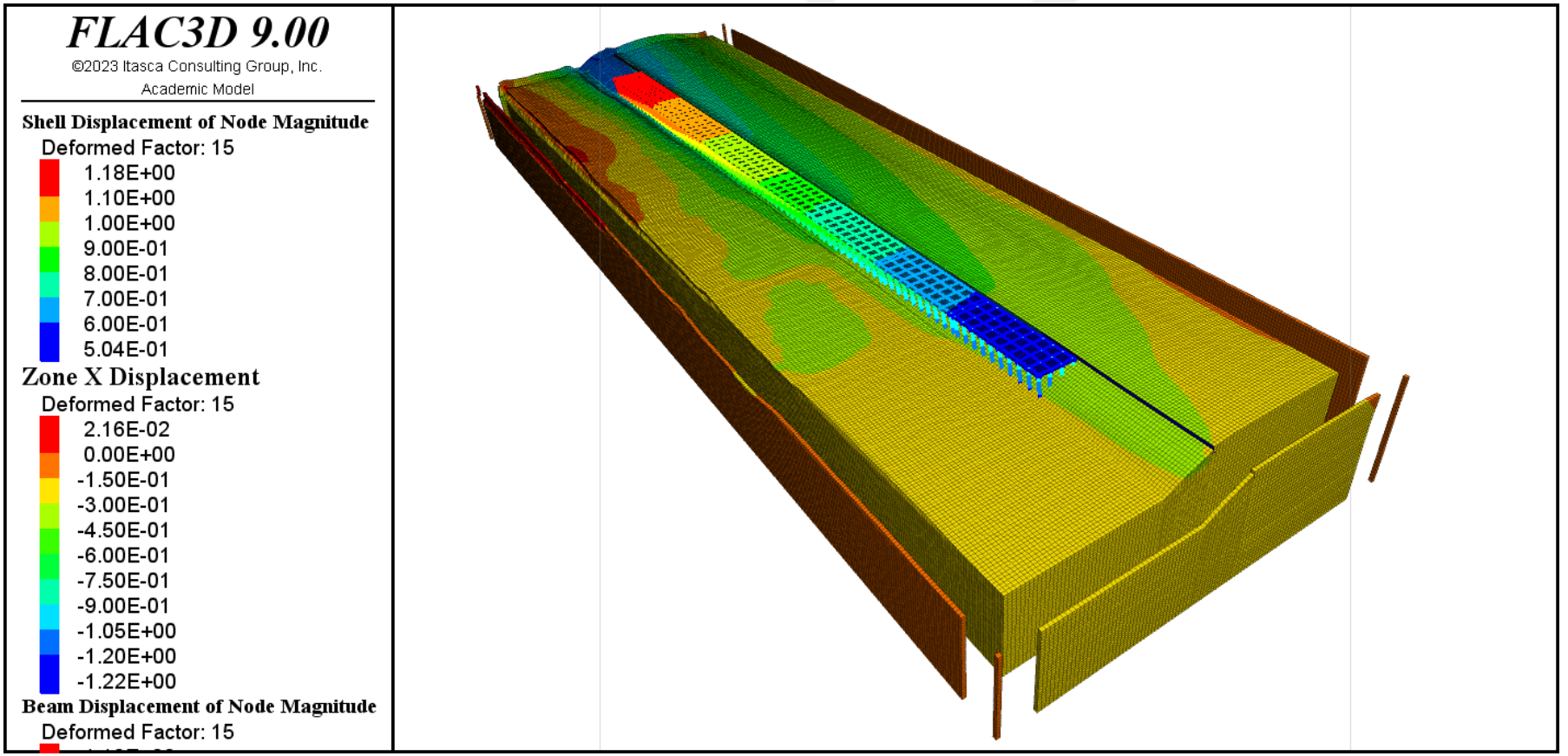

Figure 8.69. Wharf System Displacement Plot for LCS System (from First Module to Last Module).

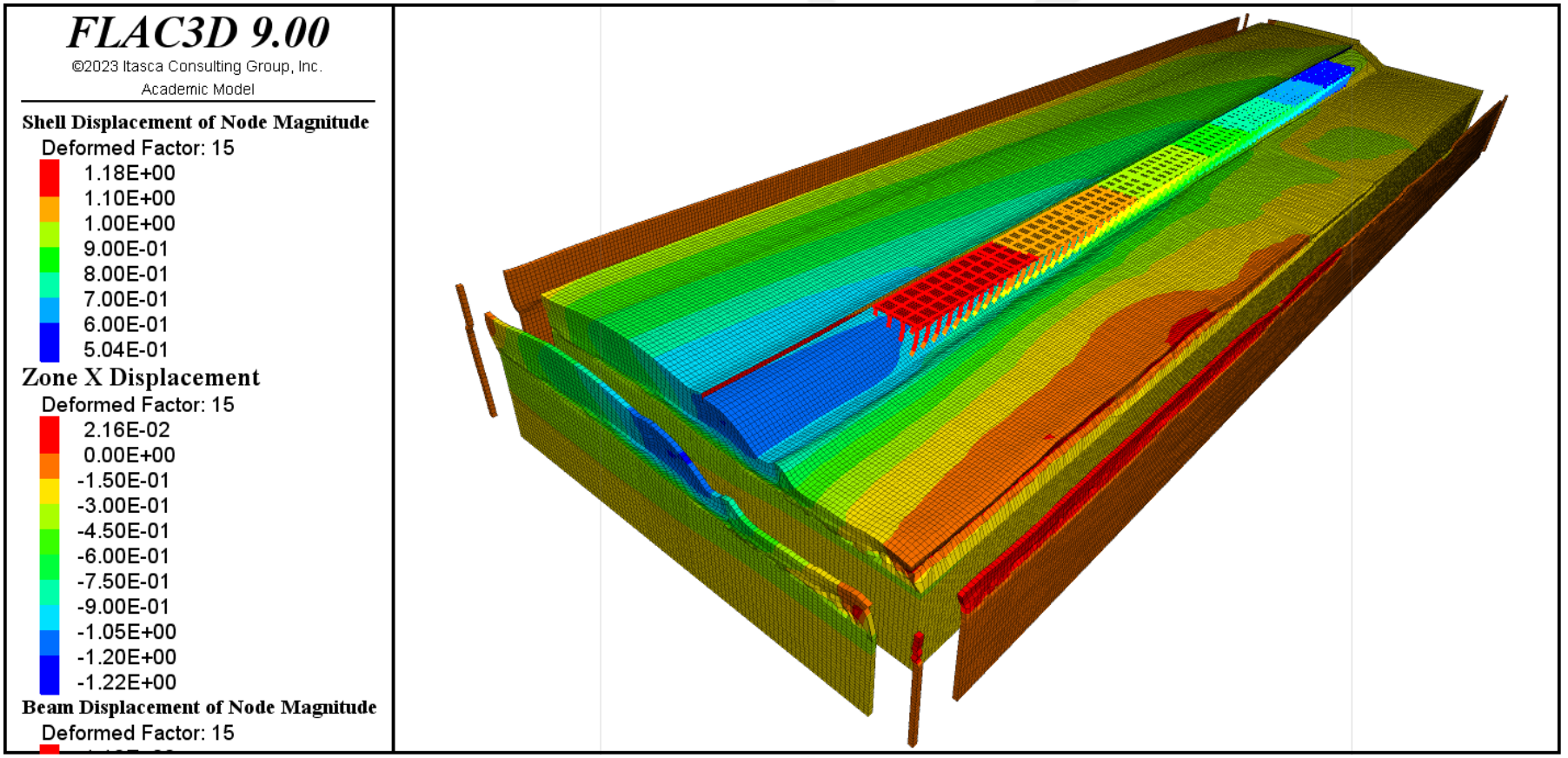

Figure 8.70. Wharf System Displacement Plot for LCS System (from Last Module to First Module).

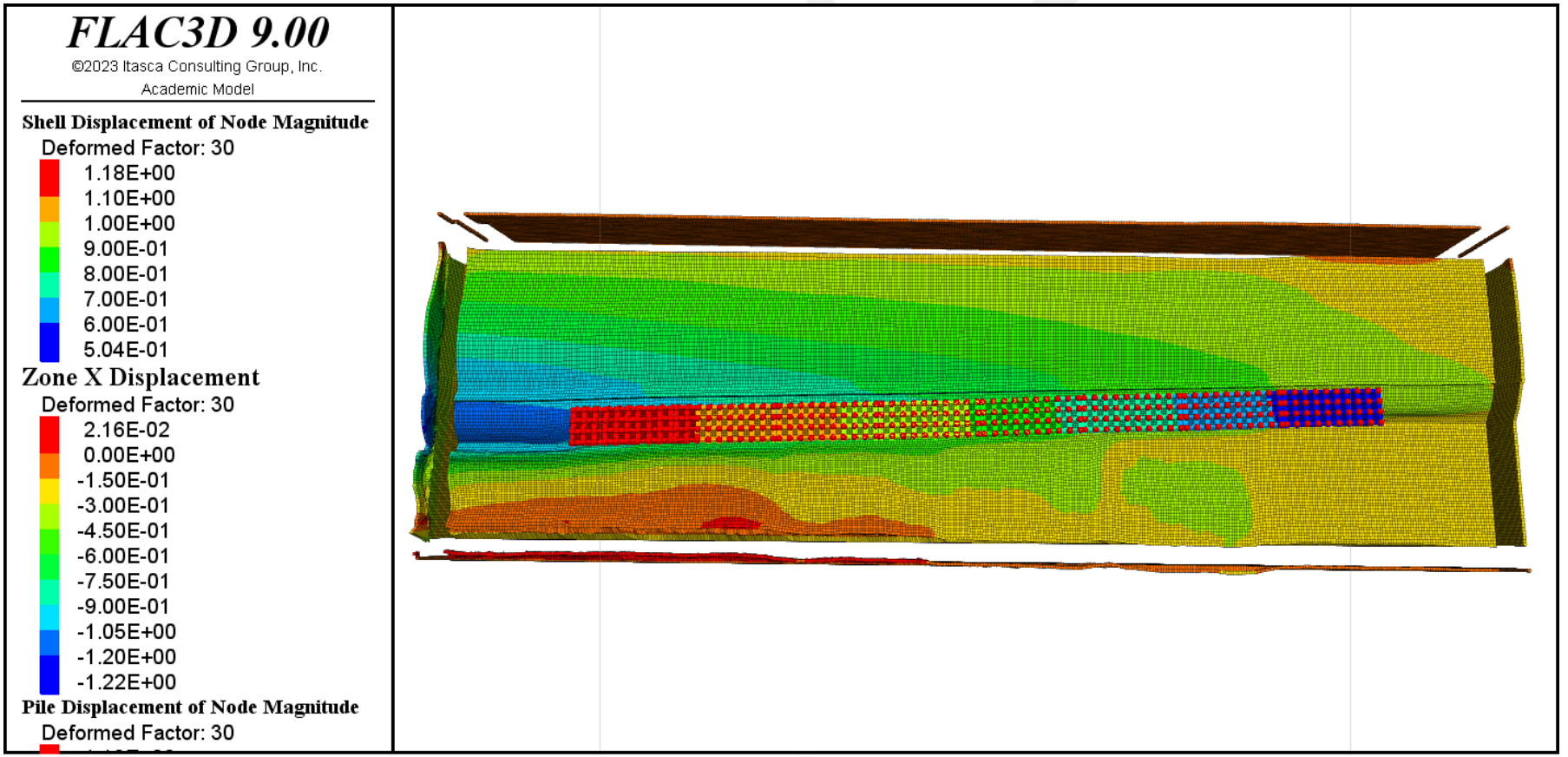

Figure 8.71. Wharf System Displacement Plot (Plan View) for LCS System.

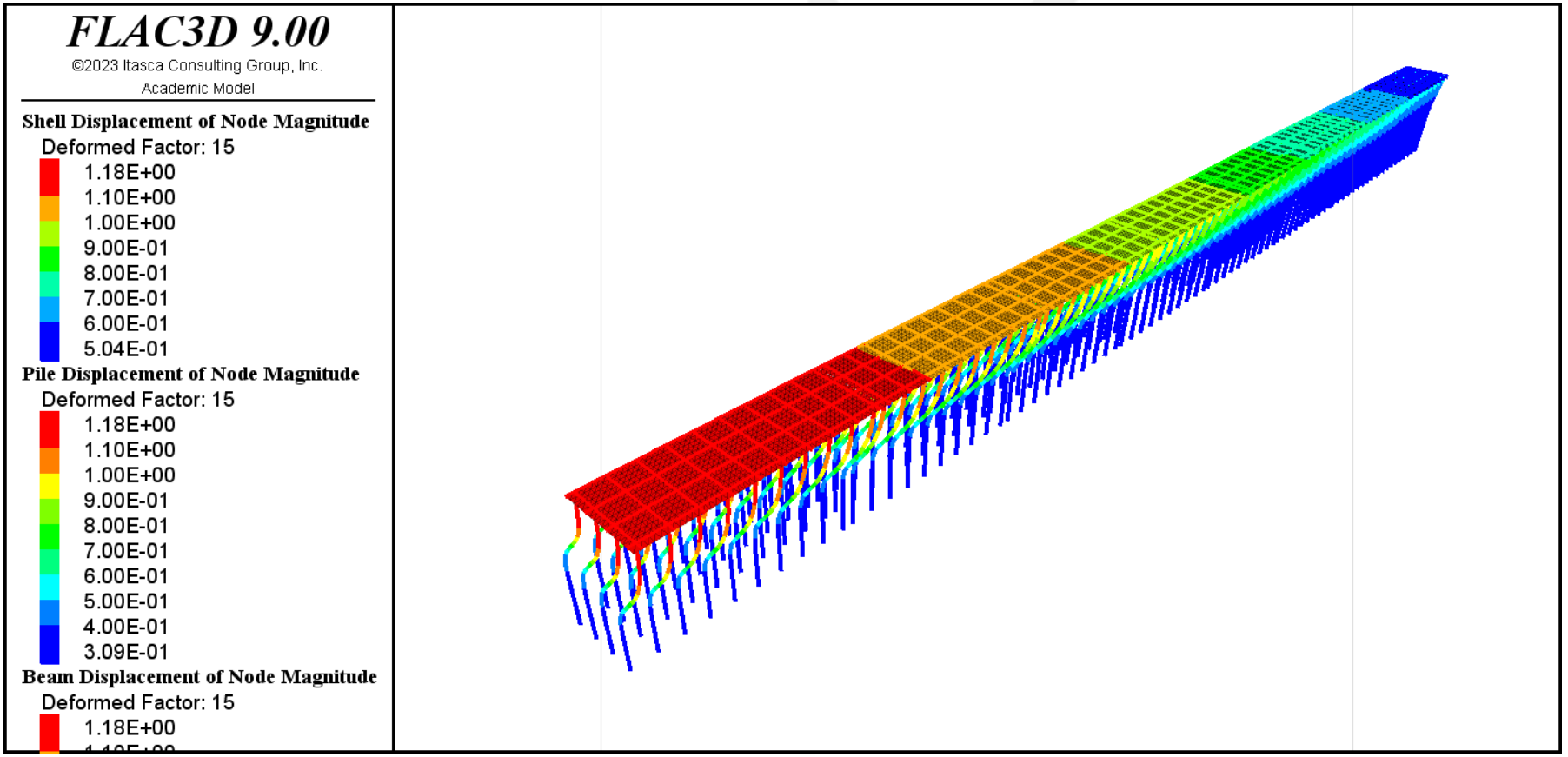

Figure 8.72. Pile and Deck Displacement Plot for LCS System.

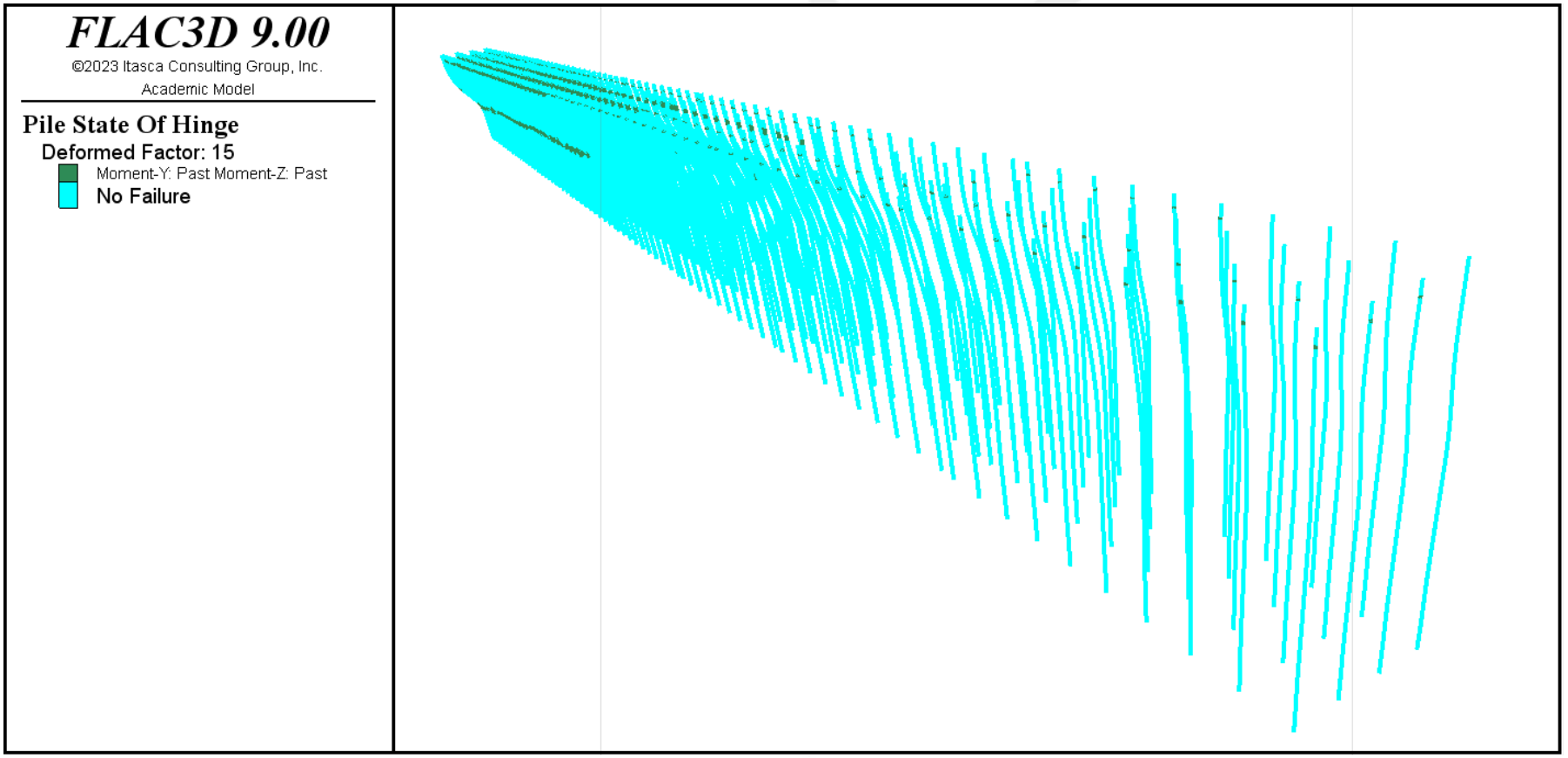

Figure 8.73. Pile Hinges for LCS Wharf System (from First Module to Last Module).

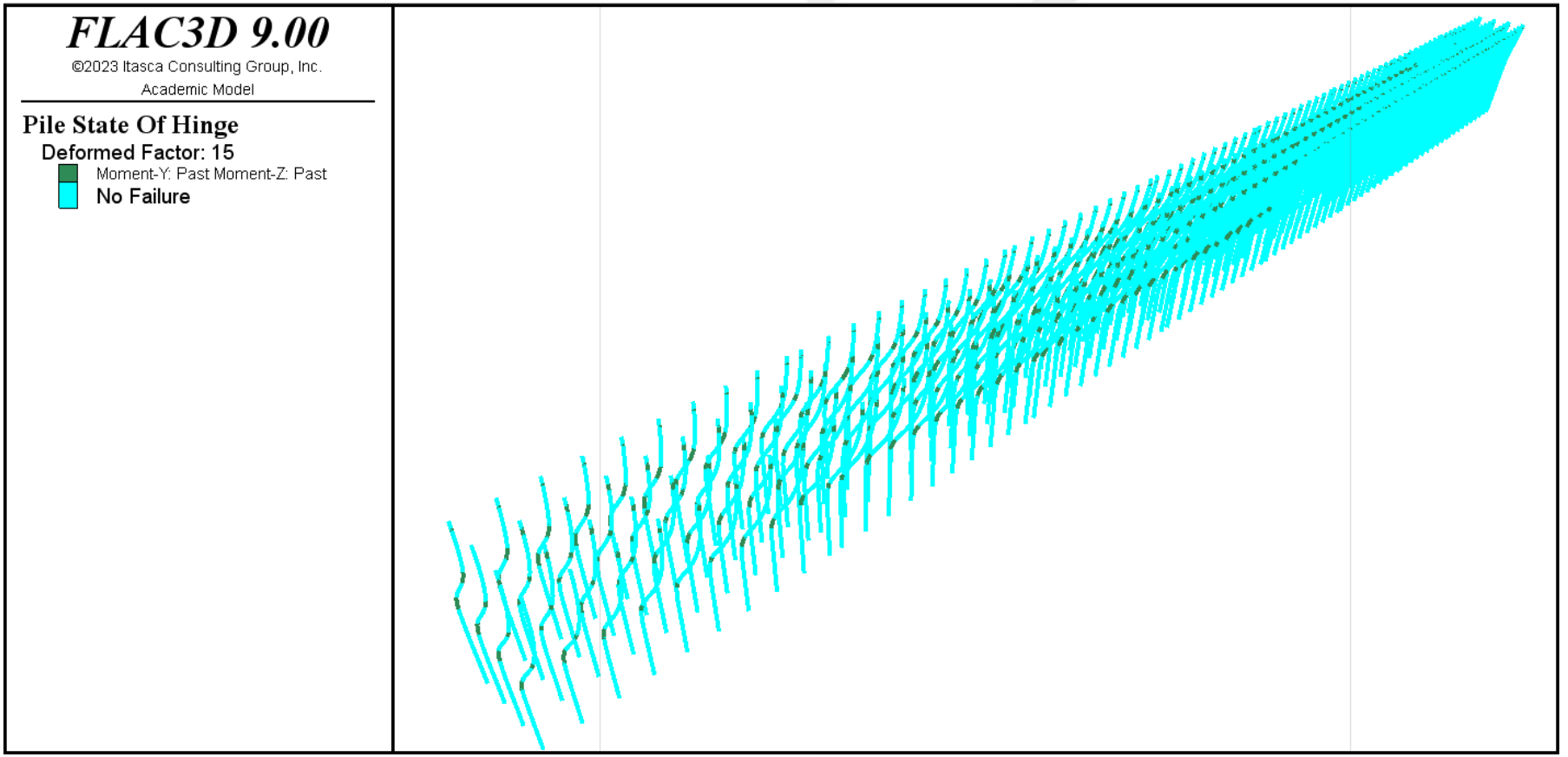

Figure 8.74. Pile Hinges for LCS Wharf System (from Last Module to First Module).

Figures 8.75 and 8.76 illustrate the pore pressure and the effective stress time histories for the 8-module wharf systems with longitudinally constant and changing (LCS) soil stratifications under TLV excitation. The response quantities are measured at soil nodes located near 1st modules. The black curves represent the responses of the system with constant soil stratification while the blue curves represent those of the system with longitudinally changing soil stratification (LCS). Significant pore pressure development and effective stress reduction are observed only at the systems with constant soil stratification. LCS system has an almost negligible thickness of the liquefiable MDS layer in the region where the first module is located. As a result, nearly linear deformation is observed at the same soil node for LCS system while approximately 4.6% and 1.2% shear strains are measured in transverse and longitudinal directions respectively for the system with constant soil stratification (Figures 8.77 and 8.78).

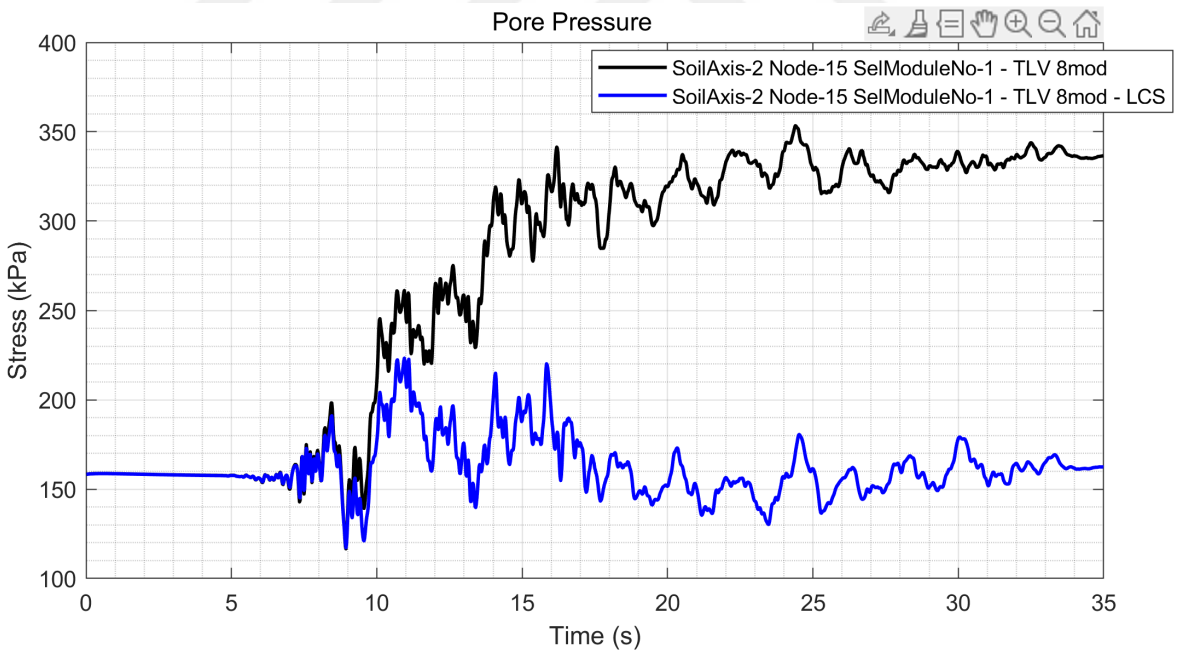

Figure 8.75. Pore Pressure Comparison for 8mod Constant System vs. 8mod LCS System (Soil Axis-2 Node-15 SelMod-1).

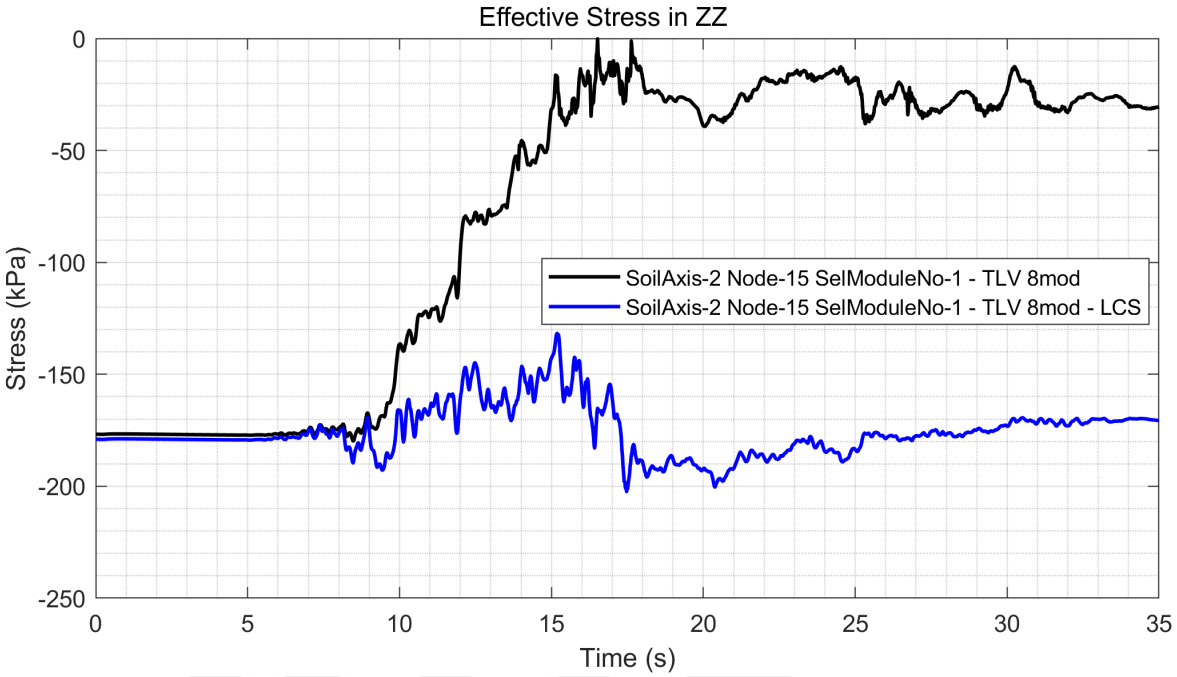

Figure 8.76. Effective Stress Comparison for 8mod Constant System vs. 8mod LCS System (Soil Axis-2 Node-15 SelMod-1).

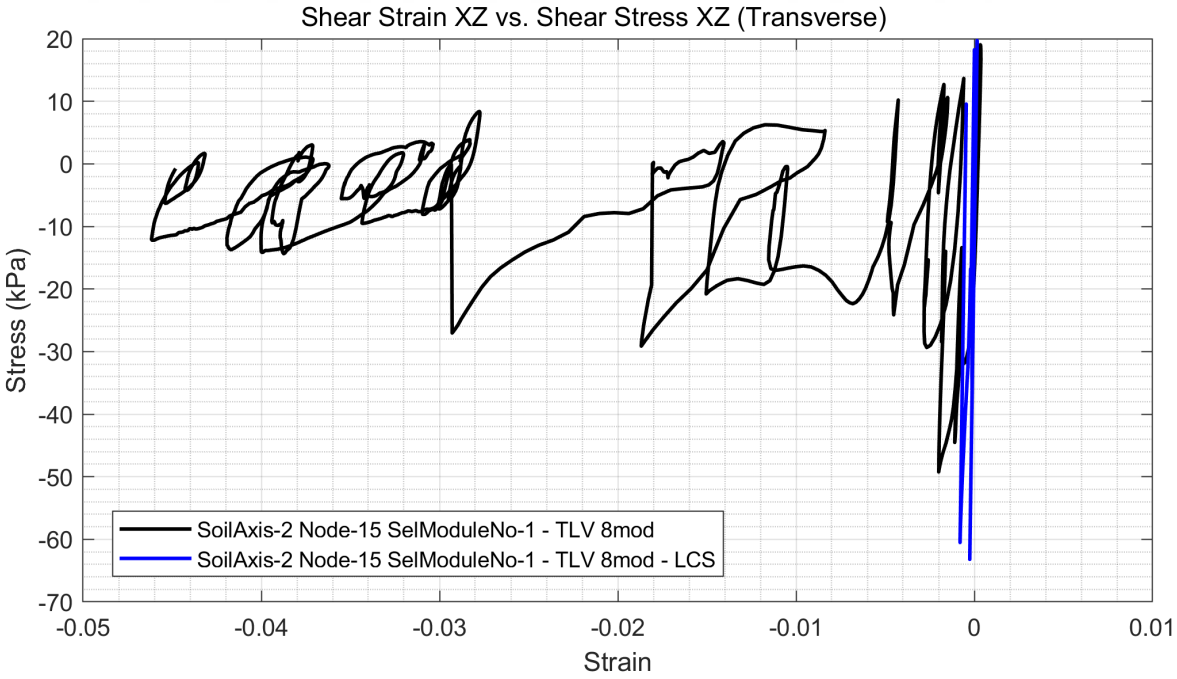

Figure 8.77. Shear Strain-Stress Comparison in Transverse Direction for 8mod Constant System vs. 8mod LCS System (Soil Axis-2 Node-15 SelMod-1).

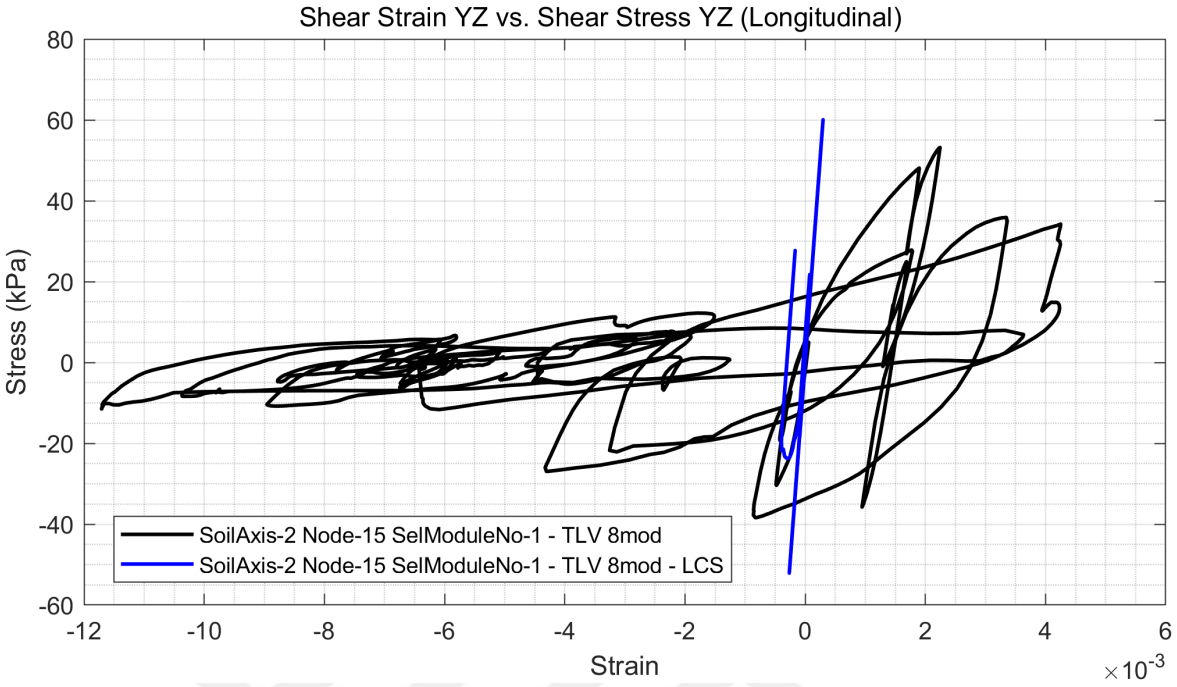

Figure 8.78. Shear Strain-Stress YZ Comparison in Longitudinal Direction for 8mod Constant System vs. 8mod LCS System (Soil Axis-2 Node-15 SelMod-1).

Figures 8.79 and 8.80 illustrate the pore pressure and effective stress time histories measured at the soil node 15, Figures 8.81 and 8.82 shows those measured at the soil node 16 (Figure 6.17). Both nodes are taken from soil axis no 2 near the 8th module (Figure 6.18). Since LCS model has a thicker MDS layer near the 8th module, pore pressure generation and effective stress reduction are present in soil node 16 for LCS model. No change is observed at the soil node 16 since it does not correspond to the MDS layer in the wharf system with constant stratification. Shear strains reach to 7.3% and 2% for LCS model in transverse and longitudinal directions respectively (Figures 8.83 and 8.84). The transverse displacements are measured as 0.48m and 0.92m at the embankment crest nodes near the 1st and 8th module respectively for LCS model whereas those are measured as 0.67m at the nodes near the 1st and 8th module for the system with constant soil stratification (Figure 8.85). The displacements in longitudinal direction have the similar trend but they are small (Figure 8.86).

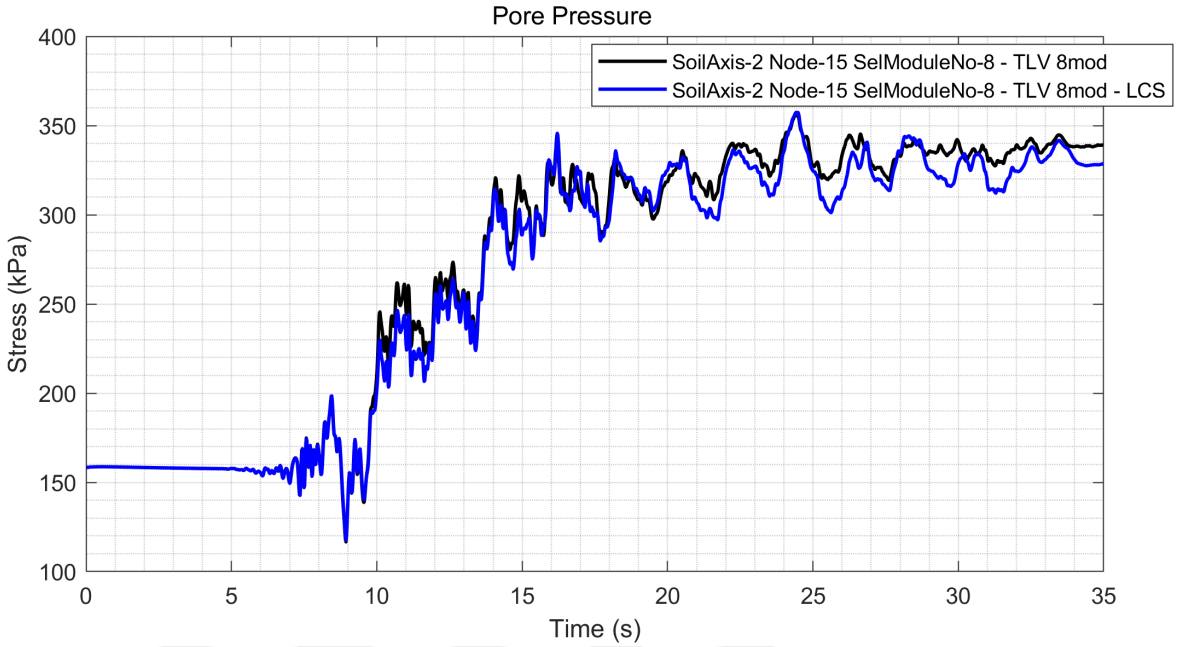

Figure 8.79. Pore Pressure Comparison for 8mod Constant System vs. 8mod LCS System (Soil Axis-2 Node-15 SelMod-8).

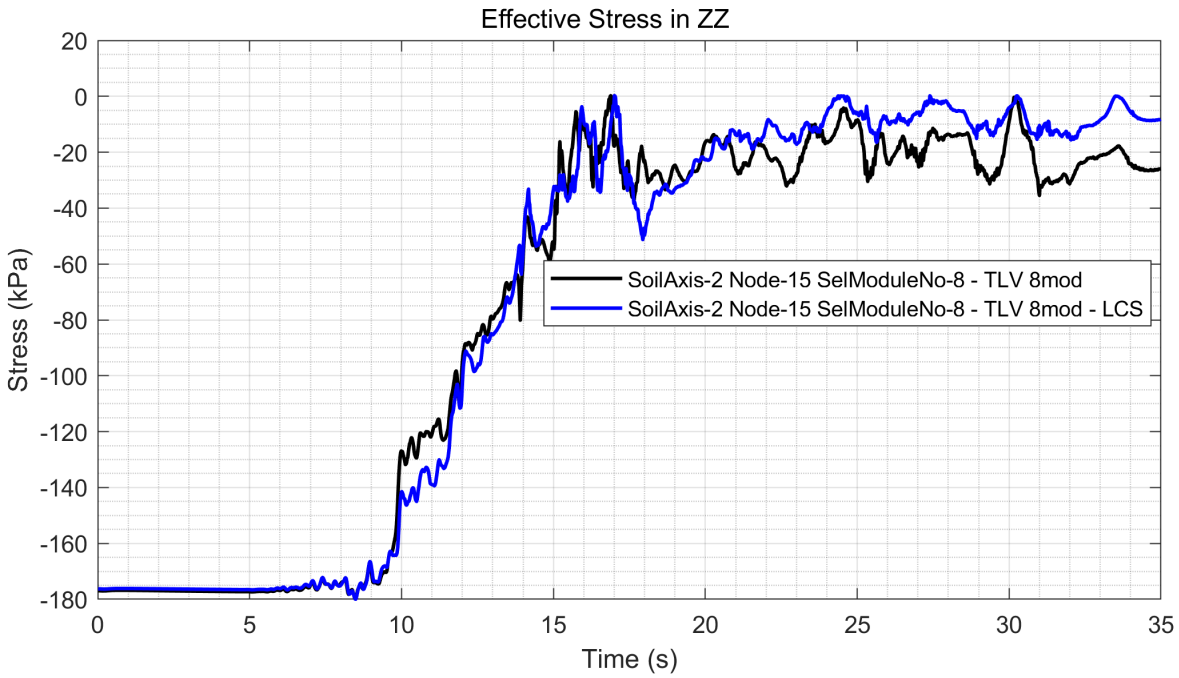

Figure 8.80. Effective Stress Comparison for 8mod Constant System vs. 8mod LCS System (Soil Axis-2 Node-15 SelMod-8).

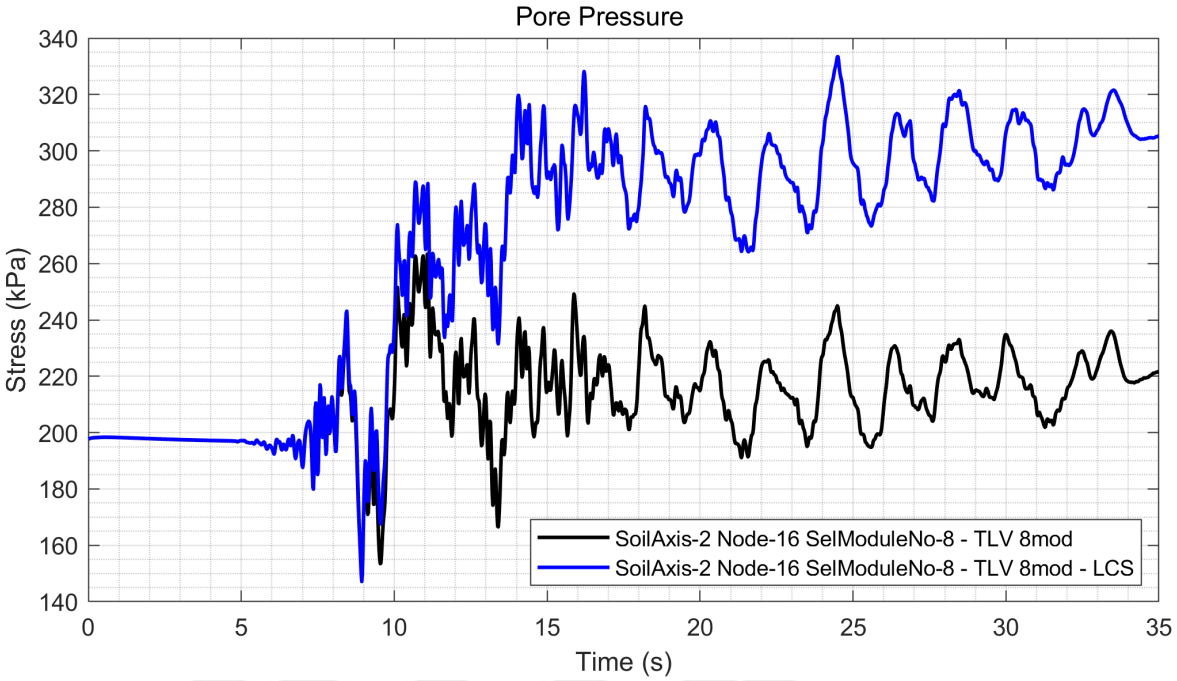

Figure 8.81. Pore Pressure Comparison for 8mod Constant System vs. 8mod LCS System (Soil Axis-2 Node-16 SelMod-8).

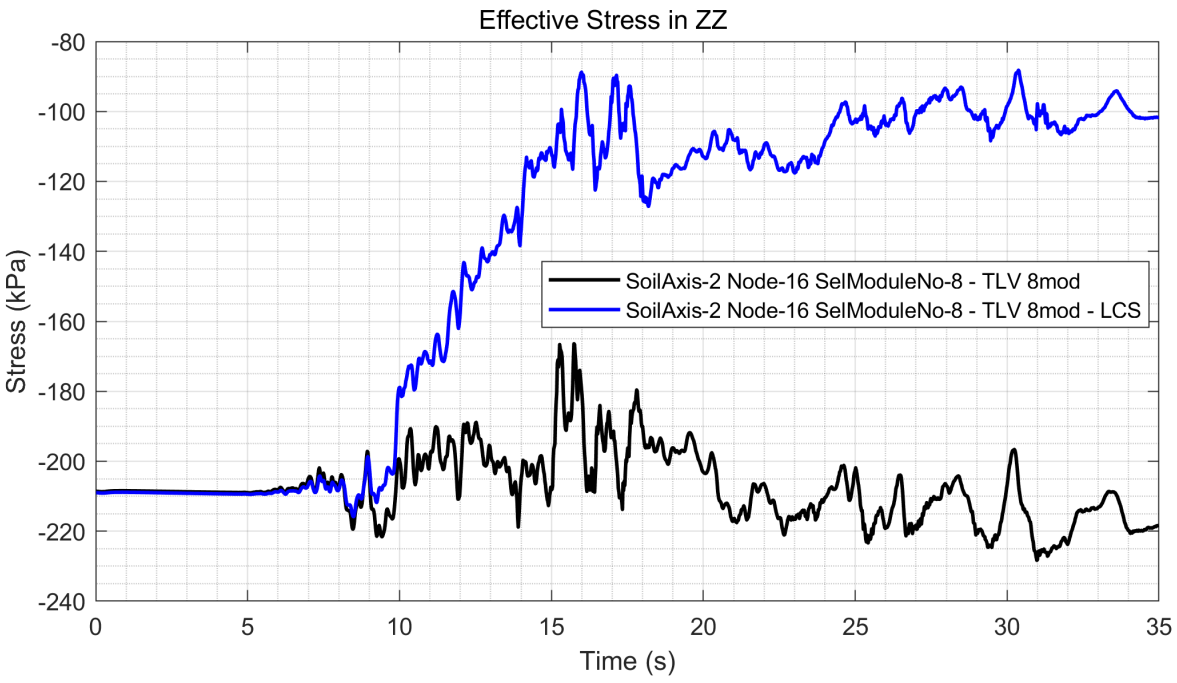

Figure 8.82. Effective Stress Comparison for 8mod Constant System vs. 8mod LCS System (Soil Axis-2 Node-16 SelMod-8).

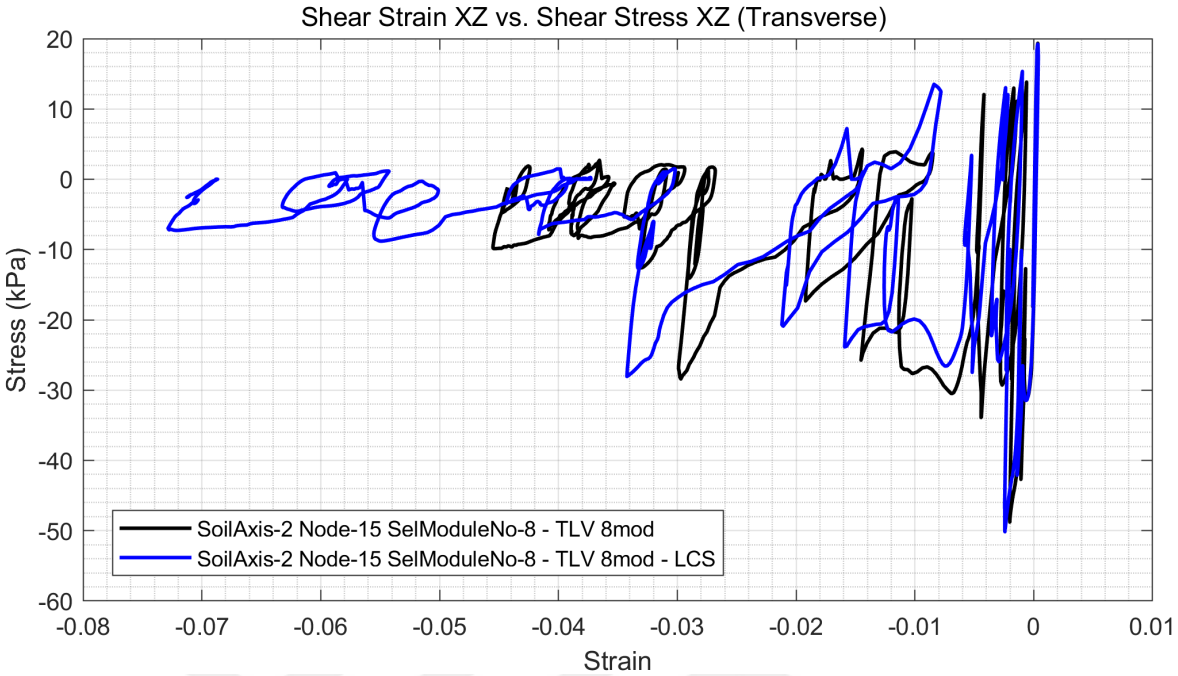

Figure 8.83. Shear Strain-Stress Comparison in Transverse Direction for 8mod Constant System vs. 8mod LCS System (Soil Axis-2 Node-15 SelMod-8).

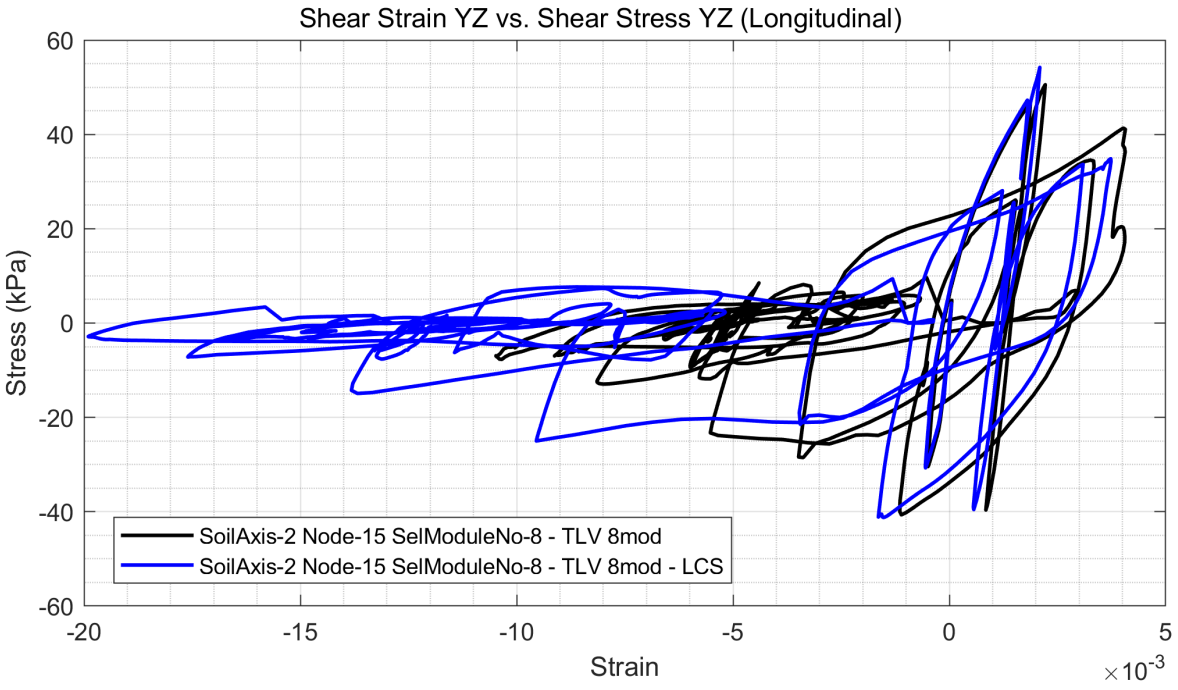

Figure 8.84. Shear Strain-Stress Comparison in Longitudinal Direction for 8mod Constant System vs. 8mod LCS System (Soil Axis-2 Node-15 SelMod-8).

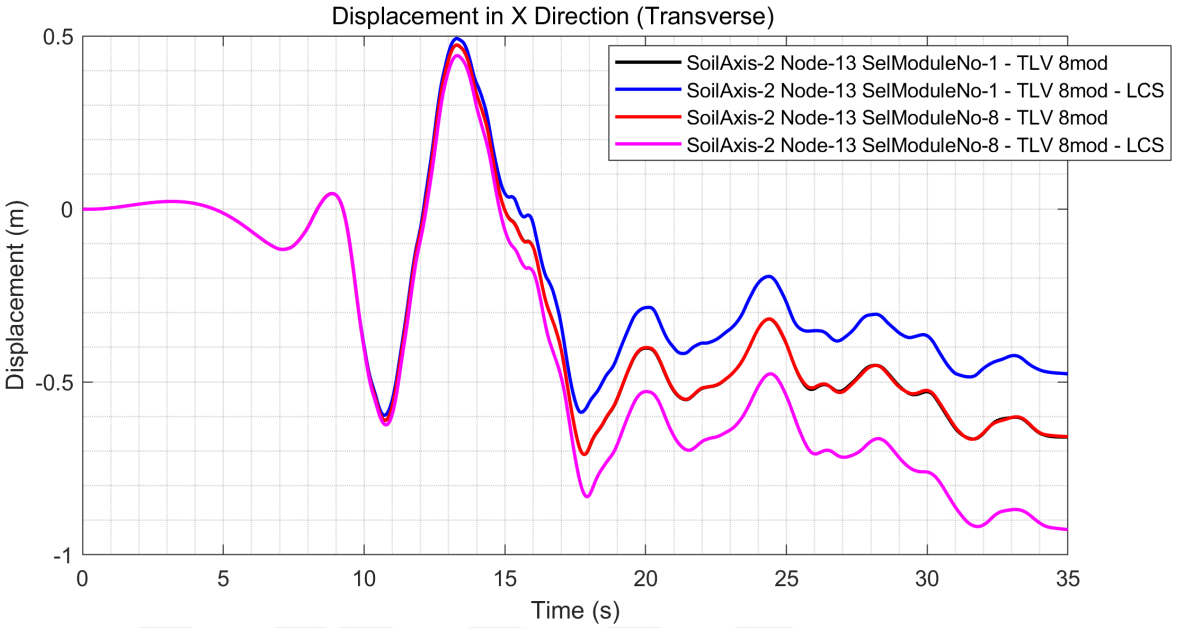

Figure 8.85. Displacement Comparison in Transverse Direction for 8mod Constant System vs. 8mod LCS System (Soil Axis-2 Node-13 SelMod-1 and SelMod-8).

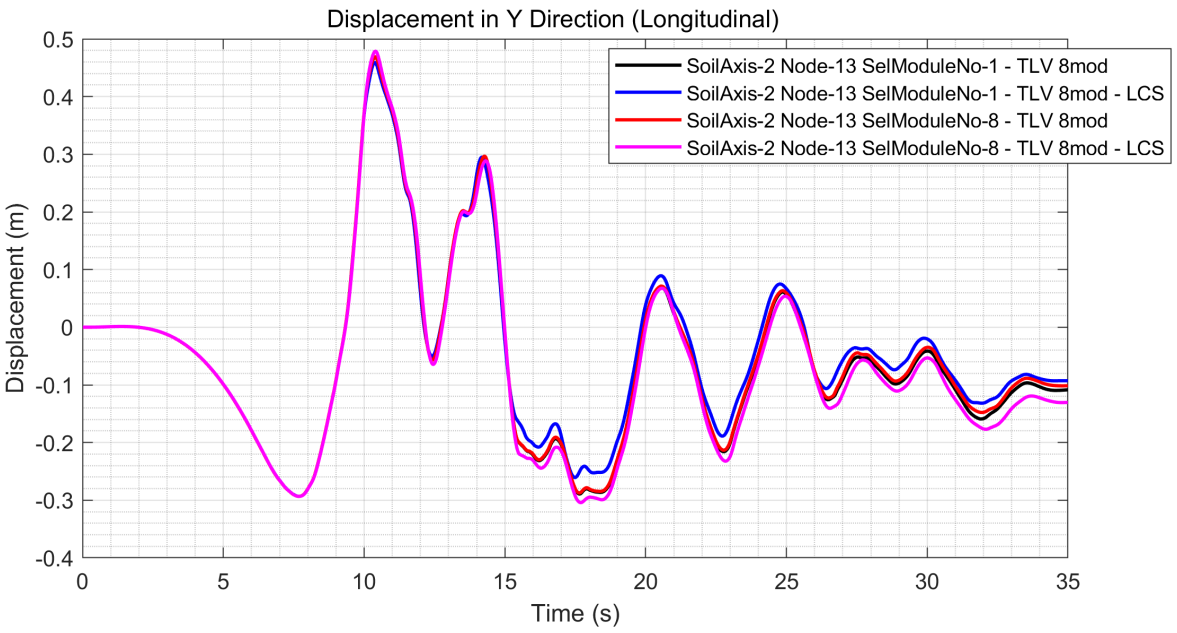

Figure 8.86. Displacement Comparison in Longitudinal Direction for 8mod Constant System vs. 8mod LCS System (Soil Axis-2 Node-13 SelMod-1 and SelMod-8).

Figures 8.87 and 8.88 illustrate the relative displacement responses, in transverse and longitudinal directions respectively, for the wharf systems with constant soil stratification and varying soil stratification. The displacement trend of the systems is consistent with the observed soil deformation. The pile displacements gradually increase towards Axis-80 where the thickness of liquefiable layer significantly larger than that near Axis-01.

The distribution of plastic hinges along the wharf system was shown in Figures 8.73 and 8.74 to depict the overall behavior of the system regarding plastification. Figures 8.89 and 8.90 show the plastic hinge locations at Axis-01 and Axis-80, respectively, to clearly observe the change in plastic deformation along the system. As explained before, there is almost no change in the response of structural elements along the wharf systems with constant soil stratification. However, the inelastic behavior of piles drastically change along the LCS system. It is seen from Figure 8.90 that plastic hinges occur at three different parts along the piles. The RC plug plastic hinge and the in-ground hinge, which occurred just behind the liquefiable MDS layer, were observed in the previous cases. In this case, a new plastification region, located between the two previously observed plastic hinges, emerged. After yielding occurred at both ends of the frame element, the MDS layer with the rockfill layer above sliding over the failure surface imposes a force in the downward direction. The considerable thickness (10m) of the liquefiable soil layer significantly increases the moment at the mid-part of the frame, which is pinned at both ends, resulting in the formation of a plastic hinge.

Significant rotation values of piles are observed at the rockfill and soil layers where the in-ground plastic hinges occurred (Figure 8.91 and 8.92). Obviously, plastic rotations increase in these locations. The relative rotations can reach approximately 2%. The locations of peak rotations shift below in LCS system compared with the other system due to the greater thickness of MDS layer in LCS system. Conversely, it is observed that the rotations at the plugs in the system with constant stratification are generally greater than LCS system. It is probably because the movement of a large soil block sliding over failure surface does not allow the deck relative movement due to its

inertia. Actually, it is similar to the behavior of base-isolated systems. Therefore, the plug regions are released and the rotations in this region are in lower value in general.

Internal force plots are given in Figures 8.93, 8.94, 8.95 and 8.96. Consistent trends with the displacement and rotations illustrated above can be observed in these figures as well.

Note that the given soil stratification in the displacement, rotation and internal force figures reflects the case of constant soil stratification. Only Figure 8.90 includes the soil stratification belonged to LCS system.

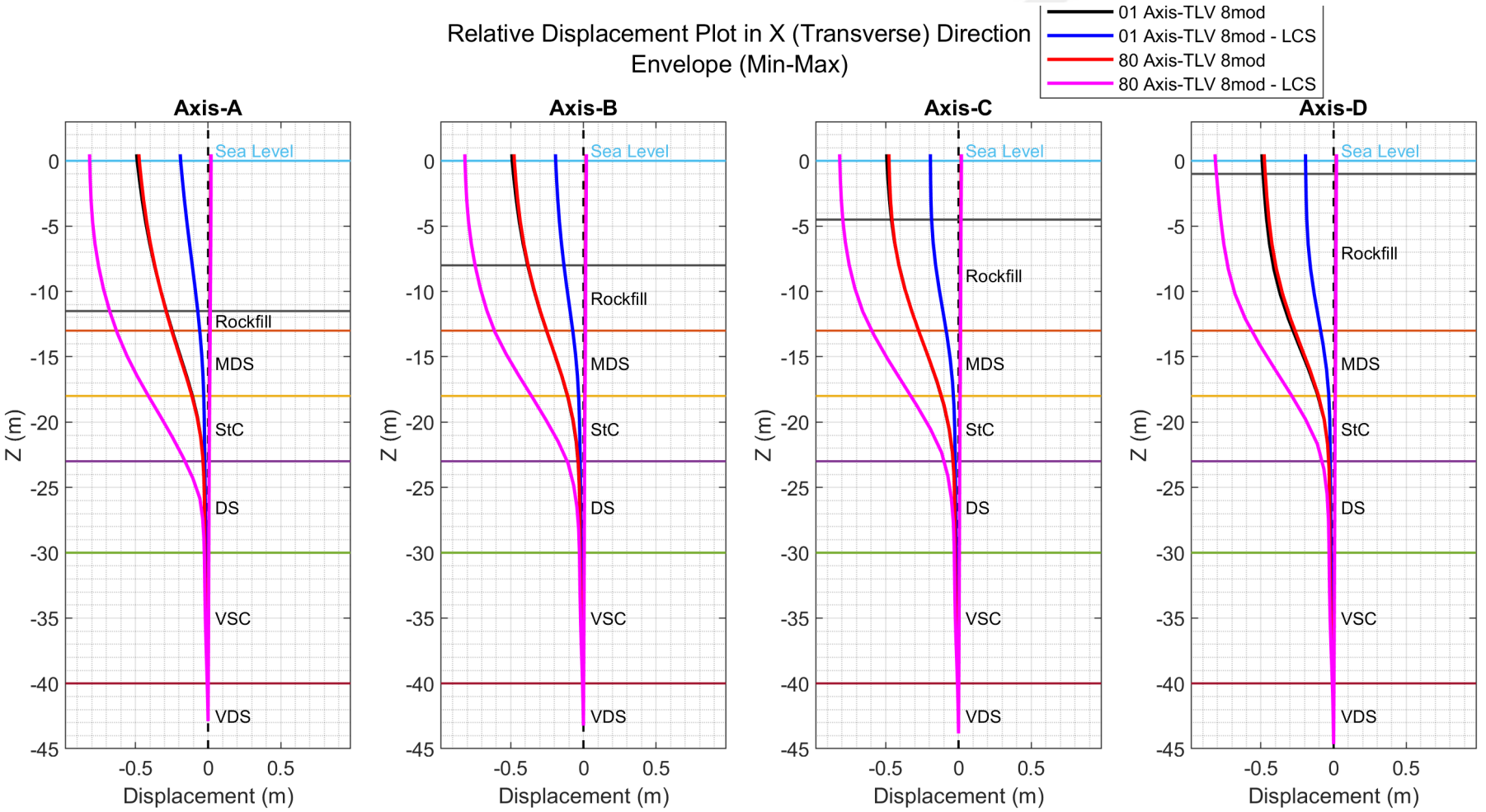

Figure 8.87. Relative Displacement Comparison in Transverse Direction for Constant System vs. LCS System.

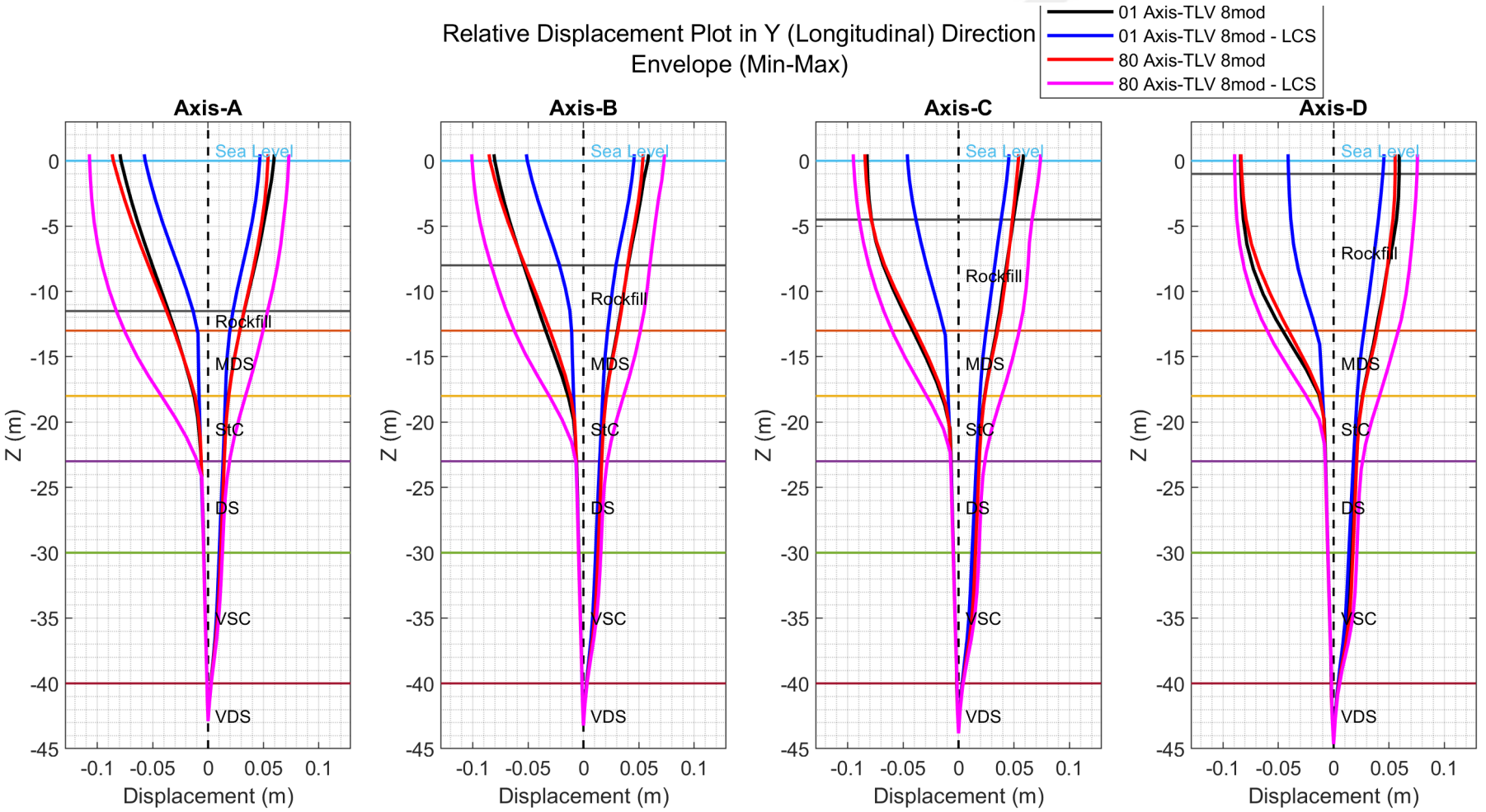

Figure 8.88. Relative Displacement Comparison in Longitudinal Direction for Constant System vs. LCS System.

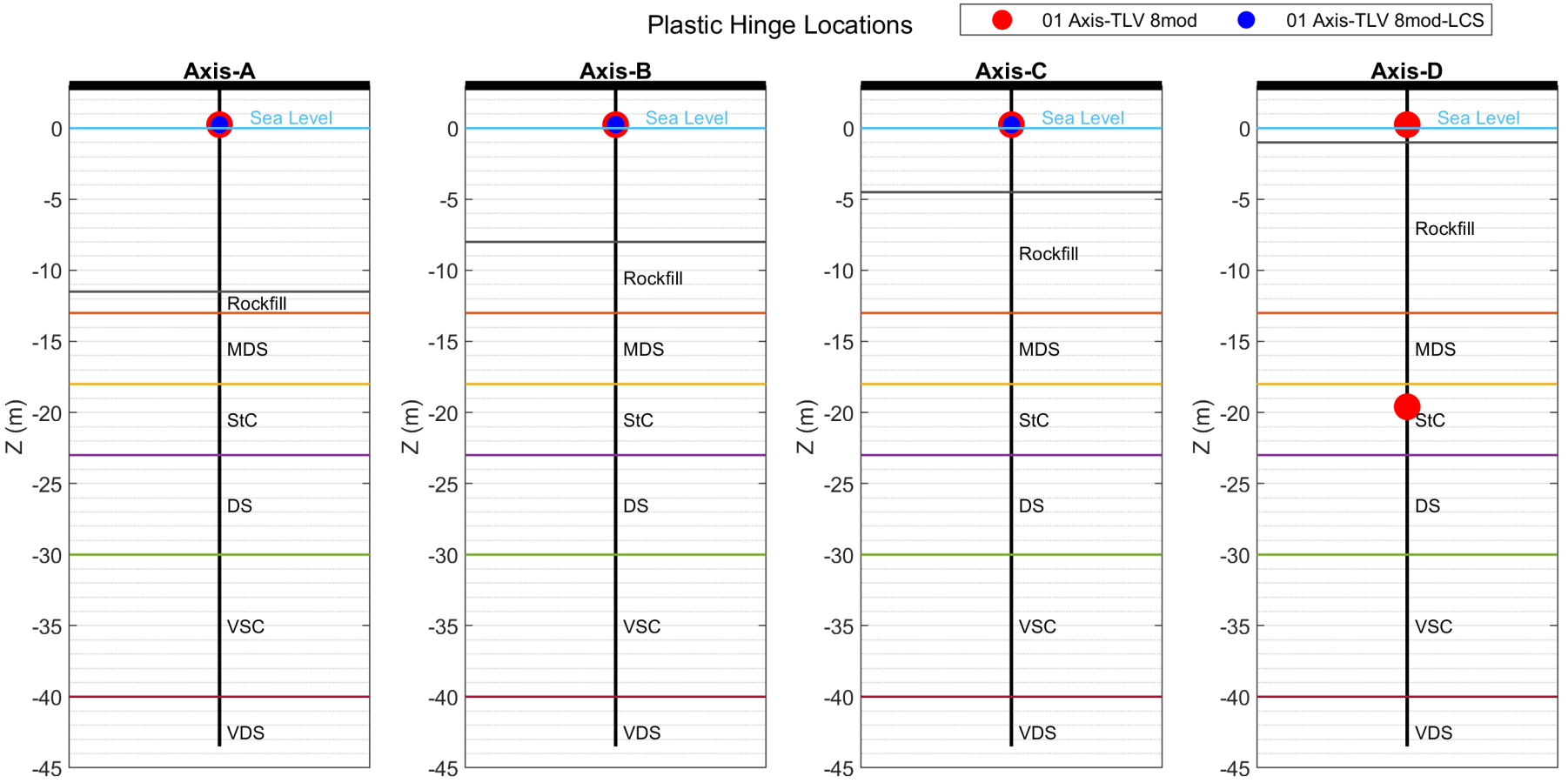

Figure 8.89. Plastic Hinge Locations for Constant System vs. LCS System (01-Axis).

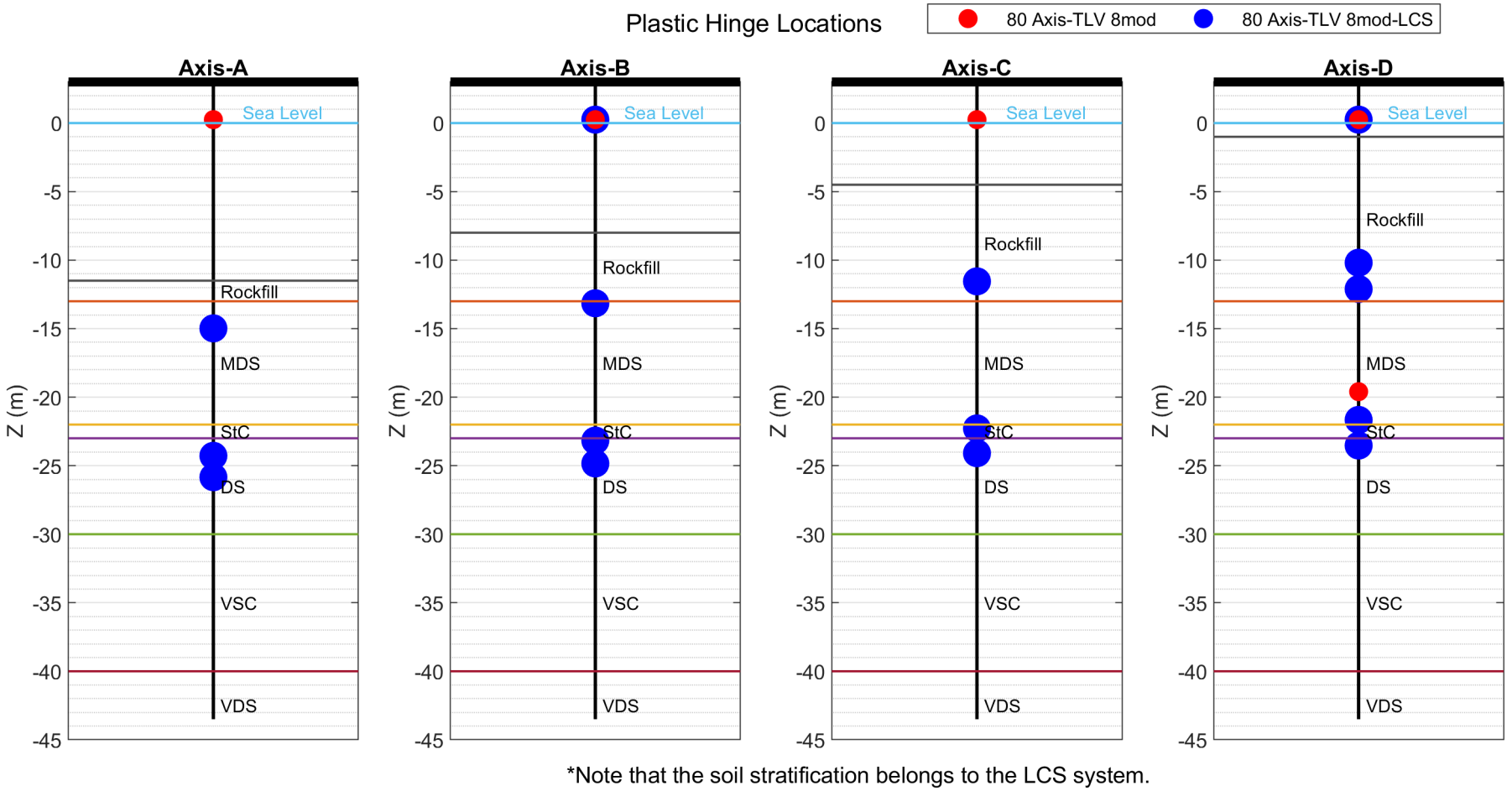

Figure 8.90. Plastic Hinge Locations for Constant System vs. LCS System (80-Axis).

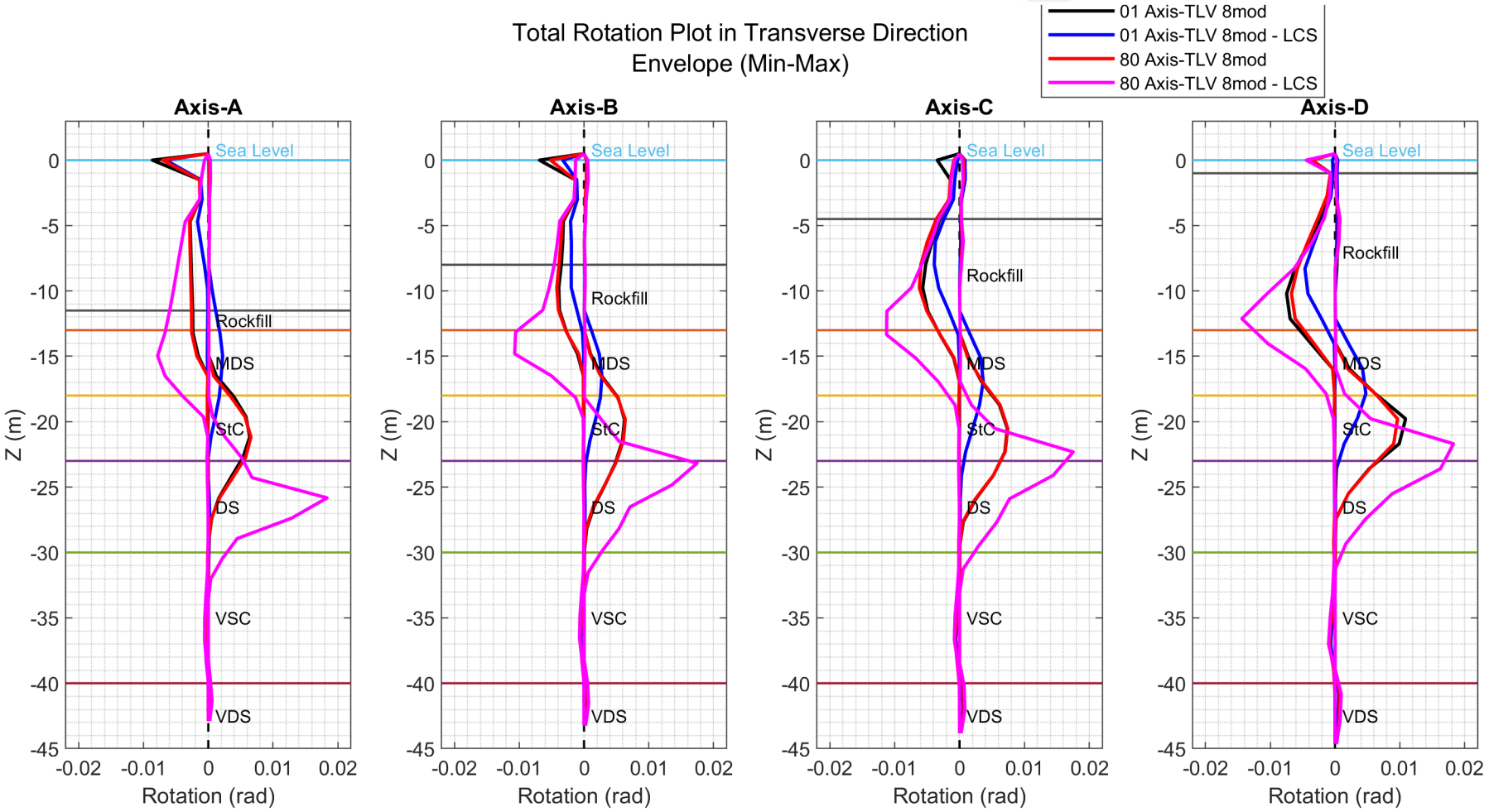

Figure 8.91. Relative Rotation Comparison in Transverse Direction for Constant System vs. LCS System.

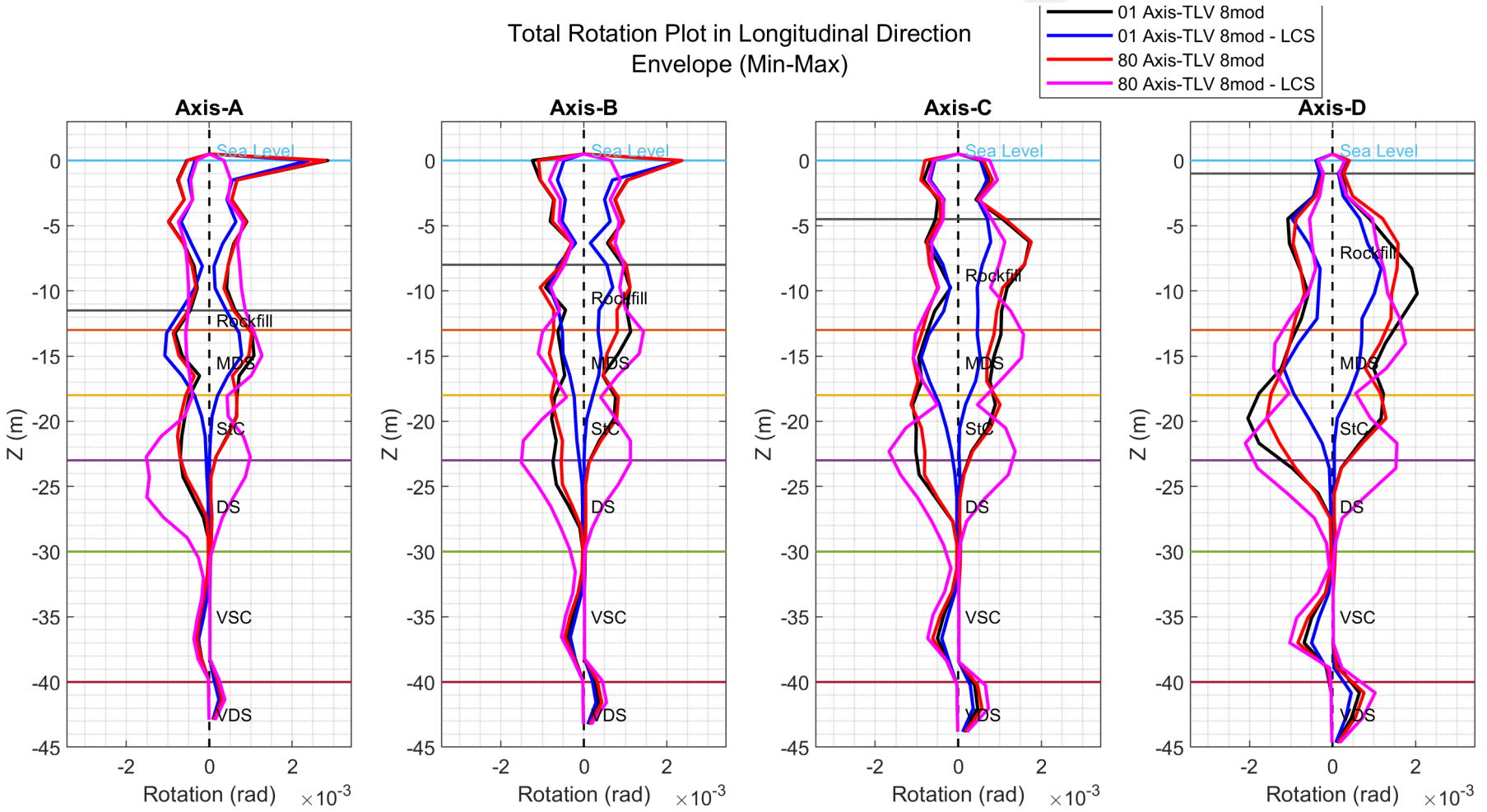

Figure 8.92. Relative Rotation Comparison in Longitudinal Direction for Constant System vs. LCS System.

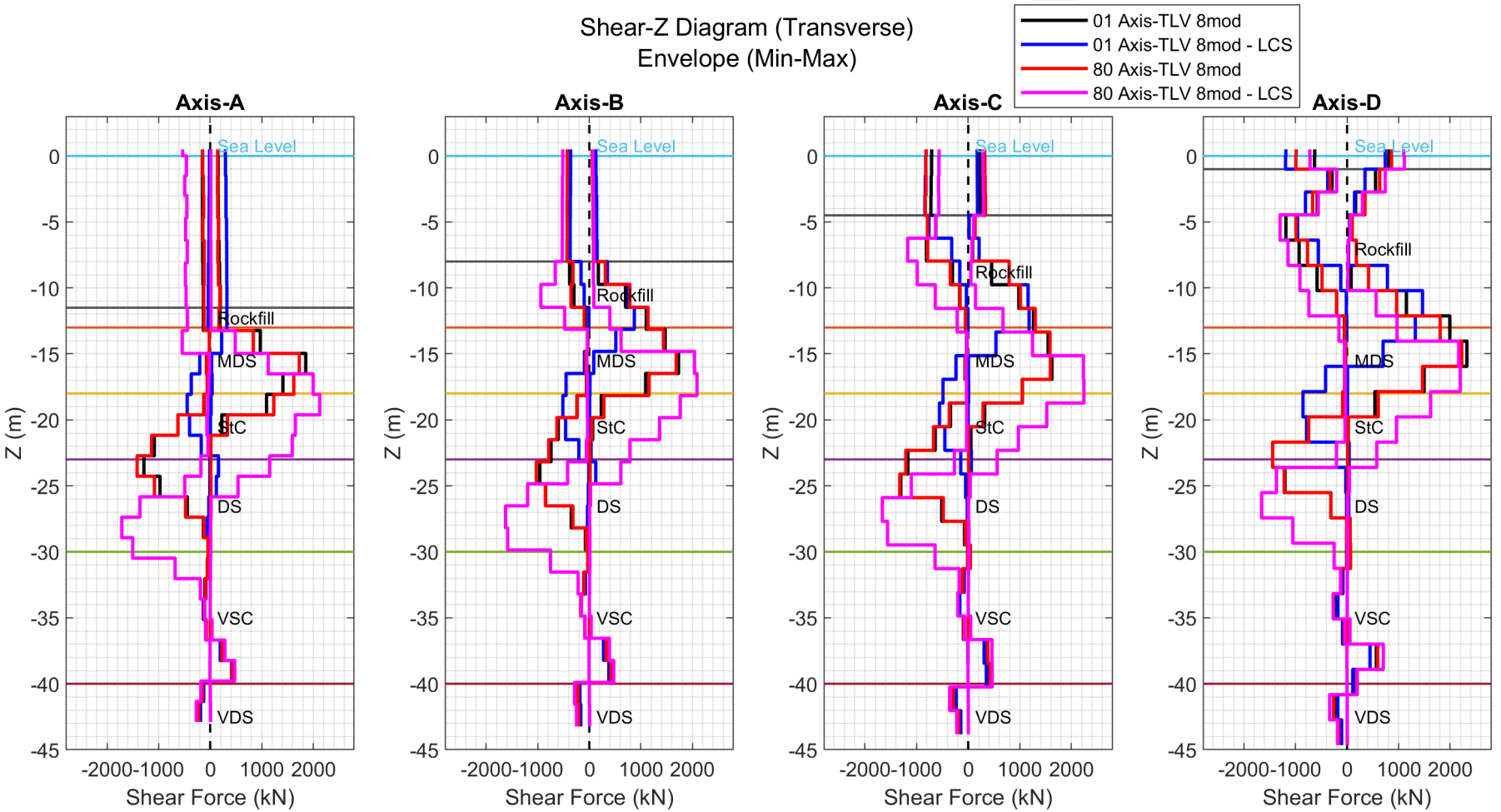

Figure 8.93. Pile Shear Force Comparison in Transverse Direction for Constant System vs. LCS System.

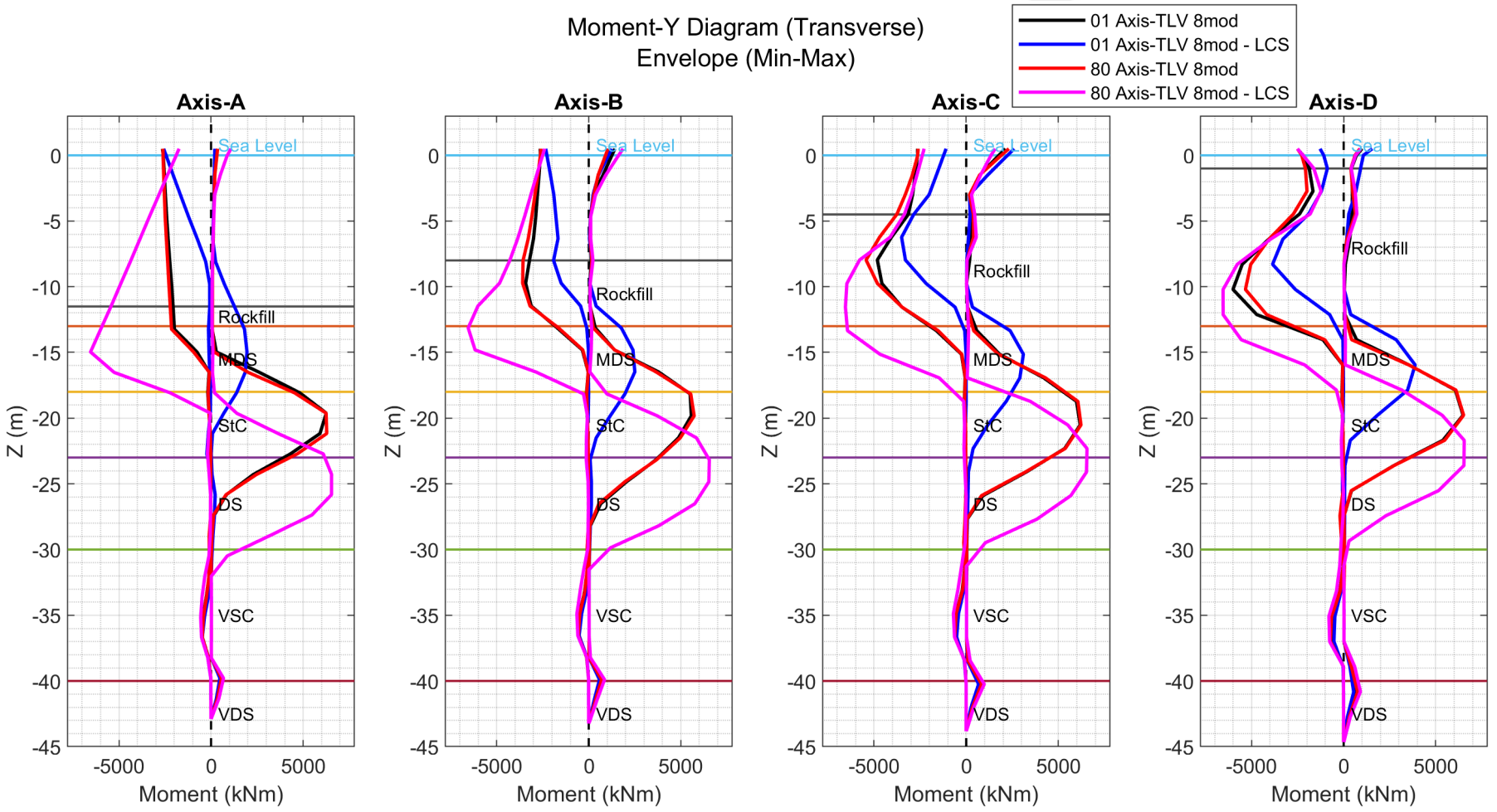

Figure 8.94. Pile Moment Comparison in Transverse Direction for Constant System vs. LCS System.

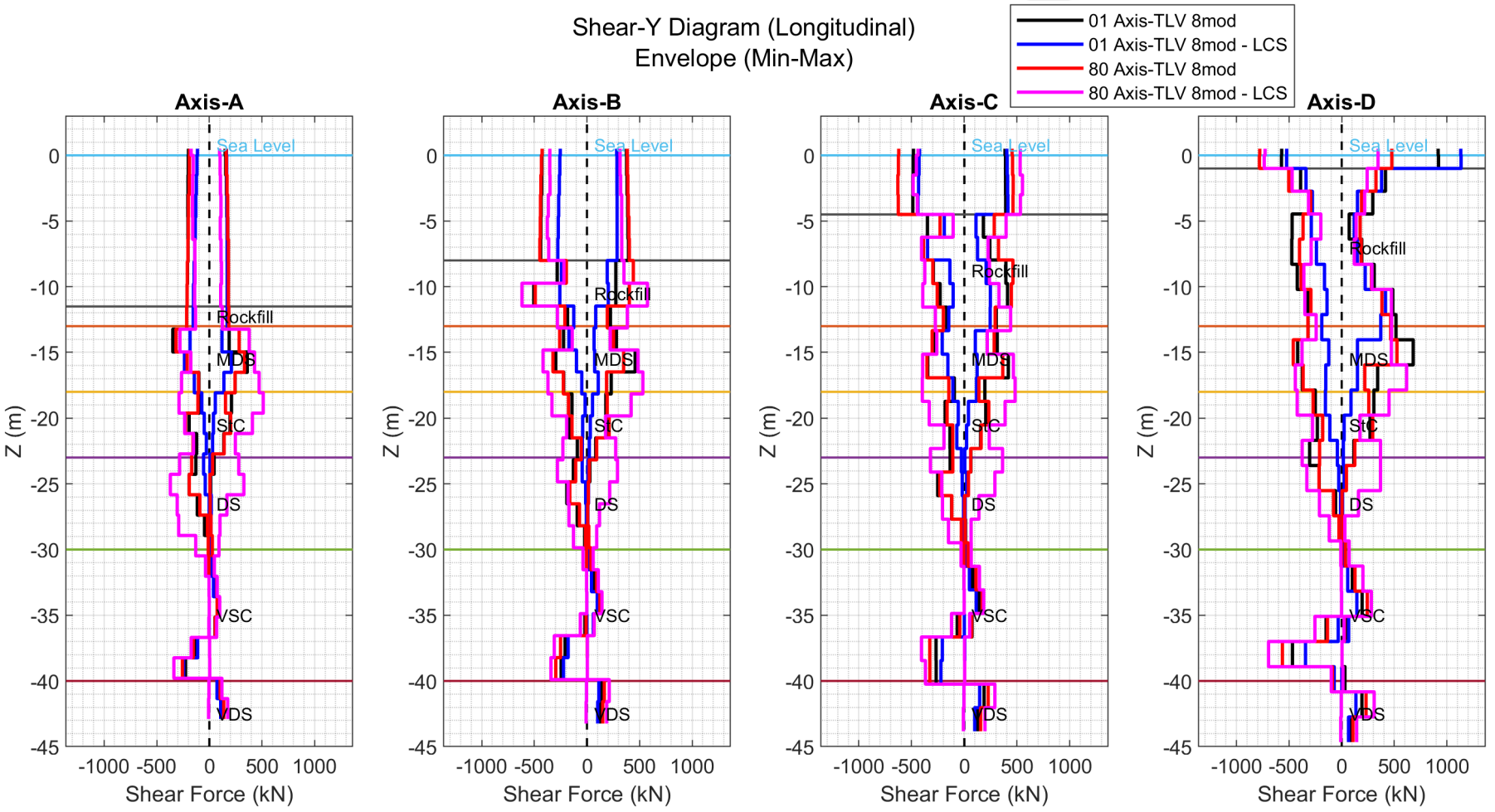

Figure 8.95. Pile Shear Force Comparison in Longitudinal Direction for Constant System vs. LCS System.

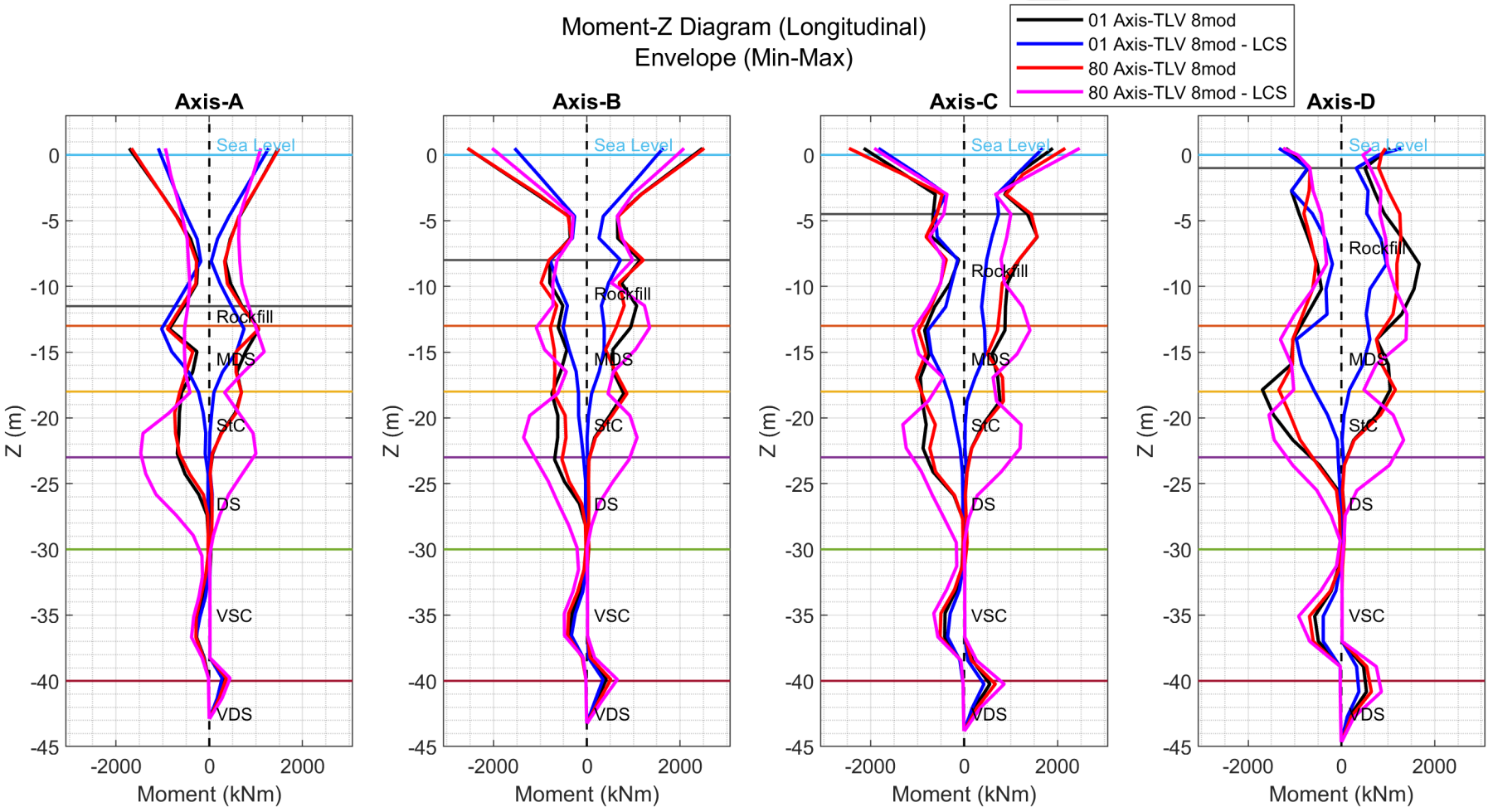

Figure 8.96. Pile Moment Comparison in Longitudinal Direction for Constant System vs. LCS System.

Shear key force time histories are compared for the two wharf systems. The comparisons are given for the shear keys between the modules 1-2, 2-3, 3-4, 4-5 in Figure 8.97 and modules 5-6, 6-7, 7-8 in Figure 8.98. The permanent shear forces are observed at the end of ground shaking for all shear keys of LCS system. The permanent shear force is the highest between modules 1 and 2, and the lowest between modules 7 and 8 in line with the overall deformation character of embankment with changing soil stratification.

It is clearly observed from the shear force time history between module 1 and 2 that the shear key force is getting increase after t=15s and reaches the highest level among all shear keys (shear key no:1) in the system. The shear key force for 8-module wharf system with constant soil stratification is measured as 684kN at the shear key no:1 (Figure 6.16). The highest shear key force for LCS system is measured as 1038kN at the shear key no:1. A 50% increase in shear key forces is observed due to the changing soil stratification.

Figures 8.99 and 8.100 show the deck acceleration time histories measured at the deck no:3 (Figure 6.15) from module-1 to module-8. The peak accelerations are prominently greater in the system with constant soil stratification at the first modules. The reason is that the soil deformation due to liquefaction alters the vibration frequency of the structural system during ground shaking and probably causing the amplification of accelerations when the structure frequency matches with forcing frequency. On the contrary, the acceleration response of LCS system decks becomes higher than the system with constant stratification as we move towards the end modules.

Note that the acceleration response tends to contain a significant amount of high frequency content and potentially causing deceptive amplification since damping is not considered for structural elements. Therefore, the level of deck accelerations should be evaluated comparatively.

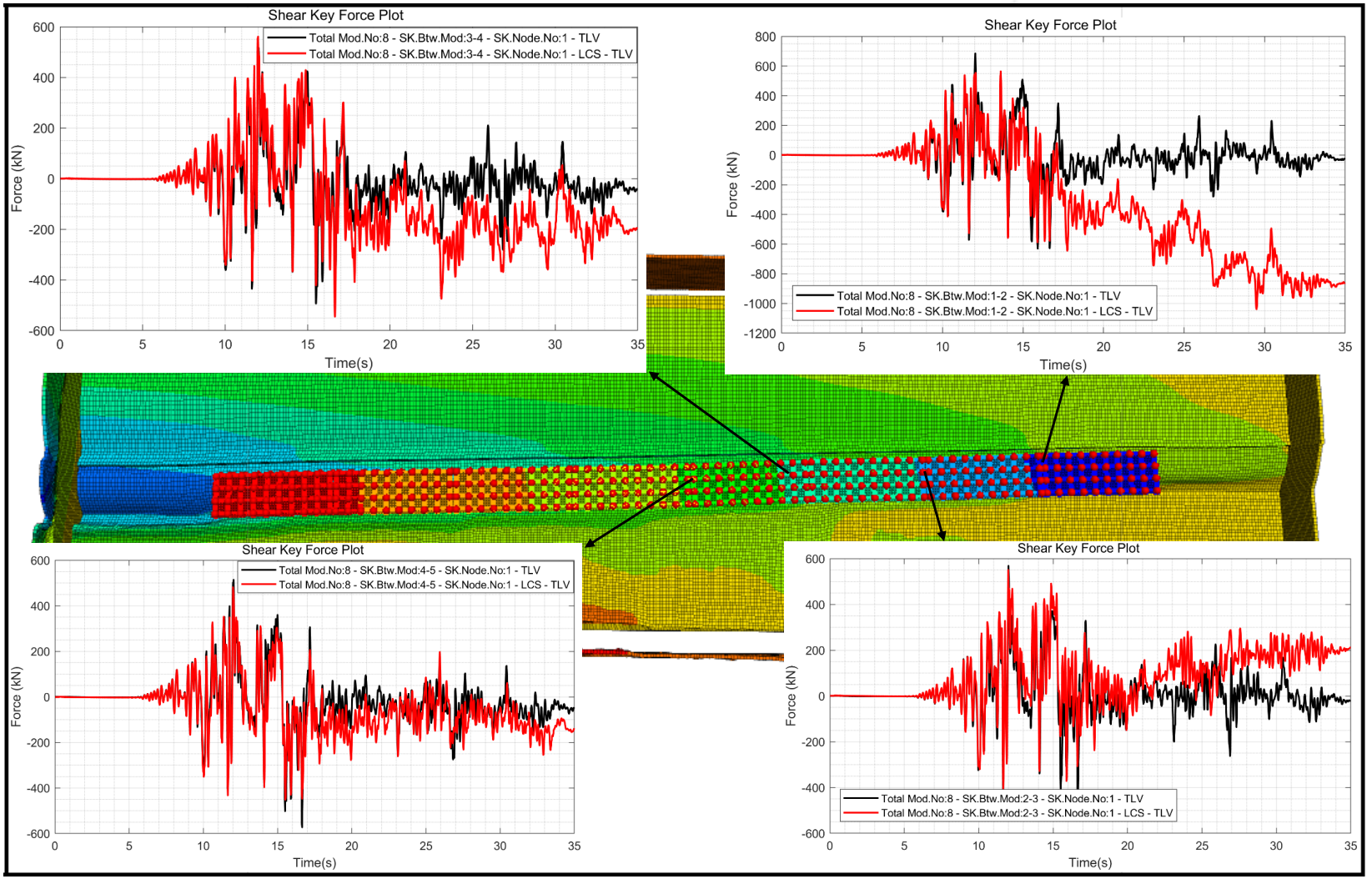

Figure 8.97. Shear Key Force Histories for LCS Wharf System (Between Modules No 1-2,2-3,3-4,4-5).

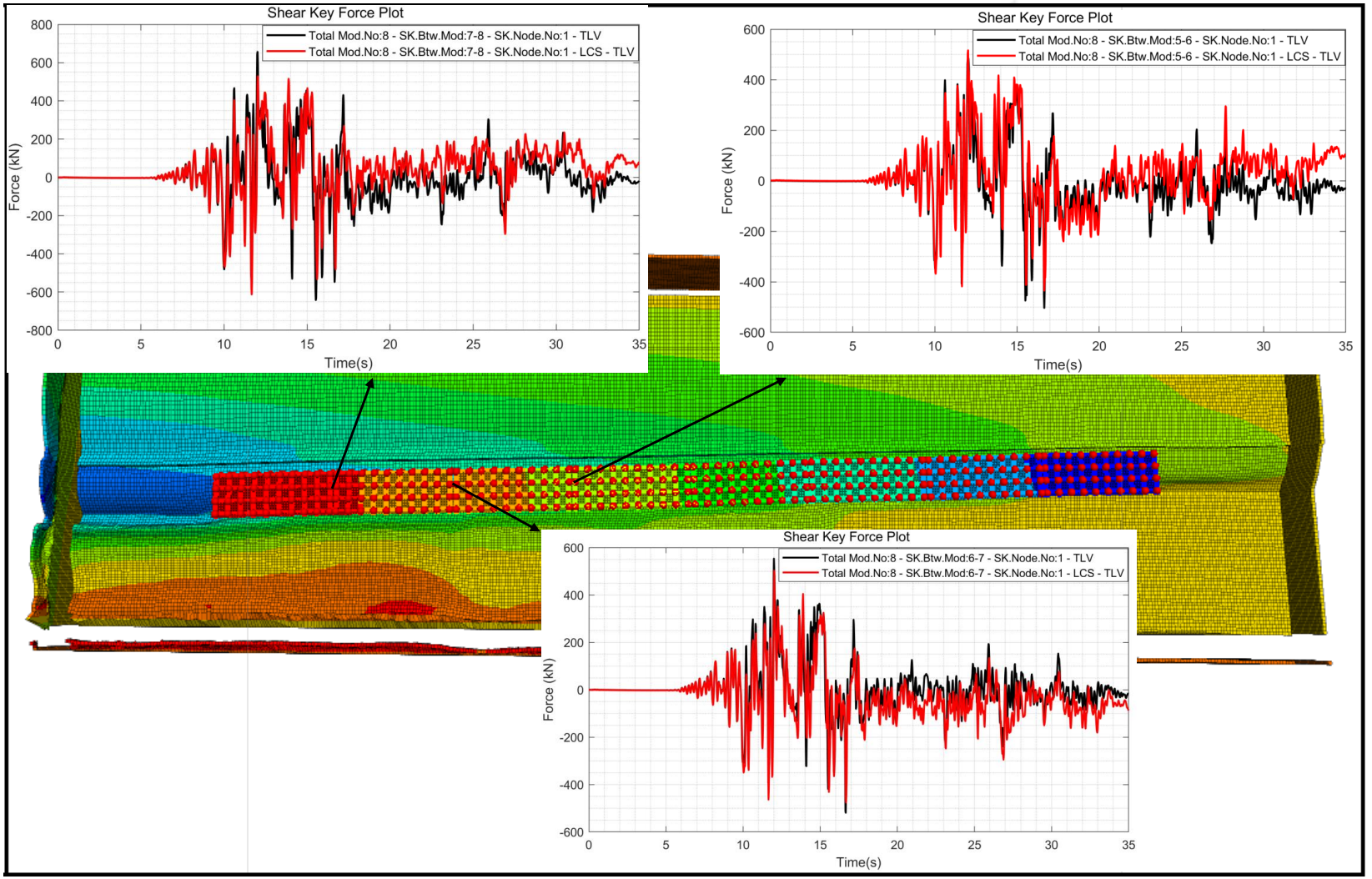

Figure 8.98. Shear Key Force Histories for LCS Wharf System (Between Modules No 5-6,6-7,7-8).

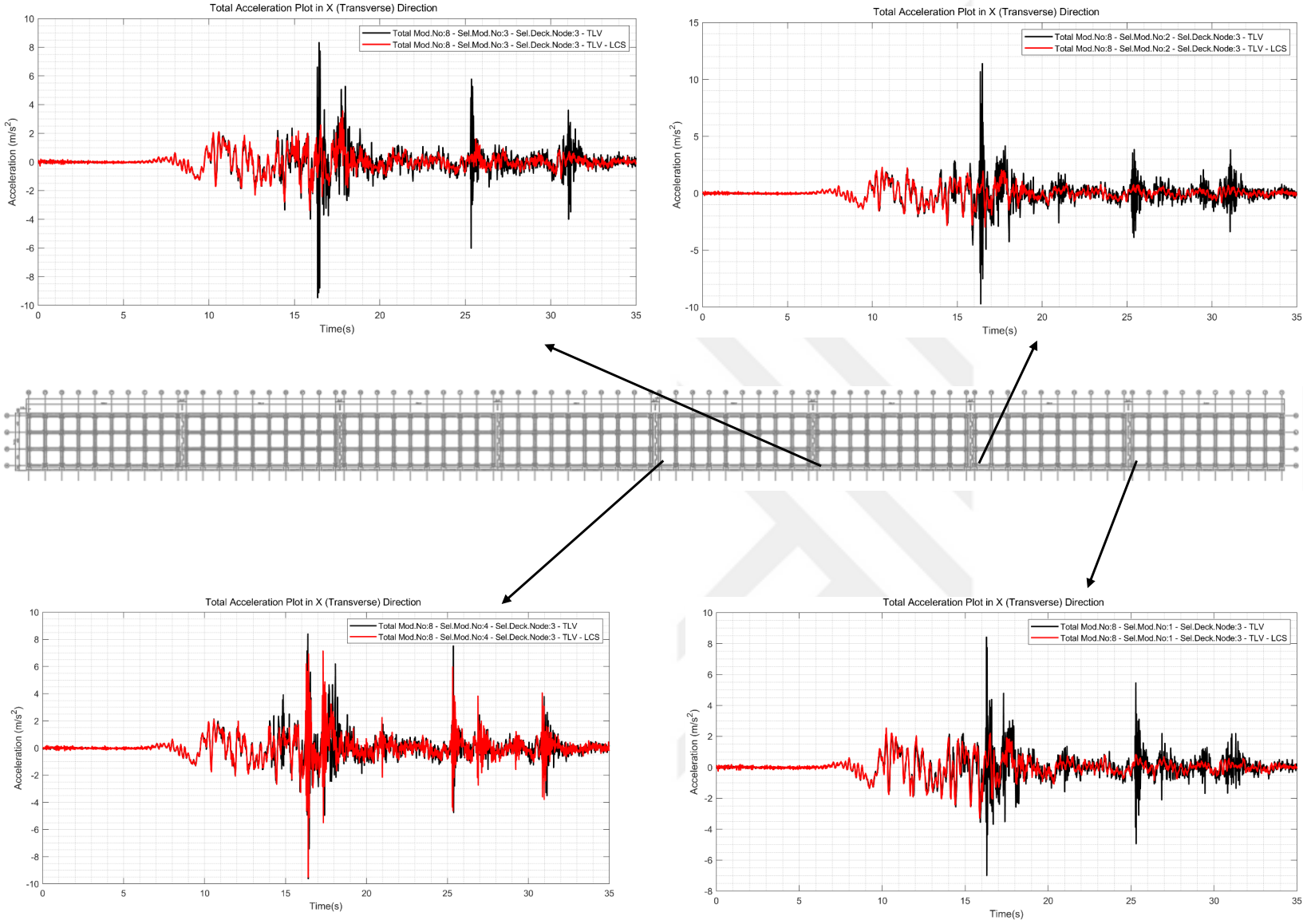

Figure 8.99. Deck Acceleration Comparison (Deck Node No:3) in Transverse Direction (Module No: 1,2,3,4).

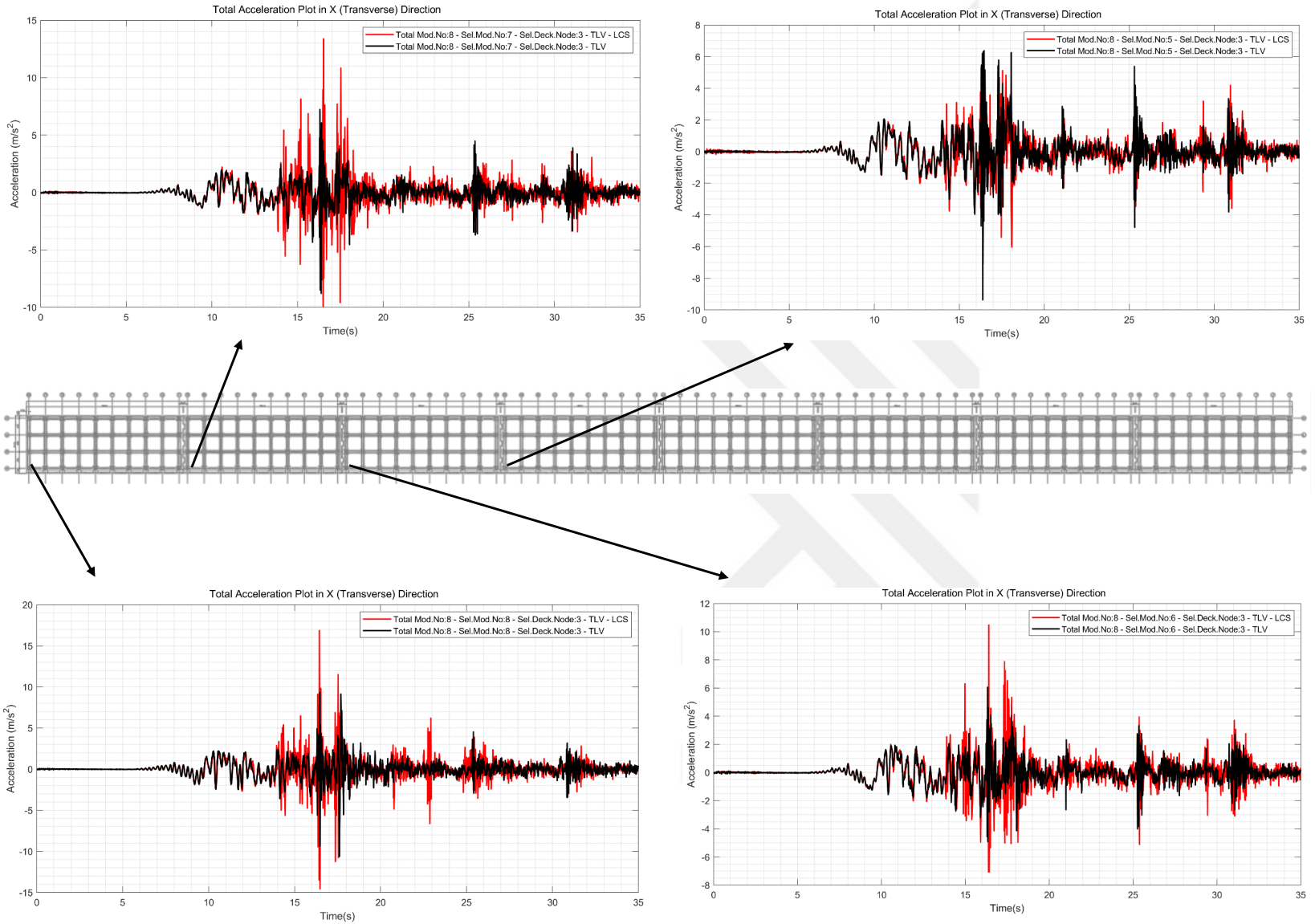

Figure 8.100. Deck Acceleration Comparison (Deck Node No:3) in Transverse Direction (Module No: 5,6,7,8).

8.3. Response Comparison for Wharf Strip Model and Single Module Analysis

In this section, the response comparisons are given for the wharf strip and single module system models. Both systems are evaluated under only transverse excitation. Although the importance of longitudinal excitation is proven and explained in the previous chapters, this section is presented to address the questions regarding commonly used plane-strain models in practice.

In general, only slight differences exists in the comparisons. It can be seen in Figures 8.101, 8.102, 8.103, 8.104 for soil response and Figures 8.105, 8.106, 8.107, 8.108, 8.109 for structural response.

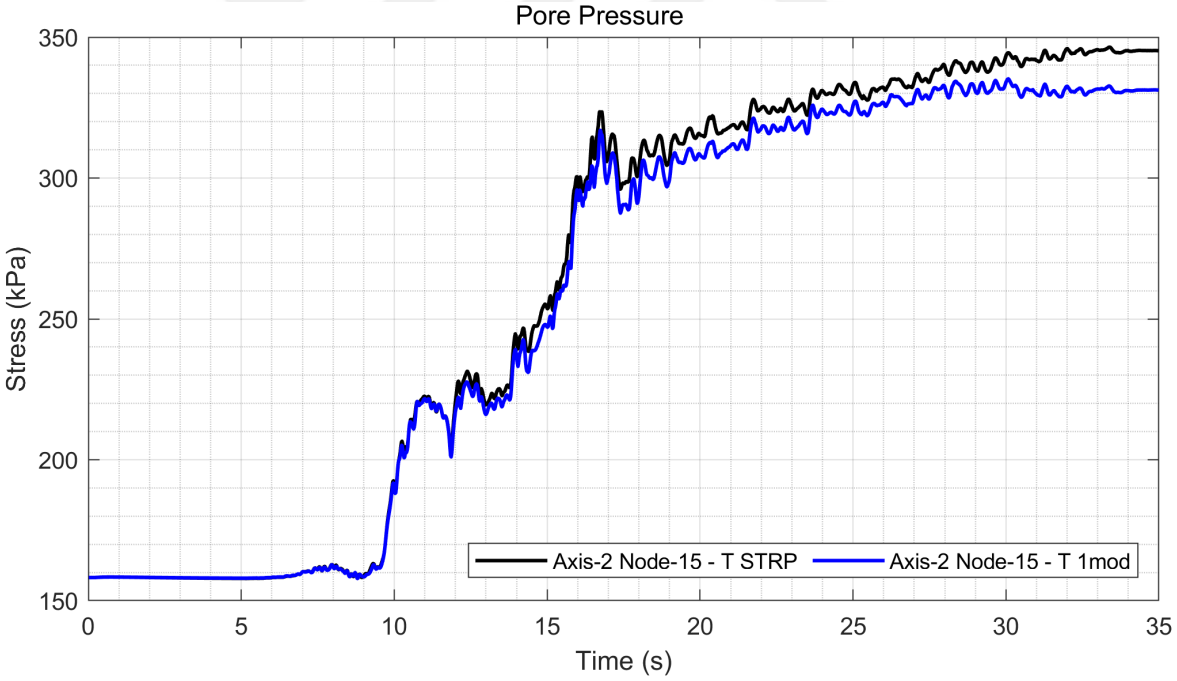

Figure 8.101. Pore Pressure Comparison for Strip vs. Single Module (Axis-2 Node:15).

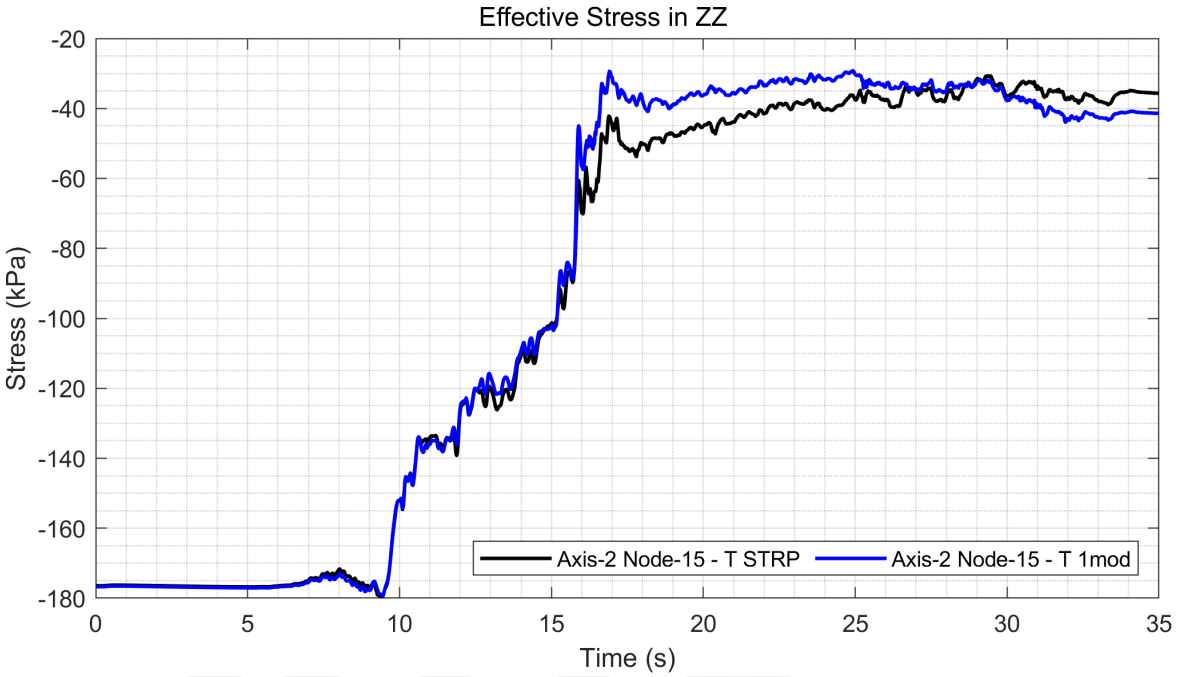

Figure 8.102. Effective Stress Comparison for Strip vs. Single Module(Axis-2 Node:15).

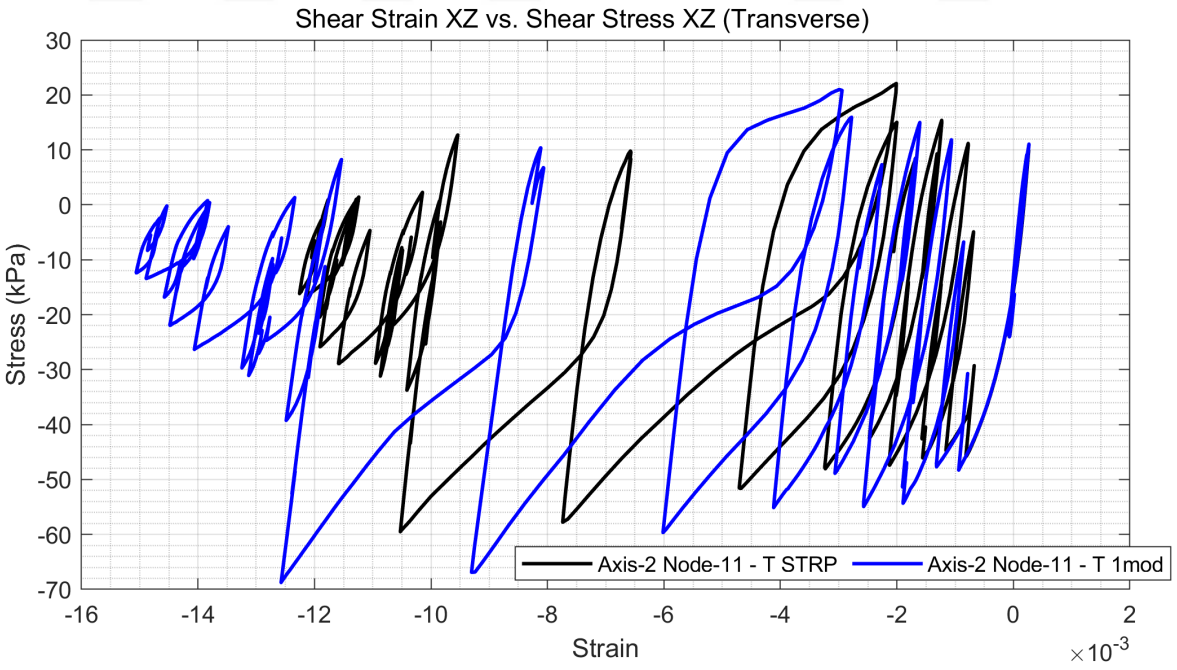

Figure 8.103. Stress-Strain Comparison for Strip vs. Single Module (Axis-2 Node:15).

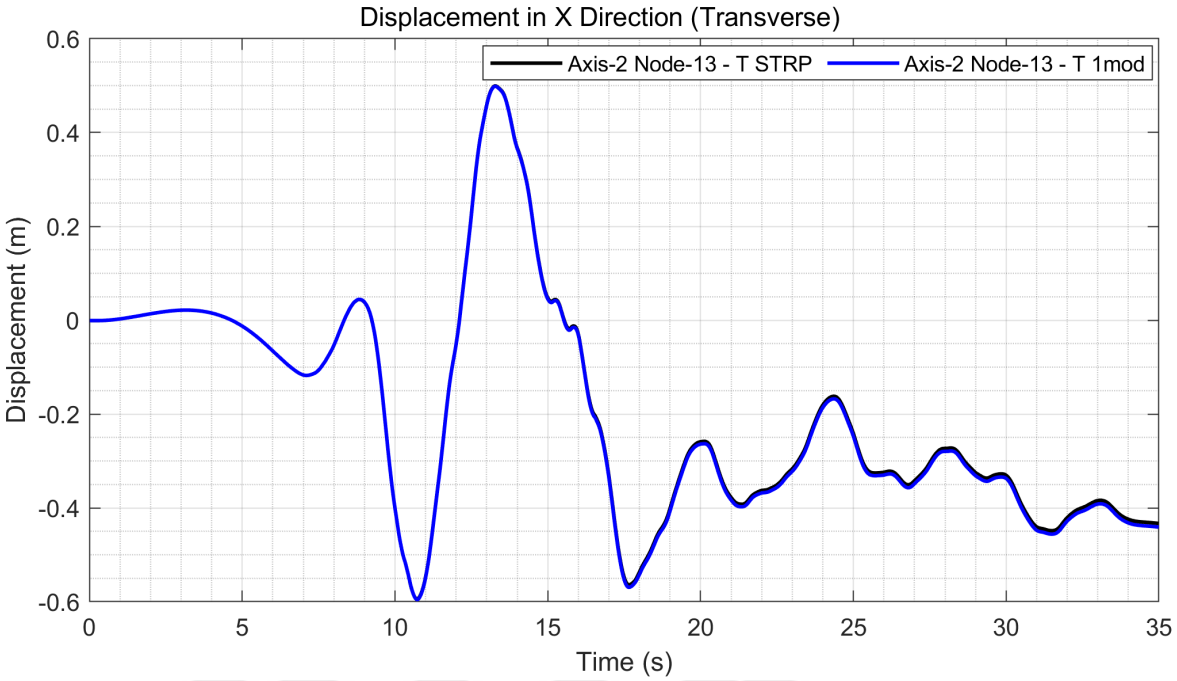

Figure 8.104. Displacement Comparison for Strip vs. Single Module (Axis-2 Node:13).

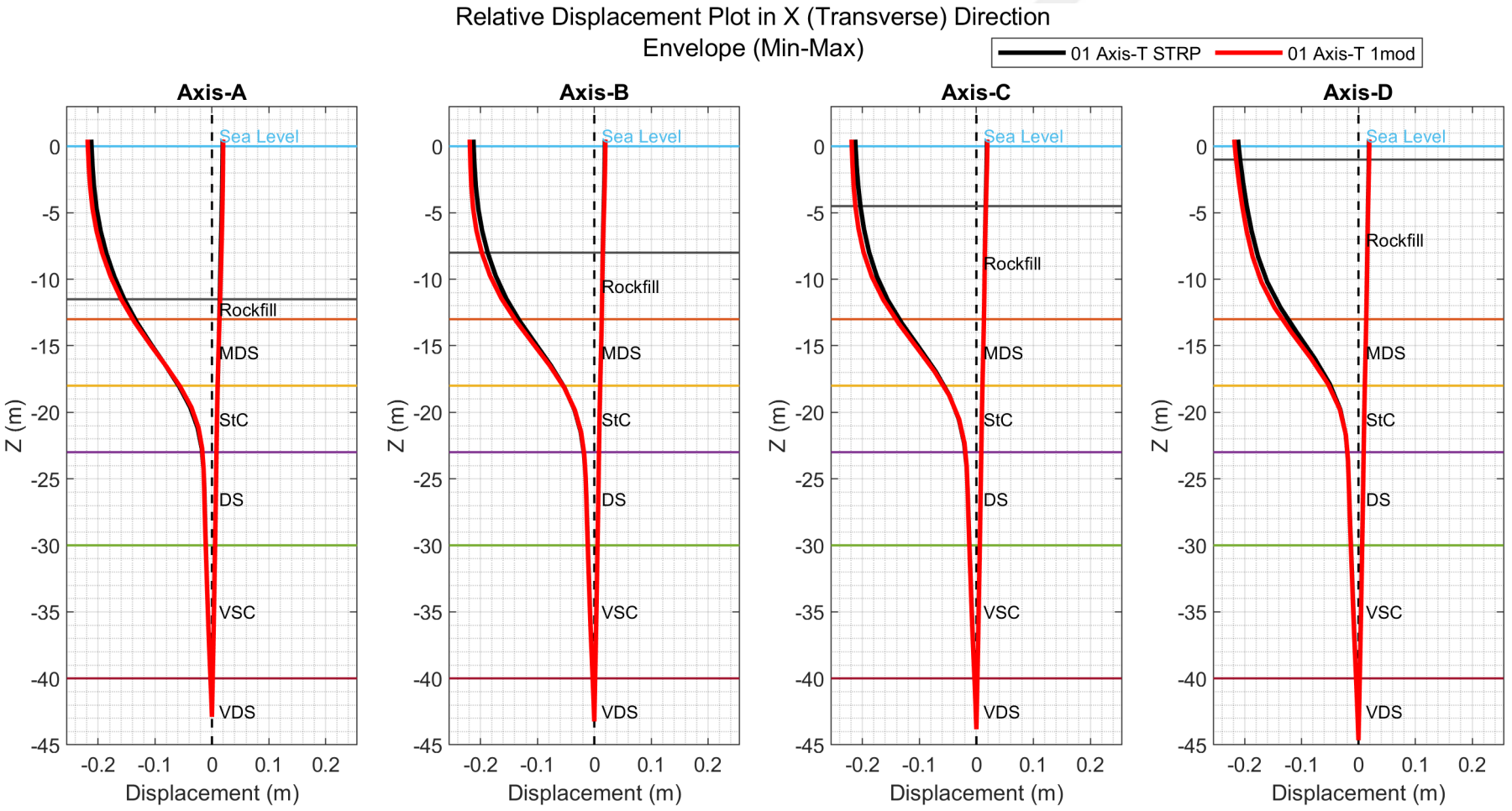

Figure 8.105. Relative Displacement Comparison for Strip vs. Single Module.

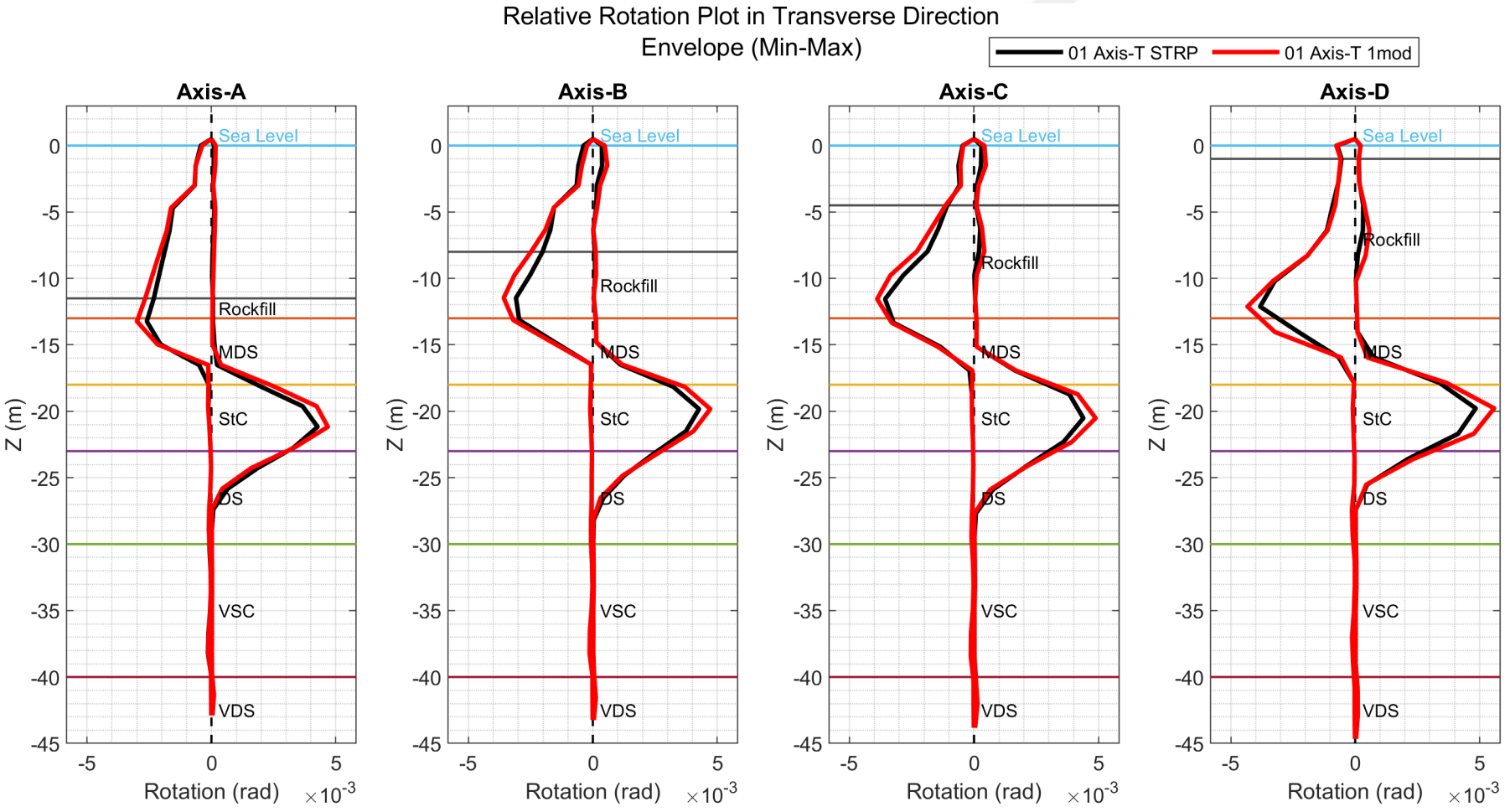

Figure 8.106. Relative Rotation Comparison for Strip vs. Single Module.

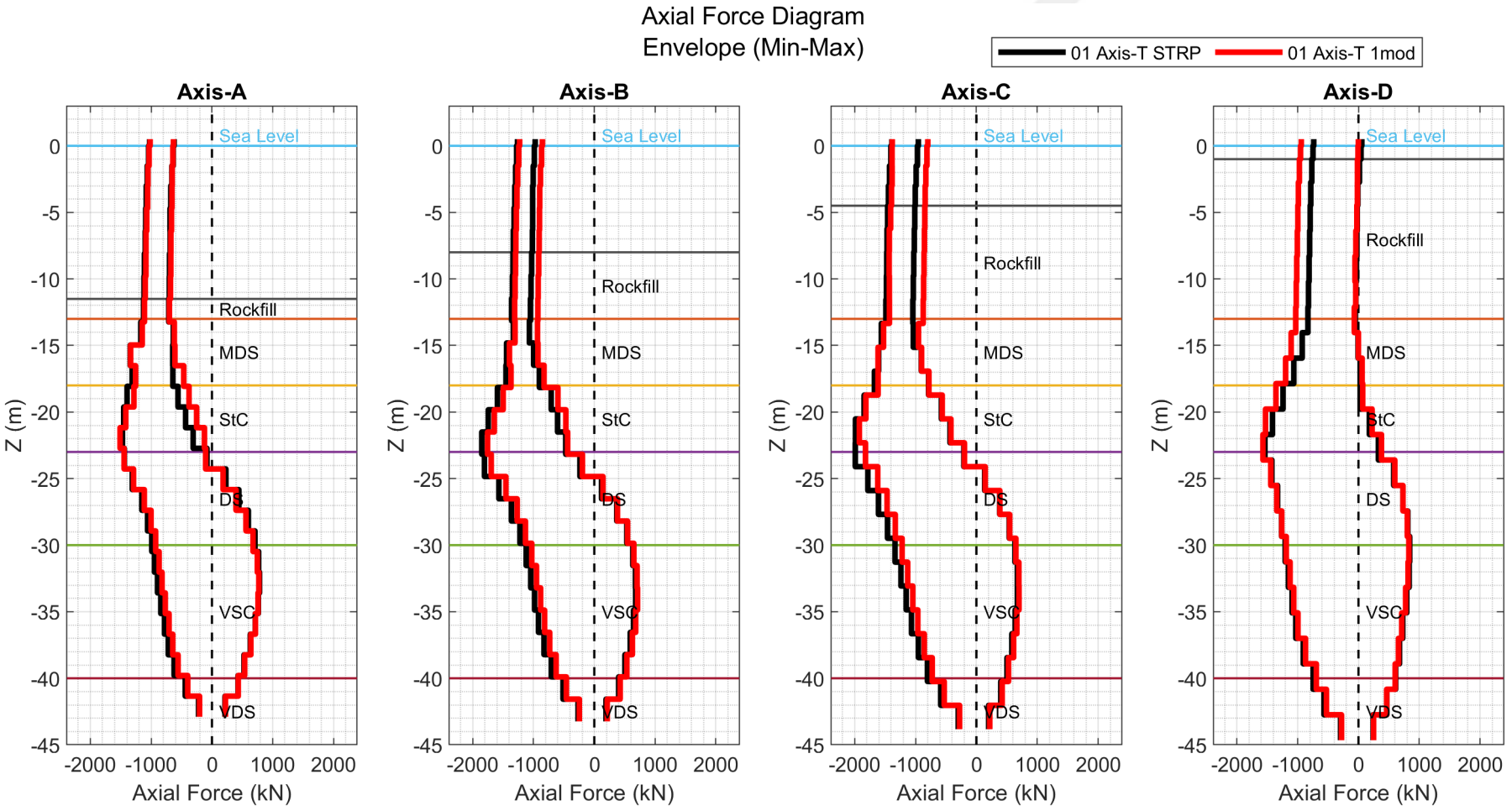

Figure 8.107. Axial Force Comparison for Strip vs. Single Module.

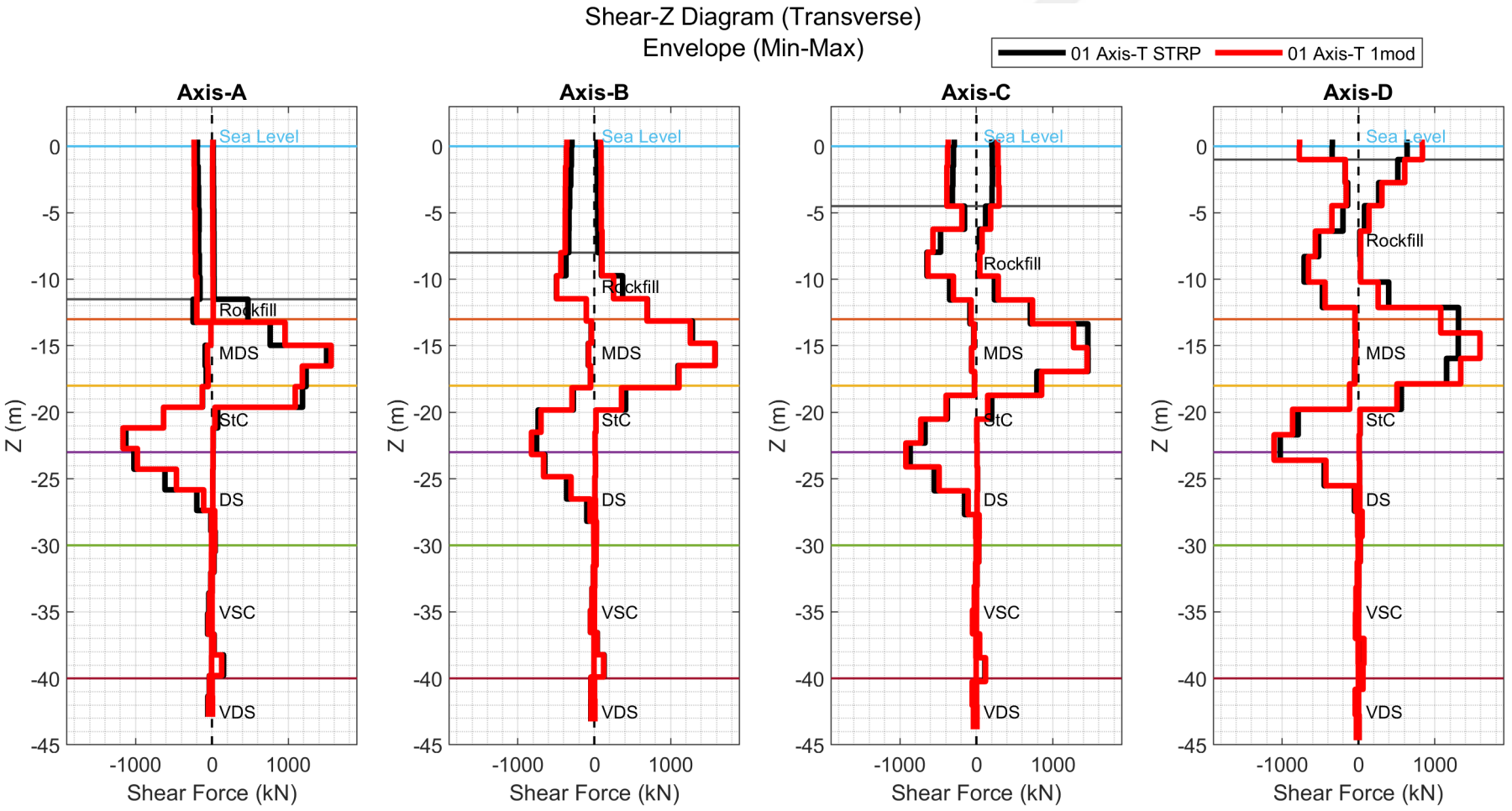

Figure 8.108. Shear Force Comparison for Strip vs. Single Module.

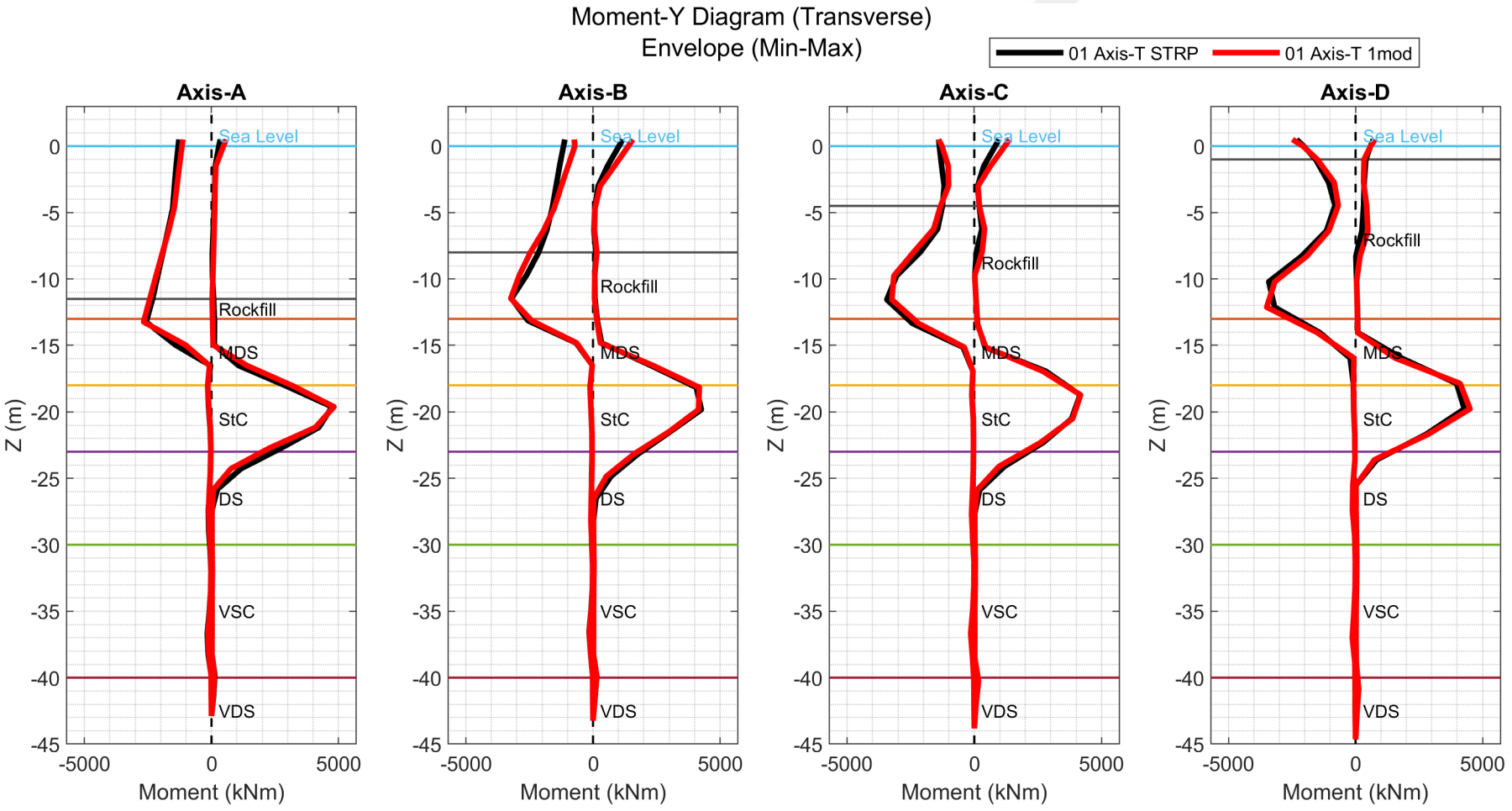

Figure 8.109. Moment Comparison for Strip vs. Single Module.

9. CONCLUSION

The current modeling and analysis procedures for pile-supported wharf systems lack consideration of several critical aspects and the impacts of those aspects have not been thoroughly investigated. To address this, multiple analysis cases were evaluated, leading to several significant conclusions.

In general, it is understood that soil liquefaction leading to excessive soil deformation has decisive role in the wharf system analysis and design. A detailed modeling of soil and the integration of soil-structure interaction play a crucial role for accurately predicting the seismic response of wharf components. The presence of a liquefiable soil layer and the level of liquefaction, when considered within a proper soil-structure interaction model, can unfavorably alter the overall vibration behavior of a structural system. Therefore, the liquefaction-induced soil deformations affect not only the occurrence of in-ground plastic hinges but also influence the plug response at the pile-deck interface. In fact, this is the direct outcome of kinematic interaction effect resulting in an amplified foundation input motion applying to the deck. This is completely disregarded in practice in uncoupled kinematic loading and inertial loading analyses, which are used to calculate the inelastic deformation demands of plug hinges and in-ground hinges separately. These effects can only be accurately captured only by direct SSI analysis models.

In case of liquefiable soil conditions, the effect of longitudinal excitation, on the seismic response of wharf components is significant. This is directly linked to embankment failure resulting from seismic excitation. A faster development of pore pressure, caused by an increase in the volumetric strain of soil elements due to bi-directional excitation at the failure surface, results in a faster increase in the effective stress compared to uni-directional excitation. Then, it leads to a sudden loss of shear strength at the failure surface. The early reduction in shear strength makes the massive soil block move over the sliding surface as it remains exposed to ground shaking in a longer time

interval. Thus, the shear strains under bi-directional excitation can reach 2.5 times of those obtained under uni-directional excitation. Such an increase in soil deformations significantly contributes to the increase in pile deformations, leading to the formation of plug and in-ground plastic hinges. This demonstrates that commonly used plane-strain analysis is inadequate, when liquefiable soil conditions are incorporated.

The torsional behavior of structural systems has been investigated by several researchers considering solely structural analysis models where soil behavior is represented by uni-axial spring elements. Hence the effect of SSI is disregarded, reducing the problem to a vibration analysis of a massive deck. Consequently, the eccentric wharf system responds as a torsionally coupled vibration under bi-directional excitation. However, the SSI analyses in this study revealed that the torsional response of wharf systems is minimal. In fact, the results of SSI analyses have altered our common perception regarding the seismic behavior of wharf based solely on inertial loading concept. SSI includes the kinematic interaction of pile and soil along with inertial interaction. The forces acting on the piles through kinematic interaction counterbalance the eccentric forces acting on deck due to inertial effects. Thus, the wharf system exhibit almost fully uncoupled bi-directional seismic response, showing negligible torsional effects. Furthermore, a parametric analysis is carried out to investigate whether the torsional response of the wharf system is associated with liquefaction or not. It is observed that the in-plane rotations of deck are not influenced by the liquefaction of soil layer. Consequently, it is concluded that torsional response is not an important aspect for the analysis and design of single module systems.

In multi-segmented wharf systems, although it does not notably influence seismic response, another source of torsion is observed. The exterior modules are driven to move by the mobilization of the free-field response on one side, while the movement of these modules are constrained by the interior modules on the other side. As a result, the deck of exterior modules experiences in-plane rotation. However, this rotation becomes noticeable only when the deck displacements are significantly amplified, with negligible impact on the seismic response of the wharf components.

Thus the seismic response of wharf systems with constant soil stratification is not significantly affected by two sources of torsion: Structural eccentricity (SE) and relative soil movement (RSM) around exterior modules. However, when evaluating the system with varying soil stratification (VSS), another source of torsion emerges due to relative movement of the liquefied soil layer along the embankment for the linked structural system. In this study, a linear variation in liquefiable layer along the embankment is adopted to simply demonstrate the effect of varying soil stratification on the seismic response. It is observed that the relative movement of liquefied soil layer along the embankment induces increasing deformation to the piles along the wharf system. This effect significantly increases the inelastic deformation demand at pile hinges and leads to a greater number of plastic hinge formations towards the end of the wharf system. Therefore, the consideration of varying soil stratification becomes particularly important in the presence of liquefiable soil conditions.

The variation of soil stratification along the embankment is also important for another significant aspect: the design of shear keys between modules. Shear keys are commonly used in wharf systems to ensure safe maritime operations by preventing relative movements of adjacent modules. The shear key forces developed during the seismic excitation are influenced by the three torsion sources mentioned earlier. The peak shear key force is calculated around 650-750kN per single-key in 8-module systems with constant soil stratification influenced by SE and RSM. In contrast, it is calculated as 1000-1150kN per single key in the systems with varying soil stratification, influenced by SE, RSM and VSS. Despite the 50% increase in shear key forces, these levels can be resisted by concrete capacity and shear reinforcement in design.

Dynamic magnification factor (DMF) is a concept developed to approximately account for the amplification of structural response resulting from longitudinal excitation when structural analysis is based on two-dimensional models. In practical applications, DMF value is specified as 1.1 for interior modules and can increase up to 1.5 for exterior modules as specified in POLB-WDC [58]. In this study, DMF values are calculated as 2.25 for both interior and exterior modules. However, this value is

due to a completely different aspect, specifically the effect of longitudinal excitation in liquefiable soil conditions.

Another interesting outcome of this study is that the relative rotation demands in piles tend to be greater at seaward piles compared to landward piles, despite the landward piles experiencing higher shear forces, as expected. In structural engineering practice, it is typically expected that the inelastic demand of plastic hinges is higher at the landward piles due to their shorter fixity length. However, in SSI analysis under liquefiable condition, the movement of landward piles is somewhat relaxed due to the mobilization of soil and rockfill block sliding over the failure surface. This results in larger deck displacement and less relative movement of pile head and rockfill beneath. It reduces the plastic deformation demands of landward piles in SSI analysis. On the other hand, the increase in effective length of seaward piles due to liquefaction, along with larger deck displacement, leads to higher plastic deformation demands in seaward pile plugs. In fact, these results are directly due to SSI analysis under liquefiable conditions.

While the analysis results indicate that vertical excitation has a minimal impact on the overall response, further investigation is needed to assess its influence on the plasticity of the pile elements.

Wharf strip analysis is computationally cheap and yields results similar to single module analysis under transverse excitation only. It may be used for the purpose of preliminary analysis.

In a nutshell, the seismic behavior of liquefiable soil and SSI has a decisive role on the seismic response of wharf systems. A rigorous approach to soil and 3D SSI modeling, considering at least simultaneous transverse and longitudinal excitation, is essential for a more accurate evaluation of wharf structural response. Although further improvement in post-processing, particularly in plasticity modeling of structural elements and their outputs, is still required, it is evident that SSI modeling and analysis

represent the future of performance-based design for pile-supported wharf systems. There may not be a need to perform a multi-segmented wharf system analysis; the single module wharf can be modeled to account for variations in soil stratification. Torsion does not influence the results of the analysis and design of wharf systems.

10. FUTURE STUDIES

The effect of topography should be investigated using real bathymetry maps with actual soil stratification. More sophisticated constitutive models can be investigated for various types of soil layers, calibrated with extensive test data.

An investigation regarding interface elements can be investigated to find out the stiffness and strength properties for various types of soils.

Investigating the use of 3-D elements for modeling piles, rather than 1-D elements, is necessary to accurately represent the pile-pinning effect. At the same time, when the use of 3-D elements for structural components becomes feasible, obtaining strain values directly from the 3-D elements would be possible for more advanced analyses in performance-based design of wharf systems.

The behavior of rockfill elements should be investigated using discrete element modeling, with calibration studies conducted through laboratory testing. Then, the wharf analysis models can be performed by combining discrete element-finite difference/finite element simulations under seismic excitation.

REFERENCES

1. "Unified Facilities Criteria (UFC) Design: Piers and Wharves", *UFC-2017*, pp. 1–171, 2017.

2. UNCTAD, "Review of Maritime Transport 2021", `https://unctad.org/system/files/official-document/rmt2021_en_0.pdf`.

3. Chang, S. E., "Disasters and transport systems: loss, recovery and competition at the Port of Kobe after the 1995 earthquake", *Journal of transport geography*, Vol. 8, No. 1, pp. 53–65, 2000.

4. Werner, S., N. McCullough, W. Bruin, A. Augustine, G. Rix, B. Crowder and J. Tomblin, "Seismic performance of Port de Port-au-Prince during the Haiti earthquake and post-earthquake restoration of cargo throughput", *Earthquake Spectra*, Vol. 27, No. 1_suppl1, pp. 387–410, 2011.

5. Ramirez-Henao, A. F. and J. P. Smith-Pardo, "Elastic stability of pile-supported wharves and piers", *Engineering Structures*, Vol. 97, pp. 140–151, 2015.

6. Wolf, J., *Dynamic soil-structure interaction*, Prentice Hall, Inc., 1985.

7. Muraleetharan, K., K. Mish, C. Yogachandran and K. Arulanandan, "DYSAC2: dynamic soil analysis code for 2-dimensional problems", *Department of Civil Engineering, University of California, Davis, California*, 1988.

8. Muraleetharan, K., S. Jagannath, K. Arulmoli and D. Thiessen, "Performance of port facilities during the Northridge earthquake", *University of Missouri–Rolla*, 1995.

9. Yang, D.-S., *Deformation-based seismic design models for waterfront structures*, Ph.D. Thesis, Oregon State University, 1999.

10. "Itasca Consulting Group, Inc.", *FLAC — Fast Lagrangian Analysis of Continua, Ver. 8.1. Minneapolis: Itasca*, 2019.

11. Roth, W. and E. Dawson, "Analyzing the seismic performance of wharves, part 2: SSI analysis with non-linear, effective-stress soil models", *Advancing Mitigation Technologies and Disaster Response for Lifeline Systems*, pp. 395–404, 2003.

12. McCullough, N. J., *The seismic geotechnical modeling, performance, and analysis of pile-supported wharves*, Ph.D. Thesis, Oregon State University, 2004.

13. Takahashi, A., "Seismic performance evaluation of pile-supported wharf by 3D finite element analysis", *Proceedings of the 12th Asian regional conference on soil mechanics and geotechnical engineering*, Vol. 1, pp. 245–248, 2003.

14. Dickenson, S. E. and N. J. McCullough, "Modeling the Seismic Performance of Pile Foundations for Port and Coastal Infrastructure", *Seismic Performance and Simulation of Pile Foundations in Liquefied and Laterally Spreading Ground*, pp. 173–191, 2006.

15. Lu, J., *Parallel finite element modeling of earthquake ground response and liquefaction*, University of California, San Diego, 2006.

16. Chiaramonte, M. M., *An analysis of conventional and improved marginal wharves*, Master's Thesis, University of Washington, 2011.

17. Heidary-Torkamani, H., K. Bargi, R. Amirabadi and N. J. McCllough, "Fragility estimation and sensitivity analysis of an idealized pile-supported wharf with batter piles", *Soil Dynamics and Earthquake Engineering*, Vol. 61, pp. 92–106, 2014.

18. Amirabadi, R., K. Bargi, M. Dolatshahi Piroz, H. Heidary Torkamani and N. Mccullough, "Determination of optimal probabilistic seismic demand models for pile-supported wharves", *Structure and Infrastructure Engineering*, Vol. 10, No. 9, pp. 1119–1145, 2014.

19. Ragued, B., *New Zealand port characterisation and wharf seismic response*, Ph.D. Thesis, ResearchSpace@ Auckland, 2017.

20. Su, L., J. Lu, A. Elgamal and A. K. Arulmoli, "Seismic performance of a pile-supported wharf: Three-dimensional finite element simulation", *Soil Dynamics and Earthquake Engineering*, Vol. 95, pp. 167–179, 2017.

21. Su, L., H.-P. Wan, Y. Dong, D. M. Frangopol and X.-Z. Ling, "Seismic fragility assessment of large-scale pile-supported wharf structures considering soil-pile interaction", *Engineering Structures*, Vol. 186, pp. 270–281, 2019.

22. Su, L., H.-P. Wan, K. Bi, Y. Li, J. Lu, X.-Z. Ling, A. Elgamal and A. K. Arulmoli, "Seismic fragility analysis of pile-supported wharves with the influence of soil permeability", *Soil Dynamics and Earthquake Engineering*, Vol. 122, pp. 211–227, 2019.

23. Su, L., H.-P. Wan, Y. Luo, Y. Dong, F. Niu, J. Lu, X.-Z. Ling, A. Elgamal and A. K. Arulmoli, "Seismic performance assessment of a pile-supported wharf retrofitted with different slope strengthening strategies", *Soil Dynamics and Earthquake Engineering*, Vol. 129, p. 105903, 2020.

24. Su, L., H.-P. Wan, J. Lu, X. Ling, A. Elgamal and A. K. Arulmoli, "Seismic performance evaluation of a pile-supported wharf system at two seismic hazard levels", *Ocean Engineering*, Vol. 219, p. 108333, 2021.

25. Souri, M., A. Khosravifar, S. Dickenson, N. McCullough and S. Schlechter, "Effects of long duration earthquakes on the interaction of inertial and liquefaction-induced kinematic demands on pile-supported wharves", *Soil Dynamics and Earthquake Engineering*, Vol. 154, p. 107155, 2022.

26. Özcebe, A. G., F. Bozzoni and B. Borzi, "Seismic Vulnerability Assessment of Critical Port Infrastructure Components by Modelling the Soil-Wharf-Crane In-

teraction", *Infrastructures*, Vol. 7, No. 8, p. 102, 2022.

27. Souri, M., A. Khosravifar, S. Dickenson, N. McCullough and S. Schlechter, "Numerical modeling of a pile-supported wharf subjected to liquefaction-induced lateral ground deformations", *Computers and Geotechnics*, Vol. 154, p. 105117, 2023.

28. Khosravifar, A. and M. Souri, "3D Modeling of Pile-Supported Wharf Subjected to Liquefaction-Induced Lateral Ground Deformations", *Geo-Congress 2023*, pp. 124–133.

29. Wang, J., L. Su, L. Xie and X. Ling, "Seismic response analysis of pile-supported wharf under three types of near-fault ground motion", *Structures*, Vol. 57, p. 105144, Elsevier, 2023.

30. Zhang, Y., S. Tian, L. Tang and X. Ling, "Experimental and numerical investigation on the response characteristic of the crane-wharf structure in liquefiable site", *Ocean Engineering*, Vol. 299, p. 117312, 2024.

31. Varun and D. Assimaki, "Integrating soil-structure interaction analyses of pile-supported wharfs in seismic risk management of port systems", *Geotechnical Earthquake Engineering and Soil Dynamics IV*, pp. 1–10, 2008.

32. Varun, *A non-linear dynamic macroelement for soil structure interaction analyses of piles in liquefiable sites*, Ph.D. Thesis, Georgia Institute of Technology, 2010.

33. Werner, S., R. DesRoches, G. Rix and A. Shafieezadeh, "Fragility models for container cargo wharves", *TCLEE 2009: Lifeline Earthquake Engineering in a Multihazard Environment*, pp. 1–12, 2009.

34. Shafieezadeh, A., *Seismic vulnerability assessment of wharf structures*, Ph.D. Thesis, Georgia Institute of Technology, 2011.

35. Vytiniotis, A., *Contributions to the analysis and mitigation of liquefaction in loose*

sand slopes, Ph.D. Thesis, Massachusetts Institute of Technology, 2011.

36. Thomopoulos, C. and C. G. Lai, "Preliminary definition of fragility curves for pile-supported wharves", *Journal of Earthquake Engineering*, Vol. 16, No. sup1, pp. 83–106, 2012.

37. Vytiniotis, A., A.-I. Panagiotidou and A. J. Whittle, "Analysis of seismic damage mitigation for a pile-supported wharf structure", *Soil Dynamics and Earthquake Engineering*, Vol. 119, pp. 21–35, 2019.

38. Weismair, M., S. Shahrestani, A. Lim, M. N. Priestley and I. Po Lam, "Seismic Design of Port of Los Angeles Pier 400 Container Wharf", *Ports' 01: America's Ports: Gateway to the Global Economy*, pp. 1–10, 2001.

39. McCullough, N. J., S. E. Dickenson and S. M. Schlechter, "The seismic performance of piles in waterfront applications", *Ports' 01: America's Ports: Gateway to the Global Economy*, pp. 1–10, 2001.

40. Singh, J., M. Tabatabaie and J. B. French, "Importance of Seismological-Geotechnical-Structural Handshake in Performance-Based Design of Waterfront Structures", *SEOAC Annual Convention Proceedings*, pp. 155–169, 2002.

41. Roth, W., E. Dawson, M. Mehrain and A. Sayegh, "Analyzing the seismic performance of wharves, part 1: Structural-engineering approach", *Advancing mitigation technologies and disaster response for lifeline systems*, pp. 385–394, 2003.

42. SAP2000, C., "Structural analysis program", *Berkeley, California*, 2005.

43. Vahdani, S., J. Egan, R. Pyke, C.-C. Chin, T. Griswold and T. LaBasco, "Evaluating the seismic capacity of a newly designed wharf at the Port of Oakland", *Ports 2007: 30 Years of Sharing Ideas: 1977-2007*, pp. 1–9, 2007.

44. Blandon, C., *Seismic analysis and design of pile supported wharves*, Ph.D. Thesis,

Rose School. Pavia, Italy, 2007.

45. Arulmoli, A. K. and G. R. Martin, "Seismic Soil-Structure Interaction Issues for Pile-Supported Piers and Wharves", *TCLEE 2009: Lifeline Earthquake Engineering in a Multihazard Environment*, pp. 1–11, 2009.

46. Jain, P., D. S. Phelps and K. H. Chin, "Structural-geotechnical procedures for new wharf design", *Ports 2010: Building on the Past, Respecting the Future*, pp. 100–109, 2010.

47. Dickenson, S., S. Yang, D. Schwarm, M. Rees and C. Hill, "Seismic performance analysis of pile-supported wharves subjected to long-duration ground motions", *M. Huang (Ed.), Proceedings of SMIP14 Seminar on Utilization of Strong-Motion Data, Berkeley, California, United states, 9 October 2014*, pp. 63–82, 2014.

48. Percher, M. and R. Iwashita, "Kinematic Loading from a Structural Perspective", *Ports 2016*, pp. 263–272, 2016.

49. Souri, M., A. Khosravifar, S. E. Dickenson, S. Schlechter and N. McCullough, "Inertial and liquefaction-induced kinematic demands on a pile-supported wharf: physical modeling", *Geotechnical earthquake engineering and soil dynamics V*, pp. 388–397, American Society of Civil Engineers Reston, VA, 2018.

50. Galbraith, J., M. Naeem and W. Bruin, "Combined Kinematic and Inertial Seismic Analysis of Marine Structures", *15th Triennial International Conference*, pp. 66–77, American Society of Civil Engineers Reston, VA, 2019.

51. Yao, S., M. A. Naeem, S. Barrett and J. Core, "Performance Based Seismic Retrofit Solutions for Wharf Preservation", *15th Triennial International Conference*, pp. 358–368, American Society of Civil Engineers Reston, VA, 2019.

52. Souri, M., A. Khosravifar, S. Dickenson, S. Schlechter and N. McCullough, "Pile-supported wharves subjected to inertial loads and lateral ground deformations. I:

Experimental results from centrifuge tests", *Journal of Geotechnical and Geoenvironmental Engineering*, Vol. 148, No. 11, p. 04022090, 2022.

53. Souri, M., A. Khosravifar, S. Dickenson, S. Schlechter and N. McCullough, "Pile-supported wharves subjected to inertial loads and lateral ground deformations. II: Guidelines for equivalent static analysis", *Journal of Geotechnical and Geoenvironmental Engineering*, Vol. 148, No. 11, p. 04022091, 2022.

54. Benzoni, G. and M. Priestley, "Seismic response of linked marginal wharf segments", *Journal of earthquake engineering*, Vol. 7, No. 04, pp. 513–539, 2003.

55. Donahue, M. J., S. E. Dickenson, T. H. Miller and S. C. Yim, "Implications of the observed seismic performance of a pile-supported wharf for numerical modeling", *Earthquake Spectra*, Vol. 21, No. 3, pp. 617–634, 2005.

56. Thach, P. N. and S. Yang, "A Simplified Method for Estimating Target Displacement of Pile-Supported Wharf under Response Spectrum Seismic Loading", *Computational Structural Engineering: Proceedings of the International Symposium on Computational Structural Engineering, held in Shanghai, China, June 22–24, 2009*, pp. 281–289, Springer, 2009.

57. Jaradat, O. A., C. Lai, G. Saad and P. Smith, "Wharf Structure Design Consideration of Pier E Redevelopment Project at the Port of Long Beach", *Ports 2010: Building on the Past, Respecting the Future*, pp. 490–499, 2010.

58. "Port of Long Beach Wharf Design Criteria", *POLB WDC v5.0*, pp. 1–125, 2021.

59. Doran, B., J. Shen and B. Akbas, "Seismic evaluation of existing wharf structures subjected to earthquake excitation: Case study", *Earthquake Spectra*, Vol. 31, No. 2, pp. 1177–1194, 2015.

60. Erdogan, H., B. Doran, A. Seckin, B. Akbas, Y. Celikoglu and T. Bostan, "Seismic performance and retrofit evaluation of an existing pile-wharf structure", *Journal*

of Performance of Constructed Facilities, Vol. 31, No. 6, p. 04017110, 2017.

61. "Turkish Seismic Code for Marine, Railway and Airport Structures (in Turkish)", *DLH-DTY*, pp. 1–180, 2007.

62. Karakaş, N., *Kazıklı bitişik rıhtım yapılarının dinamik etkileşiminin incelenmesi*, Master's Thesis, Yıldız Technical University, 2020.

63. Gao, S., J. Gong and Y. Feng, "Dynamic magnification factor of pile-supported wharf under horizontally bi-directional ground motion", *Journal of Earthquake Engineering*, Vol. 25, No. 1, pp. 139–161, 2021.

64. Shafieezadeh, A., R. DesRoches, G. J. Rix and S. D. Werner, "Three-dimensional wharf response to far-field and impulsive near-field ground motions in liquefiable soils", *Journal of Structural Engineering*, Vol. 139, No. 8, pp. 1395–1407, 2013.

65. Burden, L. I., *Forecasting earthquake losses in port systems*, Ph.D. Thesis, Georgia Institute of Technology, 2012.

66. Yin, P., N. Priestley, G. Martin, M. Weismair, O. A. Jaradat and K. Arulmoli, "Seismic Engineering Program at the Port of Los Angeles", *Ports 2007: 30 Years of Sharing Ideas: 1977-2007*, pp. 1–10, 2007.

67. Smith-Pardo, J., J. Bardi and C. Ospina, "Seismic Assessment and Retrofitting of a Container Wharf and Container Yard following the 27 February 2010 Chile Earthquake", *15th World Conference in Earthquake Engineering, Lisboa*, 2012.

68. Hung, S. and S. Werner, "An assessment of earthquake response characteristics and design procedures for port and harbor facilities", *Proc. 3rd Int. Earthq. Microzonation Conf., Seattle*, 1982.

69. Buslov, V. M., M. Rowghani and M. Weismair, "Evaluating earthquake damage to concrete wharves", *Concrete International*, Vol. 18, No. 8, pp. 50–54, 1996.

70. Boulanger, R., S. Iai, A. Ansal, K. Cetin, I. Idriss, B. Sunman and K. Sunman, "Performance of waterfront structures", *1999 Kocaeli, Turkey, Earthquake Reconnaissance Rep*, , No. Supplement A, pp. 295–310, 2000.

71. Diaz, G. M., B. W. Patton, G. L. Armstrong and M. Joolazadeh, "Lateral load tests of piles in sloping rock fill", *Analysis and Design of Pile Foundations*, pp. 214–231, ASCE, 1984.

72. McCullough, N. J. and S. E. Dickenson, "The behavior of piles in sloping rock fill at marginal wharves", *Ports 2004: Port Development in the Changing World*, pp. 1–10, 2004.

73. Kawamata, Y., *Seismic performance of a pile-supported container wharf structures in rockfill*, Ph.D. Thesis, Oregon State University, 2009.

74. Kawamata, Y., S. A. Ashford and N. Nimityongskul, "Full-scale lateral pile load test in rock fill", *Geotechnical earthquake engineering and soil dynamics IV*, pp. 1–9, 2008.

75. Code, P. S., "The Port of Los Angeles code for seismic design, upgrade and repair of container wharves", *City of Los Angeles Harbor Department, CA, USA*, 2010.

76. Dickenson, S., S. Yang, D. Schwarm, M. Rees and C. Hill, "Use of strong motion records to validate dynamic soil-foundation-structure interaction models for pile supported wharves", *California Strong Motion Instrumentation Program, Seminar Proceedings*, 2013.

77. "Turkish Seismic Code for Marine Structures 2020 (in Turkish)", *General Directorate of Infrastructure Investments, AYGM*, 2020.

78. "Seismic Design of Piers and Wharves", *American Society of Civil Engineers - ASCE/COPRI 61-14*, 2014.

79. Earth Mechanics, I., "Port-Wide Ground Motion Study Update, Port of Long Beach, California", pp. 1–X, 2020.

80. Itasca Consulting Group, I., "FLAC3D V9.0 Online Manual", 2024, https://docs.itascacg.com/itasca900/flac3d/docproject/source/flac3dhome.html.

81. Lysmer, J. and R. L. Kuhlemeyer, "Finite dynamic model for infinite media", *Journal of the engineering mechanics division*, Vol. 95, No. 4, pp. 859–877, 1969.

82. Cheng, Z. and C. Detournay, "Formulation, validation and application of a practice-oriented two-surface plasticity sand model", *Computers and Geotechnics*, Vol. 132, p. 103984, 2021.

83. Dafalias, Y. F. and M. T. Manzari, "Simple plasticity sand model accounting for fabric change effects", *Journal of Engineering mechanics*, Vol. 130, No. 6, pp. 622–634, 2004.

84. Reese, L. C., W. M. Isenhower and S.-T. Wang, *Analysis and design of shallow and deep foundations*, Vol. 10, John Wiley & Sons, 2005.

85. Council, A. T., *Quantification of building seismic performance factors*, US Department of Homeland Security, FEMA, 2009.

86. Ancheta, T. D., R. B. Darragh, J. P. Stewart, E. Seyhan, W. J. Silva, B. S.-J. Chiou, K. E. Wooddell, R. W. Graves, A. R. Kottke, D. M. Boore *et al.*, "NGA-West2 database", *Earthquake Spectra*, Vol. 30, No. 3, pp. 989–1005, 2014.

87. Asimaki, D., J. Shi and W. Li, "SeismoSoil user manual, v1.3", *California Institute of Technology: Pasadena, CA, USA*, 2017.

88. Nakamura, Y. *et al.*, "Clear identification of fundamental idea of Nakamura's technique and its applications", *Proceedings of the 12th world conference on earthquake engineering*, Vol. 2656, pp. 1–8, Auckland/New Zealand, 2000.

89. "TS-500 Design and Construction Rules of Reinforced Concrete Structures (Turkish)", *Turkish Standard Institute*, 2000.

90. "TS-708 Steel for the Reinforcement of Concrete (Turkish)", *Turkish Standard Institute*, 2016.

91. "Eurocode 3: Design of steel structures - Part 1-1: General rules and rules for buildings", *British Standard Institution*, 2005.

92. AFAD, "Turkish Seismic Design Code for Buildings (in Turkish)", *TBDY-2018*, pp. 1–395, 2018.

93. Gardner, L. and D. Nethercot, "Structural stainless steel design: a new approach", *Structural Engineer*, Vol. 82, pp. 21–30, 2004.

94. Harn, R., C. E. Ospina and D. Pachakis, "Proposed Pipe Pile Strain Limits for ASCE 61-19", *15th Triennial International Conference*, pp. 437–448, American Society of Civil Engineers Reston, VA, 2019.

95. Mander, J. B., M. J. Priestley and R. Park, "Theoretical stress-strain model for confined concrete", *Journal of structural engineering*, Vol. 114, No. 8, pp. 1804–1826, 1988.

96. "The MathWorks Inc.", *MATLAB version: 9.13.0 (R2022b)*, 2022.

97. Lee, J. M.-y. and E. Y.-c. Wong, "Suez Canal blockage: an analysis of legal impact, risks and liabilities to the global supply chain", *MATEC web of conferences*, Vol. 339, p. 01019, EDP Sciences, 2021.

98. Panagiotidou, A. I., *Seismic response of wharf structures supported in liquefiable soil*, Master's Thesis, Massachusetts Institute of Technology, 2013.

99. Werner, S., S. Dickenson, J. Egan, J. Ferritto, P. Kaldveer, D. Thiessen, G. Ser-

venti and E. Byrne, “Experience from past earthquakes”, *Seismic guidelines for ports*, 1998.

100. “Itasca Consulting Group, Inc.”, *FLAC3D Fast Lagrangian Analysis of Continua in Three-Dimensions, Ver. 9.0. Minneapolis: Itasca*, 2023.